International Journal of Polymer Science

Polymers from Biomass: Characterization, Modification, Degradation, and Applications

Guest Editors: Mukund Adsul, Deepak K. Tuli, Pratheep K. Annamalai, Dilip Depan, and Shiv Shankar

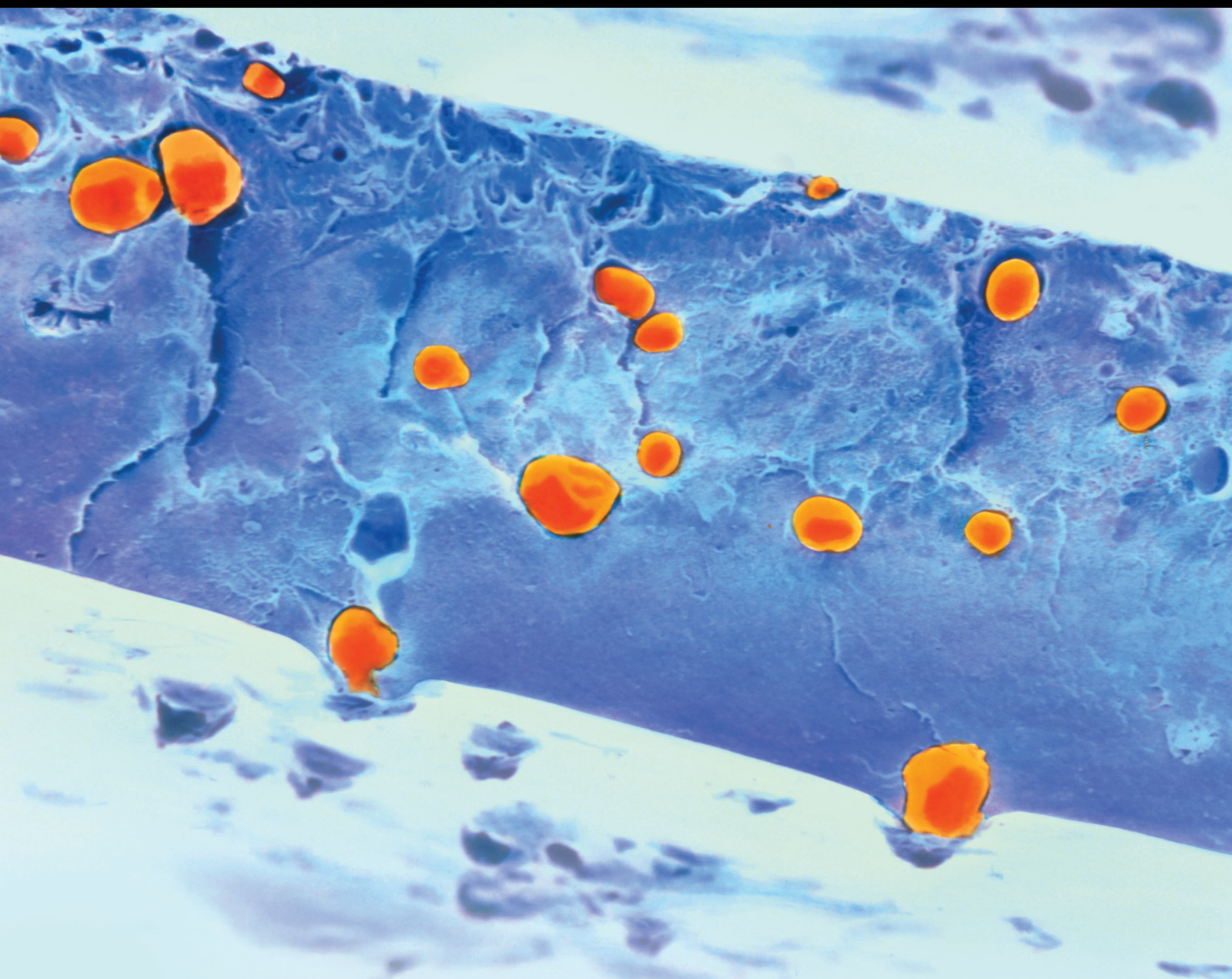

Polymers from Biomass: Characterization, Modification, Degradation, and Applications

International Journal of Polymer Science

Polymers from Biomass: Characterization, Modification, Degradation, and Applications

Guest Editors: Mukund Adsul, Deepak K. Tuli, Pratheep K. Annamalai, Dilip Depan, and Shiv Shankar

Editorial Board

Contents

Hindawi Publishing Corporation
International Journal of Polymer Science
Volume 2016, Article ID 1857297, 2 pages
http://dx.doi.org/10.1155/2016/1857297

Editorial

Polymers from Biomass: Characterization, Modification, Degradation, and Applications

Mukund Adsul,[1] Deepak K. Tuli,[1] Pratheep K. Annamalai,[2] Dilip Depan,[3] and Shiv Shankar[4]

[1] *DBT-IOC Centre for Advanced Bioenergy Research, Indian Oil R&D Center, Sector 13, Faridabad 121007, India*
[2] *Australian Institute for Bioengineering and Nanotechnology, The University of Queensland, Brisbane, QLD 4072, Australia*
[3] *Chemical Engineering Department, University of Louisiana at Lafayette, Lafayette, LA 70504, USA*
[4] *Department of Food Engineering, Mokpo National University, Jeonnam 534-729, Republic of Korea*

Correspondence should be addressed to Mukund Adsul; madsul@gmail.com

Received 23 February 2016; Accepted 23 February 2016

Polymers from biomass are of prime concern and are the cornerstone in terms of various applications such as biofuels, biomedical, and biocomposite applications. Recently, concerns on the environmental pollution and exhaust of natural resources caused by the nonbiodegradable petroleum-based plastics materials have attracted attention on the development of environmentally benign polymers for their applications in various industries and other value added utilities. Renewable and abundantly available biopolymers are the most viable alternative for the production of green materials in the near future. In order to secure the sustainable development for exponentially growing population, the increasing demands for the light-weighted high performance materials and growing concerns over environmental impact of the materials have compelled academic and industrial researchers to develop new materials from alternative or renewable resources. Renewability of resources depends on the availability and life cycle of the raw materials. In recent decades, polymeric materials from renewable biological resources such as plants, marine animals, and microbial organisms have increasingly gained the attention of researchers. The polymers which are derived/extracted from the most widely available biological renewable resources (agricultural plants, marine animals, and microorganisms) are called "biopolymers." These polymers are produced as biomass or byproduct during the growth cycles of organisms. Biopolymers or renewable polymers such as cellulose, lignin, starch, pectin, chitin, and xylan are the abundantly available polymers in nature in the form of plant biomass or other biological sources. Their importance for various applications (biofuels, nanobiocomposites, biomedical, etc.) has been analyzed for many years and still continued. There are different ways to convert these biopolymers into various chemicals, fuels, and materials for the benefit of our society. Still there are challenges to develop new methodologies or improved processes for efficient and economic utilization as well as conversion of these biopolymers.

At present few polysaccharides such as cellulose, starch, and xylan have tremendous applications in various fields such as nanoscience, biorefineries, and composites materials. Some biopolymers are yet to be exploited more such as lignin. Their separation, degradation, and aromatic nature make them more complicated but still have importance. Almost all biopolymers are degraded by microorganism by producing enzymes. They can be also degraded by chemical catalysts (e.g., solid acids) to make sugars. Recently researchers succeeded in preparing the nanoparticles of biopolymers such as cellulose and chitin, which increases their scope in nanosciences. Biological or chemical degradation of biopolymers into their simple forms (e.g., sugars) makes them applicable in biological fermentation for production of value added chemicals or fuels. These biopolymers also have medical applications such as drug delivery and tissue engineering.

Biopolymers have great potential in the growing commercial plastics market with the global production capacity

of bioplastics at about 1,161 metric tons in 2011, and this has been expected to increase up to 5,779 metric tons by 2016, as indicated by recent market survey. They are regarded as environmentally friendly materials not only due to their source but also due to their inherent biodegradability in many cases. There is also a significant portion of polymers produced from biological resources that are not biologically "degradable" according to the internationally accepted standards. In order to translate these biopolymers into real applications, there appear to be significant obstacles including poor processability, poor properties (mechanical properties, thermal stability, water absorption, and barrier properties), and performance in comparison to their synthetic counter parts. These obstacles have motivated many research activities in the field to process and evaluate materials fully or partially based on the renewable resources.

This special issue portrays the recent and significant research activities occurring around the globe, on the utilization of potential biomass into polymeric materials. Some microbial biomass based on microbiologically produced polymers (alginate) is also highlighted in this special issue along with plant based polymers. Application of chitosan in probiotic culture formulations, use of oil palm biomass for preparations of bioplastic fertilizer composites and use of starch or other carbohydrates for preparation of composite materials, and so forth are few highlights for this special issue. Being readily available, these polymers may need significant improvements for end applications. For this, novel technologies and strategies are currently being researched. Similarly, various investigations to study the thermal and environmental degradation were carried out and are highlighted in this special issue. Interestingly, renewable polymers can be also used as a binding material for construction purpose. Underdeveloped countries may harness benefits as these countries have enormous natural resources, and this aspect has been highlighted in the special issue. Apart from processing products, the biopolymers were also used to release biologically relevant materials in a controlled manner.

Acknowledgments

We acknowledge all the authors for their valuable contributions and the reviewers for their support and constructive critiques in making this special issue possible.

Mukund Adsul
Deepak K. Tuli
Pratheep K. Annamalai
Dilip Depan
Shiv Shankar

Hindawi Publishing Corporation
International Journal of Polymer Science
Volume 2016, Article ID 2062360, 12 pages
http://dx.doi.org/10.1155/2016/2062360

Review Article

Alginate Biosynthesis in *Azotobacter vinelandii*: Overview of Molecular Mechanisms in Connection with the Oxygen Availability

Ivette Pacheco-Leyva, Felipe Guevara Pezoa, and Alvaro Díaz-Barrera

Escuela de Ingeniería Bioquímica, Pontificia Universidad Católica de Valparaíso, Avenida Brasil 2147, Casilla, 4059 Valparaíso, Chile

Correspondence should be addressed to Alvaro Díaz-Barrera; alvaro.diaz@ucv.cl

Received 28 August 2015; Revised 11 January 2016; Accepted 7 February 2016

Academic Editor: Mukund Adsul

The Gram-negative bacterium *Azotobacter vinelandii* can synthetize the biopolymer alginate that has material properties appropriate for plenty of applications in industry as well as in medicine. In order to settle the foundation for improving alginate production without compromising its quality, a better understanding of the polymer biosynthesis and the mechanism of regulation during fermentation processes is necessary. This knowledge is crucial for the development of novel production strategies. Here, we highlight the key aspects of alginate biosynthesis that can lead to producing an alginate with specific material properties with particular focus on the role of oxygen availability linked with the molecular mechanisms involved in the alginate production.

1. Introduction

Increasing research on the mechanisms of synthesis and biochemical properties of biopolymers, such as polysaccharides, led to improving production process and new applications in diverse areas, mainly in food and pharmaceutical industries [1]. One of the main advantages for the use of biopolymers is its degradability, making them a renewable product option. However, the high costs of biopolymer production are still a major drawback for a widespread industrial application [2].

A particular linear polysaccharide with broad growing interest is alginate, which is a structural component of the brown marine algae and the cell wall of bacteria belonging to the *Pseudomonas* and *Azotobacter* genera [3–5]. The properties of alginates in solution largely depend on four factors: (a) its monomer chemical composition (β-D-mannuronic acid (M-residues) and its epimer, α-L-guluronic acid (G-residues)); (b) the sequence pattern of the monomers; (c) the molecular weight (MW) of the resulting polysaccharide chain; and (d) modifications of the polymer (acetylation degree) [6, 7].

However, algal alginates are complex mixtures containing polysaccharides with a wide range of MW and ratios of M : G. Hence alginates with specific defined M : G ratios or a constant range of MW cannot be easily obtained from particular algae species, due to intrinsic environmental culture conditions, thus limiting their use in the pharmaceutical and chemical industries (more details in Section 2). For this reason, the bioprocesses research area has become interested in developing strategies to produce alginates with particular molecular characteristics through microbial alginate production. In contrast to algal alginates, microbial alginates present exclusive M-residue acetylation, controlled M : G ratios, and specific MW under specific growth conditions [8–10]. A nonpathogenic bacterium able to produce alginate with high production yields in bioreactors is *Azotobacter vinelandii*. Yet, the complex regulatory pathways controlling the alginate biosynthesis and material properties in response to external environmental clues remain still unknown, despite some efforts in trying to gain new insights into gene expression patterns under different culturing conditions in *A. vinelandii* cultures [9, 11–13].

In this review, we present an up-to-date biosynthetic overview of microbial alginate biosynthesis from *Azotobacter vinelandii*, and the perspectives for production process improvement based on a better understanding on the

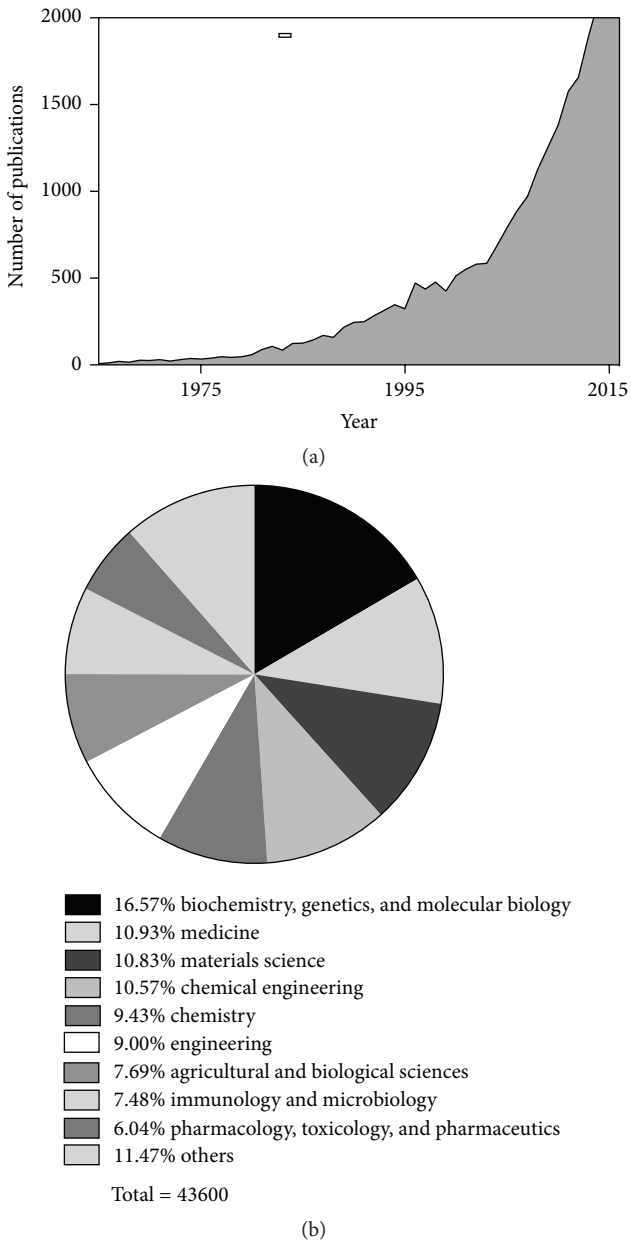

Figure 1: (a) Number of publications indexed in Scopus database (August 2015), using keyword *alginate* (–) in title, abstract, or keywords. (b) Percentage of the word *alginate* distributed in different subject areas.

molecular mechanism underlying polymer biosynthesis in relationship with the oxygen availability during the fermentation process.

2. Alginate Structure, Chemical Structure, and Applications

Over the past 40 years, a growing interest in the use of alginate has been observed including different areas, ranging from genetics to pharmaceutics (Figure 1).

Alginate has been placed as the second biopolymer derived from seaweeds with greater demand in the hydrocolloids' industry [14]. Currently, the only economic way to obtain commercial alginate used for most applications is through its extraction from marine algae, the cost of which ranges between US$ 2 and 20/kg, and with a total market value of around US$ 339 million [14]. Furthermore, alginates of very high purity are used in the pharmaceutical industry where they are sold for up to US$ 3,200/kg.

Table 1: Summary of biotechnological and pharmaceutical applications of alginates based on their molecular weights.

Application of alginate	Molecular weight (kDa)	Reference
Delivery of bioactive compounds Antioxidant *In vivo* tissue scaffolds Antibacterial Dietary supplement Cell immobilization	≈15–120	[60–66]
Food stabilizer and preserving agent Microencapsulation and storage stability Antibacterial Bioremediation Wound healing	≈120–290	[62, 63, 67–76]
Modulation of enzymatic activity Extended-release tablet compound	500–941	[71, 77]

Since alginate is a biodegradable and a biocompatible polysaccharide, it presents a panoply of food, pharmaceutical, and biotechnological applications (Figure 1(b)). In the food and pharmaceutical industries, alginate is mainly used as a stabilizing, thickening, or gel-film-forming agent [6, 15–17], Table 1; in medicine it is used as wound healing material [18], as part of medical treatments [19, 20], or as dietary fiber supplements [21, 22]. Alginate showed potential beneficial physiological effects in the gastrointestinal tract [23]. Moreover, hydrogel-alginates are being investigated in biotechnology as drug delivery agents, as cell encapsulation material, and as scaffold material in tissue engineering [24].

Alginate is the main structural component of brown marine algae (*Laminaria* and *Macrocystis*) representing about 32% of dry biomass [25], consisting in variable amounts of M-, G-, and MG-residues, linked by 1→4 glycosidic bonds [7]. On the other hand, alginates produced by bacteria are submitted to esterification with *O*-acetyl groups at the *O*-2 and/or *O*-3 of the M-residues [26], where the majority of the M-residues are mono-*O*-acetylated, and infrequently with 2,3-di-acetylated [27] (Figure 2). Because the monomeric chemical structure of bacterial alginate and the sequence length determine the mechanical properties of the alginates, one of the aims of different investigations is the possibility of manipulating the composition alginates for specific applications have been intensively investigated [28, 29].

The obligate aerobe bacterium *Azotobacter vinelandii* produces alginate that acts as a diffusion barrier for nutrients and oxygen [30, 31]. It was reported as a bacterium with a

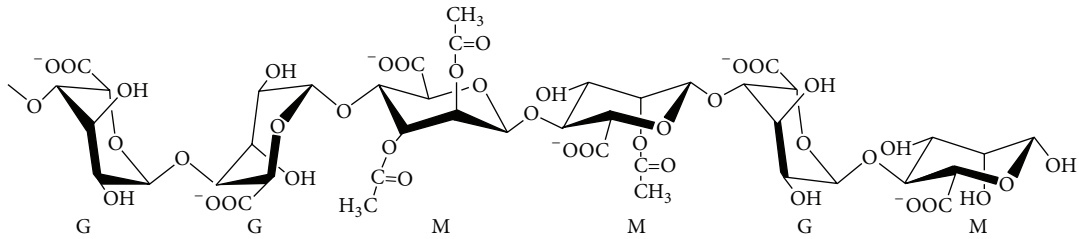

Figure 2: Representation of the chemical structure from acetylated alginates produced by *Azotobacter vinelandii* bacterium [28]. Mannuronic (M) and guluronic (G) acid residues are represented in the alginate chain.

highest respiratory rate [32], implying that it adjusts oxygen consumption rates in order to maintain low levels of cytoplasmic oxygen and in this way permitting the oxygen-sensitive enzymes to be active, like nitrogenase, which is responsible for fixing nitrogen [30, 32].

A. vinelandii under limitation of carbon source or by induction forms cysts that are more resistant to desiccation and is mainly composed of alginate [33, 34]. It also accumulates the intracellular polyester poly-β-hydroxybutyrate (PHB) as a reserve carbon and energy source [35, 36].

Consequently, an increased knowledge about the molecular mechanism involved in alginate biosynthesis will be crucial for the development of novel strategies to improve the production of alginates with defined characteristics tailored for specific applications.

3. The Biosynthetic-Secretory Route of Alginate Production in *Azotobacter vinelandii*

Microbial polysaccharides have distinct biological functions, as intracellular storage, as envelope, or as extracellular polymers [37]. Microbial alginate is an extracellular polysaccharide as xanthan, cellulose, and sphingan, among others, and they differ in their biosynthetic pathways routes (recently reviewed in Schmid et al. 2015 [37]). Moreover, alginate is secreted trough a secretion system shared among the Gram-negative bacteria [38].

The alginate biosynthesis in bacteria *Azotobacter* results from a complex regulatory network of proteins, similar to *Pseudomonas* genera [6, 28, 39].

All of the steps involved in the conversion of central sugar metabolites into the alginate precursor in *A. vinelandii* have been previously identified and characterized [6, 40]. The alginate precursor, GDP-mannuronic acid, is synthesized from fructose-6-phosphate to mannose-6-phosphate by the bifunctional enzyme phosphomannose isomerase (PMI)/guanosine-diphosphomannose pyrophosphorylase (GMP), designated as AlgA, encoded by the *algA* gene. A phosphomannomutase (AlgC) directly converts the mannose-6-phosphate into mannose-1-phosphate, which is in turn converted into GDP-mannose by the AlgA enzyme. GDP-mannose is oxidized to GDP-mannuronic acid by GDP-mannose dehydrogenase (AlgD, encoded by *algD* gene). Because the intracellular levels of GDP-mannose are high and because it is used in different pathways, it has been proposed as the limiting step of alginate biosynthesis in *P. aeruginosa* [41].

After the production of the polymer precursor GDP-mannuronic acid precursor, its polymerization and transport across the cytoplasmic membrane is carried out by proteins presumably integrating a cytoplasmic membrane complex (polymerase complex). The core of the polymerase complex is composed of the glycosyltransferase Alg8 protein and Alg44 protein [42–44]. Furthermore, the protein AlgK is thought to stabilize the polymerase complex, by interacting with Alg44 [43]. Highlighting the important role of this protein, alginate polymerization does not occur in the absence of *algK* [42, 45].

The polymannuronate polysaccharide resulting from polymerization and then translocation to the *A. vinelandii* periplasm is composed of M-residues, which can then be further modified during its passage across the periplasm [43]. These modifications consist in acetylation, epimerization, and degradation of the M-residues. More specifically, the polymannuronic molecule undergoes an *O*-acetylase modification, which is catalyzed by an acetylase enzymatic complex composed of AlgI, AlgV (AlgJ in *P. aeruginosa*), AlgF, and AlgX proteins [46–48]. While M-residue *O*-acetylation does not occur frequently in alginate, some may be acetylated. *O*-acetylated M-residues will therefore be protected from epimerization [26], because only nonacetylated M-residues can be epimerized to G-residues by the AlgG epimerase [42], so alginates with a relatively high degree of acetylation display a lower degree of epimerization [27].

Alginate depolymerization occurs at the 4-*O*-glycosidic bond via β-elimination, by alginate lyases which have been the subject of a recent review [28]. The *Azotobacter vinelandii* genome encodes six enzymes with alginate lyase activity [31]: the alginate lyase AlgL [49], the bifunctional mannuronan C-5 epimerase and alginate lyase AlgE7 [50], the three AlyA(1–3) lyases [51], and an exolyase, AlyB, that is still uncharacterized [28].

Some of the nonacetylated M-residues are then epimerized to G-residues by the bifunctional AlgG epimerase, which converts poly(β-D-mannuronate) to α-L-guluronate. In *P. aeruginosa*, AlgG is also part of the periplasmic protein complex that serves as a scaffold for leading the newly formed alginate polymer through the periplasmic space to the outer membrane secretin AlgE porin (AlgJ in *A. vinelandii*) [52]. A scaffold complex helps to transport the recently modified polysaccharide throughout the periplasm towards AlgE before secretion to the extracellular milieu. This

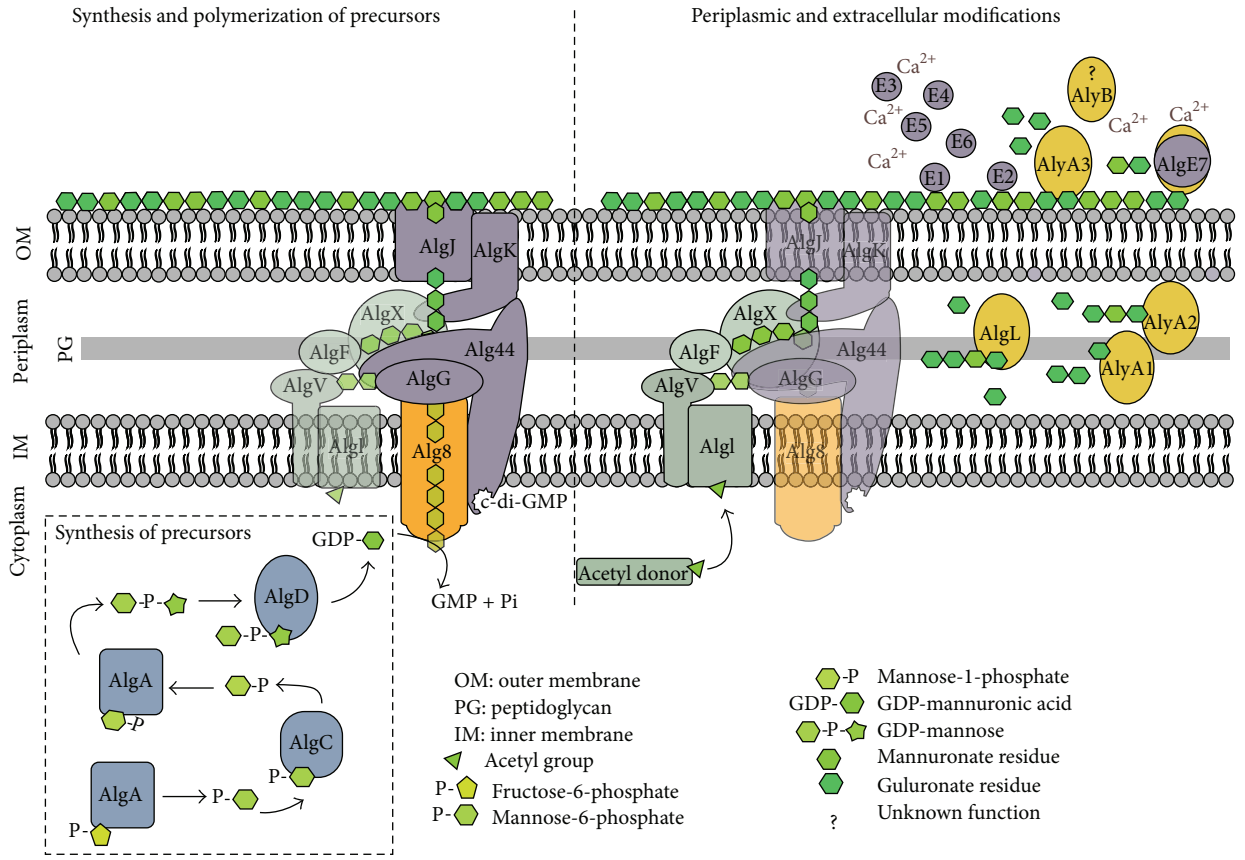

FIGURE 3: Schematic representation of the alginate biosynthetic steps in *Azotobacter vinelandii*, from evidence-based protein-protein interaction in *P. aeruginosa* [28, 42, 43]. The biosynthetic alginate pathway is represented as two complementary stages: on the left, the synthesis of the substrate precursor (GDP-mannuronic acid) and its following polymerization, including transfer from cytoplasm; on the right, the modification (periplasmic and extracellular) of the nascent polymer, as well as the export through the outer membrane of the polymer.

complex is thought to be composed of AlgG, AlgK, and AlgX proteins and possibly AlgL [40, 42, 43, 52]. The exported polysaccharide could be then epimerized by seven extracellular Ca^{2+}-dependent epimerases (AlgE1–7) [53]. Based on these evidences, Figure 3 shows a schematic representation of the alginate biosynthetic steps in *A. vinelandii*.

4. Genetic Regulation of Alginate Biosynthesis in *Azotobacter vinelandii*

In *Azotobacter vinelandii* the alginate biosynthetic gene cluster is arranged as an operon (Figure 4), containing genes coding for enzymes involved in the synthesis of the alginate precursors, as well as those involved in its polymerization, degradation, acetylation, epimerization, and secretion. The availability of the complete genome sequence of *A. vinelandii* [31] also contributes to the better knowledge of this organism.

Several promoters controlling alginate gene cluster transcription have been described: *algDp1* (σ^D promoter), *algDp2* (AlgU σ^E dependent promoter), and *algDp3* promoters, all located upstream of *algD* [54, 55], *alg8p* promoter, upstream of *alg8* [44], and a promoter for sigma 70 located upstream of *algG* [49]. In addition, two putative promoters *algCp1* and *algCp2* are situated upstream of *algC* gene (Figure 4) [56].

The alginate biosynthetic gene cluster expression is controlled by *algUmucABCD* gene cluster, where *algU* encodes the alternative sigma σ^E factor (AlgU), essential for alginate production [57]. Moreover, AlgU is responsible for transcription driven by the *algCp1* and *algDp2* promoters (Figure 5), but it does not control the *algL* or the *algA* genes, as described for *P. aeruginosa* [55].

The MucA and MucC proteins negatively regulate alginate production, acting as anti-σ^E factors [54]. MucA represses AlgU protein activity, thus suppressing *algD* transcription from the *algDp2* promoter. In contrast, *algU* gene transcription is autoregulated by AlgU interaction and activation of its σ^D promoter locus (*algUp2*) (Figure 5) [54].

Additionally, expression of the *algD* promoters is controlled by the global two-component system GacS/GacA, which is conserved among Gram-negative bacteria [58]. The GacS/GacA system controls alginate biosynthesis [58], where GacS controls the expression of *algD* from its three promoters [58]. Accordingly, mutations in *gacS* and *gacA* significantly reduce the *algD* transcript levels [58]. GacA not only is a positive regulator of the biosynthesis of alginate and PHB [58]

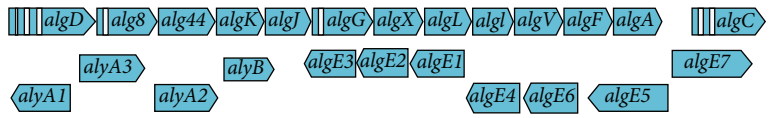

Figure 4: Genetic structure genes involved in alginate biosynthesis and modification in *Azotobacter vinelandii*. Gene operon for alginate biosynthesis *algD-A*, and *algC* gene is transcribed separately; *alyA1–3* and *alyB* alginate lyases encoding genes, and *algE1–7* the epimerases genes.

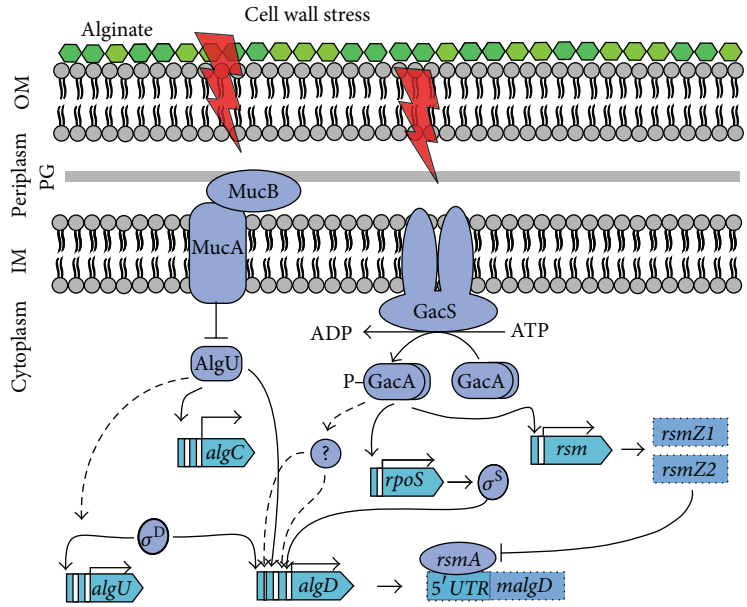

Figure 5: Regulation of alginate biosynthetic genes in *A. vinelandii* (modified according to reference [40]). Promoters are indicated as banners; mRNAs are indicated as dotted boxes; solid lines indicate the reported mechanism of regulation, and dashed lines indicate unknown mechanism of gene regulation; arrows indicate positive regulation and T-shaped bars indicate negative regulation. OM: outer membrane; PG: peptidoglycan; IM: inner membrane. See text for a more detailed description.

but also regulates alginate biosynthesis through activation of the small regulatory RNAs, Rsm (*rsmZ1* and *rsmZ2*). These RNAs interact with the rsmA protein, which binds *algD* mRNA and thus acts as a transcriptional repressor [59]. The *A. vinelandii* genome encodes nine small RNAs belonging to the Rsm posttranscriptional regulatory system (*rsmZ1–7* and *rsmY1-2*) (Figure 5) [59].

Despite the great efforts to understand the alginate biosynthetic gene regulation, little is known about how cultivation conditions could modify gene transcription in *A. vinelandii*.

5. Alginate Production in *Azotobacter vinelandii* Cultures: The Balance of Alg8 and AlgL by Oxygen Availability

The glycosyltransferase Alg8 protein belongs to the glycosyltransferase type II family and is localized in the inner cell membrane [78]. The glycosyltransferase type II enzyme family catalyzes the transfer of glycosyl residues to an acceptor molecule, during biosynthesis of polysaccharides, such as the cellulose or chitin synthase [79].

In both *Azotobacter vinelandii* and *Pseudomonas aeruginosa* the *alg8* gene encodes the Alg8 protein [44]. In *P. aeruginosa* it has been demonstrated that by adding additional copies of *alg8* it is possible to increase alginate production by at least 10 times [80], suggesting that this protein might be involved in a rate-limiting step of alginate production. As a consequence, the possibility of manipulating Alg8 protein levels in *A. vinelandii* may be a valuable approach for increased alginate production, although this has not being done so far. The attempts to reach high Alg8 protein levels were by manipulating the *alg8* gene expression via culture conditions. However, it is important to note that alginate production in *A. vinelandii* is a multienzymatic and complex process.

Moreover, the Alg44 protein acts as link between Alg8 and the AlgJ alginate exporter protein [42, 43]. Since Alg44 has a c-di-GMP intracellular binding domain, it was suggested that this protein presents a regulatory role [81]; although the c-di-GMP levels might not have an impact neither on Alg44 stability nor on its localization, it still seems to be required for the activation of Alg8 [42, 43].

Interestingly, in *A. vinelandii* batch, cultures controlling the dissolved oxygen tension (DOT) at 1% present higher

Table 2: Molecular weight of alginate and relative gene expression of *alg8* and *algL* with respect to the q_{O_2} variations.

Specific oxygen uptake rate (mmol g^{-1} h^{-1})	1–5	5–10
Alginate molecular weight (kDa)	500–1350	480–870
algL gene expression (fold change)	Until 15	0.5–1.5
alg8 gene expression (fold change)	Until 9.0	1.0–2.0

Source: [9, 11–13].

levels of *alg8* and *alg44* gene expression, when compared with control cultures (5% DOT) [9]; the authors suggested that this behavior can in turn enhance the MW of the alginate produced under low DOT conditions. Moreover, in continuous cultures under non-nitrogen-fixation conditions at different agitation rates (300, 500, and 700 rpm) and different sucrose concentration in the feed medium, the highest alginate MW (obtained at 500 rpm) is correlated with the highest *alg8* expression [12], suggesting that *alg8* gene expression can be modulated by not only oxygen availability but also carbon source feed rate, as well. The oxygen availability here is perceived as the amount of oxygen needed for full oxidation of carbon source, taking into account the oxygen transfer rate as well as the DOT level in cultures [82]. Meanwhile, in chemostat cultures under nitrogen-fixation conditions, operated at a dilution rate of 0.07 h^{-1}, expression of both *alg44* and *alg8* was affected by changes in agitation rate (400, 500, and 800 rpm), implying that the activity of both genes could be controlled by oxygen availability [13]. Although the highest alginate MW was obtained at 500 rpm, this was not correlated with higher *alg8* gene expression, which was obtained at 800 rpm. The differences between the two-chemostat culture conditions might be explained by the activation of the nitrogenase protection machinery (non-nitrogen-fixation versus fixation), where the higher alginate MW have directly linked to the *alg8* gene expression under nonfixing conditions. This notion agrees with the fact that nitrogenase activity protects cells from oxygen, thus fostering alginate production [30, 83]. Other possible explanation given is that the culture condition might activate the genes coding for alginate lyases, further discussed in this review. However, more studies are needed, especially those involving gene expression and proteomics profiles during *A. vinelandii* cultures in order to have a better insight of alginate polymerization step.

A possible link among the low specific oxygen uptake rate (q_{O_2}), the MW of the alginate synthesized, and *alg8* gene expression was found [11]. This work suggests that when the q_{O_2} value increases by double, the MW of alginate decreases (about 1.6 times), while *alg8* relative expression decreases around sixfold. Moreover, in cultures carried out in continuous mode operated at dilution rate 0.08 h^{-1}, when the q_{O_2} value was 2.2 mmol g^{-1} h^{-1}, both the alginate MW and *alg8* gene expression levels were higher than those obtained in cultures in which the q_{O_2} value was double [11]. The same correlation between low q_{O_2} value and highest alginate MW was reported [12], where a slight increment of 1 in the q_{O_2} lead to a reduction in the MW of the alginate produced by *A. vinelandii* (from 1200 to 500 kDa). Furthermore, in this condition, the lyase-encoding gene *algL* increased its expression by threefold while *alg8* expression decreased by ninefold. Interestingly, for q_{O_2} values below 2 mmol g^{-1} h^{-1} [12] or exceeding 5 mmol g^{-1} h^{-1} [9, 13], the changes in the alginate MW were not correlated with *alg8* or *algL* gene expression levels. Table 2 summarizes the major changes observed on both the alginate MW and gene expression levels, during the small increment values over the specific oxygen uptake rate of *A. vinelandii* cultures.

Furthermore, the *Azotobacter vinelandii* genome encodes six enzymes with alginate lyase activity [31]: the alginate lyase AlgL [49], the bifunctional mannuronan C-5 epimerase and alginate lyase AlgE7 [50], and the three AlyA(1–3) lyases [51].

The AlyA1, AlyA2, and AlyA3 belong to the PL7 polysaccharide lyase family, containing an alginate lyase module, linked to three calcium-binding modules [28, 51]. AlyA1 and AlyA2 are more likely to be periplasmic (AlyA1, UniProtKB-M9YEJ6; AlyA2, UniProtKB-C1DHI8) whereas the AlyA3 protein has secreted signal C-terminal domain (AlyA3, UniProtKB-C1DQS5), which is needed for efficient germination in *A. vinelandii* [51]. In chemostat cultures, conducted at dilution rate of 0.07 h^{-1} with agitation of 500 rpm, highest alginate MW was reported [13]. In this condition, an increment in the agitation rate (from 400 to 600 rpm) leads to an increment in the lyase-encoding genes *alyA1*, *algL*, and *alyA2* by twofold.

The *algGXLIVFA* operon encodes the AlgL protein responsible for the periplasmic alginate lyase activity in *A. vinelandii*. Disruption of the *algL* gene generated a strain that overproduces alginate, suggesting that this enzyme is important for alginate biosynthesis [84]. Furthermore, the increase in *algL* expression was not correlated with a decrease in alginate MW in chemostat cultures [12]. However, *algL* gene expression pattern could also be affected by the q_{O_2} (manipulated by changes in the agitation rate) in chemostat. Supporting this observation, chemostat cultures also showed an increase in *algL* gene expression (around eightfold) together with higher MW alginate production [11, 12]. By using an *A. vinelandii* mutant strain carrying algL::WGm nonpolar mutation [84] and culturing under 3% of DOT, no alterations were found in alginate lyase activity in culture broth comparing with the wild-type strain. However, alginates with a high MW were obtained [85], suggesting that the lower MW of the alginate correlates with the higher alginate lyase AlgL activity.

In *A. vinelandii* ATCC 9046 strain cultures carried out at 1 and 5% DOT, the expression of higher alginate lyase genes (*algL*, *alyA1*, *alyA2*, *alyA3*, and *algE7*) correlated with the lower DOT and with the higher MW alginate production [9]. In these conditions (1% DOT), the intracellular and extracellular lyase activities were lower, comparing with cultures grown at 5% DOT, suggesting that dissolved oxygen affected the activity of the alginate lyases and/or their gene expression. However, the alginate lyase activity (intracellular and extracellular) seemed to be associated with the exponential phase of the cultures, where, in the ATCC strain cultured, the maximum of alginate lyase activity was found in the prestationary phase and dropping in the stationary phase [9, 85].

As stated previously (Table 2), in cultures with q_{O_2} between 2 mmol g^{-1} h^{-1} and 5 mmol g^{-1} h^{-1} [9, 11–13], the

activity of intracellular lyases, namely, AlgL, presented a basal level which was not correlated with a rise in their gene transcriptional levels [9]. This behavior *per se* may explain the observed rise in alginate MW (Table 2). Even though these observations indicate that dissolved oxygen affects intracellular as well as extracellular alginate lyase activities, it is possible that different alginate lyases could be expressed at different physiological states, as suggested by the study of AlyE3, which is essential for the efficient cyst germination in *A. vinelandii* [51].

It is important to note that although the AlgL is localized in the periplasm, it has an N-terminal secretion signal (AlgL, UniProtKB-O5219), suggesting that AlgL secretion can occur in response to diverse environmental stimuli (i.e., oxygen concentration). This notion is supported by the observation that AlgL extracellular activity is highly dependent on the dissolved oxygen and that the role of alginate lyase is restricted to a postpolymerization step [9, 85]. Similarly, the alginate lyase AlyA3 also presents extracellular activity, whereas AlyA1 and AlyA2 appear to be periplasmic [51]. These data strongly suggest that alginate lyase expression and extracellular activity occur in response to dissolved oxygen concentrations. Therefore, a detailed analysis of dynamic variations in expression levels and in enzymatic activity throughout the culture is warranted to understand more deeply the alginate polymerization process.

In summary, current evidence indicates that when values of q_{O_2} vary between 2 and 5 mmol g^{-1} h^{-1} in cultures of *A. vinelandii*, a rise in expression of *algL* together with a decrease in expression of *alg8* correlates with a decrease in alginate MW (Table 2). As such, this range of q_{O_2} could be a target in the development of strategies to manipulate the characteristics of alginates.

5.1. Oxygen Sensing Mechanisms in Azotobacter vinelandii. Current evidences demonstrate that the oxygen transfer rate, the dissolved oxygen tension levels, and the oxygen uptake rate affect alginate biosynthesis in *A. vinelandii* cultures [8, 9, 12, 13, 36, 40, 86–89]. Despite the importance of the oxygen and the intrinsic relationship with it, no strong evidence of the molecular mechanism involved in sensing it during *A. vinelandii* culturing is available, as well as its further downstream mechanism still being lacking. In this section we discuss that oxygen availability during *A. vinelandii* culturing is a key factor and we suggest a possible mechanism of action.

In *A. vinelandii* the mechanism involved in sensing oxygen availability remains to be fully investigated. In bacteria, several oxygen sensing mechanisms exist. However they can be clustered in two groups based on how the signal is perceived. One category can interact with external environment while, on the other hand, the second category senses physiological changes resulting from variations in the external environment. Nevertheless, both sensing mechanisms operating together control directly the switch between aerobic and anaerobic metabolism [90]. Among the oxygen sensing mechanism, the FNR, ArcA/B, and ubiquinone-8 (Q8) are well characterized in *E. coli* [90].

In *A. vinelandii* the absence of an Fnr-like protein, CydR, overexpressing the β-ketothiolase and acetoacetyl-coA reductase [91], both enzymes catalyze the production of β-hydroxybutyryl-CoA, which is the PHB precursor [40]. It has been demonstrated that low aeration culture conditions in *A. vinelandii* cultures enhanced the metabolic flux from pyruvate towards acetyl-CoA. This had an influence on the increment on the metabolic flux towards PHB production, concomitantly with the higher alginate production [8], suggesting that the aeration conditions could affect the alginate production, by regulating possible gene targets of CydR. Supporting this observation, batch cultures of *A. vinelandii* OP mutant strain carried out at 600 rpm showed lowest q_{O_2} compared with wild-type strain (ATCC 9046) [92]. The *A. vinelandii* OP strain contains an insertion element in the *algU* gene, which in turn represses alginate synthesis [93] and it has been suggested that AlgU is required for *cydR* gene expression [94].

CydR controls the expression of *cydAB* operon that encodes a cytochrome *bd* terminal oxidase, and *cydAB* gene expression correlates with the NADH:ubiquinone oxidoreductase activity (NDHII) [91]. In *A. vinelandii*, the Na^+-translocating NADH:ubiquinone oxidoreductases (Na^+-NQR) are encoded in the *nqr* operon, and it had been linked to regulating negatively alginate production [95]. Additionally, *A. vinelandii* genome contains genes linked to NADH:ubiquinone oxidoreductases (NDH), the NDH-II type, and 13 genes encoding subunits of NDH-I type [95]. The NADH oxidation in *A. vinelandii* is mediated by two NADH:ubiquinone oxidoreductases [96], and the fast NADH oxidation is linked to a fast quinone reduction. The *ubiC-A* operon in *A. vinelandii* is responsible for the transcription of the genes necessaries for Q8 biosynthesis [95]. A mutation in the intragenic region *ubiA* correlates with lower Q8 protein levels, accompanied with an improvement in the alginate production, but all the more, with a higher expression of biosynthetic alginate genes, *algD*, *algC,* and *algA*. Moreover, the Q8 protein seems to be responsible for at least 8% of the respiratory capacity in *A. vinelandii*, during low and high aeration cultures [95].

Interestingly, in other bacteria as *E. coli*, the role of quinones as a redox signal for the pathways involved in sensing oxygen and regulation of expression of genes involved in oxidative and fermentative catabolism is well known, specifically the ArcB/A two-component system [97–99].

Figure 6 summarizes the plausible regulation of *alg* genes in *A. vinelandii*, via a signaling cascade activated by oxygen availability. On one hand, the Na^+NQR protein regulates negatively *algD* and *algC* gene targets, while the ArcB/A two-component system regulates *algD* and *alg8* gene expression under oxygen availability. When oxygen is limiting, the sensor kinase ArcB autophosphorylates and then transphosphorylates the regulator ArcA, which activates *algD*, *alg8,* and *alg44* gene expression. The autophosphorylation of ArcB is inhibited at higher oxygen concentrations, by the accumulation of Q8 (oxidized form). In this sense, in *A. vinelandii,* a tight control of *alg* genes via a signaling cascade activated by oxygen availability may exist (Figure 6).

Although recently Flores et al., 2015 [36], discussed mainly the influence of the oxygen on production of alginate during *A. vinelandii* cultures, not much attention is paid

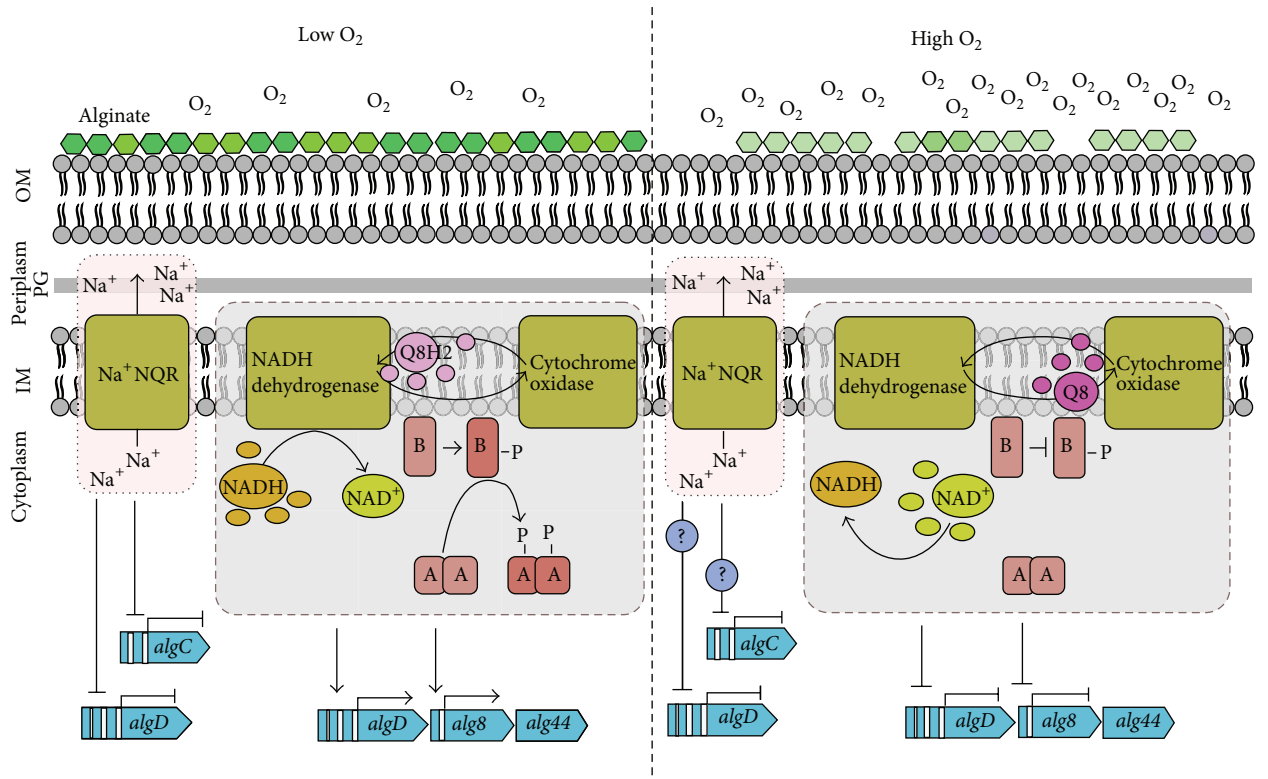

Figure 6: Schematic representation of the possible gene regulation mechanism by oxygen in *Azotobacter vinelandii*. Oxygen availability is depicted in the figure as low O_2 (left side) and high O_2 (right side). Light red dotted boxes indicate the Na^+-translocating NADH:ubiquinone oxidoreductase (Na^+NQR) that regulates negatively *algD* and *algC* gene targets, although the exact mechanism of *algD* and *algC* gene regulation at high O_2 by Na^+NQR is still unknown. Gray slashed boxes represent the ArcB/A two-component redox sensor: under high oxygen availability, the autophosphorylation of ArcB (B blocks) is inhibited by oxidized quinones (Q8). ArcA (A blocks) in the nonphosphorylated state is unable to bind specifically to *algD*, *alg8*, and *alg44* gene targets. Low oxygen causes a decrease in the level of oxidized quinones (Q8H2), allowing the autophosphorylation of ArcA. ArcA-P binds specifically to its target sites and coordinates the cellular response to oxygen availability. Arrows indicate positive regulation and T-shaped bars indicate negative regulation. Flag-type boxes indicate genes described in the figure. Question mark indicates unknown gene regulation mechanism. OM: outer membrane; PG: peptidoglycan; IM: inner membrane.

to which molecular pathways are involved during alginate biosynthesis. In our work, we propose a possible mechanism of action of the oxygen availability during *A. vinelandii* culturing, offering a new path to look at and in this way contributing to the better knowledge of controlling bacterial alginates production.

Despite the enormous efforts in understanding the microbial alginate biosynthesis under defined culture conditions, there is still a way to go. The decoding of the *A. vinelandii* genome has open the possibility to getting access to new information; however no wide genetic screen studies during alginate production have been reported yet. So, it will be necessarily an improvement in the knowledge of *A. vinelandii* alginate biosynthesis gene regulation in alginate production processes, in order to generate a tailored and affordable alginate product.

6. Conclusion

In the present review we discuss that oxygen availability during *Azotobacter vinelandii* cultures might exert a tight control over the expression of alginate-related genes, which will impact the quality of the polysaccharide or will regulate enzymatic activities that modified the nascent alginate chain. Current evidence indicates a prevailing equilibrium in *alg8* and *algL* gene expression, which is being regulated by oxygen availability. This equilibrium will further impact the alginate molecular weight. Accordingly, more information regarding oxygen sensing, transportation, and signaling pathways during specific culture conditions of *A. vinelandii* will be needed in order to obtain alginates with specific characteristics.

Conflict of Interests

The authors declare that there is no conflict of interests regarding the publication of this paper.

Acknowledgments

This work was supported by a Grant from CONICYT-Chile (Project PCCI40039) and DI-PUCV 037-98. The authors

acknowledge Dr. Nuno Rodrigues Dos Santos for his critical comments on the paper.

References

[1] B. H. A. Rehm, "Bacterial polymers: biosynthesis, modifications and applications," *Nature Reviews Microbiology*, vol. 8, no. 8, pp. 578–592, 2010.

[2] S. Bengtsson, A. R. Pisco, M. A. M. Reis, and P. C. Lemos, "Production of polyhydroxyalkanoates from fermented sugar cane molasses by a mixed culture enriched in glycogen accumulating organisms," *Journal of Biotechnology*, vol. 145, no. 3, pp. 253–263, 2010.

[3] F. Clementi, "Alginate production by *Azotobacter vinelandii*," *Critical Reviews in Biotechnology*, vol. 17, no. 4, pp. 327–361, 1997.

[4] D. E. Pszczola, "Discovering treasures of the deep," *Food Technology*, vol. 52, no. 4, pp. 74–80, 1998.

[5] I. W. Sutherland, *Biotechnology of Microbial Exopolysaccharydes*, Cambridge University Press, Cambridge, UK, 1990.

[6] U. Remminghorst and B. H. A. Rehm, "Bacterial alginates: from biosynthesis to applications," *Biotechnology Letters*, vol. 28, no. 21, pp. 1701–1712, 2006.

[7] J. L. Geddie and I. W. Sutherland, "The effect of acetylation on cation binding by algal and bacterial alginates," *Biotechnology and Applied Biochemistry*, vol. 20, no. 1, pp. 117–129, 1994.

[8] T. Castillo, E. Heinzle, S. Peifer, K. Schneider, and C. F. Peña M, "Oxygen supply strongly influences metabolic fluxes, the production of poly(3-hydroxybutyrate) and alginate, and the degree of acetylation of alginate in *Azotobacter vinelandii*," *Process Biochemistry*, vol. 48, no. 7, pp. 995–1003, 2013.

[9] C. Flores, S. Moreno, G. Espín, C. Peña, and E. Galindo, "Expression of alginases and alginate polymerase genes in response to oxygen, and their relationship with the alginate molecular weight in *Azotobacter vinelandii*," *Enzyme and Microbial Technology*, vol. 53, no. 2, pp. 85–91, 2013.

[10] Ç. Kıvılcımdan Moral, Ö. Doğan, and F. D. Sanin, "Effect of oxygen tension and medium components on monomer distribution of alginate," *Applied Biochemistry and Biotechnology*, vol. 176, no. 3, pp. 875–891, 2015.

[11] A. Díaz-Barrera, A. Aguirre, J. Berrios, and F. Acevedo, "Continuous cultures for alginate production by *Azotobacter vinelandii* growing at different oxygen uptake rates," *Process Biochemistry*, vol. 46, no. 9, pp. 1879–1883, 2011.

[12] A. Díaz-Barrera, E. Soto, and C. Altamirano, "Alginate production and *alg*8 gene expression by *Azotobacter vinelandii* in continuous cultures," *Journal of Industrial Microbiology and Biotechnology*, vol. 39, no. 4, pp. 613–621, 2012.

[13] A. Díaz-Barrera, F. Martínez, F. Guevara Pezoa, F. Acevedo, and B. Lin, "Evaluation of gene expression and alginate production in response to oxygen transfer in continuous culture of *Azotobacter vinelandii*," *PLoS ONE*, vol. 9, no. 8, Article ID e105993, 2014.

[14] N. Rhein-Knudsen, M. T. Ale, and A. S. Meyer, "Seaweed hydrocolloid production: an update on enzyme assisted extraction and modification technologies," *Marine Drugs*, vol. 13, no. 6, pp. 3340–3359, 2015.

[15] W. Sabra, A.-P. Zeng, and W.-D. Deckwer, "Bacterial alginate: physiology, product quality and process aspects," *Applied Microbiology and Biotechnology*, vol. 56, no. 3-4, pp. 315–325, 2001.

[16] B. H. A. Rehm and S. Valla, "Bacterial alginates: biosynthesis and applications," *Applied Microbiology and Biotechnology*, vol. 48, no. 3, pp. 281–288, 1997.

[17] P. Gacesa, "Bacterial alginate biosynthesis—recent progress and future prospects," *Microbiology*, vol. 144, no. 5, pp. 1133–1143, 1998.

[18] D. Hoefer, J. K. Schnepf, T. R. Hammer, M. Fischer, and C. Marquardt, "Biotechnologically produced microbial alginate dressings show enhanced gel forming capacity compared to commercial alginate dressings of marine origin," *Journal of Materials Science: Materials in Medicine*, vol. 26, no. 4, article 162, 2015.

[19] E. Ruvinov and S. Cohen, "Alginate biomaterial for the treatment of myocardial infarction: progress, translational strategies, and clinical outlook," *Advanced Drug Delivery Reviews*, vol. 96, pp. 54–76, 2016.

[20] J. Venkatesan, I. Bhatnagar, P. Manivasagan, K.-H. Kang, and S.-K. Kim, "Alginate composites for bone tissue engineering: a review," *International Journal of Biological Macromolecules*, vol. 72, pp. 269–281, 2015.

[21] I. A. Brownlee, A. Allen, J. P. Pearson et al., "Alginate as a source of dietary fiber," *Critical Reviews in Food Science and Nutrition*, vol. 45, no. 6, pp. 497–510, 2005.

[22] M. G. Jensen, M. Kristensen, and A. Astrup, "Effect of alginate supplementation on weight loss in obese subjects completing a 12-wk energy-restricted diet: a randomized controlled trial," *The American Journal of Clinical Nutrition*, vol. 96, no. 1, pp. 5–13, 2012.

[23] P. W. Dettmar, V. Strugala, and J. Craig Richardson, "The key role alginates play in health," *Food Hydrocolloids*, vol. 25, no. 2, pp. 263–266, 2011.

[24] M. Liu, L. Dai, H. Shi, S. Xiong, and C. Zhou, "*In vitro* evaluation of alginate/halloysite nanotube composite scaffolds for tissue engineering," *Materials Science and Engineering: C*, vol. 49, pp. 700–712, 2015.

[25] N. V. Konda, S. Singh, B. A. Simmons, and D. Klein-Marcuschamer, "An investigation on the economic feasibility of macroalgae as a potential feedstock for biorefineries," *BioEnergy Research*, vol. 8, no. 3, pp. 1046–1056, 2015.

[26] I. W. Davidson, I. W. Sutherland, and C. J. Lawson, "Localization of *O*-acetyl groups of bacterial alginate," *Journal of General Microbiology*, vol. 98, no. 2, pp. 603–606, 1977.

[27] G. Skjåk-Bræk, S. Paoletti, and T. Gianferrara, "Selective acetylation of mannuronic acid residues in calcium alginate gels," *Carbohydrate Research*, vol. 185, no. 1, pp. 119–129, 1989.

[28] H. Ertesvåg, "Alginate-modifying enzymes: biological roles and biotechnological uses," *Frontiers in Microbiology*, vol. 6, no. 523, 2015.

[29] H. Ertesvåg, S. Valla, and G. Skjåk-Bræk, "Enzymatic alginate modification," in *Alginates: Biology and Applications*, B. H. A. Rehm, Ed., Microbiology Monographs, pp. 95–115, Springer, Berlin, Germany, 2009.

[30] W. Sabra, A.-P. Zeng, H. Lunsdorf, and W.-D. Deckwer, "Effect of oxygen on formation and structure of *Azotobacter vinelandii* alginate and its role in protecting nitrogenase," *Applied and Environmental Microbiology*, vol. 66, no. 9, pp. 4037–4044, 2000.

[31] J. C. Setubal, P. dos Santos, B. S. Goldman et al., "Genome sequence of *Azotobacter vinelandii*, an obligate aerobe specialized to support diverse anaerobic metabolic processes," *Journal of Bacteriology*, vol. 191, no. 14, pp. 4534–4545, 2009.

[32] E. Post, D. Kleiner, and J. Oelze, "Whole cell respiration and nitrogenase activities in *Azotobacter vinelandii* growing in oxygen controlled continuous culture," *Archives of Microbiology*, vol. 134, no. 1, pp. 68–72, 1983.

[33] H. L. Sadoff, "Encystment and germination in *Azotobacter vinelandii*," *Bacteriological Reviews*, vol. 39, no. 4, pp. 516–539, 1975.

[34] D. Segura, C. Núñez, and G. Espín, "Azotobacter cysts," in *Encyclopedia of Life Sciences*, John Wiley & Sons, New York, NY, USA, 2001.

[35] A. Díaz-Barrera and E. Soto, "Biotechnological uses of *Azotobacter vinelandii*: current state, limits and prospects," *African Journal of Biotechnology*, vol. 9, no. 33, pp. 5240–5250, 2010.

[36] C. Flores, A. Díaz-Barrera, F. Martínez, E. Galindo, and C. Peña, "Role of oxygen in the polymerization and de-polymerization of alginate produced by *Azotobacter vinelandii*," *Journal of Chemical Technology and Biotechnology*, vol. 90, no. 3, pp. 356–365, 2015.

[37] J. Schmid, V. Sieber, and B. Rehm, "Bacterial exopolysaccharides: biosynthesis pathways and engineering strategies," *Frontiers in Microbiology*, vol. 6, 2015.

[38] J. C. Whitney and P. L. Howell, "Synthase-dependent exopolysaccharide secretion in Gram-negative bacteria," *Trends in Microbiology*, vol. 21, no. 2, pp. 63–72, 2013.

[39] I. D. Hay, Z. U. Rehman, A. Ghafoor, and B. H. A. Rehm, "Bacterial biosynthesis of alginates," *Journal of Chemical Technology and Biotechnology*, vol. 85, no. 6, pp. 752–759, 2010.

[40] E. Galindo, C. Peña, C. Núñez, D. Segura, and G. Espín, "Molecular and bioengineering strategies to improve alginate and polydydroxyalkanoate production by *Azotobacter vinelandii*," *Microbial Cell Factories*, vol. 6, article 7, 2007.

[41] P. J. Tatnell, N. J. Russell, and P. Gacesa, "GDP-mannose dehydrogenase is the key regulatory enzyme in alginate biosynthesis in *Pseudomonas aeruginosa*: evidence from metabolite studies," *Microbiology*, vol. 140, no. 7, pp. 1745–1754, 1994.

[42] Z. U. Rehman, Y. Wang, M. F. Moradali, I. D. Hay, and B. H. A. Rehm, "Insights into the assembly of the alginate biosynthesis machinery in *Pseudomonas aeruginosa*," *Applied and Environmental Microbiology*, vol. 79, no. 10, pp. 3264–3272, 2013.

[43] M. Fata Moradali, I. Donati, I. M. Sims, S. Ghods, and B. H. Rehm, "Alginate polymerization and modification are linked in *Pseudomonas aeruginosa*," *mBio*, vol. 6, no. 3, Article ID e00453-15, 2015.

[44] H. Mejía-Ruíz, J. Guzmán, S. Moreno, G. Soberón-Chávez, and G. Espín, "The *Azotobacter vinelandii* alg8 and *alg44* genes are essential for alginate synthesis and can be transcribed from an *algD*-independent promoter," *Gene*, vol. 199, no. 1-2, pp. 271–277, 1997.

[45] H. Mejía-Ruíz, S. Moreno, J. Guzmán et al., "Isolation and characterization of an *Azotobacter vinelandii algK* mutant," *FEMS Microbiology Letters*, vol. 156, no. 1, pp. 101–106, 1997.

[46] L. M. Riley, J. T. Weadge, P. Baker et al., "Structural and functional characterization of *Pseudomonas aeruginosa* AlgX: role of Algx in alginate acetylation," *Journal of Biological Chemistry*, vol. 288, no. 31, pp. 22299–22314, 2013.

[47] M. J. Franklin and D. E. Ohman, "Mutant analysis and cellular localization of the AlgI, AlgJ, and AlgF proteins required for *O* acetylation of alginate in *Pseudomonas aeruginosa*," *Journal of Bacteriology*, vol. 184, no. 11, pp. 3000–3007, 2002.

[48] P. Baker, T. Ricer, P. J. Moynihan et al., "*P. aeruginosa* SGNH hydrolase-like proteins AlgJ and AlgX have similar topology but separate and distinct roles in alginate acetylation," *PLoS Pathogens*, vol. 10, no. 8, Article ID e1004334, 2014.

[49] A. Vazquez, S. Moreno, J. Guzmán, A. Alvarado, and G. Espín, "Transcriptional organization of the *Azotobacter vinelandii algGXLVIFA* genes: characterization of *algF* mutants," *Gene*, vol. 232, no. 2, pp. 217–222, 1999.

[50] B. I. G. Svanem, W. I. Strand, H. Ertesvåg et al., "The catalytic activities of the bifunctional *Azotobacter vinelandii* mannuronan C-5-epimerase and alginate lyase AlgE7 probably originate from the same active site in the enzyme," *Journal of Biological Chemistry*, vol. 276, no. 34, pp. 31542–31550, 2001.

[51] M. Gimmestad, H. Ertesvåg, T. M. B. Heggeset, O. Aarstad, B. I. G. Svanem, and S. Valla, "Characterization of three new *Azotobacter vinelandii* alginate lyases, one of which is involved in cyst germination," *Journal of Bacteriology*, vol. 191, no. 15, pp. 4845–4853, 2009.

[52] S. Jain and D. E. Ohman, "Role of an alginate lyase for alginate transport in mucoid *Pseudomonas aeruginosa*," *Infection and Immunity*, vol. 73, no. 10, pp. 6429–6436, 2005.

[53] H. Ertesvåg, H. K. Høidal, I. K. Hals, A. Rian, B. Doseth, and S. Valla, "A family of modular type mannuronan C-5-epimerase genes controls alginate structure in *Azotobacter vinelandii*," *Molecular Microbiology*, vol. 16, no. 4, pp. 719–731, 1995.

[54] C. Núñez, R. León, J. Guzmán, G. Espín, and G. Soberón-Chávez, "Role of *Azotobacter vinelandii mucA* and *mucC* gene products in alginate production," *Journal of Bacteriology*, vol. 182, no. 23, pp. 6550–6556, 2000.

[55] L. Lloret, R. Barreto, R. Léon et al., "Genetic analysis of the transcriptional arrangement of *Azotobacter vinelandii* alginate biosynthetic genes: identification of two independent promoters," *Molecular Microbiology*, vol. 21, no. 3, pp. 449–457, 1996.

[56] G. Gaona, C. Núñez, J. B. Goldberg et al., "Characterization of the *Azotobacter vinelandii algC* gene involved in alginate and lipopolysaccharide production," *FEMS Microbiology Letters*, vol. 238, no. 1, pp. 199–206, 2004.

[57] S. Moreno, R. Nájera, J. Guzmán, G. Soberón-Chávez, and G. Espín, "Role of alternative σ factor AlgU in encystment of *Azotobacter vinelandii*," *Journal of Bacteriology*, vol. 180, no. 10, pp. 2766–2769, 1998.

[58] M. Castañeda, J. Sánchez, S. Moreno, C. Núñez, and G. Espín, "The global regulators GacA and σ^S form part of a cascade that controls alginate production in *Azotobacter vinelandii*," *Journal of Bacteriology*, vol. 183, no. 23, pp. 6787–6793, 2001.

[59] J. Manzo, M. Cocotl-Yañez, T. Tzontecomani et al., "Post-transcriptional regulation of the alginate biosynthetic gene *algD* by the Gac/Rsm system in *Azotobacter vinelandii*," *Journal of Molecular Microbiology and Biotechnology*, vol. 21, no. 3-4, pp. 147–159, 2012.

[60] M. A. Azevedo, A. I. Bourbon, A. A. Vicente, and M. A. Cerqueira, "Alginate/chitosan nanoparticles for encapsulation and controlled release of vitamin B_2," *International Journal of Biological Macromolecules*, vol. 71, pp. 141–146, 2014.

[61] X. Zhao, B. Li, C. Xue, and L. Sun, "Effect of molecular weight on the antioxidant property of low molecular weight alginate from *Laminaria japonica*," *Journal of Applied Phycology*, vol. 24, no. 2, pp. 295–300, 2012.

[62] C. A. Bonino, M. D. Krebs, C. D. Saquing et al., "Electrospinning alginate-based nanofibers: from blends to crosslinked low molecular weight alginate-only systems," *Carbohydrate Polymers*, vol. 85, no. 1, pp. 111–119, 2011.

[63] K. Fujiki, H. Matsuyama, and T. Yano, "Protective effect of sodium alginates against bacterial infection in common carp, *Cyprinus carpio* L.," *Journal of Fish Diseases*, vol. 17, no. 4, pp. 349–355, 1994.

[64] T. Kuda, H. Goto, M. Yokoyama, and T. Fujii, "Effects of dietary concentration of laminaran and depolymerised alginate on rat cecal microflora and plasma lipids," *Fisheries Science*, vol. 64, no. 4, pp. 589–593, 1998.

[65] T. Kuda, T. Yano, N. Matsuda, and M. Nishizawa, "Inhibitory effects of laminaran and low molecular alginate against the putrefactive compounds produced by intestinal microflora *in vitro* and in rats," *Food Chemistry*, vol. 91, no. 4, pp. 745–749, 2005.

[66] I. Pajic-Lijakovic, S. Levic, M. Hadnađev et al., "Structural changes of Ca-alginate beads caused by immobilized yeast cell growth," *Biochemical Engineering Journal*, vol. 103, pp. 32–38, 2015.

[67] F. E. Vasile, A. M. Romero, M. A. Judis, and M. F. Mazzobre, "*Prosopis alba* exudate gum as excipient for improving fish oil stability in alginate—chitosan beads," *Food Chemistry*, vol. 190, pp. 1093–1101, 2016.

[68] F. Mancini, L. Montanari, D. Peressini, and P. Fantozzi, "Influence of alginate concentration and molecular weight on functional properties of mayonnaise," *LWT—Food Science and Technology*, vol. 35, no. 6, pp. 517–525, 2002.

[69] O. Aizpurua-Olaizola, P. Navarro, A. Vallejo, M. Olivares, N. Etxebarria, and A. Usobiaga, "Microencapsulation and storage stability of polyphenols from *Vitis vinifera* grape wastes," *Food Chemistry*, vol. 190, pp. 614–621, 2016.

[70] W. Cheng, C.-H. Liu, C.-M. Kuo, and J.-C. Chen, "Dietary administration of sodium alginate enhances the immune ability of white shrimp *Litopenaeus vannamei* and its resistance against *Vibrio alginolyticus*," *Fish and Shellfish Immunology*, vol. 18, no. 1, pp. 1–12, 2005.

[71] M. D. Wilcox, I. A. Brownlee, J. C. Richardson, P. W. Dettmar, and J. P. Pearson, "The modulation of pancreatic lipase activity by alginates," *Food Chemistry*, vol. 146, pp. 479–484, 2014.

[72] B. An, H. Lee, S. Lee, S. Lee, and J. Choi, "Determining the selectivity of divalent metal cations for the carboxyl group of alginate hydrogel beads during competitive sorption," *Journal of Hazardous Materials*, vol. 298, pp. 11–18, 2015.

[73] W. Cheng, R.-T. Tsai, and C.-C. Chang, "Dietary sodium alginate administration enhances Mx gene expression of the tiger grouper, *Epinephelus fuscoguttatus* receiving poly I:C," *Aquaculture*, vol. 324-325, pp. 201–208, 2012.

[74] S.-T. Chiu, R.-T. Tsai, J.-P. Hsu, C.-H. Liu, and W. Cheng, "Dietary sodium alginate administration to enhance the non-specific immune responses, and disease resistance of the juvenile grouper *Epinephelus fuscoguttatus*," *Aquaculture*, vol. 277, no. 1-2, pp. 66–72, 2008.

[75] C.-H. Liu, S.-P. Yeh, C.-M. Kuo, W. Cheng, and C.-H. Chou, "The effect of sodium alginate on the immune response of tiger shrimp via dietary administration: activity and gene transcription," *Fish and Shellfish Immunology*, vol. 21, no. 4, pp. 442–452, 2006.

[76] K. Fujiki and T. Yano, "Effects of sodium alginate on the non-specific defence system of the common carp (*Cyprinus carpio* L.)," *Fish and Shellfish Immunology*, vol. 7, no. 6, pp. 417–427, 1997.

[77] H. Tomida, T. Yasufuku, T. Fujii, Y. Kondo, T. Kai, and M. Anraku, "Polysaccharides as potential antioxidative compounds for extended-release matrix tablets," *Carbohydrate Research*, vol. 345, no. 1, pp. 82–86, 2010.

[78] L. L. Oglesby, S. Jain, and D. E. Ohman, "Membrane topology and roles of *Pseudomonas aeruginosa* Alg8 and Alg44 in alginate polymerization," *Microbiology*, vol. 154, no. 6, pp. 1605–1615, 2008.

[79] I. M. Saxena, R. M. Jr. Brown, M. Fevre, R. A. Geremia, and B. Henrissat, "Multidomain architecture of β-glycosil tranferases: implications for mechanism of action," *Journal of Bacteriology*, vol. 177, no. 6, pp. 1419–1419, 1995.

[80] U. Remminghorst and B. H. A. Rehm, "*In vitro* alginate polymerization and the functional role of Alg8 in alginate production by *Pseudomonas aeruginosa*," *Applied and Environmental Microbiology*, vol. 72, no. 1, pp. 298–305, 2006.

[81] M. Merighi, V. T. Lee, M. Hyodo, Y. Hayakawa, and S. Lory, "The second messenger bis-(3′-5′)-cyclic-GMP and its PilZ domain-containing receptor Alg44 are required for alginate biosynthesis in *Pseudomonas aeruginosa*," *Molecular Microbiology*, vol. 65, no. 4, pp. 876–895, 2007.

[82] S. Alexeeva, K. J. Hellingwerf, and M. J. Teixeira de Mattos, "Quantitative assessment of oxygen availability: perceived aerobiosis and its effect on flux distribution in the respiratory chain of *Escherichia coli*," *Journal of Bacteriology*, vol. 184, no. 5, pp. 1402–1406, 2002.

[83] J. Oelze, "Respiratory protection of nitrogenase in Azotobacter species: Is a widely held hypothesis unequivocally supported by experimental evidence?" *FEMS Microbiology Reviews*, vol. 24, no. 4, pp. 321–333, 2000.

[84] M. A. Trujillo-Roldán, S. Moreno, D. Segura, E. Galindo, and G. Espín, "Alginate production by an *Azotobacter vinelandii* mutant unable to produce alginate lyase," *Applied Microbiology and Biotechnology*, vol. 60, no. 6, pp. 733–737, 2003.

[85] M. A. Trujillo-Roldán, S. Moreno, G. Espín, and E. Galindo, "The roles of oxygen and alginate-lyase in determining the molecular weight of alginate produced by *Azotobacter vinelandii*," *Applied Microbiology and Biotechnology*, vol. 63, no. 6, pp. 742–747, 2004.

[86] A. Díaz-Barrera, C. Peña, and E. Galindo, "The oxygen transfer rate influences the molecular mass of the alginate produced by *Azotobacter vinelandii*," *Applied Microbiology and Biotechnology*, vol. 76, no. 4, pp. 903–910, 2007.

[87] A. Díaz-Barrera, P. Silva, R. Ávalos, and F. Acevedo, "Alginate molecular mass produced by *Azotobacter vinelandii* in response to changes of the O_2 transfer rate in chemostat cultures," *Biotechnology Letters*, vol. 31, no. 6, pp. 825–829, 2009.

[88] E. Lozano, E. Galindo, and C. F. Peña, "Oxygen transfer rate during the production of alginate by *Azotobacter vinelandii* under oxygen-limited and non oxygen-limited conditions," *Microbial Cell Factories*, vol. 10, article 13, 2011.

[89] C. Peña, M. A. Trujillo-Roldán, and E. Galindo, "Influence of dissolved oxygen tension and agitation speed on alginate production and its molecular weight in cultures of *Azotobacter vinelandii*," *Enzyme and Microbial Technology*, vol. 27, no. 6, pp. 390–398, 2000.

[90] J. Green and M. S. Paget, "Bacterial redox sensors," *Nature Reviews Microbiology*, vol. 2, no. 12, pp. 954–966, 2004.

[91] G. Wu, A. J. G. Moir, G. Sawers, S. Hill, and R. K. Poole, "Biosynthesis of poly-β-hydroxybutyrate (PHB) is controlled by CydR (Fnr) in the obligate aerobe *Azotobacter vinelandii*," *FEMS Microbiology Letters*, vol. 194, no. 2, pp. 215–220, 2001.

[92] A. Díaz-Barrera, R. Andler, I. Martínez, and C. Peña, "Poly-3-hydroxybutyrate production by *Azotobacter vinelandii* strains in batch cultures at different oxygen transfer rates," *Journal of Chemical Technology & Biotechnology*, 2015.

[93] J. M. Martínez-Salazar, S. Moreno, R. Nájera et al., "Characterization of the genes coding for the putative sigma factor *AlgU* and its regulators MucA, MucB, MucC, and MucD in *Azotobacter vinelandii* and evaluation of their roles in alginate biosynthesis," *Journal of Bacteriology*, vol. 178, no. 7, pp. 1800–1808, 1996.

[94] R. León and G. Espín, "*flhDC*, but not fleQ, regulates flagella biogenesis in *Azotobacter vinelandii*, and is under AlgU and CydR negative control," *Microbiology*, vol. 154, no. 6, pp. 1719–1728, 2008.

[95] C. Núñez, A. V. Bogachev, G. Guzmán, I. Tello, J. Guzmán, and G. Espín, "The Na^+-translocating NADH: ubiquinone oxidoreductase of *Azotobacter vinelandii* negatively regulates alginate synthesis," *Microbiology*, vol. 155, no. 1, pp. 249–256, 2009.

[96] Y. V. Bertsova, A. V. Bogachev, and V. P. Skulachev, "Noncoupled NADH: ubiquinone oxidoreductase of *Azotobacter vinelandii* is required for diazotrophic growth at high oxygen concentrations," *Journal of Bacteriology*, vol. 183, no. 23, pp. 6869–6874, 2001.

[97] M. Bekker, S. Alexeeva, W. Laan, G. Sawers, J. T. De Mattos, and K. Hellingwerf, "The ArcBA two-component system of *Escherichia coli* is regulated by the redox state of both the ubiquinone and the menaquinone pool," *Journal of Bacteriology*, vol. 192, no. 3, pp. 746–754, 2010.

[98] D. Georgellis, O. Kwon, and E. C. C. Lin, "Quinones as the redox signal for the Arc two-component system of bacteria," *Science*, vol. 292, no. 5525, pp. 2314–2316, 2001.

[99] R. Malpica, G. R. Peña Sandoval, C. Rodríguez, B. Franco, and D. Georgellis, "Signaling by the Arc two-component system provides a link between the redox state of the quinone pool and gene expression," *Antioxidants and Redox Signaling*, vol. 8, no. 5-6, pp. 781–795, 2006.

Hindawi Publishing Corporation
International Journal of Polymer Science
Volume 2016, Article ID 3230109, 8 pages
http://dx.doi.org/10.1155/2016/3230109

Research Article

Thermal, Morphological, and Biodegradability Properties of Bioplastic Fertilizer Composites Made of Oil Palm Biomass, Fertilizer, and Poly(hydroxybutyrate-co-valerate)

A. S. Harmaen,[1] A. Khalina,[2] H. Mohd Ali,[3] and I. Nor Azowa[4]

[1]*Institute of Tropical Forestry and Forest Products, Universiti Putra Malaysia (UPM), 43400 Serdang, Selangor, Malaysia*
[2]*Faculty of Engineering, Universiti Putra Malaysia (UPM), 43400 Serdang, Selangor, Malaysia*
[3]*Faculty of Biotechnology and Biomolecular Sciences, Universiti Putra Malaysia (UPM), 43400 Serdang, Selangor, Malaysia*
[4]*Faculty of Science, Universiti Putra Malaysia (UPM), 43400 Serdang, Selangor, Malaysia*

Correspondence should be addressed to A. S. Harmaen; harmaen@upm.edu.my

Received 5 August 2015; Revised 20 December 2015; Accepted 21 January 2016

Academic Editor: Shiv Shankar

Slow-release bioplastic fertilizer (BpF) composites were developed by processing oil palm empty fruit bunch (EFB), fertilizer, and poly(hydroxybutyrate-co-valerate) (PHBv) using extrusion techniques with controlled formulation and temperature. The temperature was kept at 150°C for 3 to 5 min during processing using twin-screw extruder. The PHBv lost weight gradually with the increasing temperature and its thermal degradation occurred initially at 263.4°C and reached the maximum at 300.7°C. Scanning electron microscope (SEM) images showed that the bonding of all composites created small gaps between matrices polymer and fiber because the hydrophilic characteristic of EFB fibers weakened the interfacial bonding. PHBv/EFB/NPKC2 showed faster biodegradation over PHBv/NPKC1 and PHBv/NPKC2, which was 99.35% compared to 68.66% and 90.28%, respectively.

1. Introduction

Poly(3-hydroxybutyrate-*co*-3-hydroxyvalerate) commercially known as Biopol™ is a derivative of poly(3-hydroxybutyrate) (PHB). PHB has been widely studied as biomedical and biodegradable materials. One of the main hurdles in its commercial applications is the postprocessing embrittlement [1]. Some researchers claimed that the embrittlement is not related to its physical aging but actually caused by secondary crystallization during storage [2–4] where a low temperature melting peak of 75°C appears.

The use of bioplastic fertilizers (BpF) in agriculture and horticultural industry has been going on for decades. It is considered as an advanced approach within the slow-release fertilizers (SRF), which play an important role in efficiently delivering the nutrients for plant uptake while controlling the longevity of the product. Most of the SRF used in agriculture industry utilize this type of SRF [5]. Compared to traditional water-soluble fertilizers used in fertigation, BpF may only require a single application to supply enough nutrients for the plants for an extended period, hence the lower labour costs needed to apply fertilizers. Furthermore, BpF is also often applied together within the media to grow the seedlings.

Uncontrolled or excessive use of fertilizers leads to huge economic losses of resources, apart from being the main cause of environmental pollution [6, 7]. Therefore, using SRF can help solve these issues [8–10]. SRF has the ability to release nutrients at a predetermined time and rate to suit the plant uptake at different growth stages [11]. The rate and time of nutrient release are optimized by manipulating the physical and/or chemical characteristics of the fertilizer, involving mechanisms such as diffusion, degradation, and hydrolysis [12]. The rate of nutrient dissolution is also coordinated according to the plant requirements. SRF has many advantages against conventional fertilizers. One of them is the ability to allow gradual release of nutrients, which increases the efficiency of nutrient uptake and leads to higher yield [13, 14]. A setback in using polymer coating for SRF is the issue of degradability of the materials used for coating because they will remain in soil after nutrient release. The accumulation

of these materials will eventually become a bigger issue of environmental pollution. Therefore, many studies have been dedicated to developing biodegradable and environmentally safe polymer coating materials [15–19].

The demand for natural fibers has seen a drastic increase in recent years because they are renewable and environmentally friendly. Natural fibers have high potential as reinforcements in polymer composites and thus they have been extensively studied for this purpose [20]. As fillers, they have many advantages, such as lower cost, light weight, low density, high strength to weight ratio, biodegradability, and better thermal properties and other acceptable specific properties [21].

Various materials have been tested to be used as fertilizer coating, involving different methods such as spouted bed, fluidized bed, and rotating drum. Tennessee Valley Authority (TVA) tried using rotating drum to produce sulphur-coated urea (SCU) [22]. Then, another study reported the use of spouted bed to produce SCU [23]. Ten years after that, a researcher develops a technique modified fluidized bed to coat urea [24]. All the three approaches have been reviewed and studied further by more recent researchers [25–28]. Regardless of the procedures, the quality of SRF and the accuracy of nutrient release time depend on various parameters.

In this study, the extrusion process involved the compounded NPK fertilizer with EFB and biopolymer. Based on the literature review, CRF/SRF available in the market are commonly made of nonbiodegradable plastic/polymer by means of dipping, emulsion, or spraying. The novelty of this study was the use of compounding method in producing SRF, with the incorporation of biodegradable polymer PHBv. The idea was to add the EFB fibers to reinforce the bioplastic fertilizer and produce SRF bioplastic composites. This bioplastic fertilizer (BpF) composite is able to gradually degrade in soil within a shorter period of time compared to conventional fertilizers. In this study, the BpF composites have to determine degradation in soil burial test. The data on degradation of BpF composites were analyzed using ANOVA (SAS system analysis).

2. Materials and Methods

2.1. Materials. Poly(hydroxybutyrate-co-valerate) (PHBv) under the trade name Biopol, Germany, was supplied by Innovative Pultrusion Sdn. Bhd., Senawang, Negeri Sembilan. The natural fibers used as fillers were oil palm empty fruit bunch (EFB) fibers, which were supplied by Poly Composite Sdn. Bhd., Teluk Intan, Perak. NPKC1 (uncoated) and NPKC2 (coated) fertilizers were supplied by Diversatech Fertilizer Sdn. Bhd, Bangi, Selangor, Malaysia. The average particle sizes of the EFB and fertilizer in granular form were 0.25 to 0.5 mm.

2.2. Bioplastic Fertilizer (BpF) Composites Formulation and Compounding Using Extrusion Processing. The compounding of materials in this section was carried out in twin-screw extruder (Micromac, Malaysia) with a 30 mm screw diameter. Biodegradable plastics PHBv and oil palm empty fruit bunch and NPK fertilizer were dried at 103 ± 2°C overnight in a drying oven. The materials to be compounded were fed at a constant speed into the hopper extruder by means of a screw feed system. The product was bioplastic fertilizer (BpF) composites containing biodegradable plastic, empty fruit bunch, and NPK fertilizer. These components were homogenized in the mixer. The reverse barrel temperature profile from the feed throat to die exit ranged from 145°C to 160°C. The formulation of bioplastic fertilizer (BpF) composites is presented in Table 1. The premix was fed into the main feeder at the speed of 15 rpm. The extruder screw speed was 40 rpm. The temperature was about 145°C for Section I, about 150°C for Section II, and about 160°C for Section III.

Table 1: Formulation of bioplastic fertilizer (BpF) composites compounding.

Composites	PHBv (%)	EFB fibers (%)	NPK fertilizers (%)
PHBv/NPKC1	40	0	60
PHBv/NPKC2	40	0	60
PHBv/EFB/NPKC1	30	10	60
PHBv/EFB/NPKC2	30	10	60

Note: PHBv (poly(hydroxybutyrate-co-valerate)), NPKC1 (uncoated) and NPKC2 (coated), and EFB (empty fruit bunch).

2.3. Thermogravimetric Analysis (TGA). The equipment used in thermogravimetric analysis was TGA Q500, TA Instruments. Ten milligrams of samples was heated under the temperature range from 35°C to 600°C at the rate of 10°C/min. The analysis required nitrogen atmosphere with the flow rate of nitrogen at 20 mL/min. The weight reduction of samples was recorded and plotted against temperature.

2.4. Differential Scanning Calorimetry Analysis (DSC). The equipment used in DSC analysis was Differential Scanning Calorimeter DSC Q20, TA Instruments. The analysis required argon atmosphere with the flow rate of argon at 50 mL/min. Ten milligrams of samples was weighted and sealed in an aluminium pan. In the nonisothermal melt-crystallization, the melted samples were cooled to −20°C at a cooling rate of 10°C/min after melting at 200°C for 2 min. Subsequently, the crystallized samples were heated to 250°C at 10°C/min to determine their melting behavior. In the isothermal melt-crystallization, the samples melted at 200°C for 2 min were cooled at a rate of 100°C/min to the desired crystallization temperature (T_c) and allowed to crystallize. Each sample was recorded for its cold crystallization temperature (T_c), glass transition temperature (T_g), and melting temperature (T_m).

2.5. Scanning Electron Microscopy (SEM). Scanning electron microscope (S-3400N, Hitachi, Japan) was used to analyze the surfaces of the fractured samples. At the cathode, the acceleration voltage was set at 15 kV. Prior to this, the samples were sputter-coated with gold dust in the coater Emitech K550X (600 s, 35 mA, 2×10^{-1} bar).

2.6. Biodegradation Test. The BpF composites biodegradation test involved the simulation of natural soil environment in a simple soil burial test. The natural soil was collected earlier and it was made sure that it did not contain any

Table 2: TGA characterisation of pure PHBv, PHBv/NPK, and PHBv/NPK/EFB composites.

	Degradation temperature (°C)		
Composites	T_{IDT}	T_{FDT}	Residual (%) (at 550°C)
NPKC1	76.12	285.45	41.80
NPKC2	76.01	372.63	40.82
EFB	251.18	342.82	23.11
PHBv	263.44	300.73	0.257
PHBv/NPKC1	268.76	471.76	27.00
PHBv/NPKC2	269.30	495.74	29.76
PHBv/EFB/NPKC1	268.23	439.26	29.07
PHBv/EFB/NPKC2	252.78	426.47	25.41

Notes: T_{IDT}: initial decomposition temperature; T_{FDT}: final decomposition temperature.
PHBv (poly(hydroxybutyrate-co-valerate)), NPKC1 (uncoated) and NPKC2 (coated), and EFB (empty fruit bunch).

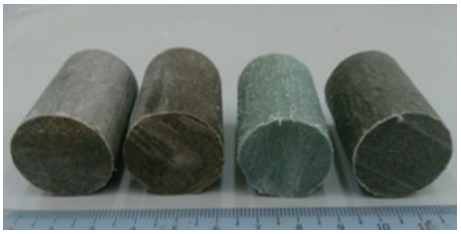

Figure 1: Bioplastic fertilizer (BpF) composites.

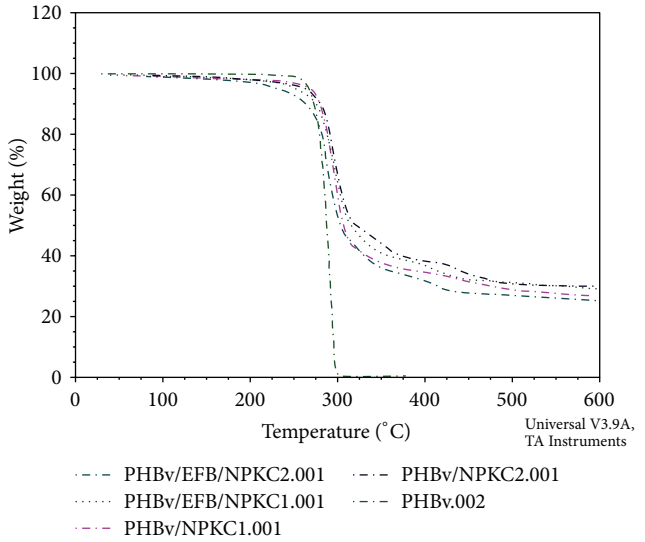

Figure 2: TGA thermograms showing the thermal properties of pure PHBv, PHBv/NPK, and PHBv/EFB/NPK composites. Note: PHBv (poly(hydroxybutyrate-co-valerate)), NPKC1 (uncoated) and NPKC2 (coated), and EFB (empty fruit bunch).

composting materials or enzyme activity. In this test, 5 replications samples were simply buried in the natural soil and were kept at temperature between 25°C and 30°C, with relative humidity of around 65%. The test spanned for a total of 16 weeks and the samples were recovered every four weeks for analysis. Thus, there were seven degradation stages, starting from Week 0, Week 4, and so on until Week 16. For each stage, the samples recovered were rinsed under running water to get rid of soil residues from the surface. Drying oven with the temperature of 80°C was used to completely remove the moisture until a constant dry weight was obtained for each sample. The weight loss after the soil burial test indicated the level of biodegradability of the samples. The calculation of weight loss involved the following equation:

$$\text{Weight loss (\%)} = \frac{W_0 - W_1}{W_0} \times 100, \quad (1)$$

where W_0 is the weight before the test while W_1 is the weight after the test.

3. Results and Discussion

3.1. Fabrication of Bioplastic Fertilizer (BpF) Composites. The samples of the BpF composites are shown in Figure 1. After compounding, the samples were extruded from mould and cut to about 30 mm in length. In this study, the samples of BpF composites were compounded to achieve homogeneity, with good bonding and dispersion. One of the best methods to obtain good dispersion of fillers in the biopolymer matrix is the twin-screw extrusion technique [29, 30]. However, the sensitivity of the temperature during compounding processes involving extrusion or injection moulding is limited [31]. The interaction between matrix and fillers (reinforcement) that provide larger surface area improves the mechanical properties as well as the dimensional and thermal stability of the composite [32, 33]. The process conditions, which determine the dispersion and the adhesion/interaction between the fillers and the matrix, influence the enhancement of the composite material [34, 35].

3.2. Thermogravimetric (TGA). Table 2 and Figure 2 show the TGA results and the curves which illustrate the weight loss of pure PHBv, EFB fibers, and the BpF composites under increasing temperature. The loss of weight was directly proportional to the increase in temperature. The thermal degradation started at 263.44°C and reached its maximum at 300.73°C. The pure PHBv has earlier been reported to have thermal instability beyond 250°C [36]. It was also mentioned that the chain scission and hydrolysis that occur

Table 3: DSC characterisation of pure PHBv, PHBv/NPK, and PHBv/NPK/EFB composites.

Sample	T_c (°C)	T_g (°C)	T_m (°C)
NPKC1	200.68	—	110.26
NPKC2	—	30.19	86.29
EFB	—	—	76.35
PHBv	46.58	94.21	171.69
PHBv/NPKC1	41.82	87.29	166.38
PHBv/NPKC2	43.71	90.84	151.63
PHBv/EFB/NPKC1	40.49	90.79	166.53
PHBv/EFB/NPKC2	44.29	89.07	161.29

Notes: crystallization temperature (T_c), glass transition temperature (T_g), and melting temperature (T_m).
PHBv (poly(hydroxybutyrate-co-valerate)), NPKC1 (uncoated) and NPKC2 (coated), and EFB (empty fruit bunch).

in the degradation process lead to weight loss and crotonic acid formation. The moist environment further catalyzes the hydrolytic degradation. The cumulative thermal degradation PHBv as the matrix and the EFB fibers as the fillers resulted as the thermal degradation of the biocomposites. The thermal degradation of the composites started at approximately 250°C and reached its maximum at 400°C. The TGA results revealed that the fibers were the final component of the composites that underwent degradation. The maximum thermal degradation of the composite was slightly higher than the pure PHBv. As seen in Figure 2, the degraded PHBv did not show any residue. The residual mass was presented as functions of fiber and fertilizer percentage because the degradation of fiber by heating (pyrolysis) in partial or total absence of oxygen produced char residue. Higher concentration of fertilizer in the composites produced higher char residue, but the residue was expected to be lower than the NPK fertilizer for all composites. The thermal degradation of PHBv largely involved *cis*-elimination mechanism and random chain scission with a six-membered ring transition state [37, 38]. The PHBv/EFB/NPKC2 composite was more stable than PHBv because it had a higher maximum degradation peak than PHBv. The composite was also found to be more thermally stable than other composites because it required higher initial degradation temperature. Thus the presence of NPK and EFB fiber did not have any degradation effect on PHBv.

3.3. Differential Scanning Calorimetry Analysis (DSC). Table 3 presents the DSC results. The addition of NPK fertilizer and EFB fiber to make the BpF composites reduced the crystallinity of the pure PHBv. The DSC thermograms in Figure 3 show reduced melting temperature and the presence of double melting peaks, which suggested a disrupted arrangement of polymer crystal structures due to the addition of EFB fiber to the PHBv matrix. Past studies have reported the nucleating effect of natural fibers which promotes the formation of transcrystalline structures along fiber surfaces during crystallization from the melt [39]. The disordered crystal growth along the interface of fiber-matrix and their interference on the crystals formation in the bulk probably caused the discontinuities in the matrix crystals and reduced the overall crystallinity of the polymer.

Figure 3 shows the thermograms of pure PHBv blended with 10 wt.% EFB fibers and 60% NPK fertilizer. The details

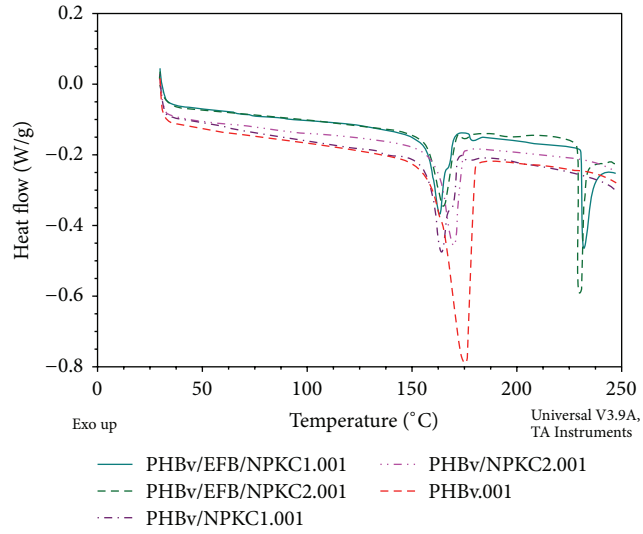

Figure 3: DSC characterisation of pure PHBv, PHBv/NPK, and PHBv/NPK/EFB composites. Note: PHBv (poly(hydroxybutyrate-co-valerate)), NPKC1 (uncoated) and NPKC2 (coated), and EFB (empty fruit bunch).

are given in Table 3 where T_m is the melting temperature, T_g is the glass transition temperature, and T_c is the crystallization temperature. The effects of EFB fibers on the crystallinity and nucleation of PHBv were studied using the nonisothermal DSC. The crystallization of the heterogenous crystal during the heating cycle led to a bimodal endotherm of PHBv [40]. In the presence of fertilizer, the addition of 10 wt.% EFB fibers increased the crystallization rate, probably because the molecular chains diffused slower through the well-distributed EFB fibers to the nucleus.

3.4. Scanning Electron Microscopy (SEM). Figure 4(a) PHBv/NPKC1 and (b) PHBv/NPKC2, shows SEM images of the PHBv and NPK fertilizer composites. These images show some NPKC1 and NPKC2 that were well bonded to the matrix. This suggests that the PHBv/NPKC1 and PHBv/NPKC2 composites had better dispersion, wetting, and interfacial adhesion. It was evident that there were weak stress transfer and bad interfacial adhesion between the interfaces of PHBv

Table 4: Weight loss of bioplastic fertilizer (BpF) composites from soil burial test.

Composites	Weeks				
	0	4	8	12	16
PHBv/NPKC1	0	50.4a (5.78)	55.85c (2.28)	60.17c (7.70)	68.66c (2.53)
PHBv/NPKC2	0	56.45a (12.23)	77.94b (6.36)	87.78b (0.98)	90.28b (1.57)
PHBv/EFB/NPKC1	0	55.76a (7.08)	79.57ab (7.37)	89.31ab (1.28)	96.48a (1.35)
PHBv/EFB/NPKC2	0	58.66a (7.47)	88.41a (0.51)	96.43a (0.57)	99.35a (0.17)

Note: means of weight loss for the weight loss labelled with the same letters (a, ab, b, c, and d) were not significantly different at $P < 0.05$. Standard deviation is given in parentheses. PHBv (poly(hydroxybutyrate-co-valerate)), NPKC1 (uncoated) and NPKC2 (coated), and EFB (empty fruit bunch), 5 replications of samples.

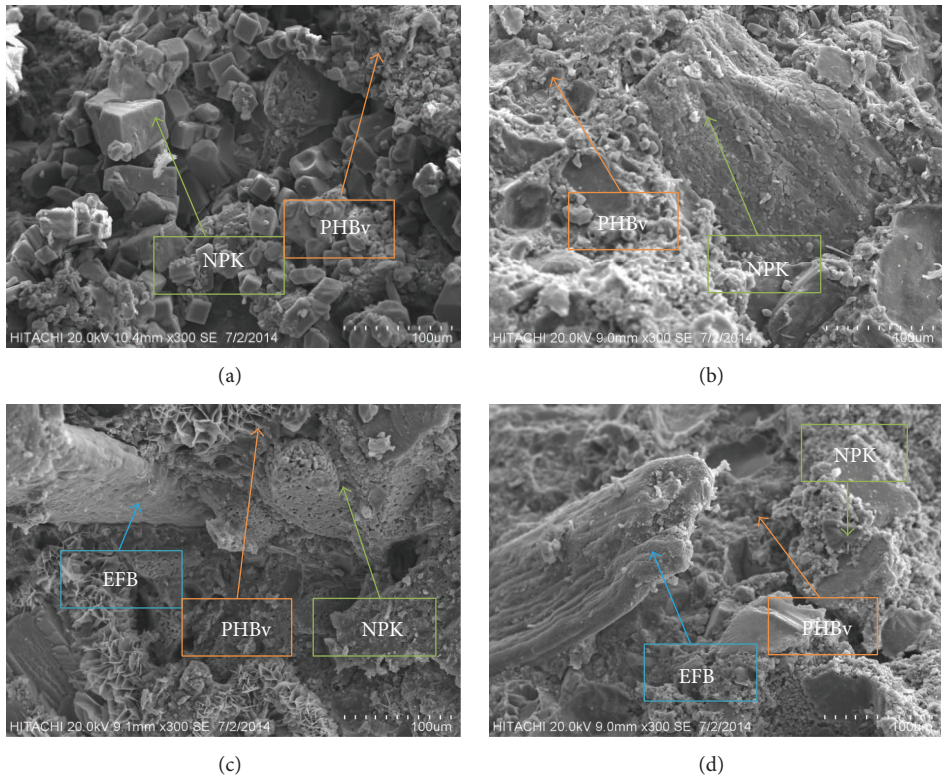

Figure 4: SEM of bioplastic fertilizer (BpF) composites. (a) PHBv/NPKC1, (b) PHBv/NPKC2, (c) PHBv/EFB/NPKC1, and (d) PHBv/EFB/NPKC2. Note: PHBv (poly(hydroxybutyrate-co-valerate)), NPKC1 (uncoated) and NPKC2 (coated), and EFB (empty fruit bunch).

matrix and EFB fibers. This could be observed in the SEM images of the compounding fractured surfaces, as shown in Figure 4(c) PHBv/EFB/NPKC1 and (d) PHBv/EFB/NPKC2. Bad interfacial adhesion caused led to total debonding of the fibers from the matrix. As shown in Figure 4(c) PHBv/EFB/NPKC1, the EFB fiber protruded from the fractured PHBv composite surfaces. For PHBv/EFB/NPK composite, it was clear that weak interfacial adhesion manifested between the small gaps of the fibers and the matrix. Figure 4(d) PHBv/EFB/NPKC2, also showed that the same situation occurred in the other PHBv composite. It has been discussed that the differences in polarity between PHBv and EFB fibers caused them to have low compatibility with each other, which led to the weak bonding.

3.5. Biodegradation of Bioplastic Fertilizer (BpF) Composites. The results from ANOVA analysis, Table 4, and Figure 5 show that the degradation rates of BpF composites were not significantly different, which was at $P < 0.05$. Table 4 shows the rate of biodegradation composite samples. From the results, PHBv/EFB/NPK composites showed highest weight loss or greatest biodegradation along the study. The first stage of biodegradation involved the microbial attack on the surface of the polymer. An increase in water absorption enhanced the hydrolysis of ester groups on the PHB backbone [37]. The water absorption also caused debonding and enhanced dispersion of EFB fibers. Consequently, all of these led to more surface area exposed to microbial degradation, further increasing the biodegradation rate.

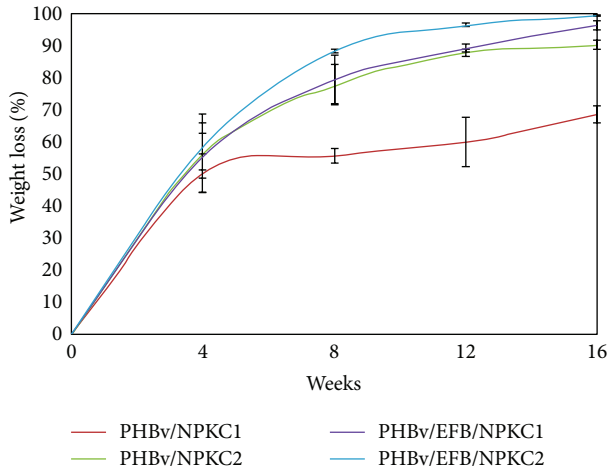

Figure 5: Mean of standard deviation and weight loss of PHBv/NPK and PHBv/EFB/NPK composites in soil burial test. Note: PHBv (poly(hydroxybutyrate-co-valerate)), NPKC1 (uncoated) and NPKC2 (coated), and EFB (empty fruit bunch), 5 replications of samples.

The biodegradation rate of polymers is influenced by multiple factors such as microbial activity, surface area, moisture, temperature, pH, and nutrients. However, PHBv is not affected by moisture and also not soluble in water. It is stable for an indefinite period in air and no degradation should occur under normal storage conditions. In anaerobic conditions, the PHA degradation produces water, CO_2, and methane (CH_4) while only water and CO_2 are produced in aerobic conditions. The extent of polymer biodegradability is mainly determined by its chemical and physical properties. PHAs with high molecular weight are more resistant to biodegradation. In studying polymer biodegradability, it is also important to consider the melting temperature of the polymer.

Figure 5 depicts some of the samples that underwent the soil burial test for 4, 8, and 16 weeks. Significant degradation could be observed between Weeks 8 and 16. Most of the polymers biocomposites have degraded starting from Week 4, though PHBv/NPKC1 and PHBv/NPKC2 still kept some of their original shapes. The percentages of total weight loss for all samples are shown in Table 4. PHBv/EFB/NPKC2 (99.35%) degraded better than PHBv/NPKC1 (68.66%) and PHBv/NPKC2 (90.28%) and had 30% higher weight loss compared with PHBv/NPK. The test was halted after 16 weeks because it was no longer possible to accurately measure the weight loss beyond that point. The samples lacked structural integrity and seemed to be a mass of EFB fibers with many of the components already degraded.

Figure 6 shows the evidence from morphological images. The bonding of all composites created small gaps between matrices polymer and fiber because hydrophilic characteristic of the EFB fiber weakened the interfacial bonding. This gave advantage to the fiber in BpF to be degraded faster than PHBv composites. EFB fiber also absorbed water, degraded slowly, and swelled, allowing the release of fertilizer into soil. Furthermore, the presence of EFB fibers increased

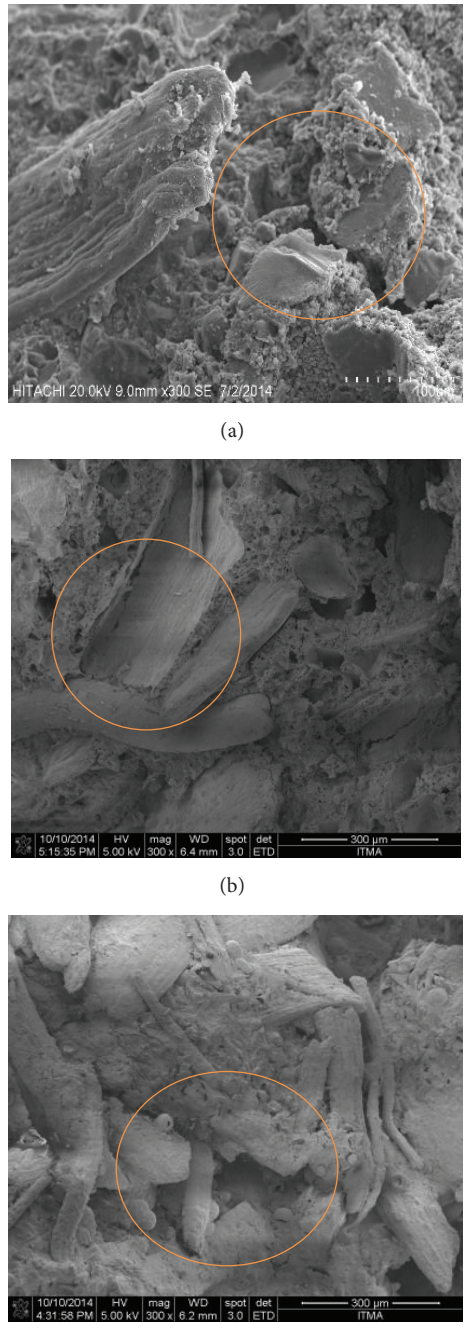

Figure 6: SEM micrographs of the soil burial samples. (a) PHBv/EFB/NPKC2, 0 weeks, (b) PHBv/EFB/NPKC2, 8 weeks, and (c) PHBv/EFB/NPKC2, 16 weeks. Note: PHBv (poly(hydroxybutyrate-co-valerate)), NPKC2 (coated), and EFB (empty fruit bunch).

the surface area for the biodegradation of the composites. Figure 6(a) shows that the presence of EFB fibers in the composites enhanced biodegradation process, as indicated by the increase in the weight loss percentages of the samples. Figure 6(b) also shows that the PHBv/EFB/NPK biocomposites underwent more degradation after 8 weeks of soil burial test. It was assumed that the enhanced degradation of

the composites was caused by the weak adhesion between the interface of PHBv matrix and EFB fibers. Figure 6(c) shows the complete detachment of components in PHBv/EFB/NPK biocomposites after 16 weeks. The formation of larger gaps due to detachment allowed more access for the microbes to reach the internal parts of the biocomposites, hence the enhanced biodegradation.

4. Conclusions

The PHBv/EFB/NPKC2 composite was more stable than pure PHBv because the former had a higher maximum degradation peak and it required higher initial degradation temperature. The PHBv composite degradability was improved by the addition of EFB fibers which increased the hydrophilicity of the composites. PHBv/NPKC1 and PHBv/NPKC2 reinforced with 10 wt.% EFB fiber were degraded faster in soil burial test. SEM results showed that the PHBv/NPKC1 and PHBv/NPKC2 composites without EFB fibers had better dispersion, wetting, and interfacial adhesion, hence the lower rate of biodegradation.

Conflict of Interests

The authors declare that there is no conflict of interests regarding the publication of this paper.

Acknowledgment

The paper was supported by Research Grant GP-IBT/2013/9420600/MST23 under Materials Science and Technology (MST) cluster supported by Research Management Centre, UPM.

References

[1] J. Zhang, S. McCarthy, and R. Whitehouse, "Reverse temperature injection molding of Biopol and effect on its properties," *Journal of Applied Polymer Science*, vol. 94, no. 2, pp. 483–491, 2004.

[2] G. J. M. de Koning and P. J. Lemstra, "Crystallization phenomena in bacterial poly[(*R*)-3-hydroxybutyrate]: 2. Embrittlement and rejuvenation," *Polymer*, vol. 34, no. 19, pp. 4089–4094, 1993.

[3] F. Biddlestone, A. Harris, J. N. Hay, and T. Hammond, "The physical ageing of amorphous poly(hydroxybutyrate)," *Polymer International*, vol. 39, no. 3, pp. 221–229, 1996.

[4] M. Scandola, G. Ceccorulli, and M. Pizzoli, "Miscibility of bacterial poly(3-hydroxybutyrate) with cellulose esters," *Macromolecules*, vol. 25, no. 24, pp. 6441–6446, 1992.

[5] D. O. Huett and B. J. Gogel, "Longevities and nitrogen, phosphorus, and potassium release patterns of polymer-coated controlled-release fertilizers at 30°C and 40°C," *Communications in Soil Science and Plant Analysis*, vol. 31, no. 7-8, pp. 959–973, 2000.

[6] C.-S. Wu, "Controlled release evaluation of bacterial fertilizer using polymer composites as matrix," *Journal of Controlled Release*, vol. 132, no. 1, pp. 42–48, 2008.

[7] M. K. Hafshejani, F. Khandani, R. Heidarpour, A. Arad, and S. Choopani, "Study the sources of mercury vapor in atmosphere as a threatening factor for human health and bio-filtering methods for removal of toxic pollution," *Life Science Journal*, vol. 10, no. 1, pp. 293–296, 2013.

[8] A. M. Dave, M. H. Mehta, T. M. Aminabhavi, A. R. Kulkarni, and K. S. Soppimath, "A review on controlled release of nitrogen fertilizers through polymeric membrane devices," *Polymer-Plastics Technology and Engineering*, vol. 38, no. 4, pp. 675–711, 1999.

[9] A. Shaviv, "Advances in controlled-release fertilizers," in *Advances in Agronomy*, vol. 71, pp. 1–49, Academic Press, New York, NY, USA, 2001.

[10] Sh. Jin, G. Yue, L. Feng, Y. Han, X. Yu, and Z. Zhang, "Preparation and properties of a coated slow-release and water-retention biuret phosphoramide fertilizer with superabsorbent," *Journal of Agricultural and Food Chemistry*, vol. 59, no. 1, pp. 322–327, 2011.

[11] S. K. Jain, 2007, http://www.Pharmainfo.net.

[12] I. Bhattacharya, S. Bandyopadhyay, Ch. Varadachari, and K. Ghosh, "Development of a novel slow-releasing iron—manganese fertilizer compound," *Industrial and Engineering Chemistry Research*, vol. 46, no. 9, pp. 2870–2876, 2007.

[13] F. Munoz, R. S. Mylavarapu, and C. M. Hutchinson, "Environmentally responsible potato production systems: a review," *Journal of Plant Nutrition*, vol. 28, no. 8, pp. 1287–1309, 2005.

[14] Z. Cong, S. Yazhen, D. Changwen, Z. Jianmin, W. Huoyan, and C. Xiaoqin, "Evaluation of waterborne coating for controlled-release fertilizer using Wurster fluidized bed," *Industrial and Engineering Chemistry Research*, vol. 49, no. 20, pp. 9644–9647, 2010.

[15] M. Tomaszewsa and A. Jarosiewicz, "Polysulfone coating with starch addition in CRF formulation," *Desalination*, vol. 163, no. 1–3, pp. 247–252, 2004.

[16] A. S. Mathews and S. Narine, "Poly[*N*-isopropyl acrylamide]-*co*-poryurethane copolymers for controlled release of urea," *Journal of Polymer Science, Part A: Polymer Chemistry*, vol. 48, no. 15, pp. 3236–3243, 2010.

[17] Z. Peng and F. Chen, "Synthesis and properties of lignin-based polyurethane hydrogels," *Journal of Polymer Materials*, vol. 60, no. 9, pp. 674–683, 2011.

[18] Z. Y. Peng and F. G. Chen, "Synthesis and properties of temperature-sensitive hydrogel based on hydroxyethyl cellulose," *International Journal of Polymeric Materials and Polymeric Biomaterials*, vol. 59, no. 6, pp. 450–461, 2010.

[19] G. E. Ibrahim, A. F. Abdel-Motaleb, and E. R. E. Mahmoud, "Achieving optimum scientific standards for producing fabrics suitable for protecting against hazardous chemical liquids," *Life Science Journal*, vol. 10, no. 1, pp. 342–353, 2013.

[20] A. K. Bledzki and J. Gassan, "Composites reinforced with cellulose based fibres," *Progress in Polymer Science*, vol. 24, no. 2, pp. 221–274, 1999.

[21] B.-J. Kim, F. Yao, G. Han, and Q. Wu, "Performance of bamboo plastic composites with hybrid bamboo and precipitated calcium carbonate fillers," *Polymer Composites*, vol. 33, no. 1, pp. 68–78, 2012.

[22] G. M. Blouin, D. W. Rindt, and O. E. Moore, "Sulfur-coated fertilizers for controlled release. Pilot-plant production," *Journal of Agricultural and Food Chemistry*, vol. 19, no. 1, p. 80, 1971.

[23] A. Meisen and K. B. Mathur, "Characteristic dimension and shape factor of particles," *Proceedings of the British Sulphur 20 Corporation*, vol. 2, 1978.

[24] O. A. Salman, "Polymer coating on urea prills to reduce dissolution rate," *Journal of Agricultural and Food Chemistry*, vol. 36, no. 3, pp. 616–621, 1988.

[25] C. H. Wu, "Controlled release evaluation of bacterial fertilizer using polymer composites as matrix," *Journal of Controlled Released*, vol. 132, no. 1, pp. 42–48, 2008.

[26] M. Tzika, S. Alexandridou, and C. Kiparissides, "Evaluation of the morphological and release characteristics of coated fertilizer granules produced in a Wurster fluidized bed," *Powder Technology*, vol. 132, no. 1, pp. 16–24, 2003.

[27] M. Devassine, F. Henry, P. Guerin, and X. Briand, "Coating of fertilizers by degradable polymers," *International Journal of Pharmaceutics*, vol. 242, no. 1-2, pp. 399–404, 2002.

[28] S. Tao, J. Liu, K. Jin et al., "Preparation and characterization of triple polymer-coated controlled-release urea with water-retention property and enhanced durability," *Journal of Applied Polymer Science*, vol. 120, no. 4, pp. 2103–2111, 2011.

[29] S. Mishra, S. Tripathy, M. Mishra, A. K. Mohanty, and S. Nayak, "Novel eco-friendly biocomposites: biofiber reinforced biodegradable polyester amide composites—fabrication and properties evaluation," *Journal of Reinforced Plastics and Composites*, vol. 21, no. 1, pp. 55–70, 2002.

[30] K. Oksman, M. Skrifvars, and J.-F. Selin, "Natural fibres as reinforcement in polylactic acid (PLA) composites," *Composites Science and Technology*, vol. 63, no. 9, pp. 1317–1324, 2003.

[31] S. Lee, D. Cho, W. Park, S. Han, and L. Drzal, "Novel silk/poly(butylene succinate) biocomposites: the effect of short fibre content on their mechanical and thermal properties," *Composites Science and Technology*, vol. 65, no. 3-4, pp. 647–657, 2005.

[32] A. Paul and S. Thomas, "Electrical properties of natural-fiber-reinforced low density polyethylene composites: a comparison with carbon black and glass-fiber-filled low density polyethylene composites," *Journal of Applied Polymer Science*, vol. 63, no. 2, pp. 247–266, 1997.

[33] J. M. Felix and P. Gatenholm, "Nature of adhesion in composites of modified cellulose fibers and polypropylene," *Journal of Applied Polymer Science*, vol. 42, no. 3, pp. 609–620, 1991.

[34] G. Williams and R. Wool, "Composites from natural fibers and soy oil resins," *Applied Composite Materials*, vol. 7, no. 5, pp. 421–432, 2000.

[35] K. Oksman and J.-F. Selin, "Plastics and composites from polylactic acid," in *Natural Fibers, Plastics and Composites*, F. T. Wallenberger and N. E. Weston, Eds., pp. 149–165, Kluwer Academic, Dordrecht, Netherlands, 2004.

[36] S. Luo and A. Netravali, "Characterization of henequen fibers and the henequen fiber/poly(hydroxybutyrate-co-hydroxyvalerate) interface," *Journal of Adhesion Science and Technology*, vol. 15, no. 4, pp. 423–437, 2001.

[37] Q.-S. Liu, M.-F. Zhu, W.-H. Wu, and Z.-Y. Qin, "Reducing the formation of six-membered ring ester during thermal degradation of biodegradable PHBV to enhance its thermal stability," *Polymer Degradation and Stability*, vol. 94, no. 1, pp. 18–24, 2009.

[38] S. Nguyen, G.-E. Yu, and R. H. Marchessault, "Thermal degradation of poly(3-hydroxyalkanoates): preparation of well-defined oligomers," *Biomacromolecules*, vol. 3, no. 1, pp. 219–224, 2002.

[39] A. Javadi, Y. Srithep, S. Pilla, J. Lee, S. Gong, and L.-S. Turng, "Processing and characterization of solid and microcellular PHBV/coir fiber composites," *Materials Science and Engineering C*, vol. 30, no. 5, pp. 749–757, 2010.

[40] C. Eldsäter, B. Erlandsson, R. Renstad, A.-C. Albertsson, and S. Karlsson, "The biodegradation of amorphous and crystalline regions in film-blown poly(ε-caprolactone)," *Polymer*, vol. 41, no. 4, pp. 1297–1304, 2000.

Hindawi Publishing Corporation
International Journal of Polymer Science
Volume 2015, Article ID 582901, 12 pages
http://dx.doi.org/10.1155/2015/582901

Research Article

Controlling the Melt Resistance to Flow as a Possibility of Improving the Miscibility and the Time Behavior of Some Blends Based on Starch

Doina Dimonie,[1] Miruna Musat,[1] Sanda Maria Doncea,[1] Celina Maria Damian,[2] Liliana Anton,[1] Eugeniu Vasile,[3] Roxana Trusca,[3] and Maria Râpă[4]

[1]*National Research and Development Institute for Chemistry and Petrochemistry, ICECHIM, 202 Splaiul Independentei, 060021 Bucharest, Romania*
[2]*Department of Bioresources and Polymer Science, University Politehnica of Bucharest, 1-7 Polizu, 011061 Bucharest, Romania*
[3]*METAV-CD S.A., 31 C.A., Rosetti, 020011 Bucharest, Romania*
[4]*Research Institute of Organic Auxiliary Products S.A., ICPAO, 8 Carpati, Medias, 551022 Sibiu, Romania*

Correspondence should be addressed to Maria Râpă; rapa_m2002@yahoo.com

Received 28 August 2015; Revised 13 November 2015; Accepted 30 November 2015

Academic Editor: Shiv Shankar

The paper proves that the miscibility of some blends based on starch can be improved by finding for each of them the melt resistance to flow at which the nonstationary flow and the melt degradation are avoided and the developed shear rate homogenizes optimally the material composition. The obtained results show that, for process sensitive materials like starches, the border between good and less miscibility is so narrow that the window of melt processing conditions and the best formulation must be found for each of them. The improving of miscibility by controlling the melt resistance to flow proves to be a good method to prevent retrogradation and plasticizer leaching and so to handle the new compounds behavior during usage.

1. Introduction

Physical modification of starch is a common practice to diminish its limitations such as poor processability, brittleness, hydrophilicity, and low compatibility [1] and involves also the obtaining of multicomponent, multiphase materials [2–4]. In this respect, the main concern is to reach high miscibility of the material components or, at least, to diminish the interface tensions [4–9] for reaching an advanced dispersion of minor components into the main polymer matrix [5].

The blends based on starch and polyvinyl alcohol (PVOH) present the advantage of being totally environmental destroyable materials and therefore were intensively studied [8–23]. PVOH is a water soluble vinyl polymer which, at first sight, seems to be not biodegradable [9]. However literature from PVOH manufacturers such as Kuraray Co. Ltd. indicated that PVOH can be biodegraded by activated sludge treatment [15]. Biodegradation of PVOH in soil is expected to be very slow and to take place only under selective microorganisms actions [8]. The PVOH-starch materials are still attractive for applications which require particular properties such as film and/or thermoforming capability, chemical resistance, and transparency [8–21]. The greatest difficulty in achieving of these materials is mainly the consequence of high interactions between the macromolecules of each polymer, both of them having well-defined semicrystalline morphology: granular with concentric crystalline-amorphous zones for starch and semicrystalline with high orthorhombic crystals for PVOH [9–12]. As a consequence, the free flow without degradation of the macromolecules of each polymer (destruction under shear) and the creation of new interactions, this time, between the chains of PVOH and those of starch are hard to be reached simultaneously [8, 12–14]. These difficulties lead to undesired blends behavior during usage as retrogradation and plasticizer leaching [14, 18], phenomena which diminish severely the quality of goods achieved from the new materials.

The paper aim was to study the possibility of improving the miscibility of some blends based on starch by controlling the melt dynamic viscosity to avoid the nonstationary flow of the melt and the retrogradation and the plasticizer leaching in the solid state and so to handle the time behavior during usage of new obtained amorphous materials designed for goods with short life.

2. Experimental

By blending of corn starch (27–32% amylose, T_g of 67°C) with PVOH (85% hydrolysis degree, T_g of 50°C) at the same ratio of 2.33 of PVOH related to starch (PVOH/starch), three new blends were obtained on both well-known Brabender roller and extrusion procedures. A partially soluble PVOH was selected to make certain the dissolution of new materials in cold water. The three new compounds contain glycerol (GLYC-2593-06) for three plasticizing levels: low (27%), medium (35%), and high (43%). These blends contain also common melt processing additives used in the same percentage for each of them. These plasticizing levels were chosen to ensure the obtaining of highly amorphous materials which can be melt processed, by various techniques, more easily [24, 25]. The obtaining of such materials based on starch is possible if the glycerol content is higher than 30% [20]. The blend miscibility was studied by FTIR [26–28] and X-ray diffraction (XRD) [27]. The obtained results were correlated with the blends melt flowability [23–25, 29–33] which was studied using the melt flow index (MFI) method [8, 25, 29, 30]. The MFI measurements were performed on a 4000 DYNISCO indexer, LMI type, which had provided the following melt properties: shear rate (ShR), melt flow index (MFI), dynamic viscosity (DV), and flow ratio (FR). The rheological measurements were done with a nozzle having 2.09 ratio between height and diameter (h/D), in the temperature range from 145°C to 175°C, at three loading levels, low (2.16 kg and 3.8 kg), medium (5 kg), and high (10 kg), and at cutting after 30 s. The FTIR spectra were recorded on a DIGILAB FTIR spectrometer, equipped with ZnSe crystal, via Attenuated Total Reflectance (ATR) method. The recording was made at 4 cm^{-1} resolution, using an average spectrum resulting from 5 other spectra. Each spectrum was processed with Grams/32 software and was analyzed in the following spectral range identified as representative for the miscibility of PVOH-starch multiphase materials: 3700 cm^{-1}–2500 cm^{-1}, 1800 cm^{-1}–1500 cm^{-1}, 1500 cm^{-1}–1170 cm^{-1}, and 1170 cm^{-1}–800 cm^{-1} [14]. The spectra were recorded on extrudates with smooth appearance melt processed from medium and highly plasticized blends at high load (10 kg) and four temperatures from the range of 145°C–175°C. The FTIR analyses were not made for low plasticized blend because of the numerous surface defects of the extrudates. A diffractometer Panalytical X'PERT MPD type with Bragg-Brentano geometry was used for XRD analysis. The heating enthalpy was measured by Differential Scanning Calorimetry (DSC) with Netzsch DSC 204 F1 Phoenix equipment by heating from −30°C to 100°C to remove thermal history, cooling again to −30°C, and heating to 200°C with 10°C/min under nitrogen (20 mL/min flow rate). Each blend was in addition analyzed in terms of extrudate surface quality, plasticizer leaching (assessed visually and according to [32]), and pellets quantities used to estimate, in the same conditions, the melt flowability and mechanical properties.

3. Results and Discussions

3.1. Melt Rheology

3.1.1. Shear Rate. The shear rate of the low (Figure 1(a)), medium (Figure 1(b)), and high (Figure 1(c)) plasticized blends at low load rises on the entire temperature range from 145°C to 175°C, from approximately 10 s^{-1} to about 20 s^{-1} and, respectively, to 50 s^{-1}. The increase of the shear rates is biggest at higher plasticizer content and great load almost on the entire temperature range, mainly from 155°C to 175°C. At 175°C and high load, the ShR of the low plasticized blend was of approx. 90 s^{-1}. In the same extrusion conditions, the ShR becomes 200 s^{-1} and approx. 500 s^{-1} for medium (Figure 1(b)) and highly (Figure 1(c)) plasticized blends. The shear rate-temperature dependence is almost linear both for the low plasticized blend, regardless of the extrusion conditions, and also for the highly plasticized blend extruded at high load. The nature of shear rate-temperature dependency characterizes the melt flow [31–33]. The melt flow can be unstable when this relationship is linear and the resulting extrudates, as a consequence, have sharkskin surface or are stable when this relationship is concave and the obtained extrudates present smooth appearance [31–33]. The magnitude of the surface defects depends on the extent of the material melt flow instability [33]. Accordingly, the extrudates obtained from the medium plasticized blend, extruded at medium and high loads, have smooth surfaces without any defect because the shear rate-temperature dependence is concave. The extrudates achieved both from the low plasticized blend and from highly plasticized ones, extruded at low load, have sharkskin surfaces because this dependency is linear.

3.1.2. Melt Flow Index. If the extrusion was made at low load, then, regardless of the plasticizing level, the blend fluidity reflected by MFI values is almost the same on the entire temperature range from 145°C to 175°C (Figure 2).

At medium and high loads, on the same temperature range, the melt fluidity increases more as the plasticizing level is high. At high load, the fluidity of the low plasticized blend is more than double as its values at small load. The melt fluidity is almost similar for the low plasticized blend extruded at high load, for the blend with medium plasticizer content extruded at medium load, and for the highly plasticized compound extruded at low load. If the temperature exceeds 165°C and the load is below medium level (3.8 kg) then the fluidity of the low plasticized blend increases sharply with about 150% considering its fluidity at the other temperatures. A similar sharp increase of the MFI because of the temperature increasing, under the same loading, was not observed for the blends with medium or high plasticizer contents.

The dependence of the blend fluidity on the plasticizing level and on the extrusion conditions can be explained

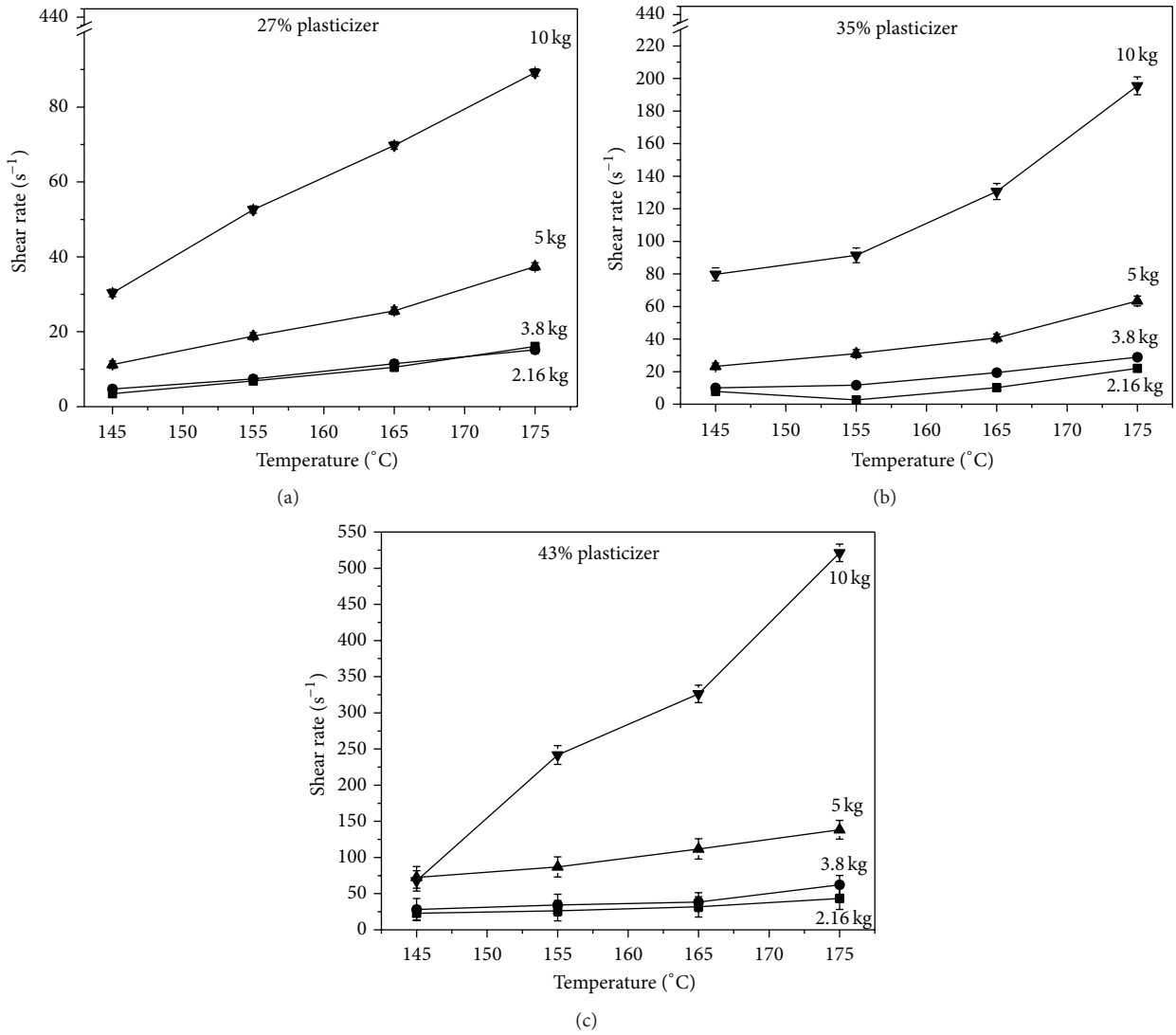

Figure 1: The dependence of the shear rate on the extrusion conditions and the plasticizing level ((a) 27%; (b) 35%; (c) 43%).

considering the macromolecules mobility and their entanglement and alignment in the flow direction. The mobility of the macromolecules is low and almost the same at loads under 5 kg, on the entire studied temperature range, regardless of the plasticizing level, probably because, in these conditions, the macromolecules are extremely entangled. At high plasticizer content and low load, in the same temperature range, the mobility remains small, probably because the macromolecules entanglement is still enhanced. At high load the fluidity has the same magnitude if the plasticizer content is low or medium and it becomes double for highly plasticized blend. At high plasticizer amount and high load, the macromolecules entanglement probably begins to decrease causing the increase of their mobility and possibly the chains alignment in the flow direction. These results show that the macromolecules mobility is dependent normally both on the plasticizing level and on the melt flow conditions. The large increase of fluidity of the low plasticized blend, extruded at high temperature, under high load, can be the consequence of the macromolecule degradation during extrusion by chain breaking [13, 34].

3.1.3. Dynamic Viscosity. As compared with its values for the low plasticized blends (Figure 3(a)), the DV decreases with up to 40%–50% for the medium (Figure 3(b)) and with about 80%–84% for the high (Figure 3(c)) plasticizer blends. At medium and high loads, regardless of plasticizing level, the DV does not show significant variations at the temperature increasing. The temperature influence on this property is more obvious at small plasticizing level and low load.

Dynamic viscosity represents the tangential force per unit area required to move, at unit rate, one horizontal plane with respect to the other (Newton's law of friction) [34]. In a simple expression, viscosity characterizes the melt flow resistance and signifies the internal friction resulting in a melt when one layer of fluid is moving in relationship to another one [34, 35]. Accordingly, the melt flow resistance of highly plasticized blend decreases more if the extrusion load is greater than

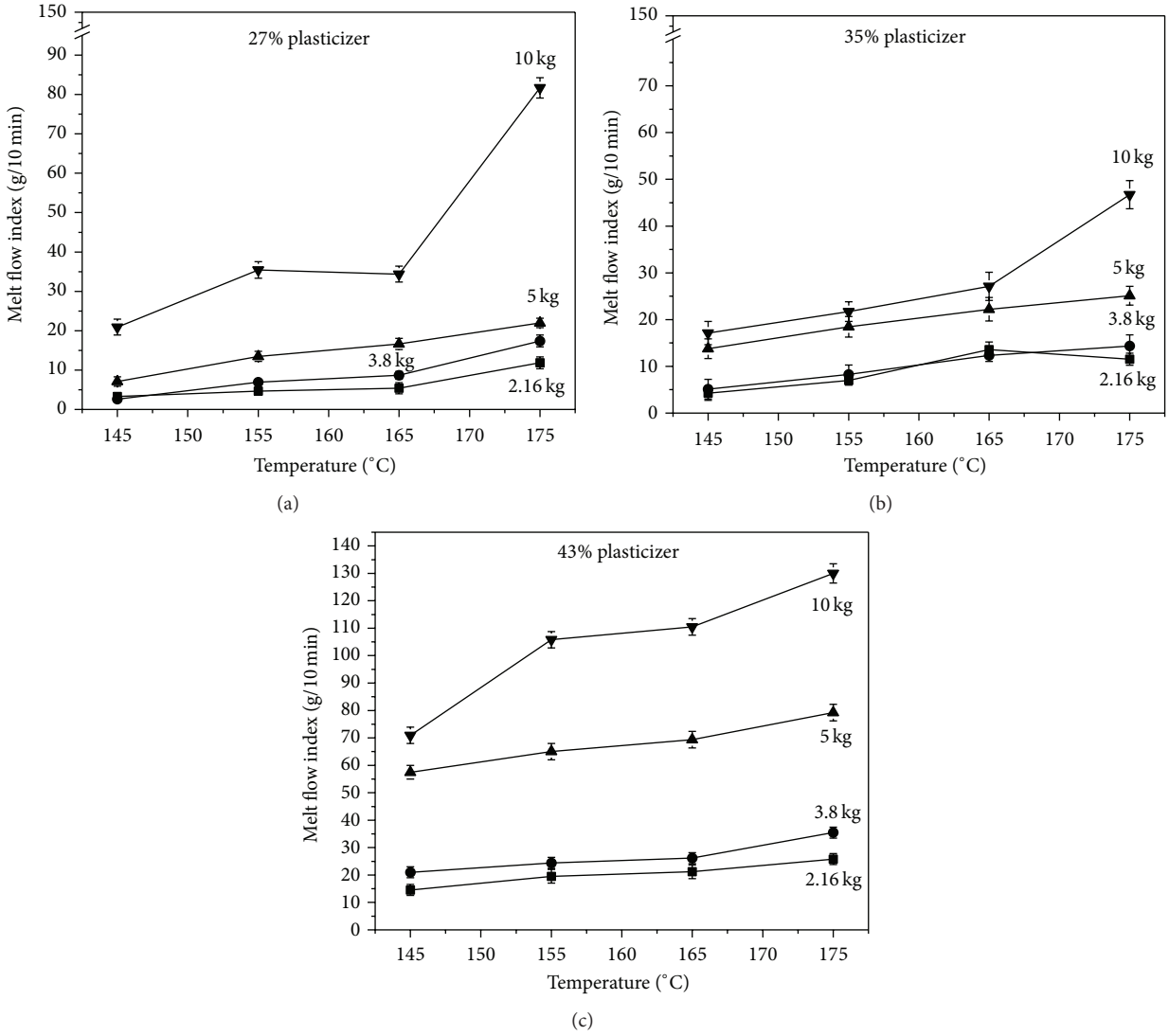

Figure 2: The dependence of the MFI on the extrusion conditions and the plasticizing level ((a) 27%; (b) 35%; (c) 43%).

3.8 kg, most likely because the chains are more disentangled and their mobility increases significantly. At low load, the melt resistance to flow decreases more at higher temperatures probably because, in these conditions, the macromolecules have greater mobility only due to the bigger kinetic energy generated by the temperature increase. The lowering of the DV with the increasing of the shear rate is in all probability the result of the alignment of disentangled macromolecules in the flow direction, aligned macromolecules having greater mobility than clew, unaligned ones. The obtained results prove that the melt flow resistance of the studied blends is more dependent on load than temperature.

3.1.4. Flow Ratio. At low load, the flow ratio practically does not depend on either the temperature value or the blend plasticizing level (Figure 4). The FR dependency on the temperature is more significant if the indexer load and plasticizer amount are higher. As compared with its values for the low plasticized blend (Figure 4(a)), the FR increases with almost 50% and, respectively, with 200% for medium (Figure 4(b)) and highly (Figure 4(c)) plasticized blends.

The flow ratio represents the ratio between two flow rates at two different loads and characterizes the melt sensitivity to the changing of the melt processing conditions [25, 29]. The increase of the flow ratio with the plasticizing degree raise is the consequence of the diminishing of the melt flow resistance due to the interposing of the plasticizer molecules between the macromolecules of the two polymers. Higher temperatures favor the FR only at high load because the melt amount which flows through the same nozzle, in the same time, under the same temperature, is higher than the quantity which flows under low load.

3.2. Blends Miscibility

3.2.1. FTIR Analysis. The perturbations of the IR spectrum are qualitative criterion of component miscibility, grounds which make from FTIR a good tool to control the material

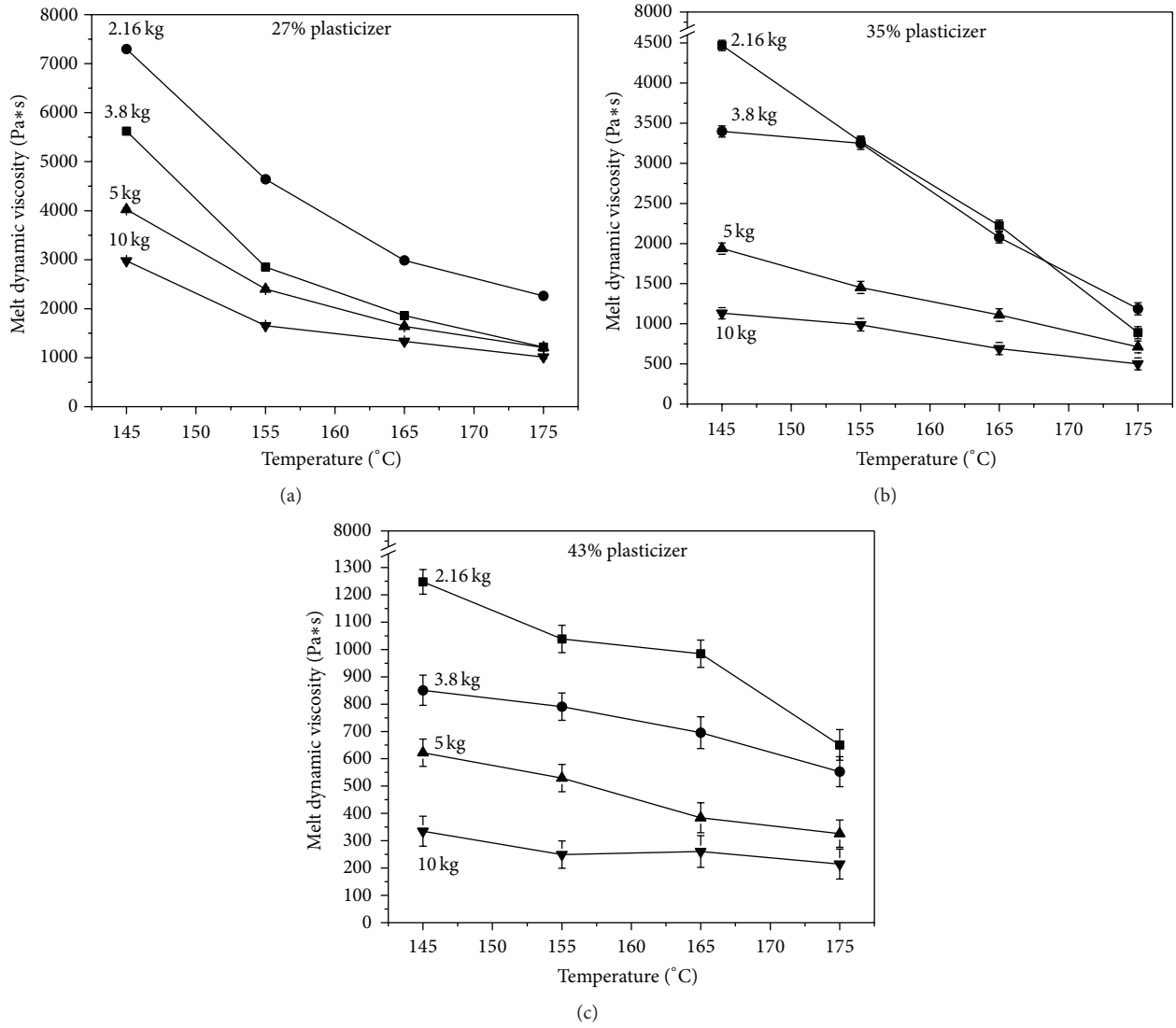

Figure 3: Dynamic viscosity dependence on the extrusion conditions and the plasticizing level ((a) 27%; (b) 35%; (c) 43%).

structure-properties relationship. The component miscibility can be revealed by *gross and/or appreciable changes* of the FTIR spectrum and/or by *small shifts* of the characteristic peaks of each component [8, 9, 14, 17, 22, 23, 26]. The *gross modifications* of the FTIR spectra refer to the new appearing spectral features and/or to the changes in intensities higher than 50% of the material peaks as compared with the component absorption. The *appreciable spectral changes* are those changes in which the component absorption is presented in the material spectrum but shifted with more than one width at the half height of the peak of components. The *small spectral shifts* refer to the shifting of the material absorption at wavenumber smaller than 10 Å considering the absorption of each component [14, 23, 26].

All the above described spectral changes are presented in the FTIR spectra of the studied blends (Figures 5–8) but with individual characteristics reliant on the plasticizing degree and the obtaining conditions of each of them.

The *main spectral change is a gross* one since it is about the appearance *of a new large peak* ranged from 1170 cm^{-1} to 955 cm^{-1}, with maximum at 1035 cm^{-1} and intensity of 1.4 ATR units (Figures 8(a) and 8(b)). This peak *was* observed in all situations with the exception of the medium plasticized blend extruded at 155°C which is smaller with about 60% as in the other cases (Figure 8(b)). With the exception of the medium plasticized blend extruded at 155°C, the intensity of this new band for all the other studied blends is *the same* with the absorption of starch at 997 cm^{-1} and nearly the same with the one of PVOH at 1087 cm^{-1} (Figure 8(a)). This new peak most likely results from the large starch saccharide band by 1.5 ATR units which lies between 1180 cm^{-1} and 960 cm^{-1} and has maximum at 970 cm^{-1} and from those of PVOH generated both by the skeletal vibrations and by stretching of the C-C-O group and is ranged between 1170 cm^{-1} and 950 cm^{-1} [26, 36]. This new appearing peak has also features of *appreciable spectral change* because its maximum *is shifted*

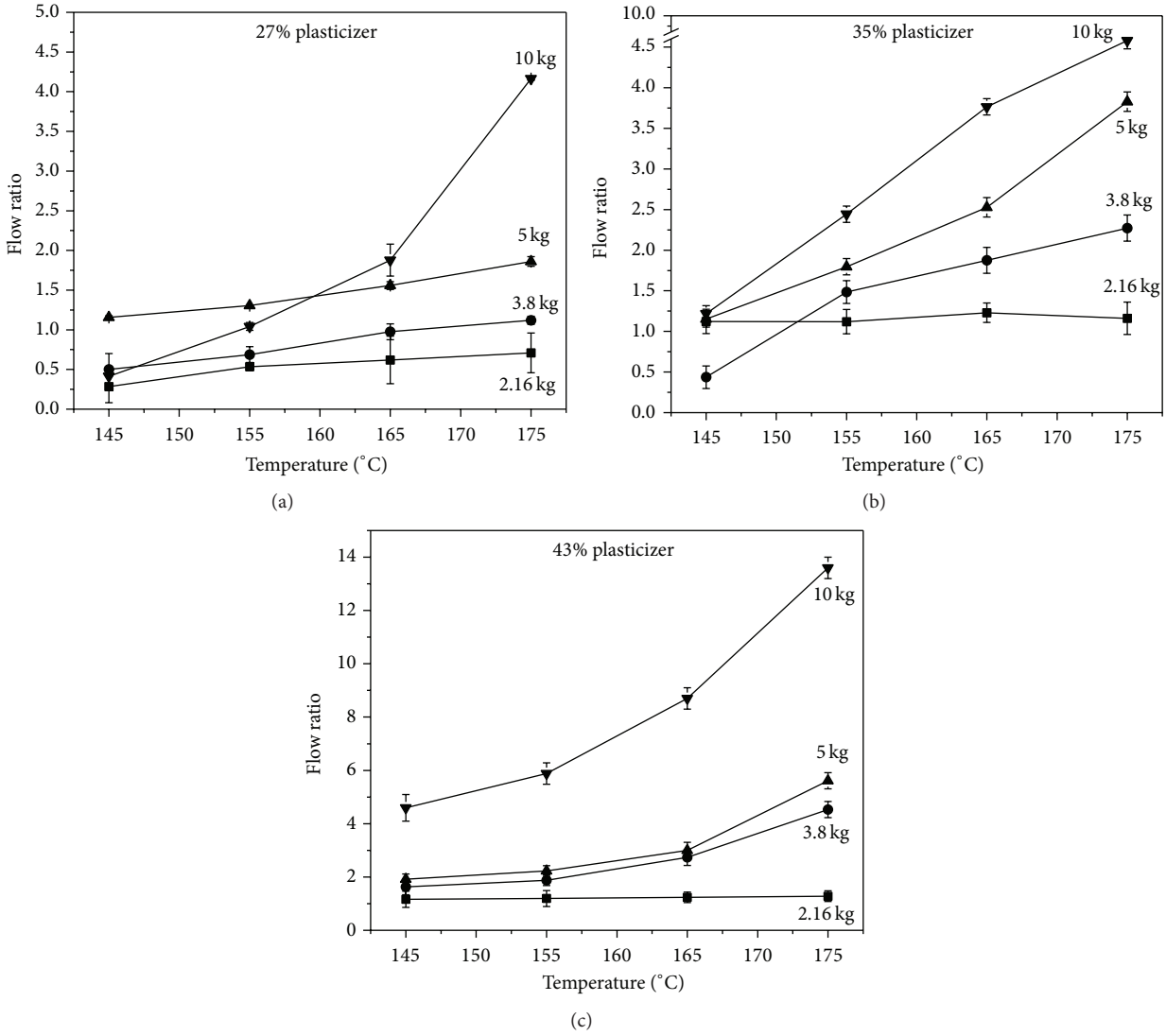

Figure 4: The dependence of flow ratio on the extrusion conditions and the plasticizing level ((a) 27%; (b) 35%; (c) 43%).

with almost 45 cm^{-1} as the maximum of the starch peak at 997 cm^{-1}.

Another *gross spectral change* registered only for the medium plasticized blend extruded at 155°C is the *disappearance of the absorption* generated by stretching and bending of the -CH_2 from PVOH with maximum at 1373 cm^{-1}, 1326 cm^{-1}, 1259 cm^{-1}, and 1246 cm^{-1} or those caused by bending and wagging of the -CH_2 and -C-H from starch with maximum at 1462 cm^{-1}, 1325 cm^{-1}, or 1243 cm^{-1} (Figure 7(b)). These spectral changes do not appear in all the other analyzed situations (Figures 7(a) and 7(b): 145°C, 165°C, and 175°C).

Another *gross spectral change* occurring only for the medium plasticized blend extruded at 155°C is the diminishing with more than 70% of the bands intensities from the PVOH at 2917 cm^{-1} and 2849 cm^{-1} generated by the -CH and the -CH_2 stretching (Figure 5(b)). For all the other cases the blends absorption is almost overlapped with the mentioned PVOH peaks (Figures 5(a) and 5(b): 145°C, 165°C, and 175°C).

A further *gross spectral change* visible only for the medium plasticized blend extruded at 155°C is represented both by the residual acetate vibration at 1715.84 cm^{-1} with shoulder at 1713.80 cm^{-1} which is smaller with about 83–89% as for PVOH (Figure 6(b)) and by the vibration of adsorbed water which is absorbed in a wide range with maximum at 1652.56 cm^{-1} and which is smaller with about 75% as for the PVOH (Figure 6(b)). The similar spectral modifications registered for all the other analyzed situations do not qualify for any changes showing the components miscibility (Figures 6(a) and 6(b): 145°C, 165°C, and 175°C).

Another *gross spectral change* appearing for the medium plasticized blend extruded at 155°C is the band generated by the stretching and bending of the -CH_2 with absorption in the range of 1418 cm^{-1}–1246 cm^{-1}. This absorption is smaller with almost 60%–80% as the similar peak from PVOH (Figure 7(b)).

A further gross spectral change visible also only for the medium plasticized blend extruded at 155°C is the absorption

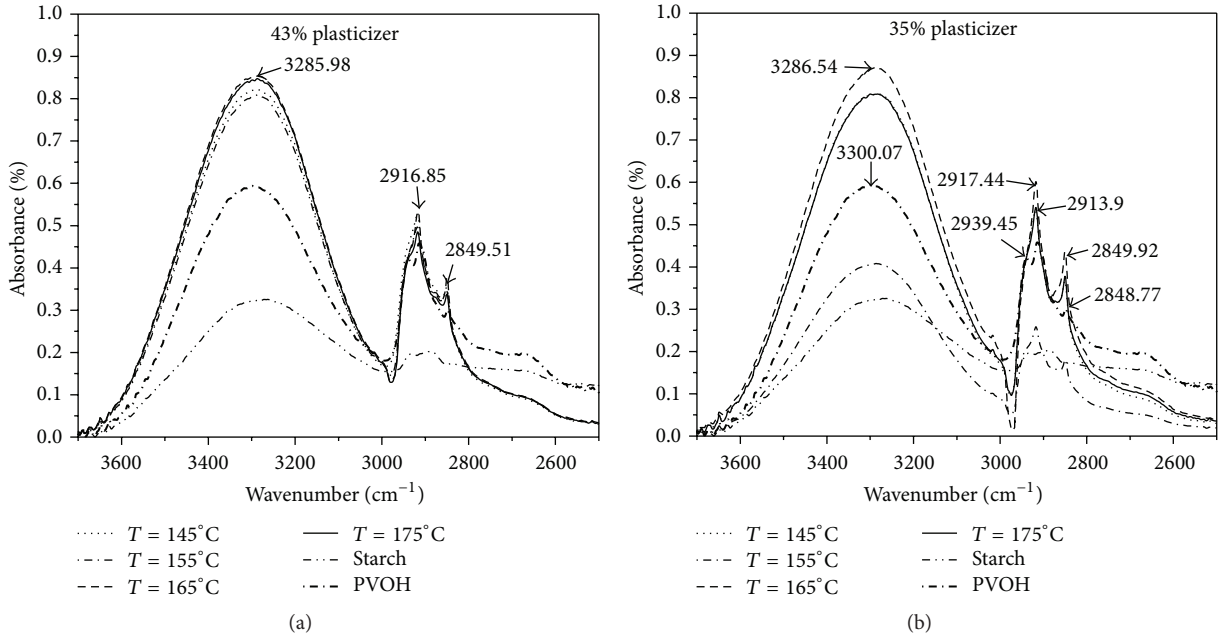

Figure 5: The dependence of ATR absorption in the absorption range of 3700 cm^{-1} to 2500 cm^{-1} on the plasticizing level ((a) 43%; (b) 35%) and the extrusion temperature (10 kg load).

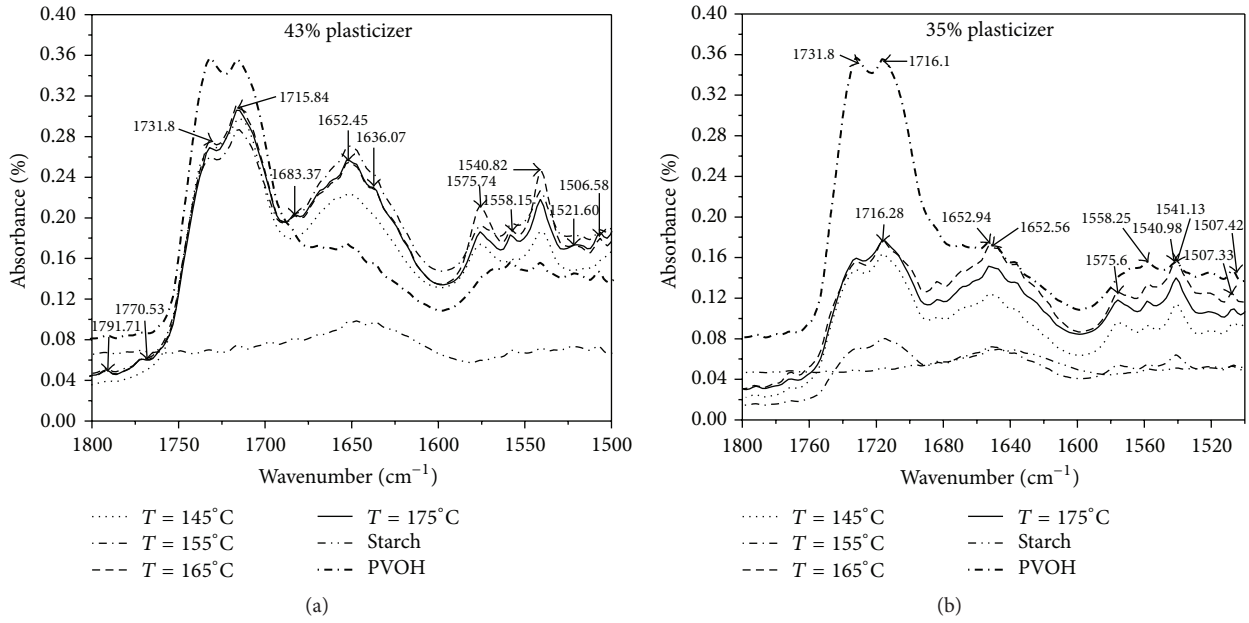

Figure 6: The dependence of ATR absorption in the range of 1800 cm^{-1} to 1520 cm^{-1} on the plasticizing level ((a) 43%; (b) 35%) and the extrusion temperature (10 kg load).

generated by the stretching vibration of the C-O-C linkage from starch at 859 cm^{-1} and by the bending vibration of -OH from PVOH at 841 cm^{-1} (Figure 8(b)). Both these blend peaks are smaller with more than 50% as the similar bands from each polymer (Figure 8(b)). The similar spectral changes which appear at these wavenumbers for the other blend and extrusion temperatures do not qualify for any spectral changes proving the component miscibility (Figures 8(a) and 8(b): 145°C, 165°C, and 175°C).

The FTIR spectra of medium plasticized blend extruded at 155°C show also *appreciable spectral changes* as larger shifting of the bands generated by the stretching vibration of the -OH at 3286 cm^{-1} which is shifted with 42 cm^{-1} as the PVOH band at 3328 cm^{-1} or with about 26 cm^{-1} as the starch peak at 3302 cm^{-1} (Figure 5(b)).

The FTIR spectra of medium plasticized blend extruded at 155°C present modifications which represent *combinations of gross with small spectral changes* as those characterizing

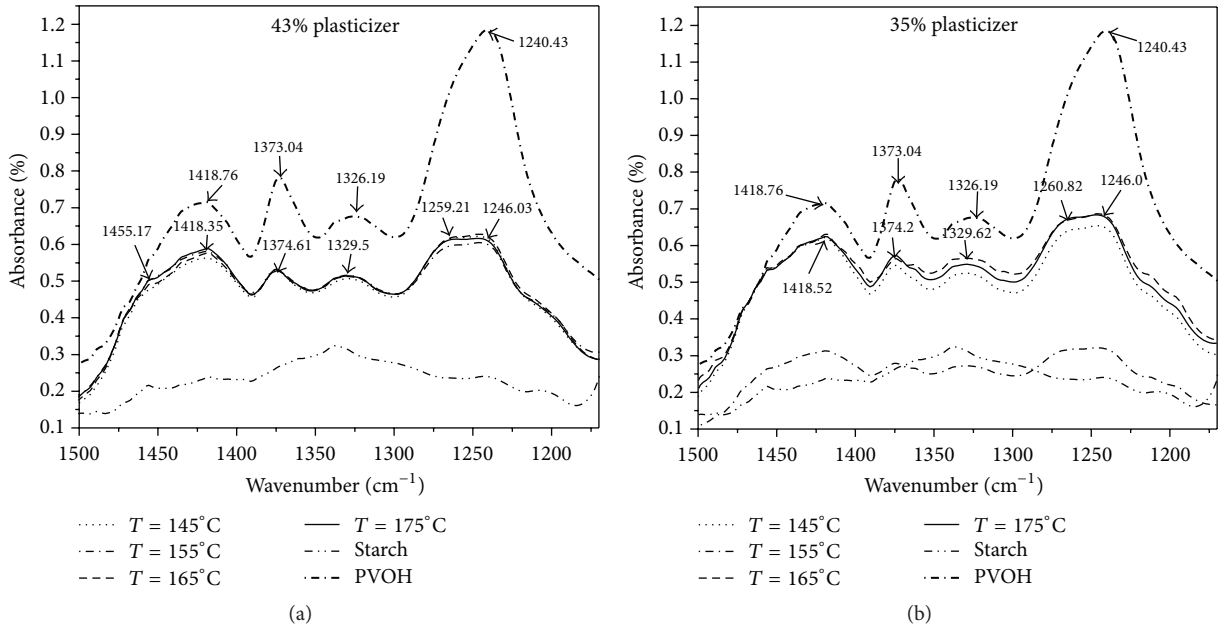

FIGURE 7: The dependence of the ATR absorption in the range of 1500 cm^{-1} to 1120 cm^{-1} on the plasticizing level ((a) 43%; (b) 35%) and the extrusion temperature (10 kg load).

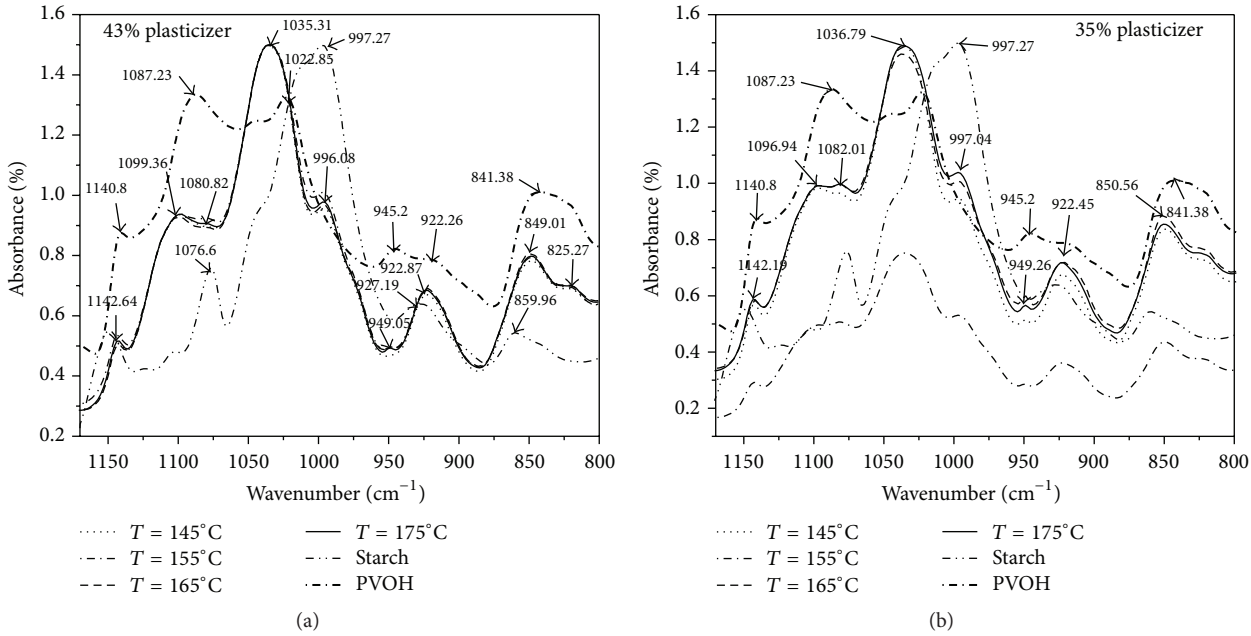

FIGURE 8: The dependence of the ATR absorption in the range of 1170 cm^{-1} to 800 cm^{-1} on the plasticizing level ((a) 43%; (b) 35%) and the extrusion temperature (10 kg load).

the stretching of the $-CH_2$ at 2849 cm^{-1} which is smaller with 50% and is shifted with 6 cm^{-1} as the similar PVOH peak (Figure 5(b)). The similar spectral changes which appear at this wavenumber for the other blend and extrusion temperatures do not mean modifications revealing component miscibility (Figures 5(a) and 5(b): 145°C, 165°C, and 175°C).

The above presented results demonstrate that the main spectral changes illustrating the component miscibility occur for medium plasticized blend extruded at 155°C. Even, in this situation, some peaks are absorbed at the same wavenumber with the two polymers; however their height is smaller with about 54%–83% as the similar peaks from the PVOH (ex. the absorption at 2918 cm^{-1}, 1541 cm^{-1}, 1142 cm^{-1}, 1036 cm^{-1}, and 850 cm^{-1}) or from the starch (at 1456 cm^{-1} or 997 cm^{-1} which in case of blends appear as shoulder at 922 cm^{-1}). These results prove that even for medium plasticized blend,

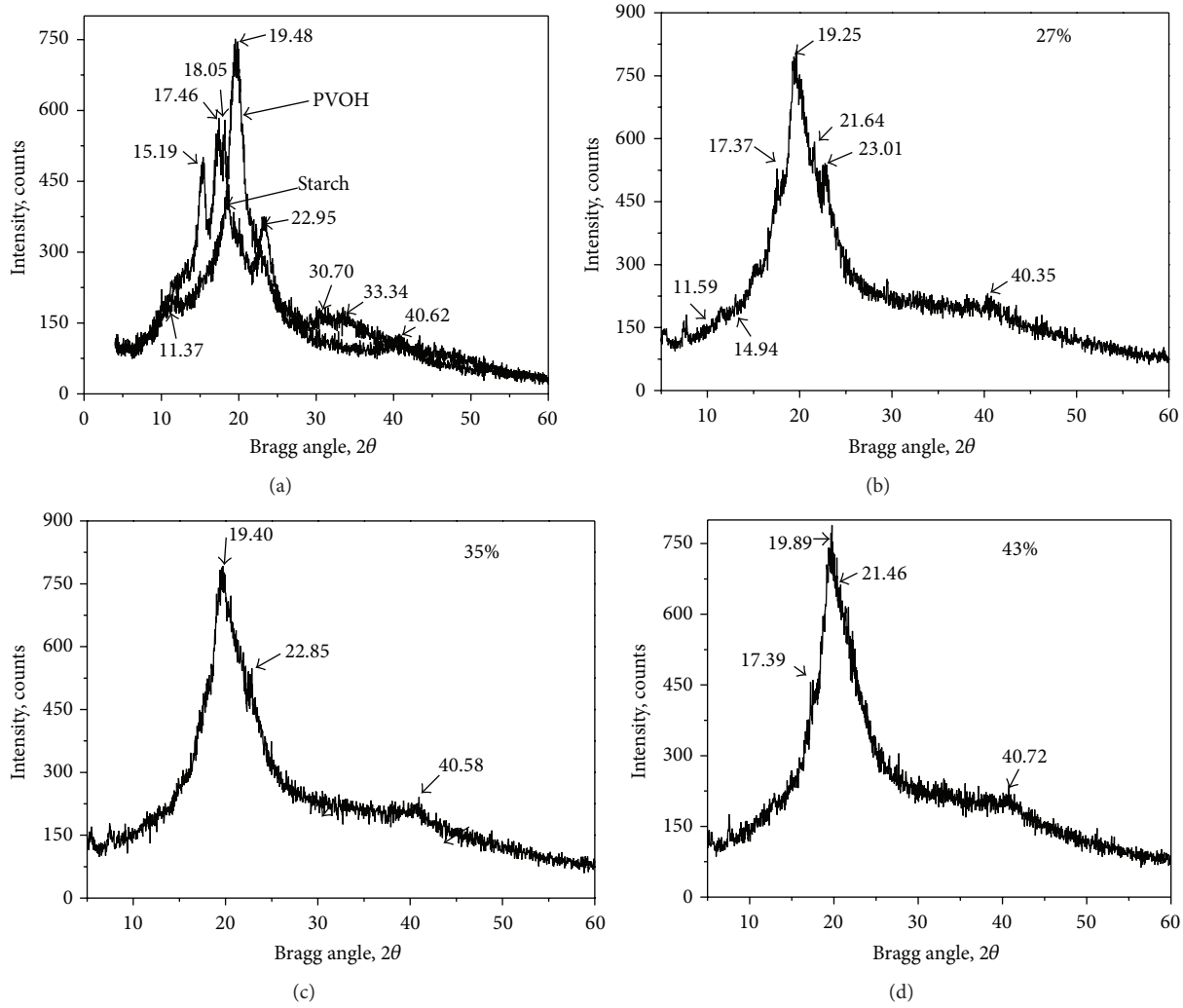

Figure 9: The diffractograms of studied blends (PVOH and starch (a); blends with plasticizing level of 27% (b); 35% (c); 43% (d)).

extruded at 155°C, the fingerprints of the two polymers are not entirely destroyed which means that the miscibility of the two polymers is not totally.

3.2.2. XRD-Retrogradation: Plasticizer Loss-Extrudates Appearance-Others. The main diffraction peak of the studied blends presents small shoulders at angles very close to those characterizing the starch diffraction, in a number depending on the plasticizing level: many at low plasticizer amount (Figure 9(b)) and a few for medium (Figure 9(c)) and high (Figure 9(d)) plasticizing levels. The mentioned shoulders (at approx. 23.01°2θ, 22.85°2θ, 21.46°2θ, 17.39°2θ, and 11.79°2θ), depending on the plasticizing degree of each blend, can be found or not on the blends diffractograms. However the main diffraction peak of each blend was registered at the same diffraction angle of around 19°2θ as for the PVOH alone. Another very small peak was registered at around 40°2θ which can represent the PVOH peak from 40.97°2θ but slightly shifted. The existence of these peaks on the blends diffractograms reminiscent from PVOH is understandable if it is considered that the PVOH represents the main matrix of the new blends and accordingly to the FTIR results it was not entirely destroyed by blending, under shear, with starch. If the amylose content of the used starch were greater, probably peaks reminiscent from starch could not be found on the blends diffractograms. The tight arrangement of starch chains between those of the PVOH was not possible almost certainly because of the uncontrolled cluster structure of amylopectin. That is why the resulting PVOH-starch compounds are microstructured materials.

If, after 8 months in the laboratory conditions, the low plasticized blend shows immediately after the obtaining the phenomenon of plasticizer leaching, the medium plasticized blend extruded at 155°C does not behave in the same way. The increase of the heating enthalpy of the low plasticized blend with about 15% immediately after obtaining shows an increase of crystallinity most likely because of retrogradation, phenomenon which generates the plasticizer leaching.

The extrudates have sharkskin appearances, without gloss (Figure 10(a)) if they were obtained from the low plasticized blend regardless of the extrusion temperatures or from the highly plasticized one extruded at low load. The only

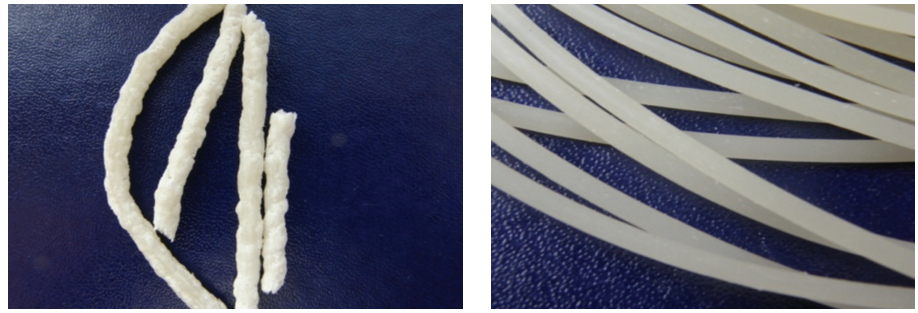

(a) (b)

Figure 10: The dependence of the extrudate surface appearance (extrusion at 155°C and 10 kg load) on the plasticizing level ((a) 27%; (b) 35%).

extrudates with gloss and smooth surface were obtained from the medium plasticized blend, extruded at 155°C and high load (Figure 10(b)).

The pellets quantity used to measure, in identical conditions, all the flow properties depends also on the plasticizing level and the obtaining conditions of the studied blends. This quantity is 235 g for the blend with medium plasticizer content and 410 g and 400 g for low and highly plasticized ones. The mechanical properties depend also on these two parameters. With the increasing of the plasticizer content the tensile strength decreases in the range of 72–38 daN/cm^2 and the break elongation increases from 418% till 520%.

These results show that the improving of the blend miscibility by finding the proper plasticizer level and the window of melt processing conditions allowed the elimination of the melt flow instability, the blend retrogradation, and the plasticizer loss.

The dependence of the miscibility on the plasticizer content and on the extrusion conditions can be explained considering the flow properties [34] of the analyzed blends. At low plasticizing level the developed shear rates are much smaller and probably not enough to well homogenize the melt which, in this condition, is less fluid and opposes a greater resistance to flow. These remarks explain the practical observations according to which the starch-PVOH blends achieved by simply blending the two polymers using a common Brabender roller sequence loss of the plasticizer immediately after the obtaining. If the melt homogeneity is poor as in case of the low plasticized blend probably the plasticizer amount is too small to be well dispersed between the macromolecules of the two polymers and so to be adsorbed onto the H-bonding sites of starch and PVOH. Poor melt homogeneity favors the plasticizer leaching probably because its molecules were not absorbed onto the H-bonding sites of the two polymers and the suprasaturation level was not reached [10, 22]. Poor melt homogeneity probably favors also the nonstationary flow which generates the sharkskin appearance of the extrudates. For the medium and highly plasticized blends extruded at medium and high loads, the conditions of more intense homogenization are fulfilled because both the shear rate and the melt fluidity are higher. In this situation the glycerol acts as a plasticizer because the adsorbed glycerol onto H-bonding sites of starch and PVOH had reached the suprasaturation level [10, 22]. Consequently the melt resistance to flow is lower and regardless of the extrusion temperature, the macromolecules of the two polymers behave similarly enough to ensure good miscibility. The medium plasticized blends have extrudates with smooth appearance because their melt flows in a stable manner. However the extrudates obtained from highly plasticized blend extruded at low load had no always very smooth appearance most likely because the homogenizing time was too short considering the greater plasticizer amount which must be dispersed between the other components. It should be recalled that the nonstationary flow of the poorly homogenized blend with high content of plasticizer was first revealed by the linearity of the shear rate-temperature dependency. The sudden increase of fluidity and of the flow ratio for the low plasticized blend at high thermal stress (T = 165°C–175°C) demonstrates that, in these conditions, beside the blend fluidization occurs a parallel process of macromolecules breaking which can be avoided if the extrusion temperature does not exceed 155°C.

The different melt flow properties of the studied blends explain the different pellets quantities used to measure for each blend, in the same conditions, the same melt flow properties. These quantities were twice greater for less miscible blends than the amount used for the high miscible blend represented by the medium plasticized blend extruded at high load and 155°C which proved to have the best flow properties in the melted state. The obtained results prove that the border between good and less miscibility of materials based on starch is so narrow that the best formulation and the window of melt processing must be found for each blend.

The best miscibility of the studied blends was reached for medium plasticized blend (37%) extruded at high load (10 kg) and 155°C almost certainly because only in these conditions does the melt resistance to flow have the smaller value. However, it should be noted that in case of the blend obtained using starch with great content of amylopectin the miscibility cannot be total, most likely because of the uncontrolled cluster structure of the amylopectin. The new materials were carried out with good results at various experimental levels into goods with short life which prove to have excellent application properties [35–41].

4. Conclusions

(1) The miscibility of some blends based on starch can be improved by finding for each of them the melt resistance to flow at which the nonstationary flow and the melt degradation are avoided and the developed shear rate can optimally homogenize the composition. The blends with improved miscibility do not show retrogradation and plasticizer leaching and flow in a molten state in a stable manner and because of this the resulting extrudates have smooth and glossy surface.

(2) The border between good and less miscibility for process sensitive materials like starch is so narrow that the best formulation and the window of melt processing must be found for each blend.

(3) The improving of miscibility by controlling the melt resistance to flow proves to be a good method to avoid the retrogradation and the plasticizer leaching and so to control the time behavior of materials based on starch during their usage.

Conflict of Interests

The authors declare that there is no conflict of interests regarding the publication of this paper.

Acknowledgments

These researches were supported by the Executive Agency for Higher Education, Research, Development and Innovation Funding (UEFISCDI), Romania, by Grant no. 59/2012. The authors thank the colleagues who carried out the experiments and prepared the rheological graphics.

References

[1] T. Mekonnen, P. Mussone, H. Khalil, and D. Bressler, "Progress in bio-based plastics and plasticizing modifications," *Journal of Materials Chemistry A*, vol. 1, no. 43, pp. 13379–13398, 2013.

[2] R. Gachter and H. Muller, *Plastics Additives*, Hanser-Gardner Publications, 2nd edition, 1987.

[3] L. H. Sperling, *Polymeric Multicomponent Materials*, Wiley-Interscience, 1997.

[4] G. Strobl, *The Physics of Polymers: Concepts for Understanding their Structures and Behavior*, Springer, Berlin, Germany, 1996.

[5] R. P. Wool, "Polymer entanglements," *Macromolecules*, vol. 26, no. 7, pp. 1564–1569, 1993.

[6] H. Ishida, "Miscibility," in *Encyclopedia of Polymer Science and Engineering*, John Wiley & Sons, 1989.

[7] L. A. Utracki, "Polymer alloys and blends. State of the art," *Polymer Networks & Blends*, vol. 1, no. 2, pp. 61–69, 1991.

[8] E. Chiellini, A. Corti, S. D'Antone, and R. Solaro, "Biodegradation of poly (vinyl alcohol) based materials," *Progress in Polymer Science*, vol. 28, no. 6, pp. 963–1014, 2003.

[9] C. A. Finch, *Polyvinyl Alcohol. Properties and Aplications*, John Wiley & Sons, London, UK, 1977.

[10] J.-H. Yu, J.-L. Wang, X. Wu, and P.-X. Zhu, "Effect of glycerol on water vapor sorption and mechanical properties of starch/clay composite films," *Starch*, vol. 60, no. 5, pp. 257–262, 2008.

[11] J.-L. Wang, F. Cheng, and P.-X. Zhu, "Structure and properties of urea-plasticized starch films with different urea contents," *Carbohydrate Polymers*, vol. 101, no. 1, pp. 1109–1115, 2014.

[12] C. M. Chaléat, P. J. Halley, and R. W. Truss, "Study on the phase separation of plasticised starch/poly(vinyl alcohol) blends," *Polymer Degradation and Stability*, vol. 97, no. 10, pp. 1930–1939, 2012.

[13] D. Dimonie, M. Petrache, C. Damian et al., "New evidences on the process sensitivity of some renewable blends based on starch considering their melt rheological properties," *International Journal of Polymer Science*, In press.

[14] D. Dimonie, S. Radu, S. Doncea et al., "The miscibility estimation of some nanocomposites based on starch," *e-Polymers*, vol. 11, no. 1, pp. 957–970, 2011.

[15] Nolan ITU in Association with ExcelPlas Australia, *Environment Australia Biodegradable Plastics—Developments and Environmental Impacts*, Ref: 3111-01, 2002.

[16] H. A. Pyshpadass, D. B. Marx, and M. A. Hanna, "Effects of extrusion temperature and plasticizers on the physical and functional properties of starch films," *Starch*, vol. 60, no. 10, pp. 527–538, 2008.

[17] F. Xie, P. Luckman, J. Milne et al., "Thermoplastic starch: current development and future trends," *Journal of Renewable Materials*, vol. 2, no. 2, pp. 95–106, 2014.

[18] F. J. R. González, "Melt blending with thermoplastic starch," in *Thermoplastic Elastomers*, A. Z. El-Sonbati, Ed., chapter 1, InTech, Rijeka, Croatia, 2012.

[19] L. Mao, S. Imam, S. Gordon, P. Cinelli, and E. Chiellini, "Extruded cornstarch-glycerol-polyvinyl alcohol blends: mechanical properties, morphology, and biodegradability," *Journal of Polymers and the Environment*, vol. 8, no. 4, pp. 205–211, 2000.

[20] P. A. Sreekumar, M. A. Al-Harthi, and S. K. De, "Effect of glycerol on thermal and mechanical properties of polyvinyl alcohol/starch blends," *Journal of Applied Polymer Science*, vol. 123, no. 1, pp. 135–142, 2012.

[21] M. S. N. B. Salleh, N. Saadon, N. Razali et al., "Effects of glycerol content in modified polyvinyl alcohol-tapioca starch blends," in *Proceedings of the IEEE Symposium on Humanities, Science and Engineering Research (SHUSER '12)*, pp. 523–526, Kuala Lumpur, Malaysia, June 2012.

[22] S. Badilescu, *Spectroscopia in Infrarosu a Polimerilor si Auxiliarilor*, Ed.Tehnica, 1982.

[23] R. Schindler, B. Lendl, and R. Kellner, "Determination of amyloglucosidase activity using flow injection analysis with Fourier transform infrared spectrometric detection," *Analyst*, vol. 122, no. 6, pp. 531–534, 1997.

[24] ISO, "Plastics—determination of the fluidity of plastics using capillary and slit die rheometers," ISO 1133, International Organization for Standardization, 2005.

[25] ASTM International, "Standard test method for melt flow rates of thermoplastics by extrusion plastograph," ASTM D1238-10, ASTM International, West Conshohocken, Pa, USA, 2010.

[26] A. Garton, *Infrared Spectroscopy of Polymer Blends, Composites and Surfaces*, Hanser Publishers, 1992.

[27] E. Franco-Marquès, J. A. Méndez, J. Gironès, M. P. Ginebra, and M. A. Pèlach, "Evaluation of the influence of the addition

of biodegradable polymer matrices in the formulation of self-curing polymer systems for biomedical purposes," *Acta Biomaterialia*, vol. 5, no. 8, pp. 2953–2962, 2009.

[28] Dynisco Polymer Test Systems, LMI 4000 Series Melt Indexer Manual, Version 3.1., http://www.dynisco.com/.

[29] V. Jinescu, *Proprietatile Fizice si Termodinamica Materialelor Plastice*, Tehnica, Bucharest, Romania, 1979.

[30] S. Zepnik, S. Kabasci, R. Kopitzky, H.-J. Radusch, and T. Wodke, "Extensional flow properties of externally plasticized cellulose acetate: influence of plasticizer content," *Polymers*, vol. 5, no. 3, pp. 873–889, 2013.

[31] C.-A. Lin and T.-H. Ku, "Shear and elongational flow properties of thermoplastic polyvinyl alcohol melts with different plasticizer contents and degrees of polymerization," *Journal of Materials Processing Technology*, vol. 200, no. 1–3, pp. 331–338, 2008.

[32] A. Peacock, *Handbook of Polyethylene: Structures, Properties and Applications*, CRC Press, 2000.

[33] H. A. Barnes, *A Handbook of Elementary Rheology*, Institute of Non-Newtonian Fluid Mechanics, London, UK, 2000.

[34] M. Tuley, *Design Engineering Manual*, Elsevier, Butterworth-Heinemann, 2010.

[35] O. Sadiku-Agboola, E. R. Sadiku, A. T. Adegbola, and O. F. Biotidara, "Rheological properties of polymers: structure and morphology of molten polymer blends," *Materials Sciences and Applications*, vol. 2, no. 1, pp. 30–41, 2011.

[36] D. Dimonie, I. Kelnar, and R. Socoteanu, "The influence of miscibility and micro-structure on the surface defects of some starch bio-hybrids," *Materiale Plastice*, vol. 47, no. 4, pp. 486–491, 2010.

[37] D. Dimonie, C. Radovici, R. M. Coserea, S. Gârea, and M. Teodorescu, "The polymer molecular weight and silicate treatment influence upon the morphology of nanocomposites for food packaging," *Revue Roumaine de Chimie*, vol. 53, no. 11, pp. 1017–1026, 2008.

[38] D. Dimonie, C. Radovici, I. Trandafir et al., "Some aspects concerning the silicate delamination for obtaining polymeric bio-hybrids based on starch," *Revue Roumaine de Chimie*, vol. 56, no. 7, pp. 685–690, 2011.

[39] D. Dimonie, I. Trandafir, M. Petrache et al., "Composition and procedure for obtaining biodegradable cell packaging," Patent Ro no. 3/143/30.12.2013A/01202/23.11.2011.

[40] D. Dimonie, R. Constantin, G. Vasilievici, M. C. Popescu, and S. Garea, "The dependence of the XRD morphology of some bionanocomposites on the silicate treatment," *Journal of Nanomaterials*, vol. 2008, Article ID 538421, 7 pages, 2008.

[41] C. Vasile, A. Stoleriu, M.-C. Popescu, C. Duncianu, I. Kelnar, and D. Dimonie, "Morphology and thermal properties of some green starch/poly(vinyl alcohol)/montmorillonite nanocomposites," *Cellulose Chemistry and Technology*, vol. 42, no. 9-10, pp. 549–568, 2008.

Hindawi Publishing Corporation
International Journal of Polymer Science
Volume 2015, Article ID 173193, 12 pages
http://dx.doi.org/10.1155/2015/173193

Research Article

Conditions to Prolonged Release of Microencapsulated Carvacrol on Alginate Films as Affected by Emulsifier Type and PH

Silvia Matiacevich,[1] Natalia Riquelme,[1] and María Lidia Herrera[2]

[1]*Departamento de Ciencia y Tecnología de los Alimentos, Facultad Tecnológica, Universidad de Santiago de Chile, Obispo Umaña 050, Estación Central, 9170201 Santiago, Chile*
[2]*Instituto de Tecnología en Polímeros y Nanotecnología ITPN (UBA-CONICET), Facultad de Ingeniería, Universidad de Buenos Aires, Avenida Las Heras 2214, Ciudad Autónoma de Buenos Aires, Argentina*

Correspondence should be addressed to Silvia Matiacevich; silvia.matiacevich@usach.cl

Received 23 July 2015; Revised 13 October 2015; Accepted 20 October 2015

Academic Editor: Dilip Depan

Alginate from algal biomass is used as edible film and the incorporation of antimicrobial agents improves its performance to increase the shelf-life of fresh foods. However, environmental conditions and intrinsic properties of films influence their release. The aim of this study was to investigate the effect of the concentration and type of encapsulating agent and pH of emulsions on the physical and antimicrobial properties of alginate-carvacrol films. Films containing alginate, carvacrol as antimicrobial agent, and Tween 20 or trehalose (0.25 and 0.75% w/w) as encapsulating agents were obtained from suspensions at pH 4 and pH 8. Physical characterization of emulsions and films and antimicrobial properties (*E. coli* and *B. cinerea*) was evaluated. Results showed that droplets size depended on trehalose concentration, but emulsion stability depended on pH and type of encapsulating agent, being more stable samples with trehalose at pH 4. Although films with Tween 20 presented the highest opacity, they showed the best antimicrobial properties at initial time; however, during storage time, they lost their activity before samples with trehalose and relative humidity (RH) was the principal factor to influence their release. Therefore, sample formulated with 0.25% trehalose at pH 4 and stored at 75% RH had the best potential as edible film for fresh fruits.

1. Introduction

Edible films and coatings can be considered an additional stress factor for preserving food products, assuring its quality as well as an increased shelf-life. The use of edible films is gaining importance in the protection and preservation of fresh food, as they have the ability to contain antimicrobial active ingredients and compounds that can prolong their shelf-life and reduce the risk of pathogen growth on its surface [1–6]. Films and coatings can support antimicrobials agents, but matrix structure stability, concentration of the product on the surface, and gradual release into food are all important characteristics for its functionality; therefore it is important to take into account these characteristics in the use of films or coatings [2].

In development of active edible films and coatings with antimicrobial properties, addition of essential oils (EOs) from herbs and spices has been extensively used as antimicrobial agents. In this sense, Rojas-Graü et al. [7, 8] evaluated the antimicrobial activities against *E. coli* O157:H7 of several EOs (oregano, cinnamon, and lemongrass) and active oil compounds (OCs), such as carvacrol, cinnamaldehyde, and citral, incorporated on alginate-apple puree edible film in concentrations lower than 0.5% w/w. In those systems, carvacrol exhibited the strongest antimicrobial activity as measured by the film disk agar diffusion assay as a qualitative test for antimicrobial activity of the films. Besides, optimal antimicrobial effects were observed using carvacrol concentration of 1.0% w/w added to the initial apple [9] and tomato [10] films preparation against *E. coli* O157:H7.

Hernández-Ochoa et al. [11] studied cumin, clove, and elecampane essential oils added to chitosan films, reporting that clove EO (2% w/w) can be considered for the preparation of active packing material. In addition, antioxidant properties from EOs are reported in gelatin based edible films [12]. Many studies are conducted in order to improve shelf-life of many fresh foods using EOs and OCs added to edible films or coatings. For example, for refrigerated chicken meat, rosemary oil incorporated into cellulose acetate based film was successfully used [13]. Oregano and clove oil added into whey protein isolate coating [14] and thyme oil in alginate coating were also investigated [15]. It was reported that films and coatings based on alginate containing cinnamon, palmarosa, and lemongrass and their main OCs improved the shelf-life and safety of fresh-cut "Piel de Sapo" melon [16] and that films containing eugenol and citral as OCs reduced microbial spoilage and preserved sensory properties of *Arbutus unedo* L. berries fruit [17]. Besides, lemongrass, oregano, and vanillin oil incorporated into an apple puree-alginate edible coatings were used for extending shelf-life of fresh-cut "Fuji" apples [18]. However, despite the lipophilic and volatile nature of the above mentioned compounds (EOs and OCs), authors did not use any type of emulsifier or encapsulating agent. It is important to remark that they can evaporate easily and decompose during preparation of these films and coatings, due to direct exposure to heat, pressure, light, or oxygen [19]. Carvacrol, the major component (50–86%) of oregano essential oil (*Origanum* sp.) [20, 21], is a phenolic compound. Its antimicrobial properties have been demonstrated in numerous studies also against bacteria [7–10, 22–25], mold [25, 26], and yeast [25, 27].

Edible films and coatings are based on proteins, polysaccharides, and lipids [28]. Among widely used polysaccharides, alginates are natural polysaccharides extracted from brown algal biomass (Phaeophyceae), and it is a salt of alginic acid composed of two uronic acids: β-D-mannuronic acid (M) and α-L-guluronic acid (G). Principal applications are based on its gel-forming ability through calcium interactions, as food additives (E400$\cdots$E405 in Europe) and in the last years as principal matrix of edible films and coatings [5, 7, 8, 15–18, 22, 29–32]. Taking into account that alginate films are hydrophilic matrices, the crosslinking process with polyvalent cations as calcium has been used to improve their water barrier properties, mechanical resistance, cohesiveness, and rigidity [31, 32]. Benavides et al. [22] suggested that physical, mechanical, and antibacterial properties of alginate films can be modified by controlling the level of internal crosslinking produced by the addition of $CaCO_3$. Therefore, the addition of $CaCO_3$ as crosslinker matrix in this study instead of $CaCl_2$ could permit a slower rate of diffusion of carvacrol into the agar as a result of the higher level of internal crosslinking achieved by the alginate matrix [22].

In order to maintain the antimicrobial properties in the film during prolonged time, encapsulation of lipid compounds (OCs) could be used, which improves the stability of the lipid, since it is a medium that provides physical protection against oxidation without antioxidants; therefore, the choice of encapsulating agent and/or emulsifier is critical, which influences the stability of the emulsion [33]. Tween 20 has been reported to be the most widely used emulsifier in the formation of emulsions and nanoemulsions [15], while the physicochemical properties of trehalose have been reported to be very promising concerning its use for microencapsulation [33]. In the other way, the storage conditions could also affect both physical and antimicrobial properties of the film [34, 35].

It is important to remark that the processing conditions of film forming suspensions, film composition, and the possible interactions between the film forming biopolymer and the other food components present in the matrix could affect additive migration and, as a consequence, its effectiveness as antimicrobial. For some applications, a quick release of the antimicrobial is required to control microbial growth in food. On the contrary, in other applications, a slow release is required so as to assure a certain level of the preservative at the surface to control the external contamination. The determination of the rate of release together with the evaluation of antimicrobial activity through the time might help to optimize the development of films and coatings as a potential active packaging material. One of the experimental design techniques to achieve this aim is the central composite rotatable design (CCRD) of response surface methodology (RSM), an effective and versatile methodological tool for the determination of optimum levels of the processing variables for the parameters studied.

Therefore, the aim of this study was to evaluate the effect of the type of emulsifier on physical, optical, and morphological properties together with antimicrobial (antibacterial and antifungal) gradual activity of alginate based films containing carvacrol during different storage conditions, in order to obtain a prolonged release of the antimicrobial agent as potential applications on coating active material. The central composite rotatable design (CCRD) of RSM was used as a statistical method to optimize the storage conditions of edible films, maximizing inhibition of bacterial growth and minimizing variation of optical properties.

2. Materials and Methods

2.1. Materials. The materials used for film formation included food-grade sodium alginate purchased from Sigma-Aldrich Chemical Co. (St. Louis, MO, USA); sorbitol (used as a plasticizing agent) obtained from Blumos (Santiago, Chile); calcium carbonate used in the crosslinking process and purchased from Winkler Ltda. (Santiago, Chile). The antimicrobial agent used in the present work was carvacrol (282197, Aldrich Company, Inc., USA) with a purity of ≥99.5%. Two different encapsulating agents were used: a synthetic one, Tween 20 (used as a surfactant) from Merck Co. (Darmstadt, Germany), and a natural one, trehalose (Blumos, Santiago, Chile). Sodium hydroxide (Aldrich Company, Inc., USA) was used to adjust pH of film forming emulsions. All reagents were analytical grade.

2.2. Microorganisms and Media. Antimicrobial characteristics of different films were measured following growth of *E. coli* (ATCC 25922), obtained from the Institute of Public Health (ISP, Santiago, Chile).

Antifungal activity of edible films was evaluated against *Botrytis cinerea*, which causes the grey mould disease and is one of the most serious diseases of a wide range of crops of worldwide importance. Postharvest losses are important due to development of this fungus during the storage and distribution of harvesting fruits [36]. *B. cinerea* were isolated from spoiled blueberries var. *Brigitta*, bought in local market (Santiago, Chile), and were inoculated on PDA medium (Potato Dextrose Agar, Biokar Diagnostics, France) and incubated at 25°C for 7 days until obtaining a pure culture (2 inoculations). Amongst the isolated strains, *Botrytis cinerea* were identified at the laboratory according to macroscopic criteria [36], and fresh cultures of 5 days were used for antifungal measurements.

2.3. Film Forming Emulsions (FFE) and Film Casting. Film forming emulsions using distilled water as solvent were prepared based on the following: 1% w/w sodium alginate, 1% w/w sorbitol (as plasticizer), and the antimicrobial agent carvacrol 0.5% w/w (concentration obtained previously through minima inhibition concentration (MIC), taking into account the presence of 1% w/w sodium alginate). Encapsulating agents were incorporated into FFE as the following concentrations: 0.25 and 0.75% w/w of trehalose and 1% w/w of Tween 20. Lower concentrations of encapsulating agents did not allow droplets formation, while higher concentrations of them modified opacity or visual appearance of films, which could affect organoleptic characteristics of the products coated with these FFE. These FFE were homogenized at room temperature for 1 min at 10.000 rpm using homogenizer (Ultraturrax Thristor Regler TR50, Germany). Then, calcium carbonate 0.02% w/w (as alginate crosslinker agent) was added using magnetic stirrer and the pH was adjusted at 4 and 8. The selected pH is the endpoints of the interval growth of both microorganisms. Vacuum was then applied in suspensions to remove bubbles. Films were obtained by warm casting; briefly 40 mL of FFE was put on Petri plates 9 cm in diameter and dried in an oven at 40°C for 20 h. Dried films were peeled from the casting surface. The thickness of each film was measured with a micrometer (Mitutoyo, Japan). Measurements were taken at five different places on the film and an average value of 0.12 ± 0.02 mm, showing uniform films.

These samples were used for determinations of physicochemical and antimicrobial properties of the films during storage time.

2.4. Characterization of FFE

2.4.1. Diameter Size of Droplets. One of the most important properties to characterize the FFE is the interfacial area of the droplets or average diameter of them, which is represented by Sauter diameter (D_{32}) [37]. It was estimated using (1) [38]. The average droplet diameter of the different FFS was calculated from images in an optical microscope with a calibrated scale at 40x (Carl Zeiss, Germany) using Motic Images Plus (v.2.0, Digital Microscopy Software, Motic China Group Co., Ltd.). At least 100 droplets were measured by quintuplicate of each FFE and the mean of data with their corresponding standard deviation is reported:

$$D_{32} = \frac{\sum_{i=0}^{n} n_i d_i^3}{\sum_{i=0}^{0} n_i d_i^2}, \quad (1)$$

where D_{32} is average droplet diameter Sauter, n_i is number of drops, and d_i is internal diameter (μm).

2.4.2. Stability of Emulsion. The stability of FFE was analyzed using a vertical scan analyzer Turbiscan MA 2000 (Formulaction, France) at different times during storage at 40°C. The samples were put in a cylindrical glass measurement cell and the backscattering (BS) profiles as a function of the sample height (total height = 70 mm), acquiring data every 40 μm, were studied in quiescent conditions at 23 ± 2°C. In this way, physical evolution of this process is followed without disturbing the original system and with good accuracy and reproducibility. Measurements were performed immediately after preparation of the emulsions by triplicate. Global stability was followed by measuring the BS mean values as a function of storage time in the middle zone of the tube [39]. The optimum zone was the one where no significant transmitted light was detected, that is, 20–60 mm for all samples.

2.5. Characterization of Films

2.5.1. Moisture Content. Moisture content of films was determined by gravimetric methodology, using an analytical balance (Mettler Toledo, Switzerland) and an oven (Wiseven Daihan Scientific WOF-105, Korea) at 105°C for 24 h until reaching constant weight (differences less than 0.5%). The analysis was performed by quadruplicate and the moisture content was expressed in % wet basis (g water/100 g wet sample) as the main value with their corresponding standard deviation.

2.5.2. Color and Opacity. The visual properties of the films can affect appearance of the products and determine acceptability for consumers. Digital images from each film (white and black background) were captured through a computer vision system (CV) setup, which consisted of a black box with four natural daylight (D65) tubes of 18 W (Philips) and a camera (Canon 14 MP PowerShot G3) placed in vertical position at 22.5 cm from samples. The camera lens angle and light were 45°, according to Pedreschi et al. [40] and Matiacevich et al. [41]. All images were acquired at the same conditions; the camera was remotely controlled by ZoomBrowser software (v6.0 Canon). Camera was calibrated using 30 color charts with a Minolta colorimeter [41]. Color data were obtained in the RGB (red-green-blue) space using Adobe Photoshop v7.0 program and convert into CIEL$^*a^*b^*$ space standard. Therefore, values of color parameters, lightness (L^*), and chromaticity parameters a^* (red–green) and b^* (yellow–blue), of each film obtained from image analysis, were equal as those values from the colorimeter. Variation of colors between each films and control film (without carvacrol) was calculated using CIEDE2000 equation [42, 43].

Film opacity is a critical property of the film if the film or coating is to be used over the surface of food. The opacity is indicative of the amount of light that can pass through the material and was determined by the Hunter lab method, using the values of lightness (L^*) obtained from the films using white (L^* white) and black (L^* black) background:

$$\text{Opacity} = \frac{L^* \text{ black}}{L^* \text{ white}}. \quad (2)$$

Data reported were the average of five films of each sample with their corresponding standard deviation.

2.5.3. Percentage of Carvacrol Release by DSC. The percentage of release (%R) of pure carvacrol from films was determined as the ratio of the fusion enthalpy of films containing carvacrol at time zero, already formed (corrected according to the water content of the samples), and the fusion enthalpy of the pure compound, as indicated in (3) [44]. The fusion enthalpy was determined by differential scanning calorimeter (DSC Diamond, Perkin Elmer, USA). The range of working temperatures was −50°C to 80°C with a heating rate of 10°C/min and cooling rate of 40°C/min. Samples films (~10 mg) were placed in hermetically sealed capsules:

$$\%R = \frac{\Delta H_S}{\Delta H_0}, \quad (3)$$

where ΔH_S is heat of melting of carvacrol in the film and ΔH_0 is heat of melting of pure carvacrol.

The calculated confidence interval for a 95% certainty was between 5% and 7% of the absolute values.

2.5.4. Molecular Mobility. Transversal or spin-spin relaxation times (T_2) were used to determine water and solids mobility and were measured by time resolved ^{1}H-NMR in a Bruker Minispec mq20 (Bruker Biospin Gmbh, Rheinstetten, Germany) with a 0.47 T magnetic field operating at a resonance frequency of 20 MHz and at 30°C. Proton populations of different mobility were measured using the free induction decay (FID) for protons from solid matrix or from water strongly interacting with the solid matrix [45], under the following conditions: pulse sequence employing a 2.74 μs, 90° pulse length and a 5.06 μs 180°, 4 scans, and relaxation delay of 2 s.

Films were placed in 10 mm diameter glass tubes (to 5 cm height) and were previously equilibrated at 30.00 ± 0.01°C in a thermal bath (Haake, model Phoenix II C35P, Thermo Electron Corp., Germany). The FID test itself is very fast, taking 10 s, and samples could be measured without appreciable temperature modification. The decay envelopes were fitted to monoexponential behavior.

2.5.5. Microstructural Characteristics of Surface (SEM). Scanning electron microscopy (SEM, Supra 40, Carl Zeiss NTS) is used to evaluate microstructural characteristics of the surface and cross sections of all films such as film homogeneity and surface smoothness. Dried samples (5 × 3 mm) were mounted on specimen stubs. Samples were freeze-dried, platinum coated, and observed using an accelerating voltage of 15 kV. For cross section observation, the samples were previously fractured using liquid nitrogen.

2.5.6. Surface Hydrophobicity. The surface hydrophobicity of the films was determined by the drop method, based on optical contact angle method. Contact angle measurements were carried out with an optic system, which comprised zoom video lens (Edmund Optics, NJ, USA) connected to a CCD camera (Pulnix, Inc., San Jose, CA, USA), controlled via software. Drops (5 μL) of ethyleneglycol (Aldrich Co.) were manually deposited on the film surface. An image analyzer (software ImageJ with the plugin Drop Shape Analysis) was used to measure the angle formed between the surface of the film in contact with the droplet and the tangent to the droplet at the point of contact with the film surface. The measurements (in both sides of the droplet) were performed within the first 15 s after dropping ethyleneglycol onto film surfaces, to avoid variations due to solvent penetration onto the specimens. Seven measurements were performed for each film at room temperature.

2.6. Antimicrobial Properties of the Films

2.6.1. Escherichia coli. *Escherichia coli* (ATCC 25922) was stored at −20°C in Mueller Hinton broth with 20% w/w skim milk until use. Bacteria culture was obtained by an inoculum in Mueller Hinton broth (DIFCO, France) at 37°C overnight. This culture served as the inoculums for the microbiological studies. The colony-forming units (CFU) counts were accurately and reproducibly obtained by absorbance value measured by optical density at 625 nm on a spectrophotometer (Shimadzu UVmini-1240, Japan), which corresponded to a 0.5 McFarland turbidity standard solution (approximately 10^8 CFU/mL) [46], and diluted with a final concentration of 10^3 CFU/mL.

The antibacterial activity of the films with carvacrol was determined using the agar diffusion method, according to Benavides et al. [22]. Briefly, the edible films were aseptically cut into 2 mm squares and placed on Muller Hinton agar plates, which had been previously spread with 1 mL of inoculum, each containing 10^3 CFU/mL of bacterial culture. The plates were incubated at 37 ± 1°C for 24 h. The diameter of the growth inhibition zones (inhibition halo) around the films was measured using a digital caliper (VWR, USA). The growth under the film discs (area of contact with the agar surface) was visually examined. The measurements were made in quadruplicate for each film.

2.6.2. Botrytis cinerea by Vapour Contact Assay. Considering the volatile characteristic of essential oils and their components, antifungal properties were observed using vapour contact [47–50]. The effect of volatile oil fraction from films was studied with invert Petri dishes method. PDA medium was poured into 90 mm of Petri dish and spot inoculated to *Botrytis cinerea*. A film slice (1 cm size) was placed into the cover of each Petri dish, so that it does not directly touch the surface of agar medium. The space inside of the

Table 1: Coded and actual values for independent factors (X_1, X_2, X_3) with 5 levels used in the experimental (central composite rotatable (CCRD)) design.

	Coded value				
	$-\alpha$ (−1.68)	−1	0	+1	$+\alpha$ (+1.68)
	Actual values				
Factors					
pH, X_1	4.8	4	6	7.2	8
Temperature (°C), X_2	4	10	20	25	30
Relative humidity (%), X_3	75	85	87	94	100

sealed Petri dish was calculated to be 70 mm^3 of air. A positive control of fungal growth was included containing inoculated PDA medium. Inhibition percentage of growth was calculated comparing fungal growth of each sample with positive control.

2.7. Data Analysis and Modeling

2.7.1. Experimental Design and Storage Conditions. The storage conditions of films were optimized using the 3-factor-5-level central composite rotatable design (CCRD), of response surface methodology (RSM) software (Statgraphics Centurion XVII). The design required 17 runs derived from 8 combinations of the independent variables performed in random order, including 3 replicates at the central point and two axial points (one variable axis at a distance of 1.68 from the center). The 3 replicates at the central point were used to determine the experimental error and the variance and check the fit. The three depended responses (pH of FFE, relative humidity, and temperature), levels, and experimental design in terms of studied values can be observed in Table 1. The experimental points were calculated as functions of the range of interest of each factor: temperature in the range of 4–30°C in order to evaluate the possible temperatures of commercial storage, pH between 4 and 8, and relative humidity (RH) from 75 to 100% and also RH of commercial storage, using the corresponding saturated salts [51]. Optima conditions were obtained using the optimization module of RSM software for each factor and for multiple responses taking into account the minima variation of color and opacity of films and the maxima inhibition of bacteria growth. All experiments were performed in randomized order to minimize bias effect. The experimental and predicted values were compared in order to determine the validity of the developed model. The verification of model was performed similar to the method applied by previous study.

2.7.2. Statistical Analysis. ANOVA was performed to determine the differences between the encapsulating types in terms of the parameters studied using GraphPad Prism version 5.03 (GraphPad Prism Inc.). Significant differences between the emulsifier types were further analyzed using Tukey's Multiple Test (GraphPad Prism v5.03). The significance of the difference was determined at a 95% confidence level ($P < 0.05$).

3. Results

The characterization of film forming emulsions and films was evaluated in order to compare different concentrations and types of encapsulating agents (0.25 and 0.75% trehalose and 1% Tween 20) at different pH (4 and 8). Then, films were stored for 14 days in order to obtain the best conditions for prolonged release of the microencapsulated carvacrol from the films.

3.1. Characterization of Film Forming Emulsions. The droplet size of each emulsion containing thyme oil and alginate using different encapsulating agents was measured since they might have a relevant impact on features such as color and mechanical properties of edible films [29]. The mean value obtained at initial time from droplet sizes (D_{32}) was 0.6 ± 0.2 μm for samples containing 0.25% of trehalose or 1% of Tween 20 and 0.3 ± 0.2 μm for samples with 0.75% of trehalose, independently of pH of emulsions. Though the high polydispersity of droplet diameters, statistical analysis shows significant differences at 95% of confidence in the diameter of droplets between both concentrations of trehalose. The high polydispersity is related to oil polarity, different interactions between components, viscosity, and solubilization rate which can influence the resulting droplet size [29, 52, 53].

The stability of the film forming emulsions (FFE) is an important factor regarding edible coatings, especially in relation to commercialization and their application by spraying process on fresh foods. The stability of emulsions was measured at 40°C because it is the temperature of casting methodology. The instability of a colloidal dispersion increases at elevated temperatures, which is attributed to accelerated Ostwald ripening and/or coalescence processes by changes in nonionic surfactant properties [53]. Therefore, 40°C was also selected in order to accelerate the instability process. The results of analysis of emulsions stability at different pH of final FFE and different type and concentrations of encapsulating agents are shown in Figure 1. In the first place, the principal instability process observed for Tween 20 emulsions, as diminution of backscattering, was coalescence/flocculation and/or Ostwald ripening at both pH, being significantly lower at pH 4 (0.5–5%) comparing to pH 8 (5–12%). Regarding type of encapsulating agents, Tween 20 is the highest instable FFE, showing, besides, sedimentation at both pH. Comparing emulsions with different concentrations of trehalose at pH 4 it may be noticed that the destabilization mechanism was creaming for 0.25% trehalose and coalescence for 0.75% trehalose, while for pH 8 the behavior was the opposite: 0.25% trehalose destabilized by coalescence and 0.75% trehalose by creaming. These results showed the relevance of pH in emulsions components interactions.

3.2. Characterization of Films at Initial Time. Moisture content of films after casting was in the range of 12 to 18% (dry basis). No significant differences ($P > 0.05$) were found for the type of encapsulating agent, concentration, or pH of the samples.

In order to obtain the variation of color of films (CIEDE2000), color parameters (L^*, a^*, b^*, Hue, and Croma)

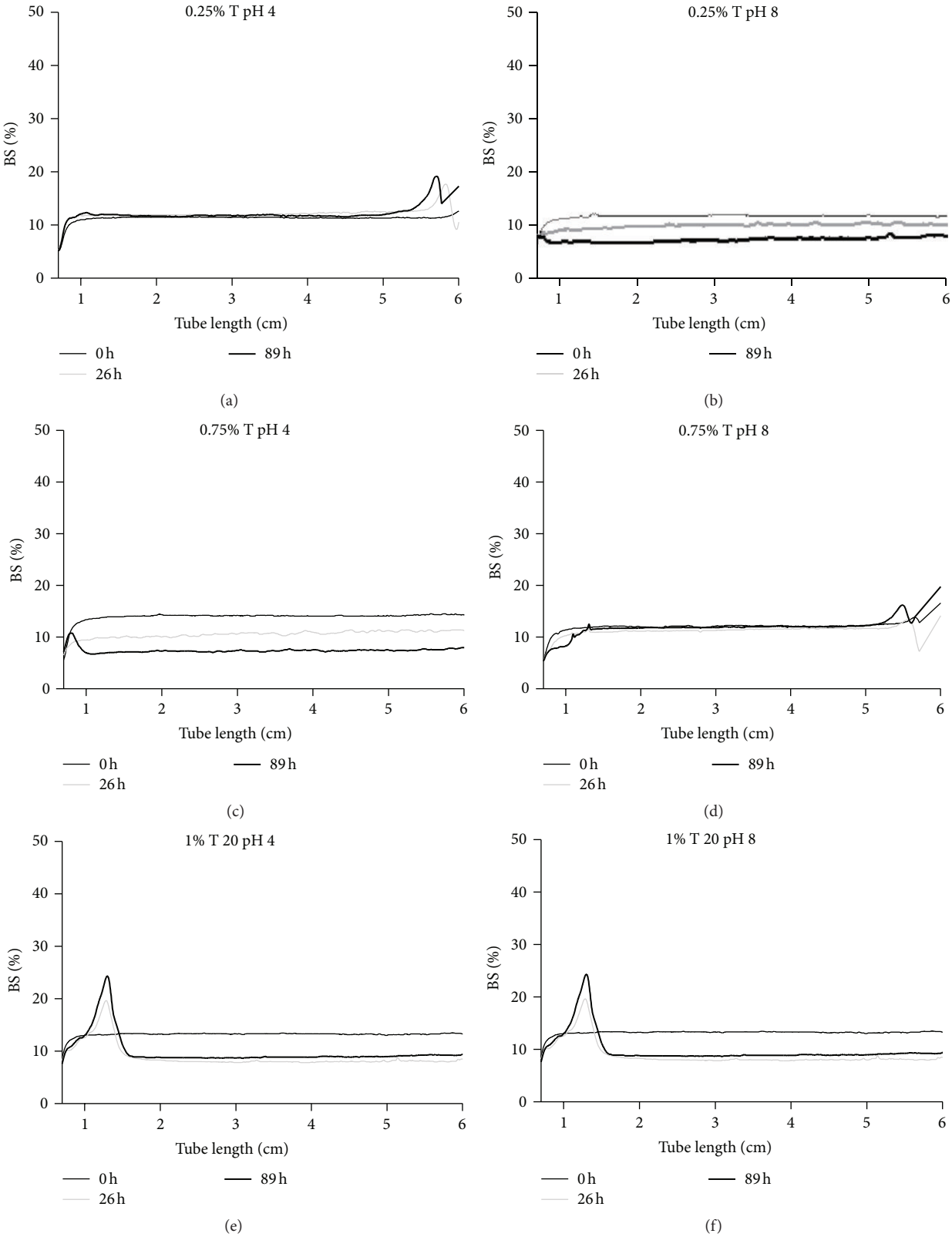

Figure 1: Stability of the emulsions stored at 40°C, comparing final pH of the emulsion and the type-concentration of the encapsulating agents. 0.25% T: 0.25% w/w trehalose; 0.75% T: 0.75% w/w trehalose; T 20: 1% w/w Tween 20.

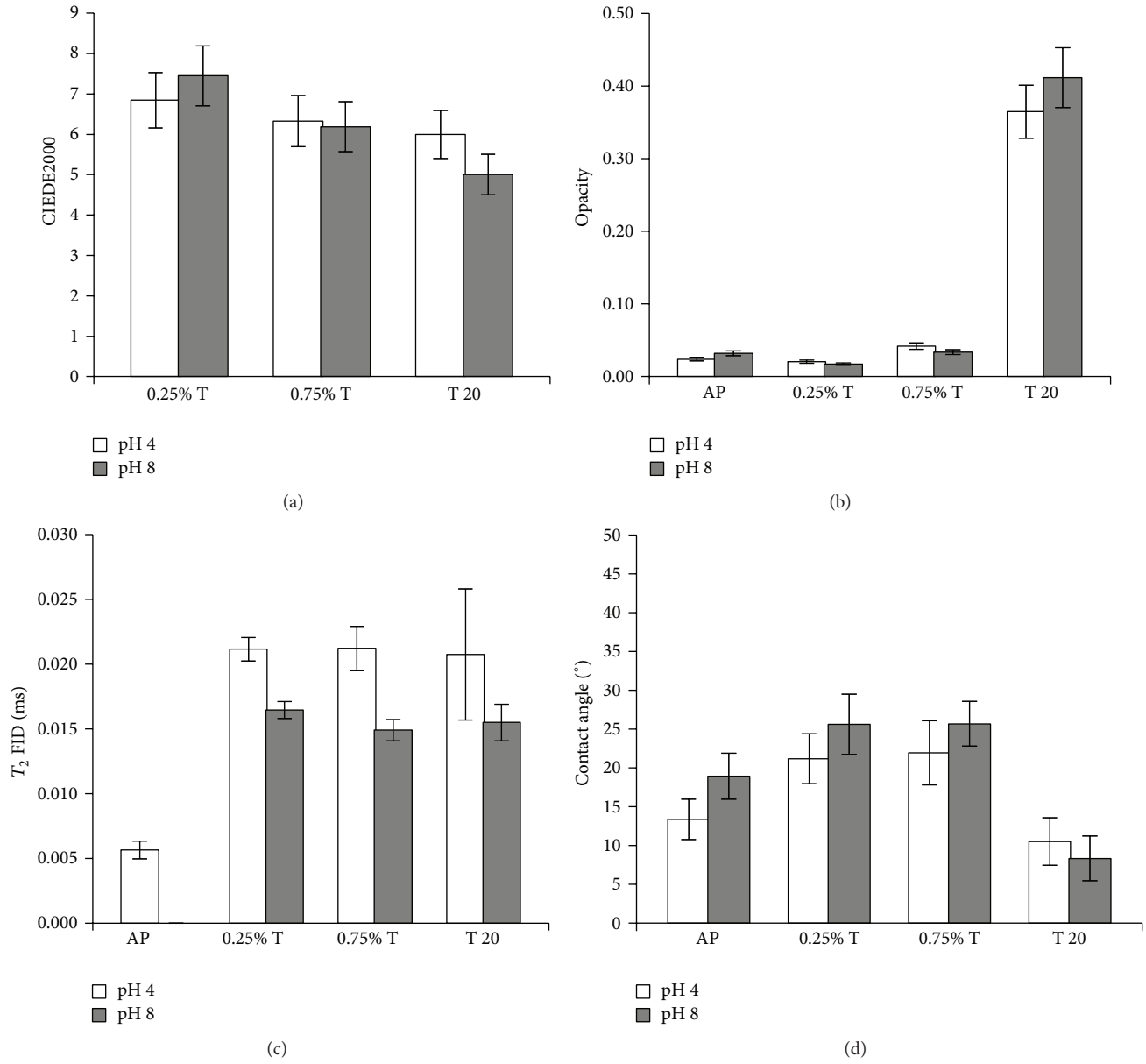

Figure 2: Characterization of each film at initial time at different pH: (a) variation of color (CIEDE2000), (b) opacity, (c) molecular mobility by T_2 FID, and (d) contact angle. Bars correspond to standard deviation of mean value. 0.25% T: 0.25% w/w trehalose; 0.75% T: 0.75% w/w trehalose; T 20: 1% w/w Tween 20.

of films were compared with control film (without antimicrobial and encapsulating agents) [42, 43]. Figure 2(a) shows significant differences ($P < 0.05$) between types of encapsulating agent, but not by pH of films. All studied films showed color variations higher than 5, indicating perceptible changes on color comparing to control [54].

Opacity, calculated using (2), was also affected by type of encapsulating agent and not by pH of films (Figure 2(b)). Films containing Tween 20 presented higher opacity (value of 0.35–0.45) than the other agents (lower than 0.05), which are considered transparent [55]. This result was attributed to sedimentation in emulsions as observed in Figures 1(e) and 1(f), which subsequently affected formation of the film, principally in opacity. In other way, molecular mobility of the films was affected principally by pH ($P < 0.05$), showing lower mobility at pH 8 than pH 4 (Figure 2(c)), where no significant differences ($P < 0.05$) were observed by type or concentration of encapsulating agent. Hydrophobicity of the films, measured by contact angle, was affected significantly ($P < 0.05$) by type of encapsulating agent but was not affected by pH of films (Figure 2(d)). Films containing Tween 20 showed the highest hydrophobicity, due to the nonpolar nature of Tween 20. On the other side, as expected from the hydrophilic nature of trehalose, their addition to films diminished hydrophobicity comparing to alginate films.

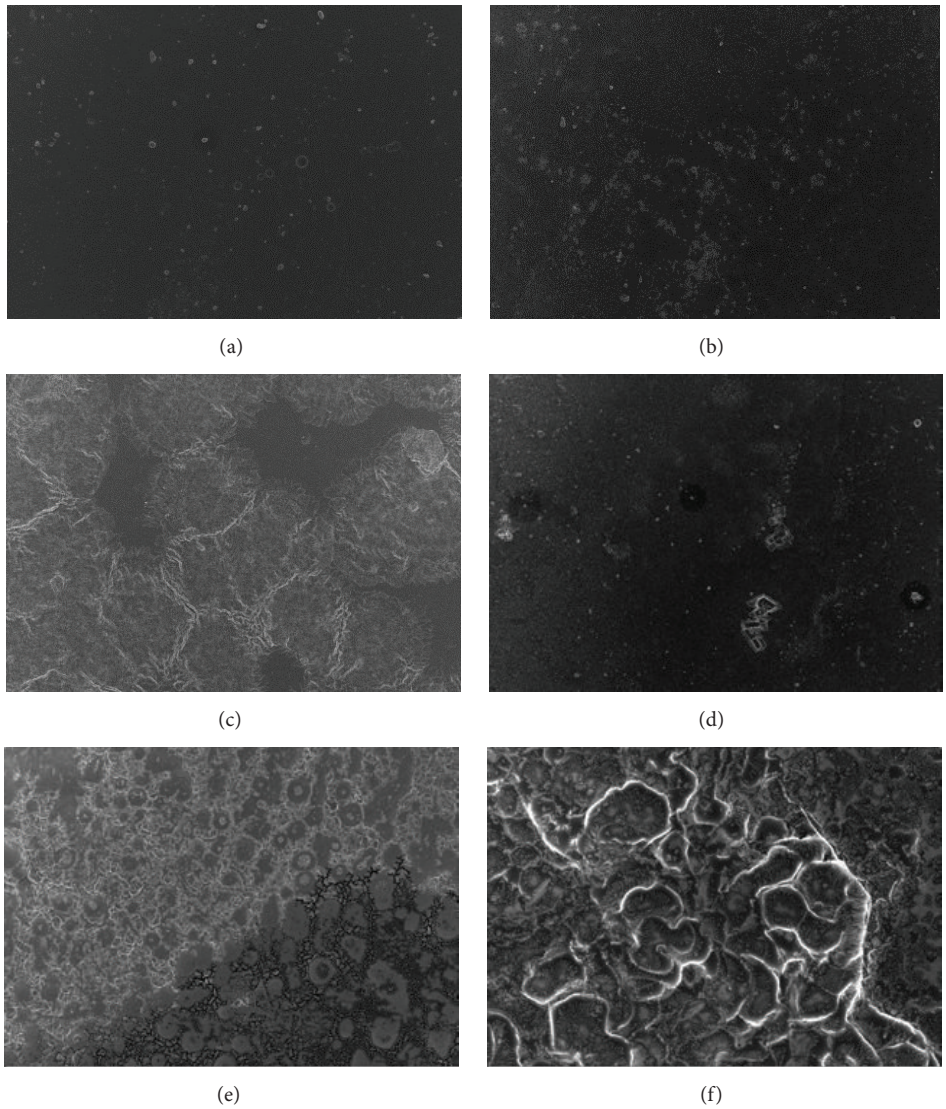

Figure 3: Scanning electron microscopy of the films at 1000x. (a) 0.25% w/w trehalose pH 4, (b) 0.25% w/w trehalose pH 8, (c) 0.75% w/w trehalose pH 4, (d) 0.75% w/w trehalose pH 8, (e) 1% w/w Tween 20 pH 4, and (f) 1% w/w Tween 20 pH 8.

Figure 3 shows the influence of type and concentration of encapsulating agents together with pH on the surface morphology of films. García et al. [56] reported that films containing lipids showed SEM images with smooth surface and compact structure, indicating an homogenous dispersion (without phase separation) of lipids in the matrix. Films containing trehalose showed a homogenous and soft structure, comparing with Tween 20, which presented a wrinkled structure. However, presence of crystals (Figure 3(d)) was observed at concentration of 0.75% of trehalose, which was associated with trehalose crystallization. Elizalde et al. [57] observed similar results during encapsulation of carotenoids by freeze-drying in a trehalose/gelatin matrix. Authors explained that sugar crystallization was influenced by water content, which promoted the release of encapsulated lipids.

The efficiency of encapsulation was measured through the % of release of carvacrol, by (3), where higher release of carvacrol indicates lower efficiency of encapsulation. The results obtained show significant differences ($P < 0.05$) between type and concentration of the encapsulating agents but not by pH. The efficiency of encapsulation was higher at 0.75% of trehalose, showing a value of 14% of carvacrol release comparing to 57% for 0.25% trehalose and 39% for Tween 20. This result is indicative that carvacrol was less released at higher concentrations of trehalose, being more encapsulated, and, therefore, it could be expected that it was released in a prolonged way during storage time.

Microbial growth such as *E. coli* on the surface of a food is a major cause of food spoilage and food-borne illness. Therefore, the use of edible active coating is interesting to inhibit spoilage and pathogenic microorganisms. Figure 4 shows that all parameters evaluated (type and concentration of encapsulating agents and pH) showed significant differences ($P < 0.05$) in the inhibition halo except for pH

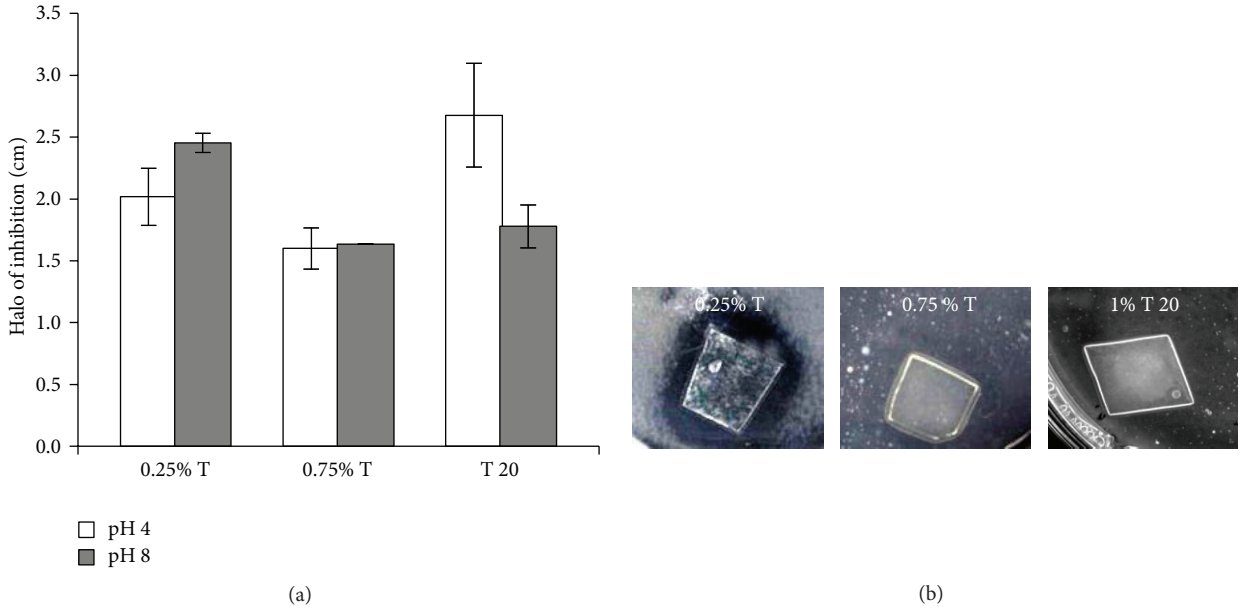

Figure 4: Halo of inhibition of the films against *Escherichia coli* by agar diffusion method. (a) Measurements. Bars correspond to standard deviation of mean value of triplicates. 0.25% T: 0.25% w/w trehalose; 0.75% T: 0.75% w/w trehalose; T 20: 1% w/w Tween 20. (b) Images of halo of inhibition as example.

in samples using 0.75% of trehalose. The high diffusion of antimicrobial agent and, therefore, higher inhibition were observed for 0.25% trehalose, followed by Tween 20 and then by 0.75% trehalose (Figure 4). Alginate films containing Tween 20 showed more interactions (measured as numbers of new peaks by FTIR) in comparison with those films containing trehalose [58]. Therefore, these differences in inhibition halo between encapsulating agents may be due to possible interactions between the hydroxyl groups of trehalose or Tween 20 and alginate polymeric chains, affecting therefore the antimicrobial agent release.

3.3. Characterization of Physical and Antimicrobial Properties of Films during Storage. Optical properties could change by humidity and temperature during storage conditions. Therefore, opacity and variation of color (CIEDE2000) for each time were evaluated during storage of 14 days comparing with the control film at initial time. Analysis was performed using the experimental design previously described, evaluating pH of film together with temperature and relative humidity as storage conditions.

Taking into account the results of CDDR experimental design (Table 1) and Pareto diagram for each parameter, it may be concluded that relative humidity is the principal factor that affects significantly ($P < 0.05$) the opacity and variation of color of all evaluated films. In addition, inhibition halo was affected significantly ($P < 0.05$) by humidity and temperature, the antimicrobial activity diminishing as humidity increases, and temperature decreases (data not shown).

The desirability function method helps determine the combination of experimental factors which simultaneously optimizes multiple answers. Therefore, the optima conditions to obtain edible films with antimicrobial activity after 14 days of storage were chosen with the aim of minimizing each property (variation of color and opacity) and of maximizing inhibition of bacteria growth (maxima halo of inhibition). The desirability maxima reached and their responses are observed in Table 2. The responses at each optimal condition showed high inhibition of *E. coli* since inhibition halo was similar to the one observed at initial time (Figure 4). The optimal conditions were similar for relative humidity but varying for pH and temperature for the three evaluated films. The results showed that these films can be used at "room" storage condition with a 75% RH. However, other conditions may affect the fresh foods where these films are intended to be applied.

Table 2: Optimal conditions for the function of desirability and optimal responses for the 14 days of storage.

Factors	0.25% trehalose	0.75% trehalose	1% Tween 20
Optimal conditions			
pH	7	8	6
Temperature (°C)	30	11	26
Relative humidity (%)	78	75	78
Responses			
Variation of color	1.4	3.2	2.7
Opacity	5.5	5.3	21.6
Halo of inhibition (cm)	3	2.7	3

Model verification was performed with an additional three sets of independent trials using the mentioned optimized conditions for each studied films. They were compared

to the predicted value from the CCRD model. All trials were not significantly ($P > 0.05$) different between them. The coefficient variation (CV) was lower than 10% and the coefficient of determination (R^2) between experimental values of each evaluated factor and the predicted value suggested by the desirability function was higher than 0.95. Therefore, the experimental results gave close values to the theoretical prediction, which meant that the results of validation parameters were satisfactory.

The high value of opacity as response of 1% of Tween 20 (Table 2) indicates that these films have no possibility of industrial applications. On the other hand, taking into account the low values of response corresponding to optical properties and the prolonged antimicrobial activity together with the optimal conditions for these values, it can be assumed that alginate films containing trehalose (at both concentrations) as encapsulating agent of carvacrol can be used as coating in fresh fruits. Taking into account these results, films containing trehalose were evaluated as antifungal films against *Botrytis cinerea* at the conditions found to be optimal. Films were stored at a relative humidity of 75% and a room temperature of 20°C, a mean of optima temperature obtained. The antifungal activity using the vapor phase methodology was evaluated at each storage time. Figure 5 showed the results obtained for inhibition of growth in edible films at both concentrations of trehalose and at different pH (4 and 8). Significant differences ($P < 0.05$) were obtained with pH but not with concentration of trehalose ($P > 0.05$), with the best antifungal film being the one prepared at pH 4. Although the antifungal activity diminished during storage time for films containing trehalose at pH 4, it is important to note that the diminution of fungal growth is higher than 50%, affirming that these films could be used by coating and/or without contact.

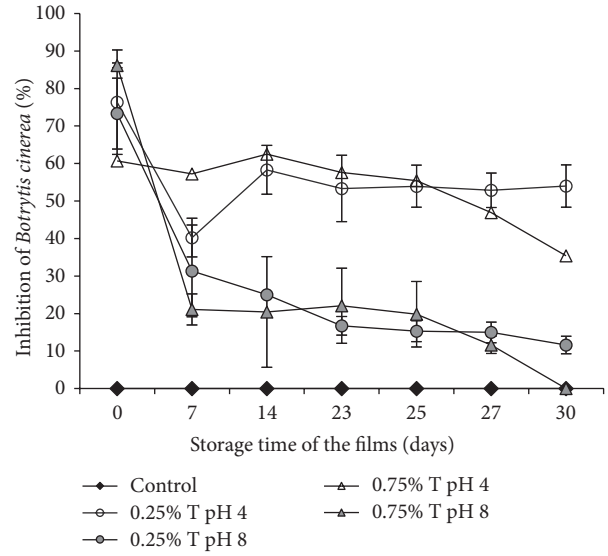

Figure 5: Inhibition percentage of growth of *Botrytis cinerea* using vapour phase methodology during storage time of the films. Bars indicate standard deviation of mean value of triplicates. 0.25% T: 0.25% w/w trehalose; 0.75% T: 0.75% w/w trehalose.

4. Conclusions

Results showed that the incorporation of trehalose improves the stability of film forming emulsion comparing to Tween 20, which presents sedimentation as instability mechanism. However, pH of emulsion was an important factor for its stability, being more stable at pH 4 than pH 8. Meanwhile, films containing trehalose were transparent comparing to opaque films with Tween 20 and differences on surface microstructure were observed between them.

During storage time, the different studied films presented different optima values of pH, relative humidity, and temperature to minimize responses as opacity and color variation and to maximize inhibition growth of bacteria. However, taking into account the multiple responses, the value of RH selected was 75%, but pH value and temperature was depending on the composition of each film. The responses observed of films stored at these optima conditions for 14 days showed that films containing trehalose (at both concentrations) are the most suitable to use in fresh foods stored at temperatures between 22 and 30°C and relative humidity of 75%. However, antifungal effect was depending on pH more than concentration of trehalose and was observed during 30 days of storage, where the inhibition of *B. cinerea* was higher than 50% at pH 4. Taking into account the microscopy of surface where crystals were observed at high concentration of trehalose, the best edible film was the sample with 0.25% trehalose at pH 4. Therefore, an antibacterial and antifungal alginate/trehalose edible film incorporated with carvacrol is a promising packaging material with good potential in many food applications.

Conflict of Interests

The authors declare that there is no conflict of interests regarding the publication of this paper.

Acknowledgments

The authors acknowledge financial support from FONDECYT Project no. 1131017, DICYT Project from VRIDEI of University of Santiago of Chile; Programa Escala Docente AUGM, Universidad de Buenos Aires-Universidad de Santiago de Chile, UBACYT Project no. 20020130100136BA.

References

[1] A. Ali, M. Maqbool, S. Ramachandran, and P. G. Alderson, "Gum arabic as a novel edible coating for enhancing shelf-life and improving postharvest quality of tomato (*Solanum lycopersicum* L.) fruit," *Postharvest Biology and Technology*, vol. 58, no. 1, pp. 42–47, 2010.

[2] C. A. Campos, L. N. Gerschenson, and S. K. Flores, "Development of edible films and coatings with antimicrobial activity," *Food and Bioprocess Technology*, vol. 4, no. 6, pp. 849–875, 2011.

[3] A. M. Durango, N. F. F. Soares, and N. J. Andrade, "Microbiological evaluation of an edible antimicrobial coating on minimally processed carrots," *Food Control*, vol. 17, no. 5, pp. 336–341, 2006.

[4] G. Oms-Oliu, M. A. Rojas-Graü, L. A. González et al., "Recent approaches using chemical treatments to preserve quality of fresh-cut fruit: a review," *Postharvest Biology and Technology*, vol. 57, no. 3, pp. 139–148, 2010.

[5] M. A. Rojas-Graü, R. Soliva-Fortuny, and O. Martín-Belloso, "Edible coatings to incorporate active ingredients to fresh-cut fruits: a review," *Trends in Food Science and Technology*, vol. 20, no. 10, pp. 438–447, 2009.

[6] K. G. Zinoviadou, K. P. Koutsoumanis, and C. G. Biliaderis, "Physico-chemical properties of whey protein isolate films containing oregano oil and their antimicrobial action against spoilage flora of fresh beef," *Meat Science*, vol. 82, no. 3, pp. 338–345, 2009.

[7] M. A. Rojas-Graü, R. J. Avena-Bustillos, M. Friedman, P. R. Henika, O. Martín-Belloso, and T. H. Mchugh, "Mechanical, barrier, and antimicrobial properties of apple puree edible films containing plant essential oils," *Journal of Agricultural and Food Chemistry*, vol. 54, no. 24, pp. 9262–9267, 2006.

[8] M. A. Rojas-Graü, R. J. Avena-Bustillos, C. Olsen et al., "Effects of plant essential oils and oil compounds on mechanical, barrier and antimicrobial properties of alginate-apple puree edible films," *Journal of Food Engineering*, vol. 81, no. 3, pp. 634–641, 2007.

[9] W.-X. Du, C. W. Olsen, R. J. Avena-Bustillos, T. H. McHugh, C. E. Levin, and M. Friedman, "Storage stability and antibacterial activity against *Escherichia coli* O157:H7 of carvacrol in edible apple films made by two different casting methods," *Journal of Agricultural and Food Chemistry*, vol. 56, no. 9, pp. 3082–3088, 2008.

[10] W.-X. Du, C. W. Olsen, R. J. Avena-Bustillos, T. H. McHugh, C. E. Levin, and M. Friedman, "Antibacterial activity against *E. coli* O157:H7, physical properties, and storage stability of novel carvacrol-containing edible tomato films," *Journal of Food Science*, vol. 73, no. 7, pp. M378–M383, 2008.

[11] L. Hernández-Ochoa, C. A. MacÍas-Castanãeda, G. V. Nevárez-Moorillón, E. Salas-Munãoz, and F. Sandoval-Salas, "Antimicrobial activity of chitosan-based films including spices essential oils and functional extracts," *CyTA-Journal of Food*, vol. 10, no. 2, pp. 85–91, 2012.

[12] J. Gómez-Estaca, L. Bravo, M. C. Gómez-Guillén, A. Alemán, and P. Montero, "Antioxidant properties of tuna-skin and bovine-hide gelatin films induced by the addition of oregano and rosemary extracts," *Food Chemistry*, vol. 112, no. 1, pp. 18–25, 2009.

[13] A. A. M. de Melo, M. G. Robson, M. F. Araujo Silveira et al., "Microbiological quality and other characteristics of refrigerated chicken meat in contact with cellulose acetate-based film incorporated with rosemary essential oil," *Brazilian Journal of Microbiology*, vol. 43, no. 4, pp. 1419–1427, 2012.

[14] I. Fernández-Pan, X. Carrión-Granda, and J. I. Maté, "Antimicrobial efficiency of edible coatings on the preservation of chicken breast fillets," *Food Control*, vol. 36, no. 1, pp. 69–75, 2014.

[15] D. López, N. Acevedo, and S. Matiacevich, "Characterization of edible active coating based on alginate-thyme oil-propionic acid for the preservation of fresh chicken breast fillets," *Journal of Food Processing and Preservation*, 2015.

[16] R. M. Raybaudi-Massilia, J. Mosqueda-Melgar, and O. Martín-Belloso, "Edible alginate-based coating as carrier of antimicrobials to improve shelf-life and safety of fresh-cut melon," *International Journal of Food Microbiology*, vol. 121, no. 3, pp. 313–327, 2008.

[17] A. C. Guerreiro, C. M. L. Gago, M. L. Faleiro, M. G. C. Miguel, and M. D. C. Antunes, "The effect of alginate-based edible coatings enriched with essential oils constituents on *Arbutus unedo* L. fresh fruit storage," *Postharvest Biology and Technology*, vol. 100, pp. 226–233, 2015.

[18] M. A. Rojas-Graü, R. M. Raybaudi-Massilia, R. C. Soliva-Fortuny, R. J. Avena-Bustillos, T. H. McHugh, and O. Martín-Belloso, "Apple puree-alginate edible coating as carrier of antimicrobial agents to prolong shelf-life of fresh-cut apples," *Postharvest Biology and Technology*, vol. 45, no. 2, pp. 254–264, 2007.

[19] L. Keawchaoon and R. Yoksan, "Preparation, characterization and in vitro release study of carvacrol-loaded chitosan nanoparticles," *Colloids and Surfaces B: Biointerfaces*, vol. 84, no. 1, pp. 163–171, 2011.

[20] T. Kulisic, A. Radonic, V. Katalinic, and M. Milos, "Use of different methods for testing antioxidative activity of oregano essential oil," *Food Chemistry*, vol. 85, no. 4, pp. 633–640, 2004.

[21] S. Burt, "Essential oils: their antibacterial properties and potential applications in foods—a review," *International Journal of Food Microbiology*, vol. 94, no. 3, pp. 223–253, 2004.

[22] S. Benavides, R. Villalobos-Carvajal, and J. E. Reyes, "Physical, mechanical and antibacterial properties of alginate film: effect of the crosslinking degree and oregano essential oil concentration," *Journal of Food Engineering*, vol. 110, no. 2, pp. 232–239, 2012.

[23] A. Guarda, J. F. Rubilar, J. Miltz, and M. J. Galotto, "The antimicrobial activity of microencapsulated thymol and carvacrol," *International Journal of Food Microbiology*, vol. 146, no. 2, pp. 144–150, 2011.

[24] P. M. Periago, B. Delgado, P. S. Fernández, and A. Palop, "Use of carvacrol and cymene to control growth and viability of *Listeria monocytogenes* cells and predictions of survivors using frequency distribution functions," *Journal of Food Protection*, vol. 67, no. 7, pp. 1408–1416, 2004.

[25] M. M. Tajkarimi, S. A. Ibrahim, and D. O. Cliver, "Antimicrobial herb and spice compounds in food," *Food Control*, vol. 21, no. 9, pp. 1199–1218, 2010.

[26] D. J. Daferera, B. N. Ziogas, and M. G. Polissiou, "The effectiveness of plant essential oils on the growth of *Botrytis cinerea*, *Fusarium* sp. and *Clavibacter michiganensis* subsp. michiganensis," *Crop Protection*, vol. 22, no. 1, pp. 39–44, 2003.

[27] D. S. Arora and J. Kaur, "Antimicrobial activity of spices," *International Journal of Antimicrobial Agents*, vol. 12, no. 3, pp. 257–262, 1999.

[28] J. Kester and O. Fennema, "Edible films and coatings: a review," *Food Technology*, vol. 40, pp. 47–59, 1986.

[29] A. Acevedo-Fani, L. Salvia-Trujillo, M. A. Rojas-Graü, and O. Martín-Belloso, "Edible films from essential-oil-loaded nanoemulsions: physicochemical characterization and antimicrobial properties," *Food Hydrocolloids*, vol. 47, pp. 168–177, 2015.

[30] K. C. Aguilar, F. Tello, A. C. K. Bierhalz, M. G. Garnica Romo, H. E. Martínez Flores, and C. R. F. Grosso, "Protein adsorption onto alginate-pectin microparticles and films produced by ionic gelation," *Journal of Food Engineering*, vol. 154, pp. 17–24, 2015.

[31] J. W. Rhim, J. H. Kim, and D. H. Kim, "Modification of Na-alginate films by CaCl2 treatment," *Korean Journal of Food Science and Technology*, vol. 37, pp. 217–221, 2003.

[32] J.-W. Rhim, "Physical and mechanical properties of water resistant sodium alginate films," *LWT—Food Science and Technology*, vol. 37, no. 3, pp. 323–330, 2004.

[33] M. S. Álvarez-Cerimedo, M. Cerdeira, R. J. Candal, and M. L. Herrera, "Microencapsulation of a low-*trans* fat in trehalose as affected by emulsifier type," *Journal of the American Oil Chemists' Society*, vol. 85, no. 9, pp. 797–807, 2008.

[34] D. Celis, M. I. Azócar, J. Enrione, M. Páez, and S. Matiacevich, "Influence of glassy or rubbery state on antimicrobial properties of chitosan-gelatin films," *Journal of Food Research*, vol. 1, pp. 184–193, 2012.

[35] S. Matiacevich, D. C. Cofré, C. Schebor, and J. Enrione, "Physicochemical and antimicrobial properties of bovine and salmon gelatin-chitosan films," *CyTA-Journal of Food*, vol. 11, no. 4, pp. 366–378, 2013.

[36] Y. Elad, B. Williamson, P. Tudzinsky, and N. Delen, *Botrytis: Biology, Phatology and Control*, Springer, Dordrecht, The Netherlands, 2007.

[37] K. Di Scipio, Y. Escalona, K. Quijada, and F. Millán, "Estudio del mezclado de emulsiones aplicando la metodología de superficie respuesta," *Revista de la Facultad de Ingeniería UCV*, vol. 23, pp. 3–7, 2008.

[38] M. Torab-Mostaedi, J. Safdari, and A. Ghaemi, "Mass transfer coefficients in pulsed perforated-plate extraction columns," *Brazilian Journal of Chemical Engineering*, vol. 27, no. 2, pp. 243–251, 2010.

[39] M. Cerdeira, G. G. Palazolo, R. J. Candal, and M. L. Herrera, "Factors affecting initial retention of a microencapsulated sunflower seed oil/milk fat fraction blend," *Journal of the American Oil Chemists' Society*, vol. 84, no. 6, pp. 523–531, 2007.

[40] F. Pedreschi, J. León, D. Mery, and P. Moyano, "Development of a computer vision system to measure the color of potato chips," *Food Research International*, vol. 39, no. 10, pp. 1092–1098, 2006.

[41] S. Matiacevich, P. Silva, F. Osorio, and J. Enrione, "Evaluation of blueberry colour during storage using image analysis," in *Colour in Food: Technological and Psychophysical Aspects*, J. L. Caivano and M. P. Buera, Eds., pp. 211–218, CRC Publisher, Buenos Aires, Argentina, 2012.

[42] M. R. Luo, G. Cui, and B. Rigg, "The development of the CIE 2000 colour-difference formula: CIEDE2000," *Color Research & Application*, vol. 26, no. 5, pp. 340–350, 2001.

[43] G. Sharma, W. Wu, and E. N. Dalal, "The CIEDE2000 color-difference formula: implementation notes, supplementary test data, and mathematical observations," *Color Research and Application*, vol. 30, no. 1, pp. 21–30, 2005.

[44] P. A. Ponce Cevallos, M. P. Buera, and B. E. Elizalde, "Encapsulation of cinnamon and thyme essential oils components (cinnamaldehyde and thymol) in β-cyclodextrin: effect of interactions with water on complex stability," *Journal of Food Engineering*, vol. 99, no. 1, pp. 70–75, 2010.

[45] E. W. Hansen, P. E. Kristiansen, and B. Pedersen, "Crystallinity of polyethylene derived from solid-state proton NMR free induction decay," *The Journal of Physical Chemistry B*, vol. 102, no. 28, pp. 5444–5450, 1998.

[46] Centers for Disease Control and Prevention (CDC) and World Health Organization (WHO), *Manual for the Laboratory Identification and Antimicrobial Susceptibility Testing of Bacterial Pathogens of Public Health Importance in the Developing World*, Centers for Disease Control and Prevention (CDC), World Health Organization (WHO), 2003.

[47] S. Inouye, M. Watanabe, Y. Nishiyama, K. Takco, M. Akao, and H. Yamaguchi, "Antisporulating and respiration-inhibitory effects of essential oils on filamentous fungi," *Mycoses*, vol. 41, no. 9-10, pp. 403–410, 1998.

[48] V. Tullio, A. Nostro, N. Mandras et al., "Antifungal activity of essential oils against filamentous fungi determined by broth microdilution and vapour contact methods," *Journal of Applied Microbiology*, vol. 102, no. 6, pp. 1544–1550, 2007.

[49] K. Laird and C. Phillips, "Vapour phase: a potential future use for essential oils as antimicrobials?" *Letters in Applied Microbiology*, vol. 54, no. 3, pp. 169–174, 2012.

[50] M. J. Velázquez-Nuñez, R. Avila-Sosa, E. Palou, and A. López-Malo, "Antifungal activity of orange (*Citrus sinensis* var. Valencia) peel essential oil applied by direct addition or vapor contact," *Food Control*, vol. 31, no. 1, pp. 1–4, 2013.

[51] L. Greenspan, "Humidity fixed points of binary saturated aqueous solutions," *Journal of Research of the National Bureau of Standards A: Physics and Chemistry*, vol. 81, no. 1, 1977.

[52] A. E. Edris and C. F. R. Malone, "Preferential solubilization behaviours and stability of some phenolic-bearing essential oils formulated in different microemulsion systems," *International Journal of Cosmetic Science*, vol. 34, no. 5, pp. 441–450, 2012.

[53] K. Ziani, Y. Fang, and D. J. McClements, "Fabrication and stability of colloidal delivery systems for flavor oils: effect of composition and storage conditions," *Food Research International*, vol. 46, no. 1, pp. 209–216, 2012.

[54] Y. Yang, J. Ming, and N. Yu, "Color image quality assessment based on CIEDE2000," *Advances in Multimedia*, vol. 2012, Article ID 273723, 6 pages, 2012.

[55] S. Banerjee and S. Bhattacharya, "Compressive textural attributes, opacity and syneresis of gels prepared from gellan, agar and their mixtures," *Journal of Food Engineering*, vol. 102, no. 3, pp. 287–292, 2011.

[56] M. A. García, A. Pinotti, M. N. Martino, and N. E. Zaritzky, "Characterization of starch and composite edible films and coatings," in *Edible Films and Coatings for Food Applications*, M. E. Embuscado and K. C. Huber, Eds., pp. 169–210, Springer, New York, NY, USA, 2009.

[57] B. E. Elizalde, M. L. Herrera, and M. P. Buera, "Retention of β-carotene encapsulated in a trehalose-based matrix as affected by water content and sugar crystallization," *Journal of Food Science*, vol. 67, no. 8, pp. 3039–3045, 2002.

[58] R. Navarro, C. Arancibia, M. L. Herrera, and S. Matiacevich, "Effect of type of encapsulating agent on physical properties of edible films based on alginate and thyme oil," *Food and Bioproducts Processing*, In press.

Hindawi Publishing Corporation
International Journal of Polymer Science
Volume 2015, Article ID 326745, 9 pages
http://dx.doi.org/10.1155/2015/326745

Research Article

Application of Microbial Biopolymers as an Alternative Construction Binder for Earth Buildings in Underdeveloped Countries

Ilhan Chang,[1] Minkyung Jeon,[2] and Gye-Chun Cho[2]

[1]*Geotechnical Engineering Research Institute (GERI), Korea Institute of Civil Engineering and Building Technology (KICT), Goyang 10223, Republic of Korea*
[2]*Department of Civil and Environmental Engineering, Korea Advanced Institute of Science and Technology (KAIST), Daejeon 34141, Republic of Korea*

Correspondence should be addressed to Gye-Chun Cho; gyechun@kaist.edu

Received 5 August 2015; Revised 3 November 2015; Accepted 11 November 2015

Academic Editor: Shiv Shankar

Earth buildings are still a common type of residence for one-third of the world's population. However, these buildings are not durable or resistant against earthquakes and floods, and this amplifies their potential harm to humans. Earthen construction without soil binders (e.g., cement) is known to result in poor strength and durability performance of earth buildings. Failure to use construction binders is related to the imbalance in binder prices in different countries. In particular, the price of cement in Africa, Middle East, and Southwest Asia countries is extremely high relative to the global trend of consumer goods and accounts for the limited usage of cement in those regions. Moreover, environmental concerns regarding cement usage have recently risen due to high CO_2 emissions. Meanwhile, biopolymers have been introduced as an alternative binder for soil strengthening. Previous studies and feasibility attempts in this area show that the mechanical properties (i.e., compressive strength) of biopolymer mixed soil blocks (i.e, both 1% xanthan gum and 1% gellan gum) satisfied the international criteria for binders used in earthen structures. Economic and market analyses have demonstrated that the biopolymer binder has high potential as a self-sufficient local construction binder for earth buildings where the usage of ordinary cement is restricted.

1. Introduction

Earth has been the most commonly used material for building and construction since the beginning of human civilization. Since the Industrial Revolution, diverse building and construction materials such as cement and steel have become the basis of modern civilization and have replaced the use of conventional building materials (i.e., earth and wood). However, it was reported that about 30% of residential buildings were still made of earth as of 1994 (Figure 1) [1]. More specifically, the portion of residential buildings made of earth is close to 50% in developing countries as well as the third world. And in developed countries (USA, EU, etc.), demand for earth buildings has been increasing in accordance with increased interest in environment-friendly architecture and construction [1].

Earth house types can be categorized by the usage of construction binders (e.g., cement) and the main formation method [2–7]. However, as a building material, soil is limited in strength and durability. Damage to earthen buildings caused by intensive rainfall, floods, and earthquakes has been widely reported [8–10]. Nonetheless, people living in Southwest Asia, the Middle East, and Africa still rely on residential buildings made of soil. The use of binders is an important factor because it influences the strength of soil buildings, regardless of the type of wall formation.

Diverse types of binders made for construction have been used widely for soil buildings, but the production of binder also entails the generation of carbon dioxide. The production process for cement (which is the most universal binder for construction) has specifically been noted as the source of about 5% of global greenhouse gases (CO_2) and accordingly

Table 1: Market price of cement[1] in each country.

Continents	Countries	Cement price (USD/ton)	Continents	Countries	Cement price (USD/ton)
Africa	Niger	280	Asia	South Korea	68
	Kenya	190		China	57
	Mali	203		Japan	125
	Mozambique	160		India	98
	Nigeria	223		Pakistan	106
	Cameroon	200		Bangladesh	112
	Rwanda	200		Indonesia	125
	Morocco	150	America	Peru	202
	Egypt	65		United States	91
Middle East	Yemen	214	Europe	Russia	89
	Afghanistan	91		Germany	93
	Iraq	120		France	132
	Kuwait	74		UK	102

[1]Source of the price of cement: global cement institute (www.globalcement.com).

Figure 1: Global distribution of earth buildings [1].

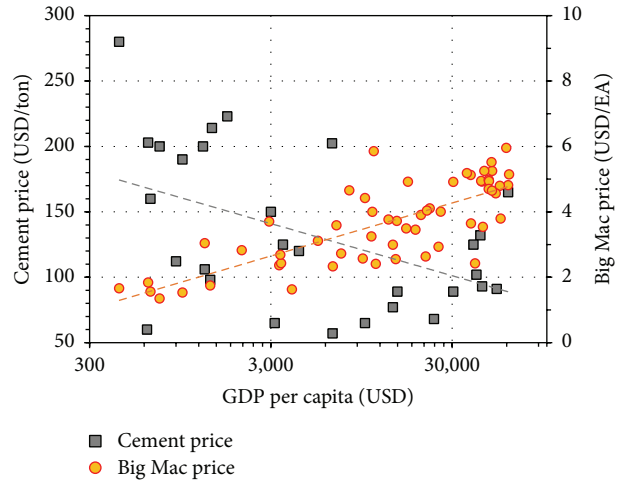

Figure 2: Global cement and Big Mac price trends with GDP per capita.

the necessity of restraining the use of cement has been raised [11]. Moreover, the global cement price distribution shows regional differences (Table 1), and cement is especially expensive in underdeveloped countries. For instance, in China, the price of 1 ton of bulk cement was 57 USD/ton, while in Nigeria it was 223 USD/ton (about 4 times higher) [12].

Generally, the market price of consumer goods tends to increase along with an increase of GDP per capita [13]. But contrary to the general market trend, the price of cement appears asymmetrically high in countries with low GDP per capita while it appears low in countries of high GDP per capita (Figure 2). This is one factor likely facilitating the imbalance in the utilization of cement. The level of market demand for cement in developed countries is comparatively lower than that in less developed or developing countries because urbanization and social infrastructure have already been largely stabilized, whereas developing countries would be expected to have higher construction demands. Therefore, it is quite important to correct such disparities in the price of cement and other construction materials.

Biopolymers are normally composed of biodegradable polysaccharides and are generated by organisms such as algae, bacteria, and fungi by consuming carbon during cultivation. Diverse kinds of biopolymers have been discovered and developed in many fields for respective applications. In particular, with rising oil prices and the threat of increasing CO_2 emissions, the market for biopolymer based plastic products has been expanding, as a replacement for high CO_2 emitting products.

Several attempts to introduce biogenic biopolymers as an additive or supplement in construction engineering have been reported. Matsuoka et al. [14] performed a study using curdlan as a viscosity agent to improve the workability of concrete, while Chang and Cho [15, 16] showed that beta-glucan treatment enhances the strength of natural soil with an increment ratio of up to 300–400% and also has low impact on the environment in terms of CO_2 emissions. Moreover, the usage of gel type biopolymers (i.e., gellan gum and agar gum) was recently introduced in the field of soil treatment [17, 18]. In this study, we performed experiments to evaluate the feasibility of gel type biopolymers (i.e., xanthan gum and

gellan gum) as construction binders for earth buildings using natural soil.

2. Materials and Methods

2.1. Biopolymers

2.1.1. Xanthan Gum. Xanthan gum is an anionic polysaccharide composed of D-glucuronic acid, D-mannose, pyruvylated mannose, 6-O-acetyl D-mannose, and 1,4-linked glucan [19], produced by the fermentation of glucose or sucrose by *Xanthomonas campestris* bacterium [20]. Xanthan gum is commonly used as a food additive and rheology modifier. A recent study showed that xanthan gum improves the strength of soil significantly, especially in the presence of clayey particles (i.e., due to hydrogen bonding between xanthan gum and clay particles) [18]. The xanthan gum (Sigma-Aldrich, CAS number 11138-66-2) used in this study is from a biological source, *Xanthomonas campestris*.

2.1.2. Gellan Gum. Gellan gum is a water-soluble polysaccharide fermented from *Sphingomonas elodea* microbe and it consists of glucose, glucuronic acid ($C_5H_9O_5$-COOH), and rhamnose ($C_6H_{12}O_5$). It forms a highly qualified gel even at low concentrations (0.05–0.25%). Gellan gum is commonly used as a thickener, emulsifier, and stabilizer for food products [21]. Due to its high stability at high temperatures and low pH conditions, gellan gum is potentially a highly durable additive for soil improvement and stabilization [22, 23]. Gelzan (CP Kelco, CAS number: 71010-52-1), a commercial gellan gum product, was used in this study.

2.2. Materials: Korean Residual Soil (KRS), Hwangtoh. To investigate the soil strengthening effect of biopolymer treatment, we used Korean residual soil (KRS) as the soil material in this study. KRS is well known as "*hwangtoh*" on the Korean peninsula and has been used as a soil building material through much of Korean history. KRS consists of quartz (8.4%), kaolinite (45.8%), halloysite (22.7%), illite (14.8), and goethite (8.3%) as its main minerals, and detailed geotechnical properties of KRS can be found in Chang and Cho [15].

Like other adobe or soil buildings, KRS buildings have weaknesses in strength and durability. Thus, we tested the use of biopolymers as a mixing binder to reinforce the strength of natural KRS. Natural KRS from Gochang, Korea, was air-dried at room temperature (18°C) and pulverized (i.e., detachment of agglomerated soil particles) to be suitable for proper mixing.

2.3. Sample Preparation and Strength Measurement. In the laboratory, we mixed KRS with xanthan gum and gellan gum to prepare biopolymer-treated KRS cube specimens. Ordinary Portland Cement (OPC) mixed and untreated (i.e., natural) KRS samples were prepared simultaneously, to compare the strengthening behavior of biopolymer treatment with preexisting soil construction (i.e., strengthening) methods.

For biopolymer (i.e., xanthan gum and gellan gum) mixing, 1000 g of dried and ground KRS was first mixed with 10 g (i.e., $m_b/m_s = 1\%$) of pure dried biopolymer powder (dry mixing stage), where m_b and m_s are the mass of the biopolymer and dry soil, respectively. Then, 600 g of distilled water (i.e., water content; $w = 60\%$) was added according to the liquid limit value (i.e., 53.7%) of natural KRS [15] to provide thorough mixing to finally obtain uniform biopolymer-soil mixtures (wet mixing stage) (Figure 3(a)).

For OPC mixing, the cement to soil ratio in mass units (m_c/m_s) was fixed at 10%, based on results of previous studies, which show compressive strength of $m_c/m_s = 10\%$ cement treatment in accordance with 1.0% biopolymer content to soil mass (i.e., m_b/m_s) conditions [15, 18]. Furthermore, 700 g of cement slurry with a water-cement ratio of 6 (i.e., $w/m_c = 600\,\text{g}/100\,\text{g}$) was prepared to obtain a cement-soil mixture with an identical initial water content condition that biopolymer-soil mixtures have (i.e., $w = 60\%$), when mixed with 1000 g of dry KRS.

The details of each mixing condition are summarized in Table 2. After mixing, the soil mixtures were poured into cubic molds (50 mm × 50 mm × 50 mm) (Figure 3(b)). Soils were compacted manually by a steel rod having a square head (i.e., 40 mm × 40 mm) and a rubber hammer to present optimal compaction and remove entrapped air voids from the soil mixtures. Cube samples were demolded and dried in air at room temperature (18°C) for 28 days, followed by unconfined compressive strength measurement at the end of drying via a UTM (Universal Testing Machine; INSTRON 5583) device (Figure 3(d)) with a 1.0%/min strain rate on three specimens to obtain average values, respectively [24]. All geometric dimensions were measured, as was the specimen mass, and top and bottom surfaces were slightly trimmed to avoid an uneven stress distribution during the testing. Additionally, in order to prevent stress localization, filter paper was placed above and below the samples during testing. Samples were loaded until failure and the residual compressive strength was observed.

3. Results and Discussion

3.1. Compressive Strength of Biopolymer-Soil Mixtures. In general, the compressive strength of soil-cement mixtures (i.e., $m_c/m_s = 10\%$) increases with dry density increment [25]. Figure 4 presents the compressive strength of xanthan gum, gellan gum, 10% cement, and untreated KRS mixtures after 28 days of dry curing (i.e., exposed to air) at room temperature (i.e., 20°C). The strength values in Figure 4 are converted strength values that correspond to 100 mm × 100 mm × 100 mm cubes, by multiplying a shape factor value $\delta = 0.85$ to the real compressive strength measurements for generalization (i.e., to avoid different shape and size effects) [26, 27].

Both 1% xanthan gum and 1% gellan gum treated soils show higher compressive strength values than the 10% cement mixed KRS. The strength of the soil mixed with 1% of xanthan gum was 6.31 MPa, which is more than 2.3 times higher than that of the soil mixed with 10% of Ordinary Portland Cement (i.e., 2.65 MPa). A previous study shows

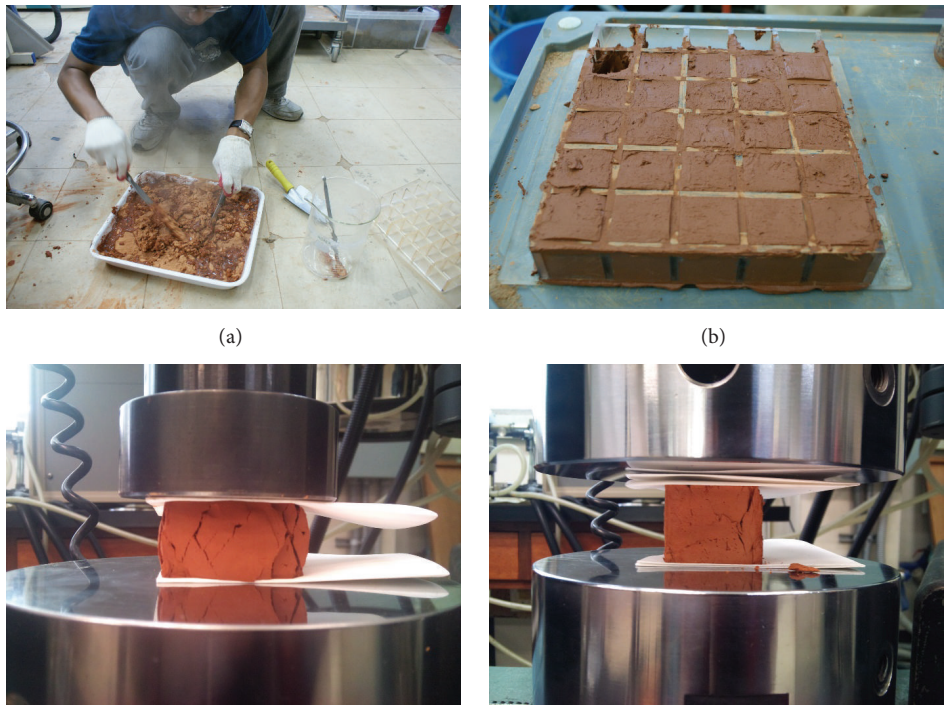

(a) (b) (c) (d)

Figure 3: Experimental program. (a) Biopolymer-soil mixing. (b) Mixture molding. (c) UTM after 1 day of curing (ductile). (d) UTM at 28 days of curing (brittle and strong).

Table 2: Mixing conditions of biopolymer-KRS mixtures.

Specimen	Mixing condition [g]			Initial mass ratio [%]	
	Dried soil	Binder	Water	Binder/soil	Water content
Xanthan gum	1,000	10	600	1.0	60
Gellan gum	1,000	10	600	1.0	60
Ordinary cement	1,000	100 (cement)	600	10.0	60
Natural (untreated) soil	1,000	—	600	—	60

that 0.5% of xanthan gum in the soil mixture could increase its strength above the level of soil mixed with 10% cement [18]. This means that either 100 kg of cement (10% of the soil) or 5 kg of xanthan gum (0.5% of the soil) would be needed to make 1 ton of soil having a strength over 2.5 MPa.

In the initial mixing stage, biopolymers tend to adsorb water immediately and form hydrogels, which enlarge the pore space between soil particles at molding. During curing and dehydration, water evaporates from the hydrogels, rendering firmer and stronger matrices between the biopolymers and soil particles. As a result, the final dried biopolymer-soil mixture can have high strength even under relatively low dry density (i.e., 1% gellan gum = 1.35 g/cm^3, 1% xanthan gum = 1.38 g/cm^3, and 10% OPC = 1.44 g/cm^3 in this study).

Several design criteria are set for bricks used for construction and building engineering (Table 3). The most common brick type in construction engineering is the cement-based brick. The Eurocode (EN 1996-3) requires a masonry cement-sand brick unit (100 mm × 100 mm × 100 mm cube) to have a compressive strength of at least 2 MPa for a 10% cement to sand ratio and 6 MPa for a 20% cement to sand ratio [28]. Another British code (BS EN 771-1) defines the minimum compressive strength for 337.5 mm (width) × 112.5 mm (length) × 112.5 mm (height) soil bricks to be 5 MPa [29], which is identical to a standard compressive strength value of 4.6 MPa by applying a shape factor value $\delta = 0.92$ [26]. Meanwhile, the International Code Council (ICC) provides

Table 3: Design criteria for earthen structures.

Design criteria	BS EN 1996-3[1]	BS EN 771-1[2]	IBC 2012[3]
Minimum compressive strength [MPa]	2 MPa (for 10% cement : soil) 6 MPa (for 20% cement : soil)	5 MPa (soil brick)	2 MPa (rammed earth brick)

[1]Eurocode 6: design of masonry structures (standard compressive strength for 100 mm × 100 mm × 100 mm cube).
[2]Specification for compacted clay masonry units (compressive strength of 337.5 mm × 112.5 mm × 112.5 mm brick).
[3]International Building Code (IBC), International Code Council (ICC) 2012.

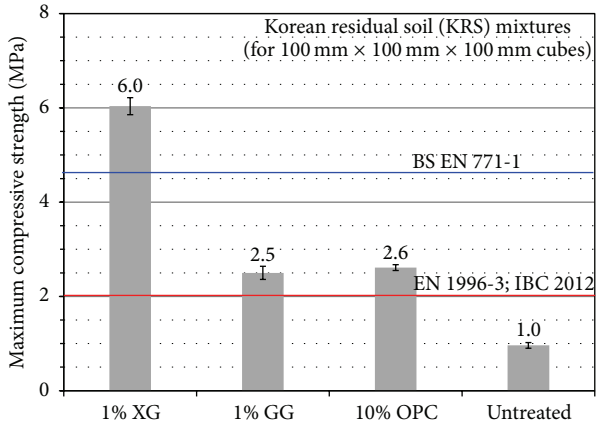

Figure 4: Maximum compressive strength values of KRS specimens and design criteria for earthen structures.

detailed requirements for earth walls, where the compressive strength of a rammed earth brick should exceed 2 MPa for a converted specimen scale (i.e., 100 mm × 100 mm × 100 mm) [30].

The average maximum compressive strength values of KRS specimens at 28 days are compared with typical design criteria of masonry structures (i.e., EN 1996-3, BS EN 771-1, and IBC 2012) in Figure 4. Untreated KRS has an unconfined compressive strength value close to 1 MPa, while 1% xanthan gum treatment produces the highest strengthening effect. The strength of 10% OPC mixed KRS (i.e., 2.65 MPa) satisfies the minimum strength criteria to be a brick. The compressive strengths of both xanthan gum (i.e., 6.3 MPa > 2 MPa) and gellan gum (i.e., 2.50 MPa > 2 MPa) mixes are in accordance with strength values in previous studies [17, 18] and satisfy the strength criteria to be used as a rammed earth brick binder [30].

Meanwhile, BS EN 1996-3 establishes the minimum strength of a wall element for a low-rise building to be higher than 5.2 MPa. In this aspect, 10% cement mixed KRS and 1% gellan gum mixed KRS are insufficient for use for single-story buildings, while 1% xanthan gum mixing is applicable for low-rise soil building construction. Moreover, the high strength of 1% xanthan gum treatment (i.e., 6.3 MPa) is a compressive strength level almost equivalent to the minimum strength of 20% ordinary cement mixing (i.e., 6 MPa), indicating the high strengthening efficiency of xanthan gum treatment, even with 1/20th (i.e., 1% versus 20%) the amount of material quantity compared to cement mixing.

Given the mechanical performance of biopolymer treatment, biopolymers are highly feasible for use as soil binders. However, the strength and stability of soil structures become critical with the presence of excess water conditions (e.g., wet or submerged). A previous study shows that the wet strength of biopolymer-treated soils is reduced to approximately 1/10th that of the dry strength when fully saturated under water [17]. Thus, water resistance or wet strength improvement methods of biopolymer-treated soils must be considered in further studies. Moreover, the economic feasibility of biopolymer application as a soil binder must be clearly demonstrated to declare biopolymers a promising construction and building material in the near future.

3.2. Future Prospects of Biopolymers as an Environment-Friendly Building Material. Petrochemical polymers have been applied diversely in modern civilization due to their demonstrated excellent performance. However, their prices are sensitive to fluctuations in oil prices, and they come with the added disadvantages of environmental damage, due to their retarded degradability, and the creation of carbon dioxide in their production process. Consequently, the need for more environment-friendly polymers has emerged, and accordingly studies to develop diverse bio-based plastics or polymers have been actively conducted [31].

Bio-based plastics or polymers can have diverse molecular structures depending on their respective polymerization processes, and this has enabled the production of customized biopolymers that have desirable strength or plasticity, with inherent biodegradability, along with low or limited carbon dioxide generation during production. On this basis, they have been regarded as a promising alternative to petrochemical products [32]. Research and market development of such products have been primarily based in regions that have strict regulations related to environment preservation, such as Japan and Europe, and the European biopolymer market currently accounts for about 60% of the entire global market.

Major global companies in the areas of chemical engineering and product manufacture are leading the development and production of biopolymers and bioplastics. Recently, several leading companies concluded an agreement together to produce environment-friendly biopolymers, and they introduced specifications and a certification system for biodegradable polymers [33]. They currently provide consumers with information about their certified products [34]. That agreement and the mutual cooperation of these corporations have brought about increased demand and improved reliability for bio-based polymer products. Biopolymers are currently applied in diverse fields including medicine, foods, cosmetics, and agrichemicals, and their markets have been growing by over 23% annually since 2010. This market growth trend is expected to continue for the time being [35, 36].

3.3. Economic Feasibility and Future Prospects for Biopolymer-Soil Treatment. The economic feasibility of biopolymers has been growing due to the expansion of biopolymer markets and the development of technologies associated with biopolymers (Figure 5). From 2009 to 2011, the global market for bioplastics increased from 249,000 tons to 1,161,000 tons annually (4.6 times), with a resulting price decrease [37–39].

The price competitiveness of biopolymers, which were 35–100 times more expensive in the early 2000s relative to conventional petrochemical polymers, has also been improving. The price gap had dropped by 2.5–7.5 times in 2007 by virtue of consistent development in technology and increased environmental regulations [39]. For instance, the price of xanthan gum in the 1960s was about 30,000 USD/ton, while it had dropped to 1/4 that amount by 2014 (Figure 6), due to expanded applications (e.g., medicine, cosmetics, construction, etc.) and subsequent technological development.

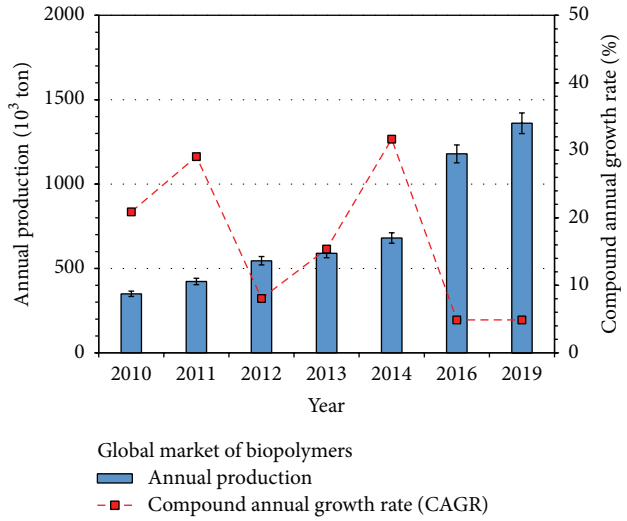

Figure 5: Expected trend and growth of the global biopolymer market.

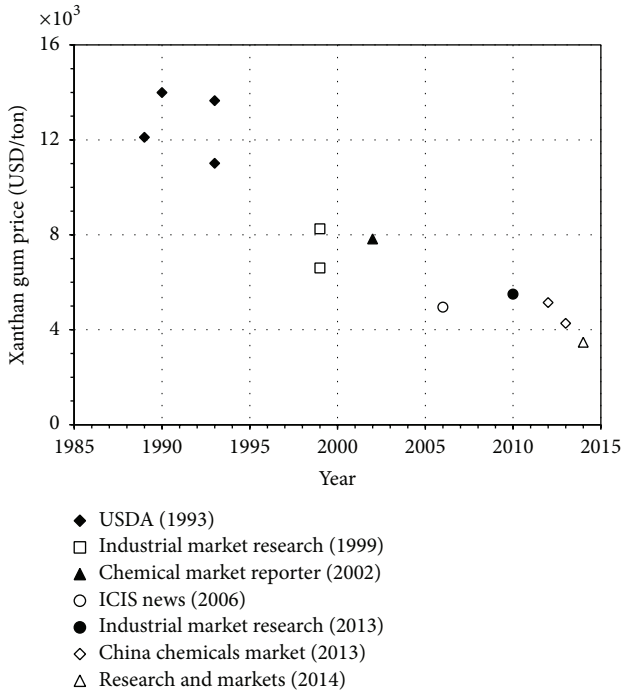

Figure 6: Market price trend of xanthan gum over 30 years (1985–2014).

In general, the major factors determining the price level of biopolymers such as xanthan gum are (1) the source of carbon, (2) the fermentation process, and (3) the recovery ratio. In particular, the level of biopolymer recovery from the fermentation medium (i.e., carbon source, e.g., sugar water and glucose) is an essential component affecting cost.

Regarding the importance of improving the recovery ratio, it was reported that a 20% increase in the recovery of biopolymers (from 60% to 80%) could reduce the price of the

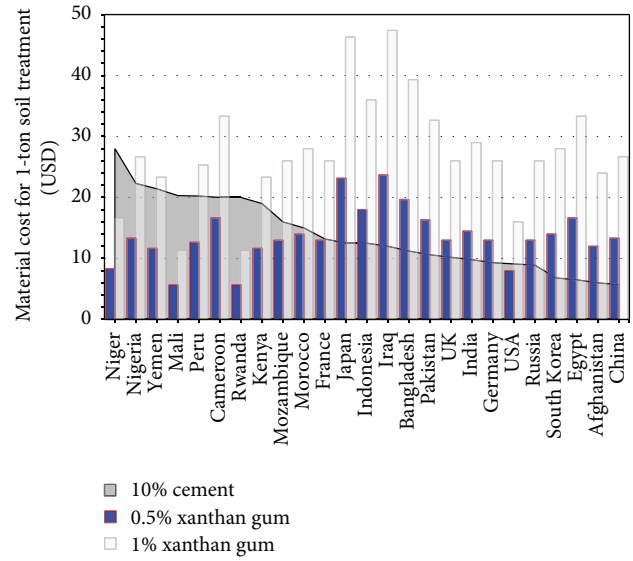

Figure 7: Estimated cost comparison for 1-ton soil treatment using cement (10%) and XG (0.5% and 1%).

biopolymer by 10% [40]. Many studies investigating methods to improve the recovery of biopolymers have focused on changing process conditions such as pH, temperature, agitation rate, nitrogen source concentration, and phosphor source concentration [41]. Consequently, biopolymer production technology has been continuously improved and the recovery ratio, which remained at a level of 30% in the 1970s, has now reached 60% in the commercial production process [42].

In addition, there have been many efforts to diversify the biopolymer carbon source, which is the major constituent of the macromolecular polysaccharide, as well as studies aimed at optimizing the production conditions of biopolymers [43–45]. The carbon source plays an important role in biopolymer commercialization because it accounts for approximately 30% of the whole production cost of biopolymers [41, 46]. Therefore, securing a sustainable and consistent carbon source is important for establishing a stable market for biopolymers.

For instance, the price of starch varies from 240 to 500 USD/ton, with a global average of 390 USD/ton in 2014 [47], reflecting much greater stability than the severe intercontinental differences in the global cement market (Table 1 and Figure 2). Thus, it becomes possible to perform cost comparisons between cement treatment and biopolymer (i.e., xanthan gum) treatment for soil strengthening by considering the cost ratio between produced xanthan gum and its carbon source (i.e., starch) [41, 46], as shown in Figure 7.

Figure 7 implies that xanthan gum treatment as a soil binder is already more competitive than cement in African countries. For instance, the price of starch in Kenya is reported to be 350 USD/ton [47]. Thus, the cost of locally produced xanthan gum can be estimated to become 2,333 USD/ton [i.e., 350 USD/ton (starch price) ÷ 0.5 (recovery ratio) ÷ 0.3 (proportion in total cost) = 2,333 USD/ton],

which indicates that the xanthan gum cost for 0.5% soil treatment (i.e., 5 kg of xanthan gum for 1 ton of soil) is 11.7 USD. Therefore, application of xanthan gum in countries with high cement prices potentially would be more economical and effective in terms of CO_2 emission reduction than cement usage, if xanthan gum is utilized for construction purposes and is locally produced. This could be accomplished by introducing an integrated commercialization process consisting of simple cultivation facility + local carbon source + germ/bacterium.

Moreover, most biopolymers sold in the current global market are food-grade, and up to 50% of the production costs of food-grade biopolymers are related to downstream purification steps, many of which would not be necessary for nonfood applications such as construction [41, 48]. Thus the price of biopolymers produced for engineering or construction purposes is expected to be lower than prices for the current commercial biopolymers estimated earlier (i.e., by 50% or so). Also, further cost reduction could be achieved by using less expensive substrates, such as agricultural product waste.

4. Conclusions

About 30%–40% of the world's population are still dwelling in buildings made of soil despite massive urbanization using modern construction technology. Such a high portion of the population is dwelling in soil buildings due to interrelated economic and environmental factors, including the availability of soil as a local and inexpensive construction material. This is problematic, since traditional soil buildings (made of soils without binders) are typically vulnerable to water and seismic loads. To cope with such problems, binders are required for soil strengthening. However, the most representative construction binder for soils (i.e., cement) accounts for more than 5% of the global annual CO_2 emissions [49–51], which becomes a concern when formulating scientific policy. In addition, the price of cement varies widely by country. In particular, it was determined that the price of cement in countries with lower GDP per capita was significantly higher than the average price in the global market. It is interesting that the countries with low GDP per capita are the most highly dependent on soil buildings, and it appears that this dependence on soil buildings is due to the very high price of construction binders, especially cement.

Thus, in this study, the use of microbially produced biopolymers as an economic and environment-friendly alternative binder for the construction of soil buildings is introduced. Feasibility studies conducted to test the comparative strength of soils treated with biopolymers confirmed that a very small amount (i.e., 0.5% of the whole contents) of biopolymers mixed with soil resulted in a higher unconfined compression strength than that of soil mixed with a large amount of cement (i.e., 10% of the whole content).

The economic feasibility of biopolymers relative to cement has yet to be improved; however with the trend of technological developments in this field it is highly likely that a market of biopolymers for construction purposes will develop. Further cost reductions are expected with the improved recovery ratio of biopolymers, together with the diversification and exploration of low priced carbon sources, and the commercialization and mass production of biopolymers specifically for construction purposes. These advances will enable countries with higher cement prices to obtain comparatively cheaper local construction binders. Furthermore, since the prices of carbon sources primarily used for the cultivation of biopolymers are lower in less developed countries, where the cost of cement is highest, the local commercialization of such biopolymers could contribute to the improvement of the strength and durability of soil buildings in countries that rely on them the most.

Conflict of Interests

The authors declare that there is no conflict of interests regarding the publication of this paper.

Acknowledgments

The research described in this paper was financially supported by a National Research Foundation of Korea (NRF) grant funded by the Korean government (MSIP) (no. 2015R1A2A2A03006268), by a grant from the Strategic Research Project (Development of Key Excavation Solutions for Expandable Urban Underground Space) funded by the Korea Institute of Civil Engineering and Building Technology (KICT), and by the KAIST End-Run Program (no. N01150661) supported by the Korea Ministry of Science, ICT and Future Planning (MISP).

References

[1] H. Houben and H. Guillaud, *Earth Construction: A Comprehensive Guide*, Intermediate Technology Publications, 1994.

[2] J. D. Revuelta-Acosta, A. García-Díaz, G. M. Soto-Zarazúa, and E. Rico-García, "Adobe as a sustainable material: a thermal performance," *Journal of Applied Sciences*, vol. 10, no. 19, pp. 2211–2216, 2010.

[3] P. J. Walker, "Strength and erosion characteristics of earth blocks and earth block masonry," *Journal of Materials in Civil Engineering*, vol. 16, no. 5, pp. 497–506, 2004.

[4] I. Evans, L. Smiley, M. G. Smith, and M. Smith, *The Hand-Sculpted House: A Philosophical and Practical Guide to Building a Cob Cottage*, Chelsea Green Publishing Company, White River Junction, Vt, USA, 2002.

[5] S. T. Maqsood and J. Schwarz, "Analysis of building damage during the 8 October 2005 earthquake in Pakistan," *Seismological Research Letters*, vol. 79, no. 2, pp. 163–177, 2008.

[6] D. Easton, *The Rammed Earth House*, Chelsea Green Publishing Company, White River Junction, Vt, USA, 2007.

[7] D. Sadek and H. Roslan, "A review on bricks and stabilized compressed earth blocks," *Scientific Research and Essays*, vol. 6, no. 3, pp. 499–506, 2011.

[8] R. Coffman, N. Agnew, G. S. Austin, and E. Doehe, "Adobe mineralogy," in *Proceedings of the 6th International Conference on the Conservation of Earthen Architecture*, pp. 424–429, Las Cruces, NM, USA, October 1990.

[9] R. Meli, O. Hernandez, and M. Padilla, "Strengthening of adobe houses for seismic actions," in *Proceedings of the 7th World*

Conference on Earthquake Engineering, pp. 465–472, Istanbul, Turkey, September 1980.

[10] M. R. Maheri, F. Naeim, and M. Mehrain, "Performance of adobe residential buildings in the 2003 Bam, Iran, earthquake," *Earthquake Spectra*, vol. 21, supplement 1, pp. S337–S344, 2005.

[11] C. A. Hendriks, E. Worrell, D. De Jager, K. Blok, and P. Riemer, "Emission reduction of greenhouse gases from the cement industry," in *Proceedings of the 4th International Conference on Greenhouse Gas Control Technologies*, pp. 939–944, 1998.

[12] International Cement Review, "Global cement report," Tech. Rep., International Cement Review, 2013.

[13] L. L. Ong, "Burgernomics: the economics of the Big Mac standard," *Journal of International Money and Finance*, vol. 16, no. 6, pp. 865–878, 1997.

[14] Y. Matsuoka, T. Shindoh, K. Yakota, and S. Kusui, "Property of β-1, 3-glucan (curdlan) as a viscosity agent for super-workable concrete," *ACI Special Publication*, vol. 173, pp. 475–491, 1997.

[15] I. Chang and G.-C. Cho, "Strengthening of Korean residual soil with β-1,3/1,6-glucan biopolymer," *Construction and Building Materials*, vol. 30, pp. 30–35, 2012.

[16] I. Chang and G.-C. Cho, "Geotechnical behavior of a beta-1,3/1,6-glucan biopolymer-treated residual soil," *Geomechanics and Engineering*, vol. 7, no. 6, pp. 633–647, 2014.

[17] I. Chang, A. K. Prasidhi, J. Im, and G.-C. Cho, "Soil strengthening using thermo-gelation biopolymers," *Construction and Building Materials*, vol. 77, pp. 430–438, 2015.

[18] I. Chang, J. Im, A. K. Prasidhi, and G.-C. Cho, "Effects of Xanthan gum biopolymer on soil strengthening," *Construction and Building Materials*, vol. 74, pp. 65–72, 2015.

[19] M. C. Cadmus, L. K. Jackson, and K. A. Burton, "Biodegradation of xanthan gum by *Bacillus sp*.," *Applied and Environmental Microbiology*, vol. 44, no. 1, pp. 5–11, 1982.

[20] A. Becker, F. Katzen, A. Pühler, and L. Ielpi, "Xanthan gum biosynthesis and application: a biochemical/genetic perspective," *Applied Microbiology and Biotechnology*, vol. 50, no. 2, pp. 145–152, 1998.

[21] P.-E. Jansson, B. Lindberg, and P. A. Sandford, "Structural studies of gellan gum, an extracellular polysaccharide elaborated by *Pseudomonas elodea*," *Carbohydrate Research*, vol. 124, no. 1, pp. 135–139, 1983.

[22] I. Giavasis, L. M. Harvey, and B. McNeil, "Gellan gum," *Critical Reviews in Biotechnology*, vol. 20, no. 3, pp. 177–211, 2000.

[23] G. G. Ferruzzi, N. Pan, and W. H. Casey, "Mechanical properties of gellan and polyacrylamide gels with implications for soil stabilization," *Soil Science*, vol. 165, no. 10, pp. 778–792, 2000.

[24] ASTM D1633-00, *Standard Test Methods for Compressive Strength of Molded Soil-Cement Cylinders*, ASTM International, West Conshohocken, Pa, USA, 2007.

[25] P. J. Walker, "Strength, durability and shrinkage characteristics of cement stabilised soil blocks," *Cement and Concrete Composites*, vol. 17, no. 4, pp. 301–310, 1995.

[26] J. R. del Viso, J. R. Carmona, and G. Ruiz, "Shape and size effects on the compressive strength of high-strength concrete," *Cement and Concrete Research*, vol. 38, no. 3, pp. 386–395, 2008.

[27] M. Tokyay and M. Özdemir, "Specimen shape and size effect on the compressive strength of higher strength concrete," *Cement and Concrete Research*, vol. 27, no. 8, pp. 1281–1289, 1997.

[28] British Standard Institute, "Eurocode 6. Design of masonry structures. Simplified calculation methods for unreinforced masonry structures," BS EN 1996-3:2006, British Standard Institute, 2006.

[29] British Standard Institute, "Specification for masonry units. Clay masonry units," BS EN 771-1:2011, British Standard Institute, 2011.

[30] International Code Council, *International Building Code 2012*, International Code Council, 2011.

[31] G. Davis and J. H. Song, "Biodegradable packaging based on raw materials from crops and their impact on waste management," *Industrial Crops and Products*, vol. 23, no. 2, pp. 147–161, 2006.

[32] G. Scott, "Green polymers," *Polymer Degradation and Stability*, vol. 68, no. 1, pp. 1–7, 2000.

[33] European Standard, "Packaging—requirements for packaging recoverable through composting and biodegradation—test scheme and evaluation criteria for the final acceptance of packaging," CSN EN 13432, 2013.

[34] P. Helby, "Environmental agreements at European Community level—reflections based on member state experience," *Journal of Cleaner Production*, vol. 10, no. 2, pp. 183–193, 2002.

[35] GBI Research, *Biopolymer Market Forecasts and Growth Trends to 2015—Starch—Based Polymers Driving the Growth*, 2010.

[36] D. K. Platt and Rapra Technology Limited, *Biodegradable Polymers: Market Report*, Rapra Technology, Shrewsbury, UK, 2006.

[37] J. Lampinen, "Trends in bioplastics and biocomposites," Developments in Adcanced Biocomposites, VTT Technical Research Centre of Finland, Espoo, Finland, 2010.

[38] R. P. Babu, K. O'Connor, and R. Seeram, "Current progress on bio-based polymers and their future trends," *Progress in Biomaterials*, vol. 2, no. 1, pp. 1–16, 2013.

[39] Frost &Sullivan, *Global Bio-Based Plastics Market*, Frost &Sullivan Research Service, 2009.

[40] W. P. Weisrock, "Method for improving xanthan yield," Google Patents, 1981.

[41] F. García-Ochoa, V. E. Santos, J. A. Casas, and E. Gómez, "Xanthan gum: production, recovery, and properties," *Biotechnology Advances*, vol. 18, no. 7, pp. 549–579, 2000.

[42] A. Palaniraj and V. Jayaraman, "Production, recovery and applications of xanthan gum by *Xanthomonas campestris*," *Journal of Food Engineering*, vol. 106, no. 1, pp. 1–12, 2011.

[43] S. Kalogiannis, G. Iakovidou, M. Liakopoulou-Kyriakides, D. A. Kyriakidis, and G. N. Skaracis, "Optimization of xanthan gum production by *Xanthomonas campestris* grown in molasses," *Process Biochemistry*, vol. 39, no. 2, pp. 249–256, 2003.

[44] Q. Li, W. Yan, K. Yang, Y. Wen, and J.-l. Tang, "Xanthan gum production by *Xanthomonas campestris* pv. campestris 8004 using cassava starch as carbon source," *African Journal of Biotechnology*, vol. 11, no. 73, pp. 13809–13813, 2012.

[45] S. Moshaf, Z. Hamidi-Esfahani, and M. H. Azizi, "Optimization of conditions for xanthan gum production from waste date in submerged fermantation," *World Academy of Science, Engineering and Technology*, vol. 57, pp. 521–524, 2011.

[46] S. Rosalam and R. England, "Review of xanthan gum production from unmodified starches by *Xanthomonas comprestris* sp.," *Enzyme and Microbial Technology*, vol. 39, no. 2, pp. 197–207, 2006.

[47] Global Industry Analysts, *Global Starch Industry*, Global Industry Analysts, 2014.

[48] I. B. Bajaj, S. A. Survase, P. S. Saudagar, and R. S. Singhal, "Gellan gum: fermentative production, downstream processing and applications," *Food Technology and Biotechnology*, vol. 45, no. 4, pp. 341–354, 2007.

[49] R. Rapier, "Global carbon dioxide emissions—facts and figures," Consumer Energy Report, 2012.

[50] R. Rehan and M. Nehdi, "Carbon dioxide emissions and climate change: policy implications for the cement industry," *Environmental Science and Policy*, vol. 8, no. 2, pp. 105–114, 2005.

[51] E. Worrell, L. Price, N. Martin, C. Hendriks, and L. O. Meida, "Carbon dioxide emissions from the global cement industry," *Annual Review of Energy and the Environment*, vol. 26, pp. 303–329, 2001.

Hindawi Publishing Corporation
International Journal of Polymer Science
Volume 2015, Article ID 615284, 11 pages
http://dx.doi.org/10.1155/2015/615284

Research Article

Thermal Degradation and Damping Characteristic of UV Irradiated Biopolymer

Anika Zafiah M. Rus and Nik Normunira Mat Hassan

Sustainable Polymer Engineering, Advanced Manufacturing and Material Center (AMMC), Universiti Tun Hussein Onn Malaysia, Parit Raja, Batu Pahat, 86400 Johor, Malaysia

Correspondence should be addressed to Anika Zafiah M. Rus; zafiah@uthm.edu.my

Received 5 April 2015; Revised 24 June 2015; Accepted 29 June 2015

Academic Editor: Dilip Depan

Biopolymer made from renewable material is one of the most important groups of polymer because of its versatility in application. In this study, biopolymers based on waste vegetable oil were synthesized and cross-link with commercial polymethane polyphenyl isocyanate (known as BF). The BF was compressed by using hot compression moulding technique at 90°C based on the evaporation of volatile matter, known as compress biopolymer (CB). Treatment with titanium dioxide (TiO_2) was found to affect the physical property of compressed biopolymer composite (CBC). The characterization of thermal degradation, activation energy, morphology structure, density, vibration, and damping of CB were determined after UV irradiation exposure. This is to evaluate the photo- and thermal stability of the treated CB or CBC. The vibration and damping characteristic of CBC samples is significantly increased with the increasing of UV irradiation time, lowest thickness, and percentages of TiO_2 loading at the frequency range of 15–25 Hz due to the potential of the sample to dissipate energy during the oscillation harmonic system. The damping property of CBC was improved markedly upon prolonged exposure to UV irradiation.

1. Introduction

Waste vegetable based palm oils are the most abundant biological sources and important raw materials for the production of biobased polyurethanes. The main components existing in waste vegetable oil are triglycerides with saturated and unsaturated fatty acids useful in many synthesis transformations and they become new polyol sources [1]. In polymer industry, waste vegetable oils which represent a major potential source of chemicals have been utilized as an alternative feedstock for biomonomers [2–4].

Synthesis of biomonomer is started with the preparation of catalyst to generate the epoxides from the unsaturated fatty compounds of the waste vegetable oil. The condensation process comprises acid-catalysed ring opening of the epoxides to form polyols. The polyol will be reacted with the crosslinking agents to produce flexible biopolymer foam and will be added to TiO_2 filler to produce biopolymer composite foam.

Polyurethane (PU) foams are versatile engineering materials with a wide range of applications because of their properties that can be readily tailored to form different types of polymer composition. Generally, PU foams are one of the major productions of urethane polymer structure [5]. The formation of biopolymer foam followed the same general reaction of isocyanate with biomonomer and both of which are derived when polymerization reactions occur similar to nearly all polymeric materials [6]. The forming process of biopolymer foam consists of three basic stages such as bubble initiation, bubble growth, and cell opening [7].

In order to enhance the photostability of biopolymer foam, the pretreatment of the physical property of biopolymer foam is needed, which includes UV stabilizer filler such as titanium dioxide (TiO_2). TiO_2 is also an inorganic pigment and is used as an additive of excellent UV screener to reflect the light away from the polymer surface [8]. This pigment is important in polymer as an inner screen for photoproducts and it limited the photooxidative phenomena. It can

also be used to reduce cost, reinforcement, and hardening, improving slip and storage stability. Furthermore, TiO_2 has been recognized as the most important photocatalyst for the degradation of many organic pollutants in water and air [9].

The development of foam block system of single degree of freedom is to measure the dynamic response of foam at different levels of compression and excitation. This is to identify the foam viscoelastic properties through a foam modeling that is designed. This concept is to design the foam block system which will contribute to seat-occupant system. The system can be applied in a wide range of polymeric materials for foam dynamic response measurement and its characterization based on the vibration of potential energy, kinetic energy, and energy loss (damping) [10, 11].

The performance of vibration transmissibility and damping characteristic of biopolymer foam using foam block system for automotive applications is important due to the method of transmissibility test that can be used in a wide range of polymeric materials which possess nonlinear viscoelastic properties. Vibration transmissibility is a ratio of the force amplitude transmitted to the amplitude foundation of the applying excitation. This method is also used to determine the damping characteristic of the system that consists of coulomb and viscous damping from free vibration decrements of mass spring system [12].

2. Experimental

2.1. Materials. The biomonomer conversions from waste vegetable oils are started with the in-house catalyst preparation to generate the epoxies from the unsaturated fatty compound. The acid-catalyst ring opening of the epoxides is to form polyols [13–17].

2.2. Preparation of Samples. The weights of compositions were determined based on the ratio of biomonomer and isocyanate with the ratio of 2 : 1 [16]. The biopolymer flexible (BF) foam was doped with titanium dioxide (TiO_2) Degussa at different percentages which is 0%, 2.5%, 5.0%, 7.5%, and 10.0%, equivalent to the weight of biomonomer. The mixture was vigorously stirred with hand mixer in a cup for 30 seconds. The mixtures were then immediately cast into an open mould to allow the biopolymer to expand out as foam. It was left for 6 hours to cure and was removed from the mould.

One hundred and sixty grams of biopolymer foam was weighed and filled in the mould cavity with internal core size of 180 × 180 × 15 mm in order to decrease the thickness and pore size by using hot compression moulding. The parameter of the hot compression machine was set at 90°C of temperature, under 26 tonnes of pressure within 1 hour [18–22]. The compress biopolymer (CB) samples and compress biopolymer composite (CBC) were further prepared into 50 mm × 50 mm × 10 mm block. CB and CBC blocks were irradiated to UV light in UV Lamp Test Chamber Model HD-703 (Haida International Equipment Co., Ltd.) at 250 hours, 500 hours, 750 hours, and 1000 hours at 50°C to simulate harsh environmental weather condition. This was carried out using an array of UV fluorescent lamps emitting light in the region from 280 to 320 nm with a tail extending to 400 nm.

2.3. Physical Characterization

2.3.1. Thermal Gravimetric Analysis (TGA). Thermal gravimetric analysis (TGA) measurement of BF and BC was performed using *Linseis TGA* to characterize the thermal properties of samples according to ISO 11358. The weight loss and derivative weight loss were measured at 20°C to 900°C with heating rate of 10°C/min under oxygen atmosphere and flow rate of 0.3 μL using alumina crucible. Furthermore, activation energy of BF and BC samples was determined by using Flynn method [23].

2.3.2. Density. The CBC samples were cut into 10 mm × 10 mm × 5 mm to conduct the density test according to ASTM D3575 [20–24] at various UV irradiation exposure times calculated as follows:

$$\text{Density, } \rho = \frac{m}{v}, \tag{1}$$

where m = mass of sample and v = volume of sample.

2.3.3. Morphology Structure. The morphology surface structure of each BF and CB sample was sputter coated with gold at 25 mA plasma current and 2 Pa of chamber pressure to make them conducting. Cellular structure images were examined by using scanning electron microscope (SEM) of JEOL-JSM6380LA operating at 15 kV at 30x magnification.

2.4. Mechanical Characterization

2.4.1. Vibration and Damping Measurement System. The vibration transmissibility test was developed to determine the effectiveness of CBC block to reduce the unwanted base vibration. The transmissibility test was generated at various base excitation levels, namely, 1 mm and 1.5 mm displacement and 0.1 G (Gravity) and 0.15 G (gravity) of the acceleration base excitation in frequency range of 2–30 Hz for 10 mm, 15 mm, and 20 mm of samples thickness. Damping characterization of CBC block is studied by modeling a mass spring damper system at low frequency following ASTM D3580-95 [18–22].

3. Result and Discussions

3.1. Physical Characterization. The predetermined UV irradiation temperatures were based on weight loss curves (TG) and derivative thermogravimetric (DTG) evaluation of BF and CB samples. The first peak appeared at the temperature range less than 100°C due to the beginning of weight loss of volatile material [24–29] in the DTG evaluation profile of the samples. The first decomposition is the first degradation of biopolymer, second decomposition is the second degradation of biopolymer, and third decomposition is attributed to the third degradation of biopolymer.

The first peak of biopolymer decomposition temperature correlates with the hard segment while the second peak correlates with the degradation of the soft segment. Qualitative characterization of the degradation process is

Table 1: Thermal property of BF and CB samples.

Samples	BF	CB
First decomposition (°C)	238	253
T_{on} (°C)	94	126
T_{max} (°C)	283	384
Weight loss (%)	20%	20%
Second decomposition (°C)	419	410
T_{on} (°C)	283	384
T_{max} (°C)	494	507
Weight loss (%)	57%	53%
Third decomposition (°C)	567	584
T_{on} (°C)	494	508
T_{max} (°C)	678	679
Weight loss (%)	17%	25%

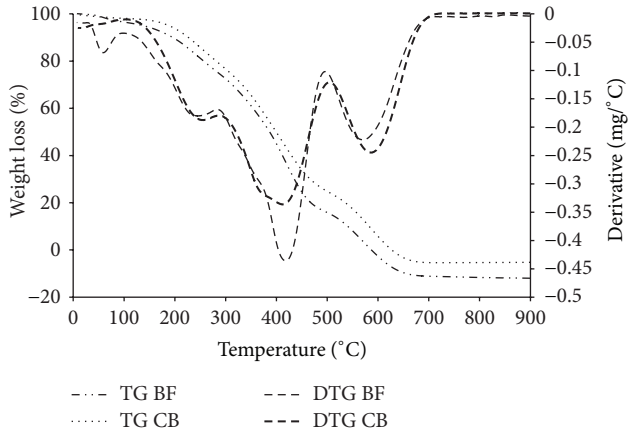

Figure 1: Thermogram (TG) and derivative weight loss (DTG) of BF and CB samples.

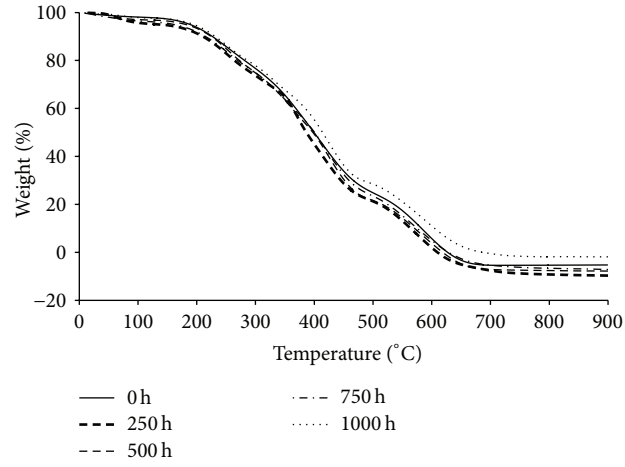

Figure 2: Thermogram weight loss of CB samples with UV irradiation.

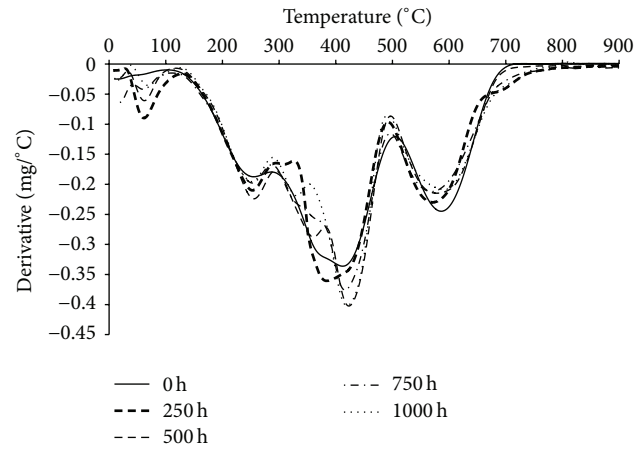

Figure 3: Thermogram DTG of CB samples with UV irradiation.

elaborated by the onset and maximum peak temperature of the first step T_{1on} and T_{1max} along with the same thing for the second step T_{2on} and T_{2max}. The details of TGA onset decomposition temperature (T_{onset}) and the maximum decomposition temperature (T_{max}) for BF and CB samples are shown in Table 1. The onset degradation temperature T_{onset} and the maximum degradation rate temperature T_{1max} of the first BF degradation stage are 238°C and 419°C. Figure 1 shows that the derivative weight loss of BF and CB was more than 94% and 98%, respectively. The weight loss of BF was started at less than 100°C indicated as volatile matter in samples which is equivalent to 4.3%. The hot compression moulding of CB samples at 90°C successfully removed the volatile matter. Therefore, the setting temperature of hot compression moulding was selected as 90°C.

The decomposition temperature is attributed to the crosslinker of flexible isocyanate content. It has been suggested that the amount of weight loss at each degradation stage may be used as a quantitative measurement of the hard and soft content in biopolymer. This is indicated by the first weight loss of BF and CB at almost the same situation for the first decomposition temperature at 238°C and 253°C, and the second decomposition temperature is at 419°C and 410°C, respectively.

Figures 2 and 3 show the major decomposition of CB samples with UV irradiation exposure in the high temperature ranges of 290°C to 510°C. This peak was attributed to hard segment of crosslinker as consequence of the relatively low thermal stability of the urethane groups. The degradation of CB samples depended on thermal stability of isocyanate (crosslinker) content in which it is less thermally stable after being UV irradiated. This is indicated by the decrease of the first weight loss of CB samples at 0 hour and 250 hours of UV irradiation for the first decomposition temperature at 253°C and 248°C. The second decomposition temperature is at 411°C and 380°C and the third decomposition temperature is at 584°C and 564°C, respectively. The duration of CB samples UV irradiation also affected the percentages of weight loss significantly. It indicated that irradiation of CB samples

Table 2: Thermal property of CB samples with UV irradiation exposure.

CB samples	UV irradiation				
	0 h	250 h	500 h	750 h	1000 h
Volatile (°C)		68	56	60	60
T_{on} (°C)		36	28	32	30
T_{max} (°C)		180	184	164	184
Weight loss (%)		5	2	3	2
First decomposition (°C)	253	248	184	248	252
T_{on} (°C)	126	180	332	164	184
T_{max} (°C)	384	312	492	280	284
Weight loss (%)	20	22	24	22	18
Second decomposition (°C)	411	380	420	416	420
T_{on} (°C)	384	312	332	280	284
T_{max} (°C)	508	460	492	494	484
Weight loss (%)	53	48	44	52	52
Third decomposition (°C)	584	564	576	572	588
T_{on} (°C)	508	460	492	494	484
T_{max} (°C)	679	660	650	650	668
Weight loss (%)	25	25	23	23	28

occurs due to photodegradation of biopolymer from the exposed CB samples surface.

Table 2 summarizes the percentages of derivative weight loss and decomposition temperature of CB samples with UV irradiation exposure from 0 hour to 1000 hours. The CB samples show that the new existing volatile peak less than 100°C is started with 250 hours of UV irradiation exposure. This is due to the formation of water soluble product in addition to volatile product at surface of CB samples during exposure to UV irradiation. The weight loss of volatile material gives 5% at 250 hours and leads to reduction of 2% at 1000 hours. The first peak of degradation of CB samples with UV irradiation was started at around 120°C to 290°C, and it is attributed to the first decomposition of biopolymer. However, the second decomposition was started from 290°C to 510°C due to the degradation of polymeric hard segment phase. Meanwhile, the third decomposition stage began at 510°C to 670°C which refers to the soft segment of polymeric degradation temperature.

3.2. Kinetic Analysis (Activation Energy). The degradation process of BF and CB samples can be characterized by activation energy, measured with TGA experimental data using analytical method proposed by Flynn. This is due to mechanism changes during the degradation of biopolymer; activation energy not only is a function of chemical structure of polymer but also varies with conversion. It provides a parameter for the assessment of thermal stability of biopolymer.

Flynn method is applied to low conversion between 1% and 5% of nonisothermal differential weight loss (DTGA) method with constant heating rate, Hr. In this study, the conversion rate α is defined as the degree of conversion (α) = weight loss at the given temperature (total weight loss of the degradation), respectively [23]. α is defined by

$$\alpha = 1 - \frac{w(t)}{w_o}, \tag{2}$$

where w_o = initial weight, $w(t)$ = weight at any time, and t = during degradation.

The fundamental rate equation in all kinetic studies is expressed as

$$\frac{d\alpha}{dt} = k(T)\, f(\alpha) = A \exp\left(\frac{-E_a}{RT}\right) f\alpha, \tag{3}$$

where k = rate constant and $f(\alpha)$ = reaction model, a function depending on the actual reaction mechanism.

For nonisothermal thermogravimetric analysis at constant heating rate, (3) may be written as (4) by using Flynn method [23]

$$\frac{d}{dt}\left[T^2 \frac{d\alpha}{dT}\right] = \frac{E_a}{T} + 2T, \tag{4}$$

where E_a = activation energy (kJ/mol), R = gas constant (8.314 J/K·mol), and T = absolute temperature (K).

In this study, it is assumed that BF and CB samples are a first order reaction. Although it is not always the case, but the simplicity and the number of parameters of the first order model allow the direct comparison of different sample to provide preliminary parameter for further and more accurate modeling. In Flynn method, $T^2(d\alpha/dt)$ is plotted against α for series of experiment performed using TGA at 10°C/min heating rate with peak temperature obtained from the DTG curve.

The activation energy of BF and CB samples is referred to in Figure 4. The activation energy of BC sample gives high values as compared to BF samples that are 1051 kJ/mol and 1022 kJ/mol, respectively. The similar trend was observed in the third decomposition of BC samples which is 1714 kJ/mol and 1680 kJ/mol, respectively. Furthermore, the activation energy of BF samples is the highest at the second decomposition which is 1384 kJ/mol as compared to that of BC

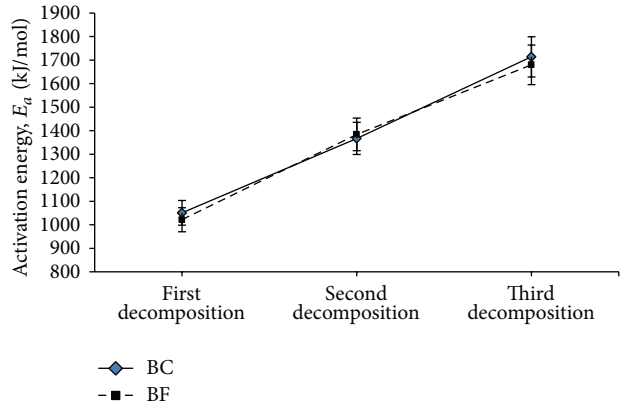

Figure 4: Activation energy of BF and CB samples before UV irradiation.

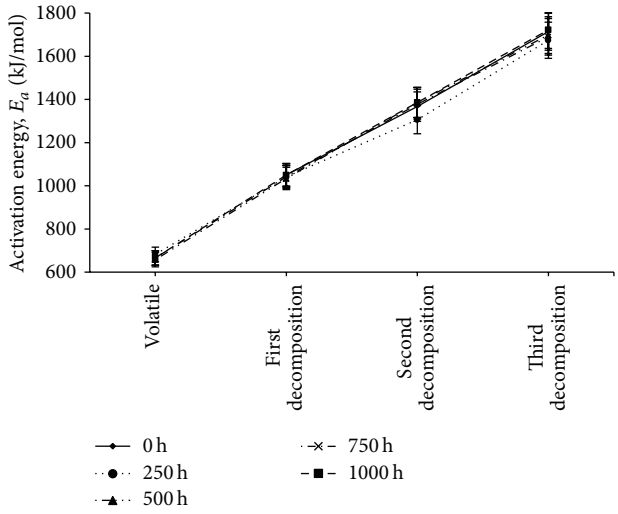

Figure 5: Activation energy of CB samples of UV irradiation.

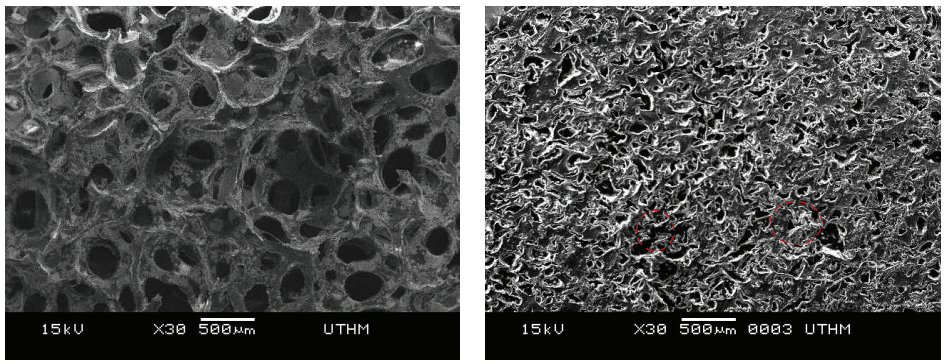

(a) (b)

Figure 6: SEM micrograph: (a) BF samples (b) CB samples.

samples which is 1367 kJ/mol. This is due to the degradation of crosslinker at the hard segment in biopolymer.

Figure 5 shows the activation energy of CB samples of UV irradiation exposure from 0 hours to 1000 hours. The activation energy of CB samples gives similar trend on the following ranges: the first decomposition temperature (1030–1050 kJ/mol), second decomposition temperature (1300–1390 kJ/mol), and third decomposition temperature (1670–1725 kJ/mol), respectively. This is due to the thermal stability of CB samples at the hard segment that has a great influence on the thermal stability of soft segment. The higher thermal stability of hard segment leads to a higher degradation temperature of soft segment whilst the activation energy of CB samples is the highest at the higher thermal stability of CB samples.

In comparison, the activation energy of CB samples of UV irradiation at the volatile matter which is less than 100°C due to evaluation of volatile matter in CB samples is the minimum activation energy of UV irradiation. As an energy barrier, activation energy provides the information of critical energy needed to start the reaction, to ensure the lower activation energy and the lowest temperature required for photostability of CB samples.

3.3. Morphology Structure. The BF samples represent having open-cell cellular structure and anisotropic. According to Gibson and Ashby (1997), it was reported that almost all man-made foams are anisotropic [30]. The open-cell structure comprises many small open windows located on the cell wall and these cause the struts formed in between the open window. The SEM results present the cell distribution of BF samples that shows uniform pore distribution, smaller cell size, and homogeneity. The larger cells were found on BF sample with 4.14 μm compared to cellular structure of CB samples of 143.71 μm as refer to Figure 6.

Table 3 shows the pore density per volume of CB and BF samples in which the highest is 5.59×10^6 cm^{-1} and the lowest is 1.56×10^6 cm^{-1} respectively before UV exposure. The Nv

Table 3: Number, diameter, and pore density per volume of BF and CB samples.

Sample	BF	CB
Number of pores	15	35
Diameter of pore (μm)	411	104
Nv (10^6) cm^{-1}	1.56	5.59

was decreased during UV exposure down to 27.786×10^6 cm^{-1} of BF samples. In addition, UV irradiation exposure changed the diameter of pores size of BF samples. The pore density of BF samples was obtained by Kumar and Suh method [31]. In this method, the number of pores was examined by counting the pore in the SEM micrographs. The magnification is M, area of SEM image is A, and $(n \cdot M^2/A)$ would give a pore density per unit area and can be converted to pore density per volume, Nv as follows:

$$Nv = \left(\frac{n \cdot M^2}{A} \right)^{3/2}. \quad (5)$$

Goren et al. (2010) investigated the pore density of foam provided by (5) based on the final foamed volume and not based on the initial volume of the sample influenced by filler sizes and filler surface [32].

The morphology structure of CB is the decrease of cell number after the tension is applied by compression technique. The spherical shapes structure of foam change to small particles and become thicker. This is due to the fact that the open-cell cellular foam is of molecular changes and is close to each other. However, the strut and cell of wall are connected to each other and elimination of cell distribution occurs. This causes the particle or cell size of CB samples to be significantly compact after using hot compression technique. This is due to the particles of the samples after being compressed.

Figure 7 shows that the morphology of the surface and cross section of CB samples were exposed to UV irradiation. The morphology of cross section structure of CB samples shows apparent small cell size distribution at the highest UV irradiation time exposure. The diameter cell size of CB samples was smaller with the increase of UV irradiation time exposure. The surface of CB samples became much rougher after UV irradiation for 1000 hours. This is caused by UV irradiation influence on the surface roughness of CB samples and photodegradation is occurring during irradiation. From the observation, the overall structure has no major difference after UV irradiation exposure, indicating that it has high photostability [21].

3.4. Density. Density is an important parameter in conjunction with the application of lightweight materials. CB density is higher than BF density which are 0.0561 g/cm^3 and 0.7838 g/cm^3, respectively, due to the porosity structure or particle structure of both biopolymer samples. The porosity of BF is higher as compared to CB due to the high porosity in the samples: 0.014 and 0.0043, respectively. This is due to the fact that the materials produced from particle structure gave higher density than the materials produced from cellular structure [18].

UV irradiation and different percentages of TiO_2 loading influence the density of samples as it is referred to in Figure 8. The density of CBC samples was significantly increased with the increment of TiO_2 loading and fluctuated with UV irradiation up to 1000 hours. Density of CBC samples was decreased at 250 hours of UV irradiation exposure and increased slowly up to 750 hours and drop at 1000 hours. The highest density of CBC samples is 10% TiO_2 loading of 1.1088 g/cm^3 due to the amount of filler loading in the samples. However, the density of CBC samples was linearly increased at 7.5% of TiO_2 loading from 0 hours to 750 hours and dropped at 1.091 g/cm^3 after 1000 hours of UV irradiation.

In general, the decrease of the density was influenced by the increase of the cell size and window cell of the foam [33]. According to the American National Standard Particleboard (1999), the material produced from particle structure gave higher density than the material produced from cellular structure [34].

3.5. Vibration Transmissibility and Damping Characteristic of CBC Samples. Vibration transmissibility and damping characteristic of CBC samples significantly changed after UV irradiated exposure at different samples thickness: 10 mm, 15 mm, and 20 mm. The maximum resonance peak for acceleration base excitation was observed at the range of 23–25 Hz, and displacement base excitation was observed at the range of 19–23 Hz. The resonance peak is equal to the vibration transmissibility of CBC samples as indicated in Figure 9. The lowest the thickness of CBC samples, the highest the reduction of vibration transmissibility. This is due to the stable vibration transmitted at the lowest thickness [22] for CBC samples, and more energy is dissipated when the density of the surface is increased. This situation occurs in relation to the resonance frequency of CBC block system which is due to the changes in stiffness during testing [35]. Furthermore, the resonance frequency and attenuation frequency shifted to the low frequency while increasing the thickness of the samples.

Damping of CBC samples was increased with the increment of UV irradiation exposure time for acceleration and displacement base excitation as it is referred to in Figure 10. The damping of CBC samples was significantly increased at the maximum transmissibility at the range of 15 to 25 Hz. The samples structure with higher porosity and higher particles density can offer better damping characteristic [36]. In this case, CBC samples are able to dissipate the vibrations through the polymer composite of long molecule chains when the moveable top plates vibrate.

Figure 11 indicated the damping of CBC with different ratio of TiO_2 loading of displacement base excitation at 1 mm and 1.5 mm with acceleration of 0.1 G and 0.15 G of 10 mm

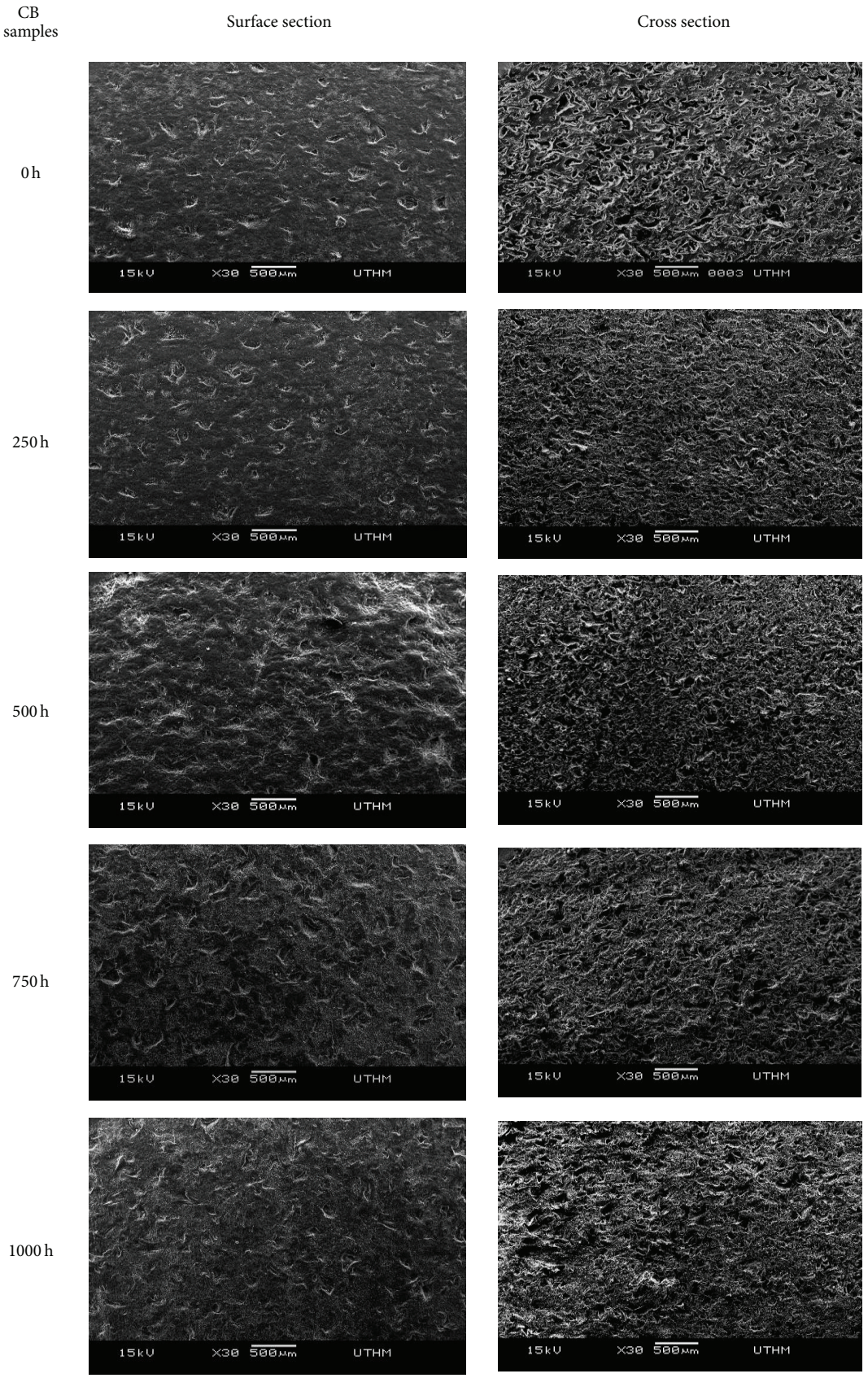

Figure 7: Morphology of CB samples with UV irradiation.

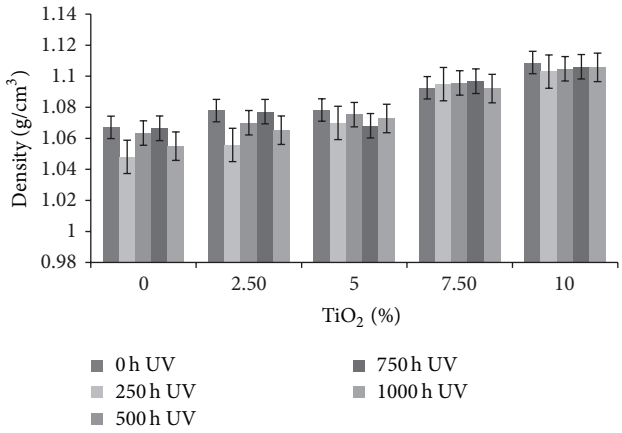

Figure 8: Density of CBC with different percentage loading of TiO_2 and UV irradiation exposure.

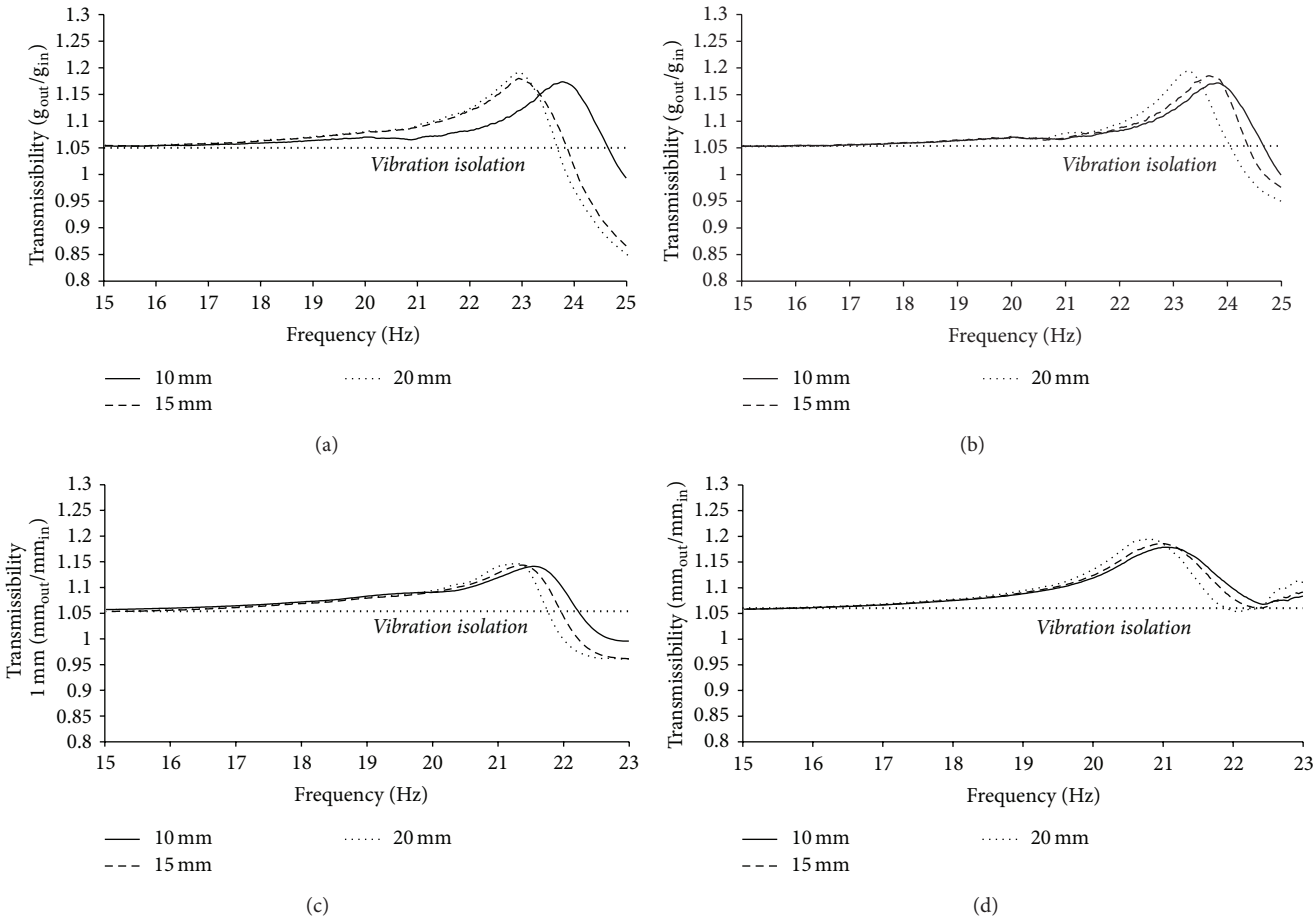

Figure 9: Transmissibility curve from base to moveable top plate: (a) 0.15 G and (b) 0.1 G and (c) 1 mm and (d) 1.5 mm base excitation.

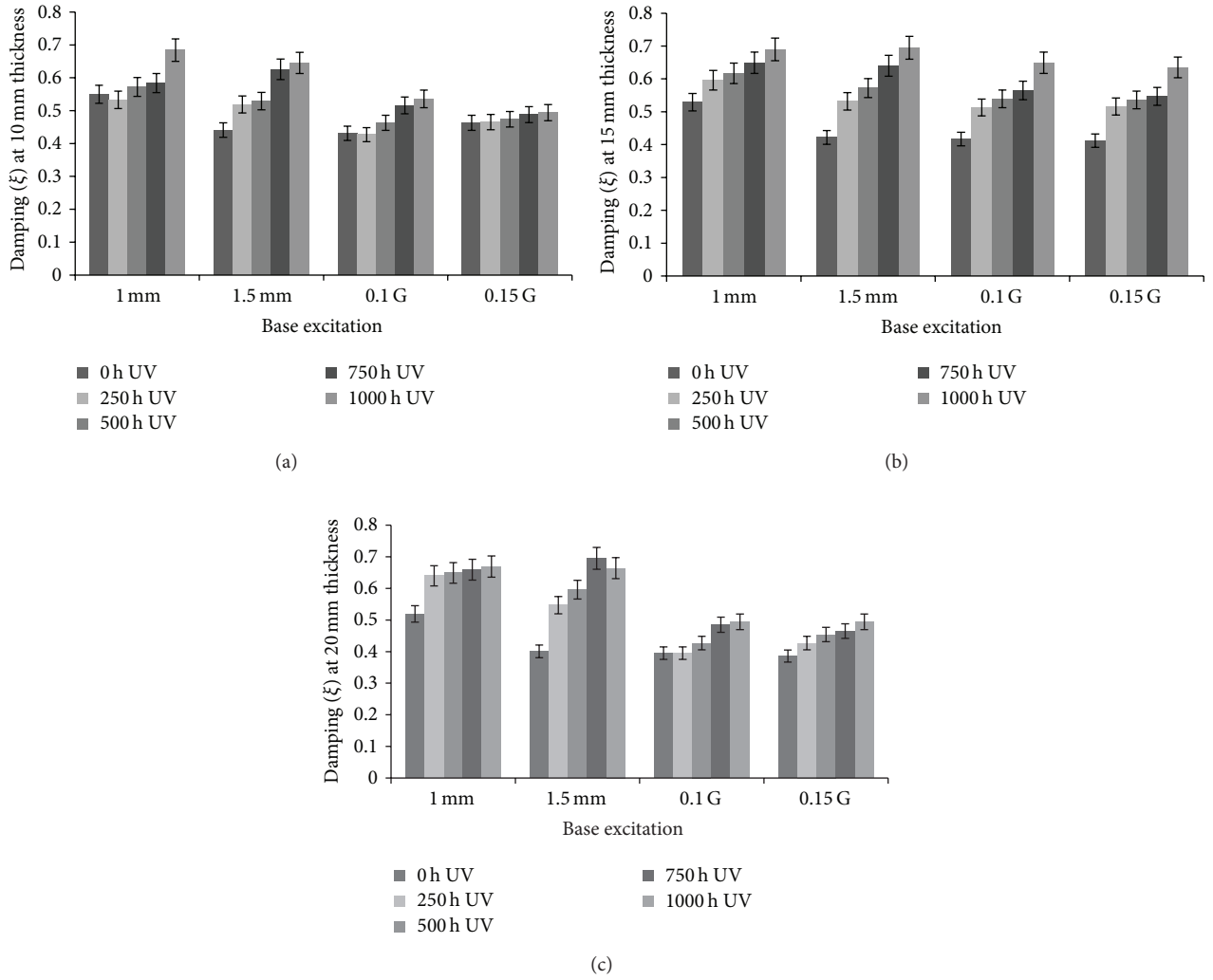

Figure 10: Damping of CBC samples of (a) 10 mm, (b) 15 mm, and (c) 20 mm thickness at different UV irradiation exposure time.

thickness. The results show that the damping of CBC samples is decreased with the increase of TiO_2 loading. Meanwhile, in average, the increase of UV irradiation exposure times revealed that the damping characteristic of CBC samples was increased. These results may indicate that the molecules of CBC samples lead to the break (chain scission), cross-link, or suffering of substitution reaction after UV irradiation [37]. Therefore, this argumentation is based on the molecular motion resulting from further cross-linking leading to higher dissipation energy throughout the thermoset during the transmissibility testing.

In addition, the characteristic of damping is an important property of materials due to the fact that the damping capacity is usually used to evaluate the material ability to dissipate elastic strain energy when it is subjected to vibratory loads [38]. Hence, the damping characteristic of CBC samples has become an important requirement in the design automotive and aerospace structures [36].

4. Conclusion

Biopolymer flexible (BF) foam is a renewable polymer based on waste vegetable cooking oil. The thermal degradation and activation energy of BF and CB samples increase with the increasing of UV irradiation time of the first degradation, second degradation, and third degradation. The morphological structure of BF and CB samples gives smaller diameter size and increased surface roughness after UV exposure. The vibration and damping characteristic of CBC samples is significantly increased with the increase of UV irradiation time, the lowest thickness, and the percentages of TiO_2 loading at the frequency range of 15–25 Hz. Cross-linking influences the properties of CBC sample. The use of high functional reactants, for example, polyol and diisocyanate, leads to a crosslink network. Moreover, an excess of diisocyanate (NCO/OH) may cause chain branching and chemical cross-link. Thus, highly crosslink CBC is useful for application, such as insulation material or automotive part.

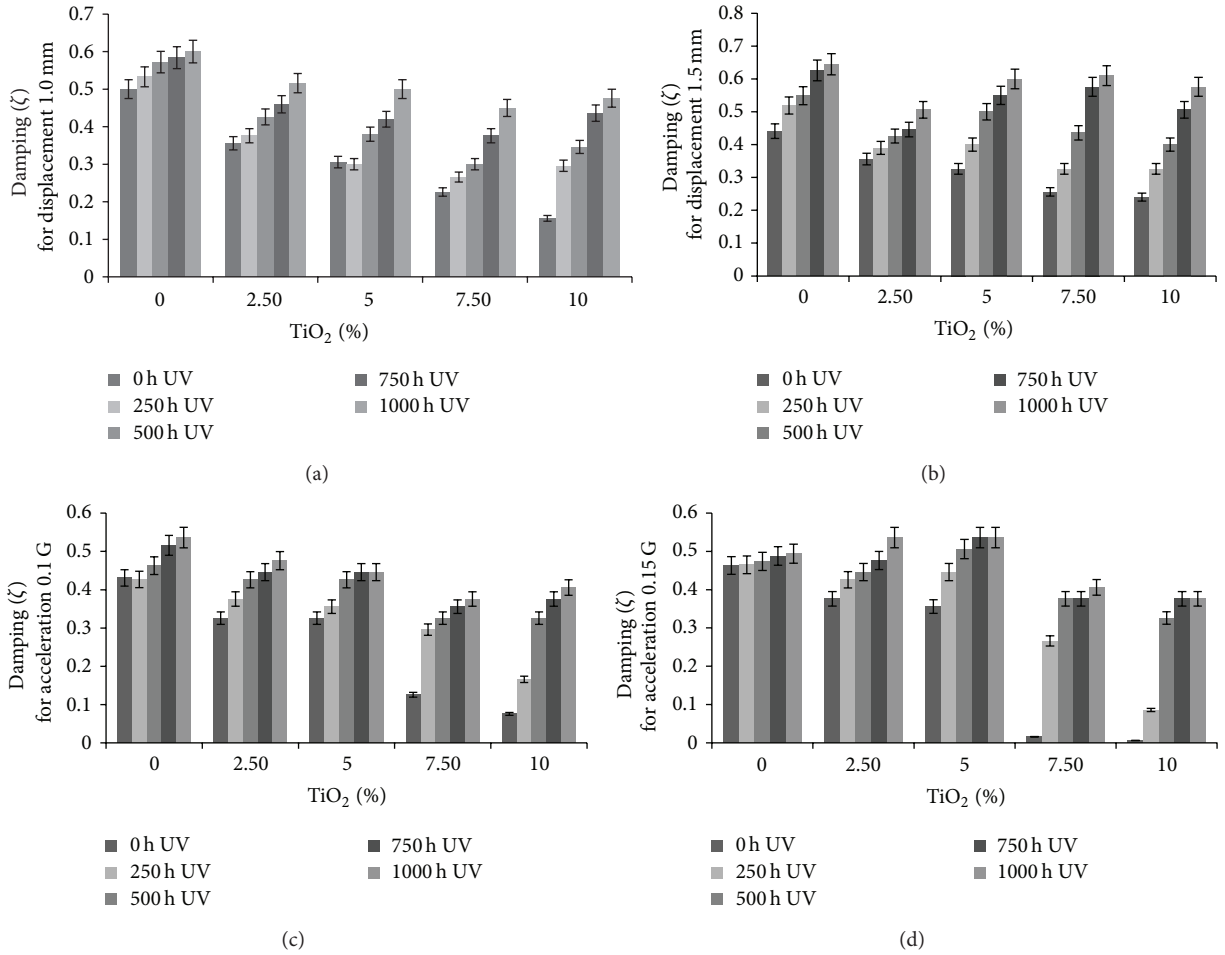

Figure 11: Damping of CBC samples: (a) 0.15 G and (b) 0.1 G and (c) 1 mm and (d) 1.5 mm base excitation of 10 mm thickness with TiO_2 with UV irradiation.

Conflict of Interests

The authors declare that there is no conflict of interests regarding the publication of this paper.

Acknowledgments

The authors would like to thank the Malaysian Government and Universiti Tun Hussein Onn Malaysia (UTHM), Johor, and the Malaysian Technical University Centre of Excellence (MTUN CoE) for supporting this research study under research Grant Vot C014, Exploratory Researched Grant Scheme, ERGS Vot E108, and Fundamental Research Grant Scheme, FRGS Vot 1481.

References

[1] J. C. Ronda, G. Lligadas, M. Galià, and V. Cádiz, "Vegetable oils as platform chemicals for polymer synthesis," *European Journal of Lipid Science and Technology*, vol. 113, no. 1, pp. 46–58, 2011.

[2] S. S. Narine, X. Kong, L. Bouzidi, and P. Sporns, "Physical properties of polyurethanes produced from polyols from seed oils: II. Foams," *Journal of the American Oil Chemists' Society*, vol. 84, no. 1, pp. 65–72, 2007.

[3] A. Z. M. Rus, "Degradation studies of polyurethanes based on vegetables oils. (Part I)," *Progress in Reaction Kinetics and Mechanism, Science Reviews*, vol. 33, pp. 363–391, 2008.

[4] A. Z. Mohd-Rus, T. J. Kemp, and A. J. Clark, "Degradation studies of polyurethanes based on vegetable oils. Part 2. thermal degradation and materials properties," *Progress in Reaction Kinetics and Mechanism*, vol. 34, no. 1, pp. 1–41, 2009.

[5] N. N. M. Hassan, A. Z. M. Rus, and M. I. Ghazali, "Acoustic performance of green polymer foam from renewable resources after UV exposure," in *Proceedings of the International Conference on Mechanical Engineering Research (ICMER '13)*, July 2013.

[6] H. Lim, S. H. Kim, and B. K. Kim, "Effects of silicon surfactant in rigid polyurethane foams," *eXPRESS Polymer Letters*, vol. 2, no. 3, pp. 194–200, 2008.

[7] D. Klempner and V. Sendijarevic, *Polymeric Foams And Foam Technology*, Hanser, Munich, Germany, 2nd edition, 2004.

[8] J. Robinson, A. Linder, A. Gemmel et al., "Comparison of standard UV test method for the ageing of cables," in *Proceedings of the 60th International Wire & Cable Symposium*, pp. 329–337, 2011.

[9] A. Hazarika and T. K. Maji, "Modification of softwood by monomers and nanofillers," *Defence Science Journal*, vol. 64, no. 3, pp. 262–272, 2014.

[10] R. Singh, P. Davies, and A. K. Bajaj, "Estimation of the dynamical properties of polyurethane foam through use of Prony series," *Journal of Sound and Vibration*, vol. 264, no. 5, pp. 1005–1043, 2003.

[11] G. Joshi, A. K. Bajaj, and P. Davies, "Whole-body vibratory response study using a nonlinear multi-body model of seat-occupant system with viscoelastic flexible polyurethane foam," *Industrial Health*, vol. 48, no. 5, pp. 663–674, 2010.

[12] J. W. Liang and B. F. Feeny, "Identifying coulomb and viscous friction from free-vibration decrements," *Nonlinear Dynamics*, vol. 16, no. 4, pp. 337–347, 1998.

[13] A. Z. M. Rus, "Polymers from renewable materials," *Science Progress*, vol. 93, no. 3, pp. 285–300, 2010.

[14] A. Z. M. Rus, "Effect of titanium dioxide on material properties for renewable rapeseed and sunflower polyurethane," *International Journal of Integrated Engineering*, vol. 1, no. 1, pp. 15–22, 2009.

[15] N. N. M. Hassan, A. Z. M. Rus, S. Nurulsaidatulsyida, and S. R. Mohid, "Acoustic study based on sustainable green polymer treated with H_2O," *Advanced Materials Research*, vol. 748, pp. 281–285, 2013.

[16] N. Sulong, *Utilization of low hydroxyl content of waste oil polymer foam doped with waste materials for sound absorption application [M.S. thesis]*, Universiti Tun Hussein Onn Malaysia, 2011.

[17] A. Z. M. Rus, N. M. H. Nik, and R. A. B. Rahim, "Influence of multilayer textile biopolymer foam doped with titanium dioxide for sound absorption materials," *Key Engineering Materials*, vol. 594-595, pp. 750–754, 2014.

[18] N. A. Latif, A. Z. M. Rus, and A. G. M. K. Zaimy, "Effect of thickness for sound absorption of high density biopolymer foams," *Key Engineering Materials*, vol. 594-595, pp. 183–187, 2014.

[19] N. A. Latif, A. Z. M. Rus, and M. K. Z. A. Ghani, "Influence of hot compression moulding of particulate biopolymer and their sandwich layups for sound absorption characteristic," *Applied Mechanics and Materials*, vol. 465-466, pp. 1044–1048, 2014.

[20] S. M. Rus, N. A. Latif, M. I. Ghazali, and A. Z. M. Rus, "Characteristics of UV irradiated waste biopolymer from renewable resources (Part 1)," *Advanced Materials Research*, vol. 974, pp. 252–256, 2014.

[21] S. M. Rus, M. I. Ghazali, and A. Z. M. Rus, "Characteristics of UV irradiated waste biopolymer from renewable resources (Part 2)," *Advanced Materials Research*, vol. 974, pp. 257–261, 2014.

[22] N. A. Latif and A. Z. M. Rus, "Vibration transmissibility study of high density solid waste biopolymer foam," *Journal of Mechanical Engineering and Sciences*, vol. 6, pp. 772–781, 2014.

[23] Y. M. Song, W. C. Chen, T. L. Yu, K. Linliu, and Y. H. Tseng, "Effect of isocyanates on the crystallinity and thermal stability of polyurethanes," *Journal of Applied Polymer Science*, vol. 62, no. 5, pp. 827–834, 1996.

[24] J. M. Cervantes-Uc, J. V. Cauich-Rodríguez, H. Vázquez-Torres, and A. Licea-Claveríe, "TGA/FTIR study on thermal degradation of polymethacrylates containing carboxylic groups," *Polymer Degradation and Stability*, vol. 91, no. 12, pp. 3312–3321, 2006.

[25] S. S. Idris, N. A. Rahman, K. Ismail, A. B. Alias, Z. A. Rashid, and M. J. Aris, "Investigation on thermochemical behaviour of low rank Malaysian coal, oil palm biomass and their blends during pyrolysis via thermogravimetric analysis (TGA)," *Bioresource Technology*, vol. 101, no. 12, pp. 4584–4592, 2010.

[26] M. Ardanuy, M. Antunes, and J. I. Velasco, "Vegetable fibres from agricultural residues as thermo-mechanical reinforcement in recycled polypropylene-based green foams," *Waste Management*, vol. 32, no. 2, pp. 256–263, 2012.

[27] S. Ibrahim and M. R. Johan, "Thermolysis and conductivity studies of poly (ethylene oxide) (PEO) based polymer electrolytes doped with carbon nanotube," *International Journal of Electrochemical Science*, vol. 7, no. 3, pp. 2596–2615, 2012.

[28] S. Gopalakrishnan, N. T. Nevaditha, and C. V. Mythili, "Synthesis and characterization of bifunctional monomers for high performance polymers from renewable resource," *International Journal of ChemTech Research*, vol. 4, no. 1, pp. 48–54, 2012.

[29] R. Artiaga, S. Naya, A. García, F. Barbadillo, and L. García, "Subtracting the water effect from DSC curves by using simultaneous TGA data," *Thermochimica Acta*, vol. 428, no. 1-2, pp. 137–139, 2005.

[30] L. J. Gibson and M. F. Ashby, *Cellular Solid: Structure and Properties*, Cambridge University Press, Cambridge, UK, 2nd edition, 1997.

[31] V. Kumar and N. P. Suh, "A process for making microcellular thermoplastic parts," *Polymer Engineering and Science*, vol. 30, no. 20, pp. 1323–1329, 1990.

[32] K. Goren, L. Chen, L. S. Schadler, and R. Ozisik, "Influence of nanoparticle surface chemistry and size on supercritical carbon dioxide processed nanocomposite foam morphology," *The Journal of Supercritical Fluids*, vol. 51, no. 3, pp. 420–427, 2010.

[33] X. Mao, S. Shimai, and S. Wang, "Gelcasting of alumina foams consolidated by epoxy resin," *Journal of the European Ceramic Society*, vol. 28, no. 1, pp. 217–222, 2008.

[34] Composite Panel Association, *American National Standard Particleboard*, Premiere Court, Gaithersburg, Md, USA, 1999.

[35] H. R. Sankar, P. Krishna, V. B. Rao, and P. B. Babu, "The effect of natural rubber particle inclusions on the mechanical and damping properties of epoxy-filled glass fibre composites," *Proceedings of the Institution of Mechanical Engineers, Part L: Journal of Materials: Design and Applications*, vol. 224, no. 2, pp. 63–70, 2010.

[36] R. F. Gibson and I. C. Finegan, "Recent research on enhancement of damping in polymer composites," *Composite Structures*, vol. 44, no. 2-3, pp. 89–98, 1999.

[37] T. Xu, G. Li, and S.-S. Pang, "Effects of ultraviolet radiation on morphology and thermo-mechanical properties of shape memory polymer based syntactic foam," *Composites—Part A: Applied Science and Manufacturing*, vol. 42, no. 10, pp. 1525–1533, 2011.

[38] J. Gu, G. Wu, and Q. Zhang, "Effect of porosity on the damping properties of modified epoxy composites filled with fly ash," *Scripta Materialia*, vol. 57, no. 6, pp. 529–532, 2007.

Hindawi Publishing Corporation
International Journal of Polymer Science
Volume 2015, Article ID 627268, 9 pages
http://dx.doi.org/10.1155/2015/627268

Research Article

Obtaining a Flexible Film Elaborated from Cassava Thermoplastic Starch and Polylactic Acid

Germán A. Arboleda,[1] Camilo E. Montilla,[1] Héctor S. Villada,[2] and Giovanni A. Varona[1]

[1]*Grupo de Investigación Ciencia y Tecnología de Biomoléculas de Interés Agroindustrial, (CYTBIA), Popayán, Colombia*
[2]*Departamento de Agroindustria, Universidad del Cauca, Popayán, Colombia*

Correspondence should be addressed to Germán A. Arboleda; ganar215@hotmail.com

Received 8 May 2015; Revised 18 July 2015; Accepted 21 July 2015

Academic Editor: Mukund Adsul

A flexible film was obtained from a blend of cassava thermoplastic starch and polylactic acid, using maleic anhydride as coupling agent. For this, an experimental design with three factors was used: polylactic acid content, coupling agent content, and temperature profile of the blown extrusion. It was found that the three factors generated significant differences on the response variables of tensile mechanical properties individually as in their triple interaction. Differential scanning calorimetry (DSC) was used by understanding the behavior of thermal properties of TPS/PLA blends with and without coupling agent, finding similar results between both. From this, the combination with 28% polylactic acid, 0.87% coupling agent, and 155.75°C temperature profile permitted the obtaining of a material with outstanding mechanical properties and offered advantages from the economic point of view.

1. Introduction

The global production of plastics is estimated at 300 million tons for 2015, being a serious environmental problem due to the slow degradation in nature of these materials produced from nonrenewable sources like petroleum, carbon, and natural gas [1], a situation that has triggered the development of new products from raw materials based on renewable sources, where biopolymers appear as the best alternative to petroleum-based polymers.

These bioplastics represent a broad spectrum of thermoplastic materials obtained from biological resources, fossils, or combinations of these [2] and they are generating growing interest in general society, plastics industry, and agricultural sector, given that it would suppose the exposure of its products to different markets [3]. In this order of ideas, starch, which is a storage polysaccharide in plants [2], is a widely used bioplastic because it is cheap, abundantly produced, and available in many renewable sources [4]. It has high potential for use in the synthesis of biodegradable materials [3] for which it is used as a thermoplastic material obtained through the interruption of its molecular interactions using plasticizers under specific conditions [2], achieving thermoplastic starch (TPS). However, they present disadvantages like their high solubility in water, hygroscopicity, and rapid aging due to retrogradation and low mechanical properties, limiting some of their applications [3]. Although these inconveniences can be reduced by mixing with other polymers [5] like polycaprolactone (PCL) [6], polylactic acid (PLA) [7], PLA/PCL binary blends [8], polyvinyl alcohol [9], and polyhydroxybutyrate [9], among others.

Of these, PLA stands out especially because of its properties, by being a renewable, biocompatible, and biodegradable polymer. It is one of the widely used bioplastics [2], so much so that in 2012 it was along with starch, the two commercial biodegradable polymers of highest importance, representing close to 47 and 41%, respectively, of the total consumption of biodegradable polymers [10]. It is obtained from renewable resources like corn, beets, wheat, and other products rich in starch [11] whose fermentation generates lactic acid polymerization, originated by the opening of the cyclic dimer ring [12]. It has higher stability of the melted mass, although its films are fragile due to the high crystallinity and level of physical aging.

However, the principal inconvenience presented by these types of blends is their immiscible phases due to the lack of

affinity between the hydroxyl groups and carboxyl terminals of hydrophobic PLA and hydroxyl groups of hydrophilic TPS [12]; additionally, it has been found that the mechanical properties of these blends diminish as TPS content increases, thus, limiting TPS content in said blends [5]. To increase compatibility among the phases, different coupling agents have been used like citric acid [13], formamide [14], and especially maleic anhydride [15] as compatibilizing agent. One advantage of using anhydrides, and in this particular case, maleic anhydride, is that it does not generate by-products when the change is made, since it is only a reaction ring opening [16]. Additionally, small amounts should be used, which reduces the costs of the final film.

This research studied the possibility of obtaining a material constituted by thermoplastic starch (TPS) from cassava and polylactic acid grafted with maleic anhydride to evaluate its mechanical and thermal properties to, thus, determine the combination of polylactic acid content, coupling agent, and temperature profile of the blown extrusion that would offer the highest characteristics regarding tensile properties.

2. Materials and Methods

This research was developed in the Rheology and Packages Laboratory at Universidad del Cauca (Popayán, Colombia).

2.1. Materials. Thermoplastic starch was obtained from cassava starch (Almidones de Sucre, Colombia). To produce polylactic acid, PLA reference 4032D (Cargill Dow Polymers LLC) was used. Some of the additives used included glycerin (99.5% purity, Disan S.A.) as plasticizer, maleic anhydride (99.0% purity, Merck) as coupling agent, benzoyl peroxide (reagent grade, Merck) as indicator agent, and stearic acid (99.3% purity, Merck) as TPS extrusion adjuvant.

2.2. Processing. To obtain TPS, the starch was first dried in a forced convection oven (Memmert) at 60°C for 15 h, and then the dry starch was mixed with glycerol at a 70 : 30 starch/glycerol ratio and 0.5% of stearic acid, for 10 min by using a high-speed blender (Kitchen Aid, model K45SS, USA). The blend was stored in a polypropylene sealed container for 48 h. After this time, the starch was thermoplasticized in a single-screw extruder (Thermo Scientific, model Haake Polylab OS, Germany) equipped with a 19 mm diameter barrel, a screw with a 5 : 1 compression ratio, and an L/D ratio of 25. A strand die was used along with a nozzle with 1 mm diameter opening. The TPS strand was gathered, dried at 80°C for 1 h, and pelletized to finally be packed in a sealed container. This extrusion used a screw rate of 50 rpm and a temperature profile of 112.25°C.

Thereafter, the grafted polylactic acid 4032D was processed, experimenting with three concentrations of maleic anhydride 0.5, 0.87, and 1.23% based on the weight of the polylactic acid. Prior to this, the polylactic acid was dried for 4 h at 80°C, by following manufacturer's specifications. Extrusion conditions for the grafted PLA were temperature of 177.50°C and 30 rpm screw rate, obtained from preliminary tests, as well as a strand nozzle with 1 mm opening.

Lastly, the TPS and grafted PLA blend was carried out in proportions of 22, 25, and 28% of PLA. This was processed under three different temperature profiles: 153.30, 155.75, and 158.00°C, in a single-screw extruder at a 35 rpm rate, using a blow die with a 70 μm opening and a set of rollers to standardize the thickness of the flexible film.

2.3. Evaluation of Tensile Mechanical Properties. The tensile mechanical properties of the flexible films obtained were measured: elastic modulus (MPa), maximum tensile strength (MPa), and maximum elongation (%). The samples were taken to a temperature chamber (Binder, model KBF 115), where they were stored under constant relative humidity conditions (50 ± 10%) and temperature (23 ± 2°C) for 8 days. Universal test equipment was used (Shimadzu model EZ-L) following the ASTM D882-10 standard [17], which establishes the procedure to execute the tensile test on films. The following operating conditions were taken: a 500 N cell, 25 mm/min spindle speed, data collection rate of 500 points/s, and 50 mm distance between vises. Samples were cut in longitudinal and transversal directions with dimensions of 90 mm length by 20 mm width. Sample thicknesses were taken by using a micrometer (Testing Machine, Inc., model 549).

2.4. Differential Scanning Calorimetry (DSC). This was conducted according to that established in the ASTM D3418-08 standard by using a TA Instruments calorimeter (model Q20, USA). The samples of the films of approximately 10 mg were previously conditioned for an 8-day period at 23 ± 2°C and 50 ± 10% RH. The sample was deposited into an aluminum capsule, sealed, and placed in the calorimeter's thermal chamber. A first heating cycle was conducted from ambient temperature to 190°C to erase the thermal history at a heating rate of 10°C/min, followed by an isotherm of 190°C for 5 min. Thereafter, a cooling cycle was carried out from 190°C to −80°C at a cooling rate of 20°C/min and an isotherm of −80°C for 5 min. Finally, a heating cycle was conducted from −80 to 200°C to determine the glass transition temperature (T_g), crystallization temperature (T_c), and melting temperature (T_m) in the respective samples.

2.5. Statistical Analysis. An analysis of variance (ANOVA) was performed to establish significant differences among treatments ($P < 0.05$), employing Tukey and T3 tests by Dunnett; SPSS software was used (version 21.0 for Windows). The analysis verified the normality assumptions of the samples by using the Shapiro-Wilk test, as well as the presence or lack of homogeneity of variance through Levene's test, all with a significance value of 0.05. For the comparison of the two treatments, Student's t-test was used.

3. Results and Discussion

3.1. Tensile Mechanical Properties. According to the experimental design, 27 factor combinations were obtained: polylactic acid content, coupling agent, and temperature profile of blown extrusion; each of these with the three response

variables was employed in the study. This was done to determine the formulation with which the highest indices of tensile mechanical properties were obtained. First, these were subjected to a Shapiro-Wilk test, proving that the samples, both in longitudinal and transversal direction, were extracted from populations with normal probability distribution, a necessary condition for a reliable study of variance. After determining the normal condition of the data, an ANOVA was conducted in both directions, finding that the totality of the response variables was influenced by the three factors evaluated and by their interactions, both double (AA-PLA, AA-temperature, and PLA-temperature) and triple (AA-PLA-temperature), which demonstrated that the result generated by the different factors was not present in isolated manner but that the effect was influenced by the other two. In this sense, it was determined which of the treatments with the AA, PLA content combination and temperature profile yielded outstanding mechanical properties.

An ANOVA test was used, finding that at least two treatments presented statistic differences in the three response variables. Upon this finding, the Levene variance homogeneity test was executed; from this test, it was found that, both in longitudinal and transversal directions, for the three response variables, the postulate of variance homogeneity was not fulfilled, which is why Dunnett's T3 multiple comparisons were performed.

Dunnett's T3 test yielded different results. In longitudinal direction, treatment 26 had the highest elastic modulus values and maximum tensile strength, while treatment 20 stood out with the maximum elongation at the rupture point, although both belonged to the same subgroup. Also, in the transversal direction, treatment 17 showed the highest values of elastic modulus; in spite of not presenting outstanding indicators regarding maximum tensile strength, it was not significantly different from the higher value treatment (treatment 16). With respect to the maximum elongation at the rupture point, treatment 19 stood out. Table 1 shows the results obtained regarding tensile mechanical properties in longitudinal and transversal directions for each of the 27 treatments obtained during the experimental design.

The PLA content was the factor with the highest influence upon the response variables: elastic modulus and tensile strength in longitudinal direction, which evidenced a tendency to find higher values of these properties as PLA content was increased. An average 28% PLA content obtained indices of 279.48 MPa in the elastic modulus, 77.7% above that found in the treatment with lower value, while, at this level, the maximum tensile strength showed an average of 4.97 MPa, representing a 33.3% increase with respect to the lower level, as evidenced in Figure 1.

These results evidenced that reported by [18–20], indicating that with higher PLA content there was higher modulus and tensile strength, given that adding PLA can increase the material's rigidity [12] functioning as a reinforcement for [21]. Upon being mixed, it is possible that the PLA characteristics increased the low mechanical properties of the pure TPS, perhaps because of a higher polar interaction between the starch and PLA carboxyl groups, attributable to the possible hydrogen bond produced between the carbonyl group

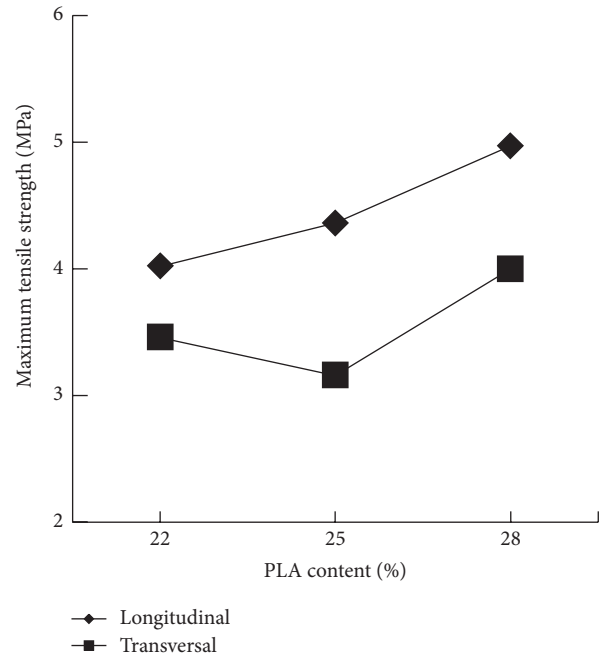

Figure 1: Behavior of maximum tensile strength against polylactic acid content.

(i.e., ester bond) of the PLA and the hydroxyl group in the starch [22].

In addition, with lower PLA values (22%), mechanical properties decreased [23]; this was probably because the humidity present in the starch reduced the PLA molecular weight caused by hydrolysis [24], given that PLA degradation is generally attributed to hydrolysis of the ester bonds in the presence of a given level of water [25], which is why a higher TPS content generated higher humidity, causing a negative effect on mechanical properties, like elastic modulus and maximum tensile strength. For the grafted PLA, its molecules contain some anhydride residues capable of activating chain scissions of the PLA molecules, for the blend in melted state, through a hydrolysis mechanism diminishing the PLA molecular weight. This reduction of the PLA chain length in the blend may have contributed to the diminishing of the tensile properties of some blends [26].

Regarding elongation, [27, 28] reported that the main inconvenience in TPS/PLA blends is precisely their low elongation, with values even below 6% as soon as the TPS concentration in the blend exceeds 10% (Figure 4). In light of this, [29] considered the possibility that PLA formed immiscible dispersions within TPS, leading to the little elongation of the final material. It has been found that elongation diminishes as starch concentration increases [30, 31], a situation contrasting with the case analyzed, where, with the higher starch content, the highest elongation indices were found, coinciding with that reported by [23]. For 22% PLA, elongation was on average 17.72%; for treatments with higher PLA concentration, elongation was 9%. Against this, the hygroscopic properties of starch and the plasticizer

Table 1: Results of tensile mechanical properties.

	Treatment*	Elastic modulus (MPa)		Maximum tensile strength (MPa)		Maximum elongation at the rupture point (%)	
		Long	Trans	Long	Trans	Long	Trans
1	A1P1T1	104.71 ± 0.20	85.46 ± 1.24	3.19 ± 0.19	2.57 ± 0.05	14.02 ± 3.47	16.22 ± 0.53
2	A1P1T2	211.96 ± 1.51	146.41 ± 0.49	4.23 ± 0.13	3.68 ± 0.25	9.92 ± 0.92	13.88 ± 3.81
3	A1P1T3	161.63 ± 0.06	99.05 ± 0.70	3.45 ± 0.12	2.76 ± 0.06	10.41 ± 0.49	7.63 ± 0.76
4	A1P2T1	230.06 ± 0.31	139.13 ± 0.42	4.25 ± 0.20	3.53 ± 0.04	7.92 ± 1.61	10.47 ± 0.42
5	A1P2T2	231.32 ± 2.00	165.90 ± 1.51	4.06 ± 0.04	3.77 ± 0.06	6.01 ± 0.54	11.45 ± 0.61
6	A1P2T3	193.41 ± 0.50	98.17 ± 0.92	3.63 ± 0.06	2.15 ± 0.07	7.15 ± 0.74	6.81 ± 0.96
7	A1P3T1	259.05 ± 0.71	112.23 ± 0.55	4.76 ± 0.28	2.73 ± 0.12	13.09 ± 2.74	5.84 ± 1.11
8	A1P3T2	189.07 ± 0.50	205.65 ± 0.68	3.53 ± 0.12	4.47 ± 0.28	5.86 ± 0.68	10.95 ± 0.19
9	A1P3T3	291.02 ± 1.2	146.73 ± 0.66	4.99 ± 0.37	4.06 ± 1.17	9.36 ± 1.96	10.62 ± 0.87
10	A2P1T1	141.62 ± 0.25	119.60 ± 0.24	3.51 ± 0.18	3.77 ± 0.09	9.41 ± 1.68	17.59 ± 1.09
11	A2P1T2	209.13 ± 1.58	87.13 ± 1.02	4.32 ± 0.12	3.48 ± 0.14	11.43 ± 0.46	22.76 ± 2.68
12	A2P1T3	195.77 ± 0.46	149.32 ± 0.64	4.22 ± 0.02	3.73 ± 0.07	12.12 ± 0.73	12.17 ± 2.71
13	A2P2T1	151.56 ± 0.79	121.33 ± 0.04	4.03 ± 0.18	3.72 ± 0.14	16.92 ± 1.81	18.46 ± 2.02
14	A2P2T2	216.35 ± 0.55	174.56 ± 0.36	4.32 ± 0.18	4.39 ± 0.05	8.90 ± 0.21	18.60 ± 2.12
15	A2P2T3	257.91 ± 0.56	118.28 ± 0.30	4.60 ± 0.13	3.02 ± 0.02	12.15 ± 1.05	10.46 ± 1.75
16	A2P3T1	234.89 ± 2.48	271.52 ± 0.85	4.55 ± 0.10	5.55 ± 0.31	8.46 ± 1.09	8.57 ± 0.77
17	A2P3T2	323.69 ± 0.85	277.03 ± 0.27	5.69 ± 0.32	4.87 ± 0.34	8.84 ± 1.14	7.63 ± 1.92
18	A2P3T3	309.57 ± 1.17	228.26 ± 3.86	5.09 ± 0.26	4.48 ± 0.12	6.10 ± 1.06	11.04 ± 2.36
19	A3P1T1	188.97 ± 1.35	86.43 ± 0.25	4.30 ± 0.09	3.67 ± 0.07	24.38 ± 1.46	31.14 ± 0.42
20	A3P1T2	232.86 ± 2.92	142.60 ± 0.22	4.93 ± 0.22	4.32 ± 0.21	25.88 ± 1.92	23.35 ± 0.99
21	A3P1T3	146.33 ± 2.68	90.33 ± 0.13	4.01 ± 0.09	3.16 ± 0.07	18.92 ± 1.53	14.75 ± 3.63
22	A3P2T1	138.93 ± 5.35	72.90 ± 0.36	3.65 ± 0.09	1.70 ± 0.18	15.99 ± 2.28	9.26 ± 1.10
23	A3P2T2	278.58 ± 2.99	63.84 ± 0.38	5.11 ± 0.33	2.64 ± 0.04	19.48 ± 2.19	10.37 ± 1.09
24	A3P2T3	332.50 ± 1.34	163.73 ± 0.40	5.62 ± 0.09	3.57 ± 0.20	13.84 ± 1.66	11.58 ± 1.29
25	A3P3T1	227.07 ± 0.35	95.02 ± 0.68	4.38 ± 0.13	2.98 ± 0.29	10.46 ± 2.52	9.98 ± 1.07
26	A3P3T2	406.32 ± 1.21	200.44 ± 0.30	6.77 ± 0.11	3.59 ± 0.05	20.72 ± 1.40	5.82 ± 0.55
27	A3P3T3	274.65 ± 1.18	109.74 ± 0.59	4.94 ± 0.28	3.32 ± 0.44	25.18 ± 0.20	10.58 ± 2.33

*Coupling agent: A1 = 0.5%; A2 = 0.87%; A3 = 1.23%. Polylactic acid: P1 = 22%; P2 = 25%; P3 = 28%. Temperature profile: T1 = 153.30°C; T2 = 155.75°C; T3 = 158.00°C.

could have interrupted the polymer-polymer and polymer-plasticizer interactions by substituting the polymer-water and water-plasticizer interactions, leading to reduced rigidity of the polymer, allowing the water absorbed by TPS to facilitate mobility of starch chains, thus resulting in increased elongation [20].

In most cases, it was seen how higher PLA content provided higher elastic modulus values in longitudinal and transversal direction. A similar situation occurred with maximum tensile strength, but contrary to what happened with maximum elongation in the transversal direction where the higher PLA content generated minor results of this response variable.

Also, the coupling agent content was the most influential factor on maximum elongation in longitudinal direction. It was found that with the maximum coupling agent content the highest maximum elongation values were obtained, increasing this property by approximately 163%, compared to treatments presenting lower elongation values, showing in 71.4% of the cases a directly proportional relationship between increased coupling agent content and maximum elongation values.

Miscibility and interface adhesion play an essential role in the mechanical properties of the polymer blends, where, generally, higher mechanical properties are expected when high interface adhesion and miscibility of the components exist [28]. Additionally, it may be expected that with higher AA content the percentage of graft in the PLA would be higher, increasing the possibilities of forming macroradicals that can react [18] and, because the effectiveness of the graft will depend on the monomer concentration [32], it is then feasible that under this coupling agent content there would

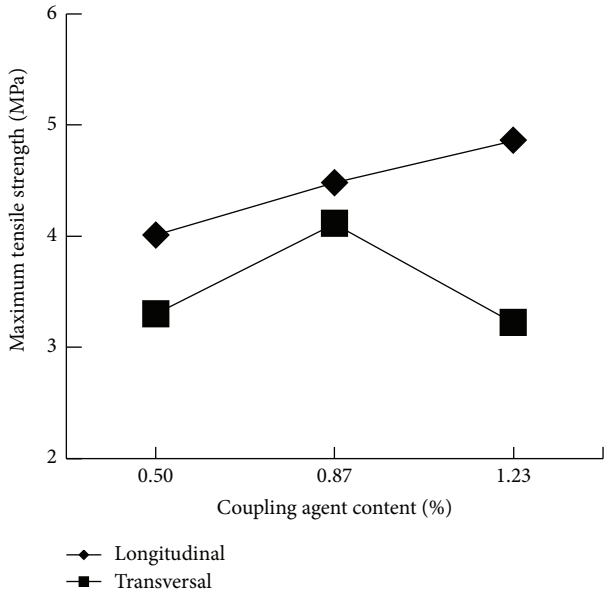

Figure 2: Behavior of maximum tensile strength against the coupling agent content.

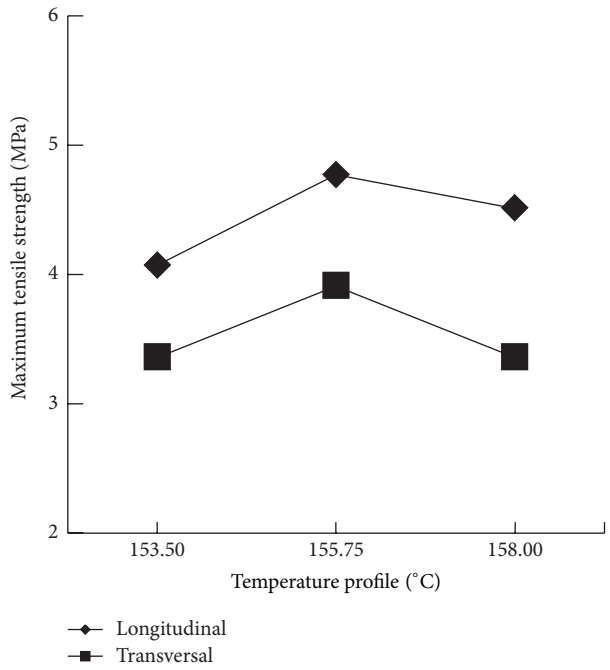

Figure 3: Behavior of maximum tensile strength against the temperature profile.

be outstanding indices of miscibility among the phases, positively affecting the mechanical properties of the final material.

However, excessive coupling agent may act as plasticizer and be responsible for the decrease in the maximum tensile strength [11], thus explaining how the maximum tensile strength values coincided with the intermediate level of coupling agent content, noted in Figure 2, due possibly to a separation of phases induced by secondary reactions (chain degradation, homopolymerization of maleic anhydride, discoloration, and reticulation) or terminal reactions [20], produced after a concentration beyond the optimal one. Secondary reactions are common in the reaction of free radicals, like, for example, β-scission. The probability of these occurring depends largely on the nature of the macroradicals and the polymer chain. For grafted PLA systems, two possible secondary reactions may have occurred: scission of the chain caused by thermohydrolysis and ramification of the PLA substrate. Excessive scission may have led to lower molecular weight and decreased properties of the polymer, while the ramification may have been disadvantageous to monomer attachment, given that most of its free radicals could attach to the lateral chains produced by this secondary reaction, thus limiting the action of the graft [18].

Also, it is feasible that, in the combinations where the minimum level of the coupling agent (0.5%) was managed, there would be inconveniences in compatibility due to an insufficient amount of the monomer, incapable of efficiently binding the TPS and PLA phases, an issue that evidenced the difficulty for film production with this coupling level where blowing problems emerged, presenting materials with great amounts of agglomerations, often with greater thickness, and maintaining a rather low torque, making the bubble output occur too slowly.

The temperature profile was the factor that generated the least effect on the maximum tensile strength. With respect to elongation, no significant differences were evident between its levels. Although its effect was not the highest, compared to the PLA content and AA, some tendencies can be highlighted. For the elastic modulus and maximum tensile strength, the highest values were found for these response variables in the intermediate temperature profile, while for elongation a clear tendency was not evidenced, given that the higher indices were shared between the first two profiles. Perhaps the action of 155.75°C may have permitted higher compatibilization of the blends, favoring polymerization of graft of free radicals, where the indicator agent could decompose rapidly and completely, producing higher amounts of macroradicals that, in turn, gave way to a higher degree of graft, as reported by [18], evidenced in the behavior shown in Figure 3.

Excessive temperatures could cause degradation of both reaction initiators [33] as maleic anhydride, causing the breaking of the coupling between phases [34], in films processed with the maximum temperature, possibly reducing the molecular weight of PLA [20]. Likewise, TPS molecular weight could lose excessive action of temperature limiting function to reinforce this PLA [21] negatively influencing the material's final properties. From the aforementioned, it has been postulated that the PLA's thermal degradation is produced principally through random scissions of the principal chain, and several of these include hydrolysis, depolymerization, oxidative degradation, and intramolecular transesterification reactions, which could have participated in the degradation process for the thermal treatments [35], associated mainly with hydrolysis of the ester groups and accelerated by –COOH terminal groups [25].

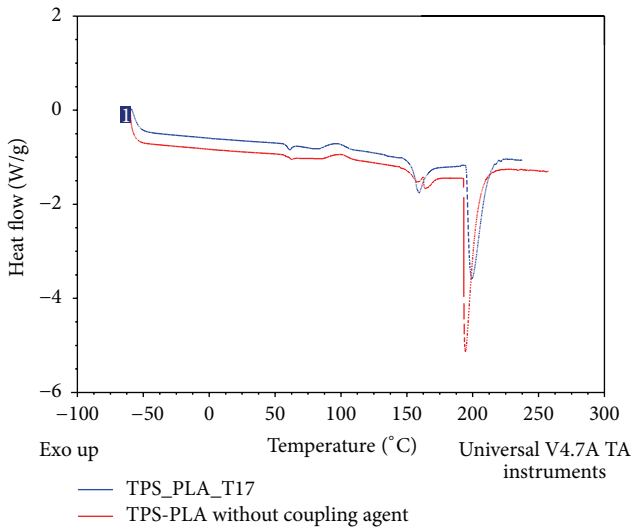

Figure 4: DSC of samples of TPS/PLA blends.

The interaction of the PLA-AA-temperature profile factors presented a significant effect upon the three response variables. In light of this, it is well known that the mechanical behavior of heterogeneous materials like TPS/PLA depends on some principal parameters, which include the modulus of each component, the volume fraction of each element, the ratio of the morphology aspect, the filler material, distribution of the length, orientation of the chains, and properties of the interface, given their responsibility in charge transfer. The last parameter depends mainly upon the degree of the interactions among the phases [36]. Due to the aforementioned, it could be deducted how the triple interaction of the factors could have been generated on the response variables, bearing in mind that the PLA content was employed, which has to do with the first and second parameters previously mentioned, the concentration of AA, directly implied in the interface properties, and the temperature profile, related to the morphology and blend coupling.

Of the three response variables observed, the elastic modulus was the variable upon which the highest effect was generated by the three factors, in both longitudinal and transversal directions. With respect to this, it was found that the minimum value obtained was 104.71 ± 0.20 MPa, corresponding to treatment 1 (A1P1T1), while the maximum was 406.32 ± 1.21 MPa in treatment 26 (A3P3T2), in longitudinal direction. Additionally, in transversal direction in treatment 23 (A3P2T2), the lowest value was found with 63.84 ± 0.38 MPa, while, with a value of 277.03 ± 0.27 MPa, treatment 17 (A2P3T2) offered the highest indices in this variable. From this, it may be seen how with the highest PLA content (28%) and with the second temperature profile (155.75°C) the highest indices of elastic modulus were found, in both directions. This, somehow, evidences the behavior reflected upon analyzing both factors separately.

Regarding the maximum tensile strength, it was found that the values are within a range from 3.19 ± 0.19 MPa from treatment 1 (A1P1T1) to 6.77 ± 0.11 MPa, corresponding to treatment 26 (A3P3T2) in longitudinal direction. For the transversal direction, treatment 22 (A3P2T2) yielded the lowest value with 1.70 ± 0.18 MPa and treatment 17 (A2P3T2) yielded the highest index with 4.87 ± 0.34 MPa. This permits observing that, as with the elastic modulus, higher indicators of maximum tensile strength were obtained with the highest PLA content and the second temperature profile. The values obtained are higher than those found by some studies on TPS/PLA blends. For elongation, treatment 8 (A1P3T2) yielded the lowest value with 5.86 ± 0.68%, while treatment 20 (A3P1T2) presented the highest indices with 25.88 ± 1.92%, in longitudinal direction. Additionally, in transversal direction, the treatment with the lowest value was 26 (A3P3T2) with 5.82 ± 0.55% and treatment 19 (A3P1T1) with 31.14 ± 0.42% offered the highest values.

According to [37], for a composite material that includes a coupling agent or grafted compatibilizer, wetting and the bond to the interface significantly influence the properties of composite materials.

The formation of interfacial molecular contact through wetting is the prerequisite for adhesive bond [24]. Due to this, the molecules diffuse and react chemically to establish covalent bonds through the interface while molecular diffusion is generally accelerated by reduced surface tension [36], which can be achieved by adding compatibilizer and subsequent establishment of chemically stable covalent bonds [18], where, possibly, in treatments with outstanding mechanical properties, high degrees of wetting and consequential bond of their interface were reached. This is perhaps because the blend conditions permitted adjusted homopolymerization of maleic anhydride, without being excessive, through a secondary reaction, producing low-molecular weight polymers that acted as plasticizers and diminished the interface energy between both phases, facilitating the wetting of the starch with the PLA [38], causing its final properties to be increased against other treatments in which these phenomena could have been reduced by diverse factors, like the insufficient amount of AA or the excessive action of temperature.

Between the two treatments shown, some considerations were kept in mind: treatment 26 (A3P3T2) offered higher values in the three response variables in longitudinal direction, but the situation was inverted in transversal direction, where treatment 17 (A2P3T2) showed the highest indices. If bidirectionality is considered, it can be seen that, for maximum tensile strength, treatment 26 presented an unbalance of 103% in the transversal direction with respect to the longitudinal direction, while for treatment 17 this disproportion was reduced to 16.8%. The same occurred with the other response variables, where treatment 17 presented the highest bidirectionality, a favorable issue for a material, given its functionality and quality, which permitted more uniform chain distribution and not as unbalanced as in treatment 26. Another advantage of treatment 17 against treatment 26 was the cost of the materials. As observed, the only difference between the combinations lies in the coupling agent content; the first presents a content of 0.87%, while the second is of 1.23%. This 0.36% difference is significant in terms of costs, given that at industrial scale it can represent considerable amounts of money, bearing in mind the high cost of commercial AA.

Table 2: Comparison results of tensile mechanical properties.

	Treatment*	Elastic modulus (MPa)		Maximum tensile strength (MPa)		Maximum elongation at the rupture point (%)	
		Long	Trans	Long	Trans	Long	Trans
1	T17	323.69 ± 0.85	277.03 ± 0.27	5.69 ± 0.32	4.87 ± 0.34	8.84 ± 1.14	7.63 ± 1.92
2	TPS/PLA*	266.23 ± 0.39	173.49 ± 0.58	4.13 ± 0.10	3.40 ± 0.19	17.11 ± 2.65	16.54 ± 2.23

*Without coupling agent.

Maleic anhydride concentration of 0.87% is lower than other reports such as [39], which used higher levels, resulting in low mechanical properties possibly caused by a greater degree of hydrolysis of starch polymer chains. According to the above, [40], who used a concentration of 2%, suggested using smaller amounts of maleic anhydride in order to improve the adhesion and compatibility of TPS and PLA. Considering the above suggestion, [38] employed a concentration of 1% of maleic anhydride to generate adhesion TPS with PLA because, at higher concentrations, possibly hydrolysis is generated, which could cause a decrease in properties.

For comparison, a film with PLA and TPS blend without inclusion of coupling agent was obtained using the same methodology. The mechanical properties of the material obtained are shown in Table 2. Treatment 17 was compared with another mixture of TPS and PLA without coupling agent, by Student t-test ($P < 0.05$), finding in their mechanical properties significant differences in elastic modulus, high tensile strength, and elongation, in longitudinal and transverse directions. Treatment 17 had higher strength values 38.0 and 42.9% lengthwise and crosswise, respectively, as compared to the film without coupling agent, demonstrating that greater interaction between material phases can cause increases in strength properties. The film without coupling agent provided a surface from which the phase separation of the PLA and TPS, with some cracks and irregularities, also evidenced its thickness which was 37.5% higher than the film thickness of treatment 17.

3.2. Differential Scanning Calorimetry (DSC). The results in Table 3 correspond to data obtained from thermograms; herein, temperatures and melting enthalpies (T_m and ΔH_m) are indicated along with a temperature signal and crystallization enthalpy (T_c and ΔH_c), as well as a glass transition temperature (T_g). During the test, two heating moments were carried out; the first, denominated run 1, obtained data corresponding to TPS, given that the second no longer showed the transitions for this component, which explains an amorphous state of the TPS after subjecting it to high temperatures with its subsequent cooling [2], while the second, called run 2, presented PLA values according to the blend analyzed.

For the film made up of the TPS/PLA binary blend (T17), some behaviors took place, for example, in run 1, although other melting peaks were present, the last of these was assigned to the TPS, found between 190 and 210°C, approximately, determining only its temperature and melting enthalpy. Additionally, for the second run, it was possible to establish that the glass transition temperature of PLA was 59.04°C, followed by crystallization signals, between 90 and 110°C, approximately. Finally, the melting temperature for PLA was found at 159.17°C, corresponding to the last peak presented in run 2.

Table 3: Phase transitions of the flexible films.

Blend	Components	T_g (°C)	T_c (°C)	ΔH_c (J/g)	T_m (°C)	ΔH_m (J/g)
T17	TPS	—	—	—	199.35	72.55
	PLA	59.04	97.48	5.48	159.17	17.23
TPS/PLA*	TPS	—	—	—	194.50	80.96
	PLA	60.90	100.74	4.11	163.88	11.59

*Without coupling agent.

Some dispositions were evidenced in the pattern film of TPS/PLA without coupling agent. As with the previous case, the first run analyzed the TPS behavior; from here, its melting temperature was obtained at 194.50°C. For the second run, crystallization signal and, lastly, the PLA melting peak of PLA were determined. From this, it was observed how the PLA melting enthalpy for the pattern film was quite inferior to that presented by the PLA in the TPS/PLA blend, which could be an indicator of the percentage of crystallinity of the composite materials. Thereby, diminished ΔH_m could be indicative of diminished crystallinity [18]. This crystallinity increase produced in the TPS/PLA film may have been caused by the nucleation of starch and the degradation of PLA polymer chains, given that starch was able to act as nucleation agent for crystallization and the molecular weight affected polymer crystallization [24]. Further, the plasticizer-like glycerol could have also migrated to the PLA matrix, causing increased mobility of the polymer chain, thus, increasing the PLA crystallization rate [31]. Diminished ΔH_m and hence crystallinity in starch and PLA blends could have been because the starch limits the movement of the polymer segments, hindering reorganization of the polymer chain [18]. Regarding crystallization enthalpy, ΔH_c was presented by the polylactic acid in both films, where the one containing TPS/PLA without coupling agent presented 33.3% reduction against the TPS/PLA blend film. Although starch may function as nucleation agent, it is also possible that it interferes with the mobility of the PLA chain, slightly reducing the PLA crystallinity [24] of the pattern film. When comparing

crystallinity according to [32], taking as a reference that ΔH_m of the 100% crystalline PLA is of 93 J/g [33], the PLA of the TPS/PLA film would present a crystallinity of 18.5%, quite above the 12.5% shown with the PLA of the pattern film. This would indicate that in the film of the treatment chosen a higher degree of crystallization may have been generated.

Authors like [33] have reported that pure PLA 4032 presents T_g of 61.3°C. For the case presented, T_g of the PLA in the TPS/PLA blend was of 59.04°C. This may be because the mobility of the PLA chain was increased due to the plasticization effect brought by the glycerol gelatinized starch [6], as well as the formation of cyclic oligomers through "backbiting" reactions [34]. However, authors like [24, 31] state that the glass transition temperature (T_g) of PLA is not affected by the incorporation of TPS; thereby, more in-depth studies would be needed to test the certainty or falsehood of this hypothesis. It is known that the plasticizer can diminish the polymer's glass transition temperature. Although the coupling agent was introduced as a reactive compatibilizer, it could also have acted as a plasticizer [24] reducing the PLA's glass transition temperature in the TPS/PLA blend. The melting enthalpy (ΔH_m) for the pure PLA (36.5 J/g) is higher than that presented by the PLA of the TPS/PLA blend (17.23 J/g). This reduction was possibly because the ramifications generated in the grafted PLA disturbed the regularity of the PLA chain structures, thus, increasing the space among them [18].

Although, according to the results of differential scanning calorimetry, films TPS/PLA with and without coupling agent showed a similar behavior in terms of values of thermal transitions, there were differences in mechanical and surface properties between the two films. In the film TPS/PLA (T17), higher values of tensile strength, a more homogeneous surface, and fineness, without irregularities and with a significantly reduced thickness, were found.

The maleic anhydride can promote transesterification/esterification reactions between the starch and MA molecules improving its compatibility with other biopolymers as manifested [39]. In the investigation by [41], they found that the inclusion of maleic anhydride to PLA further mixed with starch improves the mechanical properties of the flexible film obtained, achieving compatible polar groups starch, with the nonpolar component of PLA. Meanwhile, [42] used the maleic anhydride because it reduces the interfacial tension between phases improving adhesion of starch and PLA, resulting in thinner films and a more uniform and stable morphology, showing improved mechanical properties.

Due to the aforementioned reasons, it was determined that treatment 17 (A2P3T2) represented the formulation that offered outstanding mechanical properties, higher bidirectional balance, and the possibility of greater cost reduction of raw materials to obtain the flexible film.

4. Conclusions

The factors evaluated, polylactic acid content, coupling agent, and temperature profile, as well as their interaction, generated significant effects on the response variables in both longitudinal and transversal directions. From this, the formulation that included 28% PLA content, 0.87% coupling agent processed at extrusion temperature of 155.75°C presented outstanding mechanical properties against the remaining combinations included in the design. With the formulation found, we managed to reduce by 55.6% the coupling agent content in the material, compared to prior research conducted by the CYTBIA research group, probably influencing the diminished costs of the final material; although against starch-based materials, we managed to obtain a film with outstanding mechanical properties, but still with deficiencies against synthetic materials.

Conflict of Interests

The authors declare that they have no conflict of interests regarding the publication of this paper.

References

[1] L. Reddy, S. Reddy, and A. Gupta, "Study of bio-plastics as green and sustainable alternative to plastics," *International Journal of Emerging Technology and Advanced Engineering*, vol. 3, no. 5, pp. 76–81, 2013.

[2] M. M. Reddy, S. Vivekanandhan, M. Misra, S. K. Bhatia, and A. K. Mohanty, "Biobased plastics and bionanocomposites: current status and future opportunities," *Progress in Polymer Science*, vol. 38, no. 10-11, pp. 1653–1689, 2013.

[3] M. Valero, M. Ortegón, and Y. Uscategui, "Biopolímeros: avances y perspectivas," *Dyna*, vol. 80, no. 181, pp. 171–180, 2013.

[4] J. J. G. Van Soest and J. F. G. Vliegenthart, "Crystallinity in starch plastics: consequences for material properties," *Trends in Biotechnology*, vol. 15, no. 6, pp. 208–213, 1997.

[5] L. Jiang and J. Zhang, "Biodegradable polymers and polymer blends," in *Handbook of Biopolymers and Biodegradable Plastics: Properties, Processing and Applications*, S. Ebnesajjad, Ed., pp. 109–128, 2012.

[6] J. Cai, Z. Xiong, M. Zhou et al., "Thermal properties and crystallization behavior of thermoplastic starch/poly(ε-caprolactone) composites," *Carbohydrate Polymers*, vol. 102, pp. 746–754, 2014.

[7] F. C. Soares, F. Yamashita, C. M. O. Müller, and A. T. N. Pires, "Effect of cooling and coating on thermoplastic starch/poly(lactic acid) blend sheets," *Polymer Testing*, vol. 33, pp. 34–39, 2014.

[8] P. Sarazin, G. Li, W. J. Orts, and B. D. Favis, "Binary and ternary blends of polylactide, polycaprolactone and thermoplastic starch," *Polymer*, vol. 49, no. 2, pp. 599–609, 2008.

[9] J. Zhou, Y. Ma, L. Ren, J. Tong, Z. Liu, and L. Xie, "Preparation and characterization of surface crosslinked TPS/PVA blend films," *Carbohydrate Polymers*, vol. 76, no. 4, pp. 632–638, 2009.

[10] IHSQUÍMICA, "Biodegradable polymer," 2012, http://www.ihs.com/products/chemical/planning/ceh/biodegradable-polymers.aspx.

[11] M. Yao, "Modification of poly(lactic acid)/poly(propylene carbonate) blends through melt compounding with maleic anhydride," *Express Polymer Letters*, vol. 5, no. 11, pp. 937–949, 2011.

[12] M. A. Shirai, M. V. E. Grossmann, S. Mali, F. Yamashita, P. S. García, and C. M. O. Müller, "Development of biodegradable flexible films of starch and poly(lactic acid) plasticized with

adipate or citrate esters," *Carbohydrate Polymers*, vol. 92, no. 1, pp. 19–22, 2013.

[13] N. Wang, J. Yu, P. R. Chang, and X. Ma, "Influence of citric acid on the properties of glycerol-plasticized dry starch (DTPS) and DTPS/poly(lactic acid) blends," *Starch*, vol. 59, no. 9, pp. 409–417, 2007.

[14] N. Wang, J. Yu, P. R. Chang, and X. Ma, "Influence of formamide and water on the properties of thermoplastic starch/poly(lactic acid) blends," *Carbohydrate Polymers*, vol. 71, no. 1, pp. 109–118, 2008.

[15] M. Enriquez, R. Velasco, and V. Ortiz, "Composición y procesamiento de películas biodegradables basadas en almidón," *Biotecnología en el Sector Agropecuario y Agroindustrial*, vol. 10, no. 1, pp. 182–192, 2012.

[16] G. Moad, "Chemical modification of starch by reactive extrusion," *Progress in Polymer Science*, vol. 36, no. 2, pp. 218–237, 2011.

[17] ASTM International, *ASTM D882-10. Standard Test Method for Tensile Properties of Thin Plastic Sheeting*, ASTM International, West Conshohocken, Pa, USA, 2010.

[18] R. Zhu, *Preparation of maleic anhydride grafted poly(lactid acid) (PLA) and its compatibilization effects on PLA/Soy protein composites, Tesis de Master en Ciencia de Materiales [M.S. thesis]*, Departamento de Ingeniería Mecánica y Materiales, Washington State University, Washington, DC, USA, 2011.

[19] R. Mendoza and J. Medina, "Propiedades adhesivas de mezclas de almidón de yuca termoplastificado y ácido poliláctico (TPS/PLA)," *Revista INGE CUC*, vol. 7, no. 1, pp. 217–228, 2011.

[20] S. Detyothin, *Production and characterization of thermoplastic cassava starch, functionalized poly(lactic acid), and their reactive compatibilized blends [Tesis Doctor en Filosofía]*, Michigan State University, East Lansing, Mich, USA, 2012.

[21] T. Ke and X. Sun, "Effects of moisture content and heat treatment on the physical properties of starch and poly (lactic acid) blends," *Journal of Applied Polymer Science*, vol. 81, no. 12, pp. 3069–3082, 2001.

[22] T. Wittaya, "Rice starch-based biodegradable films: properties enhancement," in *Structure and Function of Food Engineering*, A. Amer, Ed., chapter 5, pp. 103–134, InTech, Rijeka, Croatia, 2012.

[23] N. Chapleau, M. A. Huneault, and H. Li, "Biaxial orientation of polylactide/thermoplastic starch blends," *International Polymer Processing*, vol. 22, no. 5, pp. 402–409, 2007.

[24] W. Y. Jang, B. Y. Shin, T. J. Lee, and R. Narayan, "Thermal properties and morphology of biodegradable PLA/starch compatibilized blends," *Journal of Industrial and Engineering Chemistry*, vol. 13, no. 3, pp. 457–464, 2007.

[25] P. Ma, P. Xu, M. Chen et al., "Structure-property relationships of reactively compatibilized PHB/EVA/starch blends," *Carbohydrate Polymers*, vol. 108, no. 1, pp. 299–306, 2014.

[26] J. Wootthikanokkhan, P. Kasemwananimit, N. Sombatsompop, A. Kositchaiyong, S. Isarankura na Ayutthaya, and N. Kaabbuathong, "Preparation of modified starch-grafted poly(lactic acid) and a study on compatibilizing efficacy of the copolymers in poly(lactic acid)/thermoplastic starch blends," *Journal of Applied Polymer Science*, vol. 126, supplement 1, pp. E389–E396, 2012.

[27] M. A. Huneault and H. Li, "Morphology and properties of compatibilized polylactide/thermoplastic starch blends," *Polymer*, vol. 48, no. 1, pp. 270–280, 2007.

[28] S. Falah, *Processing and properties of biodegradable polymer blends based on gelatinized potato starch [M.S. thesis]*, McMaster University, Hamilton, Canada, 2010.

[29] O. Martin and L. Avérous, "Poly(lactic acid): plasticization and properties of biodegradable multiphase systems," *Polymer*, vol. 42, no. 14, pp. 6209–6219, 2001.

[30] K. M. Nampoothiri, N. R. Nair, and R. P. John, "An overview of the recent developments in polylactide (PLA) research," *Bioresource Technology*, vol. 101, no. 22, pp. 8493–8501, 2010.

[31] C. M. O. Müller, A. T. N. Pires, and F. Yamashita, "Characterization of thermoplastic starch/poly(lactic acid) blends obtained by extrusion and thermopressing," *Journal of the Brazilian Chemical Society*, vol. 23, no. 3, pp. 426–434, 2012.

[32] A. Bhattacharya and B. N. Misra, "Grafting, a versatile means to modify polymers: techniques, factors and applications," *Progress in Polymer Science*, vol. 29, no. 8, pp. 767–814, 2004.

[33] J. Karl, *Reactive Polymers Fundamentals and Applications. A Concise Guide to Industrial Polymers*, William Andrew Publishing, Norwich, NY, USA, 2005.

[34] J. Castañeda, *Estudio de la retrogradación en películas flexibles obtenidas a partir de mezclas de almidón nativo de yuca, ácido poli-láctico (PLA) y policaprolactona (PCL) [M.S. thesis]*, Escuela de Ingeniería de Materiales, Universidad del Valle, Cali, Colombia, 2012.

[35] M. Jamshidian, E. A. Tehrany, M. Imran, M. Jacquot, and S. Desobry, "Poly-Lactic Acid: production, applications, nanocomposites, and release studies," *Comprehensive Reviews in Food Science and Food Safety*, vol. 9, no. 5, pp. 552–571, 2010.

[36] A. Wang, R. Qi, C. Xiong, and M. Huang, "Effects of coupling agent and interfacial modifiers on mechanical properties of poly(lactic acid) and wood flour biocomposites," *Iranian Polymer Journal*, vol. 20, no. 4, pp. 281–294, 2011.

[37] S. Wu, *Polymer Interface and Adhesion*, Marcel Dekker, New York, NY, USA, 1982.

[38] V. H. Orozco, W. Brostow, W. Chonkaew, and B. L. López, "Preparation and characterization of poly (lactic acid)g-maleic anhydride and starch blends," *Macromolecular Symposia*, vol. 277, no. 1, pp. 69–80, 2009.

[39] J. B. Olivato, M. V. E. Grossmann, F. Yamashita, D. Eiras, and L. A. Pessan, "Citric acid and maleic anhydride as compatibilizers in starch/poly(butylene adipate-co-terephthalate) blends by one-step reactive extrusion," *Carbohydrate Polymers*, vol. 87, no. 4, pp. 2614–2618, 2012.

[40] D. Carlson, L. Nie, R. Narayan, and P. Dubois, "Maleation of polylactide (PLA) by reactive extrusion," *Journal of Applied Polymer Science*, vol. 72, no. 4, pp. 477–485, 1999.

[41] T. Yu, N. Jiang, and Y. Li, "Study on short ramie fiber/poly(lactic acid) composites compatibilized by maleic anhydride," *Composites Part A: Applied Science and Manufacturing*, vol. 64, pp. 139–146, 2014.

[42] S. Detyothin, S. Selke, R. Narayan, M. Rubino, and R. Auras, "Effects of molecular weight and grafted maleic anhydride of functionalized polylactic acid used in reactive compatibilized binary and ternary blends of polylactic acid and thermoplastic cassava starch," *Journal of Applied Polymer Science*, vol. 132, no. 28, 15 pages, 2015.

Hindawi Publishing Corporation
International Journal of Polymer Science
Volume 2015, Article ID 732858, 8 pages
http://dx.doi.org/10.1155/2015/732858

Research Article

Influence of Chitosan Coating on Mechanical Stability of Biopolymer Carriers with Probiotic Starter Culture in Fermented Whey Beverages

Nataša S. Obradović,[1] Tanja Ž. Krunić,[1] Kata T. Trifković,[2] Maja Lj. Bulatović,[2] Marko P. Rakin,[2] Marica B. Rakin,[2] and Branko M. Bugarski[2]

[1]*Innovation Centre of the Faculty of Technology and Metallurgy, University of Belgrade, Karnegijeva 4, 11000 Belgrade, Serbia*
[2]*Faculty of Technology and Metallurgy, University of Belgrade, Karnegijeva 4, 11000 Belgrade, Serbia*

Correspondence should be addressed to Nataša S. Obradović; ntomovic@tmf.bg.ac.rs

Received 19 August 2015; Revised 29 September 2015; Accepted 30 September 2015

Academic Editor: Mukund Adsul

The aim of this study was to improve the mechanical stability of biopolymer carriers and cell viability with addition of chitosan coating during fermentation process and product storage. Dairy starter culture (1% (w/v)) was diluted in whey and mixed with sodium alginate solution and the beads were made using extrusion technique. The mechanical stability of coated and uncoated beads, the release behavior, and the viability of encapsulated probiotic dairy starter culture in fermented whey beverages were analyzed. The mechanical properties of the beads were determined according to force-displacement and engineering stress-strain curves obtained after compression testing. It was observed that addition of chitosan as a coating on the beads as well as the fermentation process increased the elastic modulus of the calcium alginate-whey beads and cell survival. The current study revealed that the coating did not significantly improve the viability of probiotics during the fermentation but had an important influence on preservation of the strength of the carrier during storage. Our results indicate that whey-based substrate has positive effect on the mechanical stability of biopolymer beads with encapsulated probiotics.

1. Introduction

Probiotic bacteria have been incorporated into a wide range of dairy products and orally administrated in various forms, such as food products, capsules, and tablets. The advantage of dairy products is that the addition of probiotics to these products enhances their functionality [1]. The viability of probiotic cells is very important because of their numerous health benefits but the desired number of viable bacteria is difficult to achieve as their number decreases due to the influence of processing, storage, and gastrointestinal conditions. Probiotic bacteria have poor survivability in yoghurt and fermented milk as they do not tolerate exposure to highly acidic and aerated media [2]. Providing probiotic living cells with a physical barrier to resist unfavorable environmental conditions is an approach currently receiving considerable attention as acceptable systems for probiotic products could be achieved [3–5]. Encapsulation is a valuable method that has been recognized for use in the food industry for increasing the viability and stability of probiotic bacteria against unfavorable environmental conditions during processing and storage [6–9]. Polysaccharides, such as alginate, chitosan, gellan gum, and κ-carrageenan, are the most commonly used materials for the encapsulation of probiotics [10–13]. Alginate is a linear polysaccharide consisting of β-D-mannuronic and α-L-guluronic acids, which has been used for the encapsulation of probiotics, proteins, antioxidants, polyphenols, and vitamins [14, 15]. Some authors reported that the mechanical and chemical stability of alginate beads could be improved by using different coating materials, which beside the protection could enable greater control over bacterial release and improved the viability of encapsulated probiotic organisms [12, 16, 17]. Chitosan, the cationic (1-4)-2-amino-2-deoxy-β-D-glucan, is industrially produced from marine and fungal chitin is being used in the food industry. This material is biodegradable, biocompatible, and

nontoxic. Due to its film forming properties, chitosan has been used for the encapsulation of probiotics and prebiotics, aromatic compounds, enzymes, and antioxidants [18–20]. It has a high modulus along with low elongation-at-break but mixing or copolymerizing chitosan with different polymers can influence its morphology and plasticity [21].

In the recent studies, the textural properties of biopolymer beads of different compositions were tested. These results indicated that differences in mechanical responses to deformation exist because of different crosslinking reactions between biopolymers networks [22].

The textural and physical properties, as well as the entrapment efficiency of the carriers, were greatly affected by the total biopolymer concentration and the employed ratio between both biopolymers [23–25].

The objective of this study was to evaluate the mechanical properties of the beads prepared from a sodium alginate solution containing whey solution with probiotic cells with a chitosan coating formed after the extrusion process. Cell survival during the preparation processes was also investigated. The influence of the fermentation medium on cell viability, mechanical strength, and elastic modulus of the biopolymer carriers before and during storage time was also examined using a Universal Testing Machine (AG-Xplus).

2. Materials and Methods

2.1. Materials. Commercially available powdered alginic acid sodium salt (medium viscosity) from brown algae (Sigma Aldrich, USA) was used for the production of the beads. The alginic acid was composed of 61% mannuronic and 39% guluronic acid with an M/G ratio of 1.56. Low molecular weight chitosan (Acros Organics, USA) was used as the coating material. Calcium chloride $CaCl_2$ dihydrate (Acros Organics, USA) was used as the gelling cation. Whey and cow milk were obtained from a domestic dairy plant Imlek d.o.o. (Belgrade, Serbia). The chemical composition of whey was total solids 9.8 ± 0.03% (w/v); protein 2.6 ± 0.012% (w/v); fat 1.05 ± 0.08% (w/v); and lactose 5.6 ± 0.114% (w/v). The pH value of the whey before fermentation was 6.4. The chemical composition of the milk was fat 0.5% (w/v); proteins 3.1% (w/v); carbohydrates 4.7% (w/v); and calcium 0.12% (w/v). The whey and cow milk were pasteurized at 60°C for 60 min and cooled to room temperature.

2.2. Preparation of Cell Culture. A freeze-dried dairy starter culture known as "Lactoferm ABY- 6" (containing *Streptococcus salivarius* ssp. *thermophilus, Lactobacillus delbrueckii* ssp. *bulgaricus, Lactobacillus acidophilus, and Bifidobacterium bifidum*) was supplied by Biochem S.R.L. (Monterotondo, Roma, Italy). For all experiments, the cell-whey suspension was prepared by dissolving 1.0% (w/v) of frozen starter culture in whey.

2.3. Encapsulation of Probiotics

2.3.1. Preparation of the Beads. Sodium alginate suspension was mixed with cell-whey suspension in the ratio 1 : 1 (v/v). The alginate beads were made by extruding the alginate-cell suspension into 2.0% (w/v) of calcium chloride using a syringe pump (Racel, Scientific Instruments, Stamford, CT, USA). Alginate-cell suspension contains 1.70% (w/v) sodium alginate. Ca-alginate beads were obtained at a collecting distance of 3 cm between the blunt stainless steel needle tip (18 gauges) and the calcium chloride solution. After collection, the beads were allowed to harden for 30 min. The beads were separated by filtration, transferred to a sterile Petri dish, and stored at 4 ± 1°C in 0.2% (w/v) yeast extract solution [26].

2.3.2. Coating of Alginate Beads with Chitosan. The chitosan and sodium alginate solutions were prepared according to the method of Zhou et al. [27]. Beads with chitosan coating were prepared as follows: the alginate beads were immersed in 100 mL of chitosan solution (4 g L^{-1}), shaken on an orbital shaker at 100 rpm for 40 min for coating, and rinsed with sterile water to remove the excess chitosan. All steps were performed under aseptic conditions.

2.4. Fermentation. Experiments were conducted in 100 mL Erlenmeyer flasks containing 50 mL of medium (70% pasteurized whey and 30% milk). Based on preliminary experiments (data not shown) 30% of milk was used for beverage formulation as concentration that is appropriate for sensory quality improvement. Samples were inoculated by adding 6% (w/v) of encapsulated starter culture. The fermentation was realized at 42°C. During the incubation, samples were taken every 2 h for the determination of the pH value. The fermentations were performed until a pH of 4.6 was attained and the stopped by rapid cooling. After the fermentation, samples were stored at 4 ± 1°C for 21 days to determine the viability of the cells and the mechanical stability of the beads.

2.5. Cell Release during the Fermentation. The influence of the alginate concentration and chitosan on the encapsulation efficiency was performed by determination of the viable cell count (log CFU mL^{-1}) and cell release from the beads. Prepared beads (1 g) were dissolved in sterile sodium citrate solution (2.0% (w/v)) by gently shaking at room temperature for 5 min. The cell release was determined based on the quotients of the number of free cells in the fermentation medium (CFU mL^{-1}) and the total number of free (CFU mL^{-1}) and encapsulated cells (CFU g^{-1}), as was presented in the literature [26].

2.6. Analytical Methods

2.6.1. Enumeration of the Encapsulated Probiotic Bacteria. For quantitative measurements of cell viability, it was necessary to liquefy the beads and release the encapsulated probiotic cells. The beads were dissolved in sterile sodium citrate solution (2.0% (w/v)) by gently shaking at room temperature. The number of *S. thermophilus* cells was determined by the pour plate counting method on M17 agar. The number of viable cells *L. bulgaricus, L. acidophilus,* and *B. bifidum* was determined by the pour plate counting method on MRS agar [28].

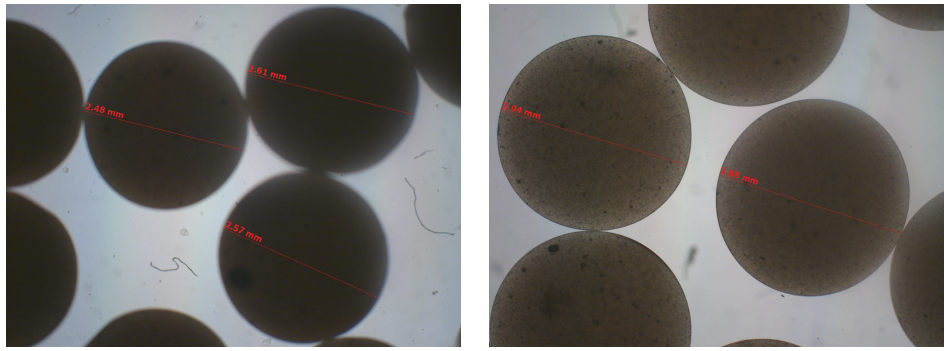

(a) (b)

Figure 1: The size of the beads measured using optical microscopy, 5 × 10: (a) alginate beads and (b) alginate beads coated with chitosan.

The results are presented as the total number of viable cells on both substrate (M17 and MRS) and cell number expressed in log (CFU mL^{-1}) for free cells and log (CFU g^{-1}) for encapsulated cells.

2.6.2. Optical Microscopy. The beads shape and existence of aggregates were examined after the encapsulation process using an optical microscope. The diameters of randomly selected wet beads in distilled water were measured by optical microscopy (Carl Zeiss Microscopy GmbH, UK) using a magnification of 5 × 10. The average diameter was calculated from the measurements of 30 beads.

2.6.3. Scanning Electron Microscopy. Scanning electron microscopy (SEM) was used to analyze the morphology of the Ca-alginate beads according to the method of Stojkovska et al. [29]. Samples were fixed on a sample holder and visualized using a TESCAN MIRA3 XMU SEM (USA Inc., Cranberry Twp, PA, USA), operated at 20 keV.

2.6.4. Mechanical Properties of the Beads. Compression tests of single beads submerged in distilled water were performed using Universal Testing Machine, AG-Xplus (Shimadzu, Japan), equipped with a 100 N force load cell (force range from 0.01 to 100 N). The compression was performed up to 30% sample deformation (ratio of displacement to initial bead diameter) at a compression speed of 1 mm/min and ambient temperature of 25 ± 1°C according to the method described in a previous work [30]. During the compression test, a single bead was submerged in distilled water in a Petri dish and placed on a flat plate. The distance between the plate (50 mm in diameter) position at a given deformation and the plate at the first contact with the bead was measured. Thirty beads from each sample were compressed and automatic detection of the contact between plate and bead was performed with a contact force of 0.1 N under identical conditions. The values of elastic modulus and maximal forces were determined using the force-displacement and engineering stress-strain curves (in the remaining text, stress-strain curves).

2.6.5. Fourier Transform Infrared Spectroscopy (FTIR). FTIR spectra of freeze-dried alginate beads before and after fermentation were analyzed in the wavenumber region of 4000 to 400 cm^{-1}. FTIR was used to verify the chemical interaction between alginate and the fermentation medium (FTIR spectrometer Bomem MB, series Hartmann & Braun).

2.6.6. Statistical Analysis. The experiments were performed in triplicate. All values are expressed as mean ± standard deviation. Mean values were analyzed using one-way ANOVA. The Tukey post hoc test was performed for means comparison [Origin Pro 8 (1991–2007) computer package; Origin Lab Co., Northampton, MA, USA]. Data were considered significantly different when $P < 0.05$. The mean values of the mechanical properties of the beads were determined using equipment software, TRAPEZIUMX 1.13.

3. Results and Discussion

3.1. Size, Shape, and Morphology of the Beads. The mean diameter of the formed Ca-alginate beads was 2.60 ± 0.025 mm. The shape of the beads did not change with the addition of chitosan and the average size of the beads with coating was 2.95 ± 0.11 mm, as shown in Figure 1.

From the SEM images of cross sections of the sample, encapsulated rod-shaped and spherical bacteria and their binding in the carrier could be seen. The probiotic bacteria were randomly grouped and placed in the cavity of carriers, as shown in Figure 2.

Void spaces that were recorded around the bacteria in this study were also similar spaces recorded by Sathyabama et al. [31] in SEM micrographs of probiotic strains, namely, *Staphylococcus succinus* (MAbB4) and *Enterococcus faecium* (FIdM3) encapsulated in alginate spheres. Based on the observed micrographs, it could be said that the gelation process of alginate beads was disrupted especially in area around the bacteria.

3.2. Influence of the Coating on the Viability of the Encapsulated Probiotic Cells. The initial number of viable cells was

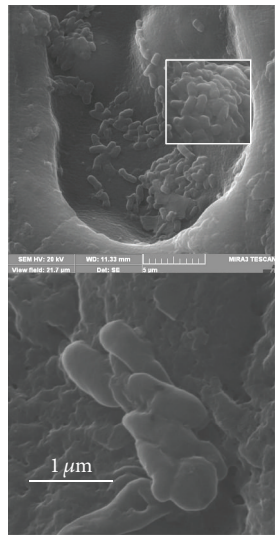

Figure 2: SEM micrographs of cross sections of alginate beads with probiotic cells, magnification 10000x.

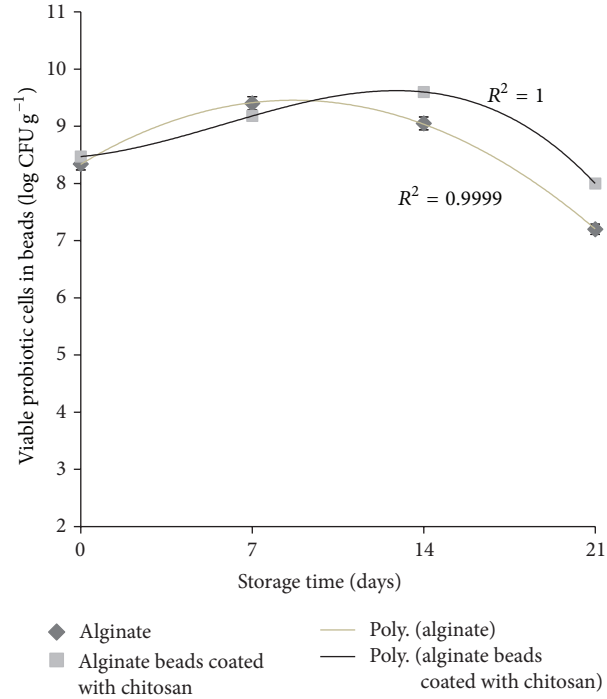

Figure 3: Viable cell number of bacteria during 21 days of refrigerated storage, at 7 days of interval for cells in alginate beads (log CFU g^{-1}) and coated alginate beads (log CFU g^{-1}).

7.55 ± 0.11 (log CFU g^{-1}) for uncoated beads and 7.59 ± 0.16 (log CFU g^{-1}) for coated alginate beads. During the fermentation, the number of viable cells in the beads without chitosan increased by 0.79 while in the beads with chitosan they increased by 0.88 (log CFU g^{-1}) log units and reached values of 8.34 ± 0.14 (log CFU g^{-1}) and 8.47 ± 0.29 (log CFU g^{-1}), respectively. Based on these results, it could be concluded that addition of chitosan did not have a statistically significant effect on cell viability during the fermentation.

In addition, comparing the coated and uncoated alginate beads, a significant difference in cell release was observed. The number of cells released into the fermentation medium from the uncoated beads was 5.33±0.05%, while a slightly lower cell leakage of 4.98±0.09% was observed for alginate beads coated with chitosan. This could be explained by the fact that, during the fermentation, electrostatic interaction between alginate carboxylate groups and ammonium chitosan groups leads to a suppression of cell release [32, 33]. Based on the obtained results, it could be stated that chitosan as coat decreased cell leakage and enhanced retention of the cells within the beads. Influence of chitosan coating on the fermentative activity and survival of encapsulated probiotic cells in simulated gastrointestinal conditions was a subject of our previous work [34]. According to the presented results in mentioned paper, chitosan-coated beads had higher probiotic viable cell count than samples with alginate beads after fermentation, and especially in simulated gastric conditions at pH 3.0 and 2.5. Chávarri et al. [35] also reported that chitosan coating provides better protection of the probiotics in comparison with uncoated microcapsules.

In this study, the influence of the coating on cell viability during storage was also considered. As shown in Figure 3, the chitosan coating improved the viability of the encapsulated probiotics during storage. After 21 days, it was observed that, in the chitosan-coated alginate beads, a greater number of bacteria survived in comparison with those in the uncoated beads, which indicated that the coating improved the viability of the probiotic strains. These findings are in agreement with previous results for the encapsulation of the probiotic strain *L. plantarum* in alginate beads coated with chitosan [12]. Thus, the chitosan coating did not adversely influence the growth of the bacteria during fermentation but stimulated their survival during storage.

3.3. Effect of the Fermentation Process on the Chemical Structure of the Alginate Beads. The results of FTIR analysis and the position of the characteristic bands are shown in Figure 4. The band at 3370.2 cm^{-1} corresponds to stretching vibrations of –OH linked to –NH_2. The band at 1411.5 cm^{-1} (related to asymmetric COO-stretching vibration) became broader after interaction of beads with fermentation medium [36]. The results showed changes in the peaks of the amino and carboxyl groups before and after fermentation, which indicates ionic interactions between the carbonyl groups of alginate and the amino groups of the proteins. Hydrogels are potential absorbers of ions present in the medium [37]. The diffusion of Ca^{2+} into the alginate network is confirmed by the shift of the –C–O and the C–O–H vibrations to lower frequencies; additionally, spectral changes in the regions of the COO-antisymmetric and symmetric stretching vibrations occurred. The bands around 1400 cm^{-1} and 1000 cm^{-1} correspond to –C–O, –C–C, and –C–OH groups [38].

3.4. Influence of the Fermentation Process, the Coating, and the Storage Time on the Mechanical Stability of the Beads. Mechanical strength and elastic modulus of the carriers with

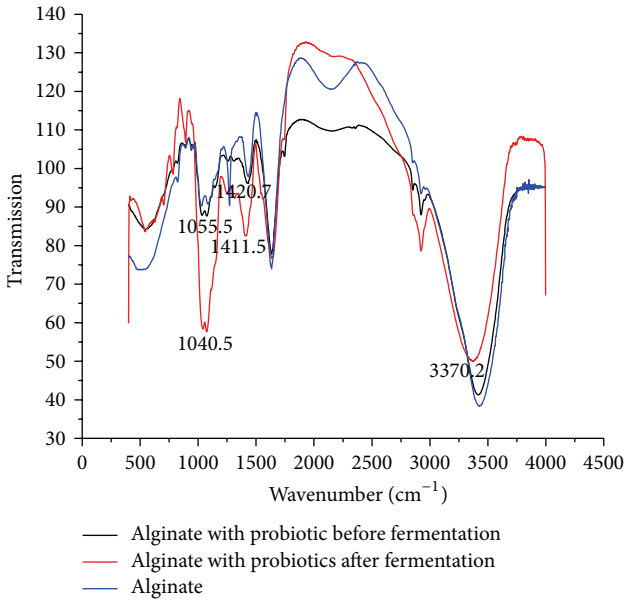

FIGURE 4: FTIR analysis of alginate beads with probiotics before and after fermentation.

probiotic cells were determined with the aim of defining the mechanical stability of the carriers that could be of significance for their further application. The viscoelastic properties of alginate gels have been assessed so far by using static or dynamic compression tests [24, 39–42]. The principle of the measurements was to impose a strain on the beads by compression and to measure the corresponding force and the resulting stress.

According to the results presented in Figure 5, it could be seen that the addition of whey with probiotic cells into the sodium alginate solution led to stabilization of the carriers and increased force values. Based on this observation, it could be stated that the calcium ions and proteins from milk and whey had an additional effect on the stability of the carriers. This effect could be explained by the ability of whey proteins to form a gel in the presence of Ca^{2+} ions. This type of gel, resulting from a dimeric association of guluronic acid regions with Ca^{2+} in the "egg box" formation, is similar to the alginate gel [15, 43]. pH is also an important factor during the fermentation and has effect on mechanical stability of the beads. The proteins from the milk and whey are pH dependent and improve gelation process in the pH range 4,5–5,5 [44]. Comparing the results obtained for the force before and after fermentation, it could be concluded that the fermentation process increased the strength of the alginate beads.

Elastic modulus of the beads was calculated from the slope using least squares regression of the plot of the stress versus strain data obtained from the compression testing. The resulting force-displacement data pairs were converted into corresponding stress and strain values, based on the initial bead diameter. Curves fitting for force-displacement and stress-strain experimental data and quality of the fit ($R^2 > 0.99$) are shown in Figure 5. Since alginate particles are viscoelastic, the slopes of the tangents in the elastic parts of the stress-strain curves before and after fermentation were used for the determination of the modulus. Elastic parts of the stress-strain curves (mostly from 10% to 20% strain) were selected according to tested degree of recovery after compression and elastic limits studied in literature data [23, 42]. Ca-alginate beads of approximate size 3.01 ± 0.11 mm were used for compression testing because of the possibility of comparisons with beads coated with chitosan.

The values of elastic modulus of the alginate beads obtained before the fermentation (0.059 ± 0.0029 N) were slightly higher than beads made of calcium alginate without addition of cell-whey suspension (0.048 ± 0.0049 N). However, results for the elastic modulus of calcium alginate beads reported by Chan et al. [42] are significantly higher compared to the results in this study. The main difference between the two studies is compression speed used during the assays. Wang et al. [40] demonstrated that the compression speed has influence on the modulus of alginate beads because the wet alginate beads are generally considered to be viscoelastic and may lose liquid under compression. The modulus values of calcium alginate beads (made of medium viscosity alginate without addition of cell-whey suspension, M/G ratio 1.56) obtained at 30% sample deformation are in good agreement with results reported by Ouwerx et al. [24]. From the force-displacement curves presented in Figure 5, it could be noticed that the presence of chitosan coating reduced the interaction between alginate and the fermentation medium which resulted in a decrease of the measured force of the coated beads after the fermentation process in comparison with the uncoated beads. The results of the elastic modulus of the beads shown in Figure 6 indicate that coating and fermentation increased the modulus of the beads.

The mechanical stability of the beads is important during storage in order to assume the quality and shelf life of fermented beverages. From Figure 7, it could be seen that the maximal forces for alginate beads increased in the first 24 h because of their direct contact with Ca^{2+} ions from the fermentation medium. Maximal forces were higher for alginate beads up to the 7th day of storage in comparison with the force for the coated beads. After 1 day, the alginate strength began to decline and this trend continued until the end of the storage. On the other hand, the strength of chitosan-coated beads increased up to the 7th day when it began to decrease because of intensive cells growth in the cavity of the material and erosion of the bead network. Based on the results, chitosan as a coating material contributed significantly to the preservation of the strength of the carrier during the storage.

4. Conclusions

The probiotic starter culture was successfully encapsulated in uncoated and coated alginate beads prepared by the extrusion method. The present study showed that the fermentation process improved the mechanical stability of the biopolymer beads because of the presence of calcium ions and proteins from the milk and whey in the fermentation medium. According to the obtained results, the presence of the chitosan coating improved the carrier strength during storage. Chitosan enables the physical isolation of bacteria from the

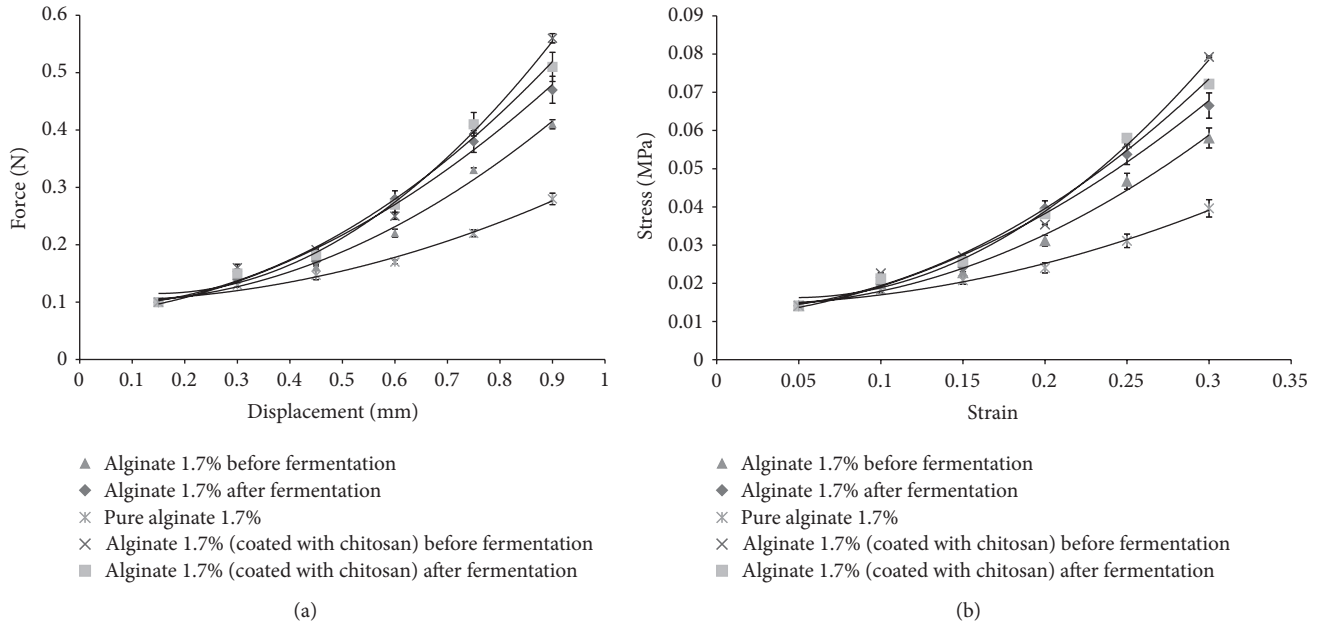

Figure 5: Comparison of the force-displacement (a) and stress-strain (b) polynomial fitted curves of the biopolymer carriers before and after the fermentation process (30% deformation, compression speed 1 mm/min, and means values ± SD, $n = 30$).

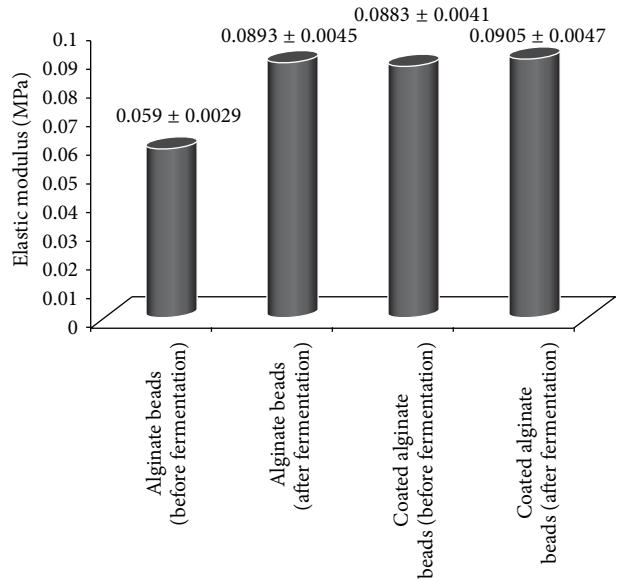

Figure 6: Elastic modulus of alginate beads with encapsulated probiotics before and after the fermentation process for 30% sample deformation (means values ± SD, $n = 30$), alginate concentration 1.7% (w/v).

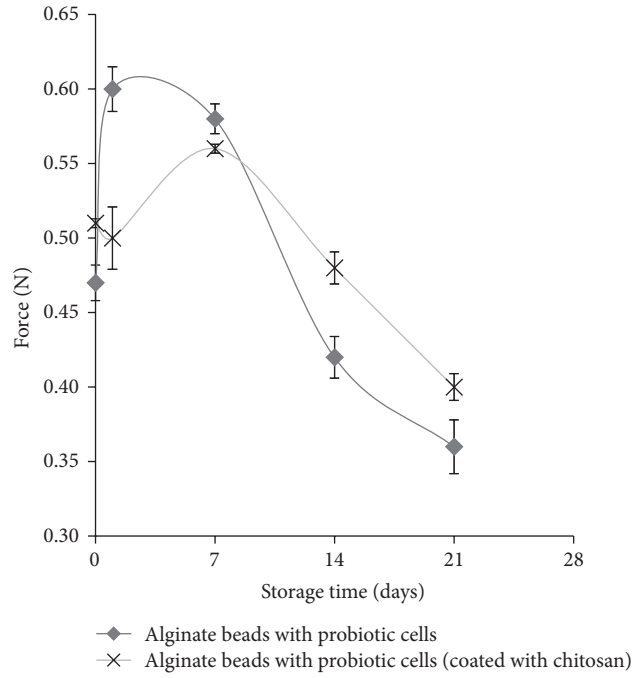

Figure 7: Influence of the chitosan coating on mechanical strength of the beads (alginate concentration 1.7% (w/v), means ± SD, $n = 30$).

external environment and decreases cell release during the fermentation. The results also indicate that fermentation increased the maximal force in comparison with freshly made uncoated beads with probiotic cells (before fermentation) and extended the shelf life of the product. We have concluded that whey-based fermentation medium had a positive effect on the stability of the material for encapsulation of probiotics, which is a very significant finding for the future applications of whey-based fermentation medium in combination with biopolymer beads for the production of fermented beverages.

Conflict of Interests

The authors declare that there is no conflict of interests regarding the publication of this paper.

Acknowledgments

The authors gratefully acknowledge the support from the Ministry of Education, Science and Technological Development of the Republic of Serbia through Projects III 46010 and ON 174004. In addition, the authors would like to give special thanks to the Shimadzu Branch Belgrade (Shimadzu Corporation, Japan) for the technical support during the experiments and Maja Vukašinović-Sekulić, Ph.D., Assistant Professor, University of Belgrade, Faculty of Technology and Metallurgy, for the pictures from the optical microscope, as well as Đordje Veljović, Ph.D., for the SEM measurements.

References

[1] E. Weichselbaum, "Probiotics and health: a review of the evidence," *Nutrition Bulletin*, vol. 34, no. 4, pp. 340–373, 2009.

[2] P. Muthukumarasamy, P. Allan-Wojtas, and R. A. Holley, "Stability of *Lactobacillus reuteri* in different types of microcapsules," *Journal of Food Science*, vol. 71, no. 1, pp. M20–M24, 2006.

[3] J. Burgain, C. Gaiani, M. Linder, and J. Scher, "Encapsulation of probiotic living cells: from laboratory scale to industrial applications," *Journal of Food Engineering*, vol. 104, no. 4, pp. 467–483, 2011.

[4] C. P. Champagne and K. Kailasapathy, "Encapsulation of probiotics," in *Delivery and Controlled Release of Bioactives in Foods and Nutraceuticals*, N. Garti, Ed., pp. 344–369, Woodhead Publishing, Cambridge, UK, 2008.

[5] D. Poncelet, C. Dreffier, P. Subra-Paternault, and T. F. Vandamme, "Introduction aux techniques de microencapsulation," in *Microencapsulation: Des Sciences aux Technologies*, T. Vandamme, D. Poncelet, and P. Subra-Paternault, Eds., pp. 3–7, Ed. Tec & doc, Paris, France, 2007.

[6] G. K. Gbassi, T. Vandamme, S. Ennahar, and E. Marchioni, "Microencapsulation of *Lactobacillus plantarum* spp. in an alginate matrix coated with whey proteins," *International Journal of Food Microbiology*, vol. 129, no. 1, pp. 103–105, 2009.

[7] L.-E. Shi, Z.-H. Li, D.-T. Li et al., "Encapsulation of probiotic *Lactobacillus bulgaricus* in alginate–milk microspheres and evaluation of the survival in simulated gastrointestinal conditions," *Journal of Food Engineering*, vol. 117, no. 1, pp. 99–104, 2013.

[8] K. Sultana, G. Godward, N. Reynolds, R. Arumugaswamy, P. Peiris, and K. Kailasapathy, "Encapsulation of probiotic bacteria with alginate–starch and evaluation of survival in simulated gastrointestinal conditions and in yoghurt," *International Journal of Food Microbiology*, vol. 62, no. 1-2, pp. 47–55, 2000.

[9] M. K. Tripathi and S. K. Giri, "Probiotic functional foods: survival of probiotics during processing and storage," *Journal of Functional Foods*, vol. 9, no. 1, pp. 225–241, 2014.

[10] N. Kamalian, H. Mirhosseini, S. Mustafa, and M. Y. A. Manap, "Effect of alginate and chitosan on viability and release behavior of *Bifidobacterium pseudocatenulatum* G4 in simulated gastrointestinal fluid," *Carbohydrate Polymers*, vol. 111, pp. 700–706, 2014.

[11] F. Nazzaro, F. Fratianni, R. Coppola, A. Sada, and P. Orlando, "Fermentative ability of alginate-prebiotic encapsulated *Lactobacillus acidophilus* and survival under simulated gastrointestinal conditions," *Journal of Functional Foods*, vol. 1, no. 3, pp. 319–323, 2009.

[12] I. Trabelsi, D. Ayadi, W. Bejar, S. Bejar, H. Chouayekh, and R. Ben Salah, "Effects of *Lactobacillus plantarum* immobilization in alginate coated with chitosan and gelatin on antibacterial activity," *International Journal of Biological Macromolecules*, vol. 64, pp. 84–89, 2014.

[13] C. Wandrey, A. Bartkowiak, and S. E. Harding, "Materials for encapsulation," in *Encapsulation Technologies for Active Food Ingredients and Food Processing*, N. J. Zuidam and V. C. Nedovic, Eds., pp. 31–100, Springer, New York, NY, USA, 2010.

[14] N. T. Annan, L. T. Hansen, and A. D. Borza, "Encapsulation in alginate-coated gelatin microspheres improves survival of the probiotic *Bifidobacterium adolescentis* 15703T during exposure to simulated gastro-intestinal conditions," *Food Research International*, vol. 41, no. 2, pp. 184–193, 2008.

[15] S. Wichchukit, M. H. Oztop, M. J. McCarthy, and K. L. McCarthy, "Whey protein/alginate beads as carriers of a bioactive component," *Food Hydrocolloids*, vol. 33, no. 1, pp. 66–73, 2013.

[16] M. T. Cook, G. Tzortzis, D. Charalampopoulos, and V. V. Khutoryanskiy, "Microencapsulation of probiotics for gastrointestinal delivery," *Journal of Controlled Release*, vol. 162, no. 1, pp. 56–67, 2012.

[17] W. Krasaekoopt, B. Bhandari, and H. Deeth, "The influence of coating materials on some properties of alginate beads and survivability of microencapsulated probiotic bacteria," *International Dairy Journal*, vol. 14, no. 8, pp. 737–743, 2004.

[18] M. Chávarri, I. Marañón, R. Ares, F. C. Ibáñez, F. Marzo, and M. D. C. Villarán, "Microencapsulation of a probiotic and prebiotic in alginate-chitosan capsules improves survival in simulated gastro-intestinal conditions," *International Journal of Food Microbiology*, vol. 142, no. 1-2, pp. 185–189, 2010.

[19] M. G. Žuža, B. M. Obradović, and Z. D. Knežević-Jugović, "Hydrolysis of penicillin G by penicillin G acylase immobilized on chitosan microbeads in different reactor systems," *Chemical Engineering & Technology*, vol. 34, no. 10, pp. 1706–1714, 2011.

[20] K. T. Trifković, N. Z. Milašinović, V. B. Djordjević et al., "Chitosan microbeads for encapsulation of thyme (*Thymus serpyllum* L.) polyphenols," *Carbohydrate Polymers*, vol. 111, pp. 901–907, 2014.

[21] E. Brychcy, D. Kulig, A. Zimoch-Korzycka, K. Marycz, and A. Jarmoluk, "Physicochemical properties of edible chitosan/hydroxypropyl methylcellulose/lysozyme films incorporated with acidic electrolyzed water," *International Journal of Polymer Science*, vol. 2015, Article ID 604759, 10 pages, 2015.

[22] O. Sandoval-Castilla, C. Lobato-Calleros, H. S. García-Galindo, J. Alvarez-Ramírez, and E. J. Vernon-Carter, "Textural properties of alginate-pectin beads and survivability of entrapped *Lb. casei* in simulated gastrointestinal conditions and in yoghurt," *Food Research International*, vol. 43, no. 1, pp. 111–117, 2010.

[23] G. Kostov, M. Angelov, I. Mihaylov, and D. Poncelet, "Mechanical properties of Ca-alginate beads for ethanol fermentation with immobilized yeast," *Revue de Génie Industriel*, vol. 5, pp. 25–35, 2010.

[24] C. Ouwerx, N. Velings, M. M. Mestdagh, and M. A. V. Axelos, "Physico-chemical properties and rheology of alginate gel beads formed with various divalent cations," *Polymer Gels and Networks*, vol. 6, no. 5, pp. 393–408, 1998.

[25] W.-P. Voo, P. Ravindra, B.-T. Tey, and E.-S. Chan, "Comparison of alginate and pectin based beads for production of poultry probiotic cells," *Journal of Bioscience and Bioengineering*, vol. 111, no. 3, pp. 294–299, 2011.

[26] M. Gündüz, *Lactic acid production by lactobacillus casei nrrl b-441 immobilized in chitosan stabilized Ca-alginate beads [M.S. thesis]*, Izmir Institute of Technology, Izmir, Turkey, 2005.

[27] Y. Zhou, E. Martins, A. Groboillot, C. P. Champagne, and R. J. Neufeld, "Spectrophotometric quantification of lactic bacteria in alginate and control of cell release with chitosan coating," *Journal of Applied Microbiology*, vol. 84, no. 3, pp. 342–348, 1998.

[28] L. J. Vrbaški and S. Markov, *Praktikum iz mikrobiologije*, Prometej, Novi Sad, Serbia, 1993 (Serbian).

[29] J. Stojkovska, D. Kostić, Ž. Jovanović, M. Vukašinović-Sekulić, V. Mišković-Stanković, and B. Obradović, "A comprehensive approach to in vitro functional evaluation of Ag/alginate nanocomposite hydrogels," *Carbohydrate Polymers*, vol. 111, pp. 305–314, 2014.

[30] N. S. Tomović, K. T. Trifković, M. P. Rakin, M. B. Rakin, and B. M. Bugarski, "Influence of compression speed and deformation percentage on mechanical properties of calcium alginate particles," *Chemical Industry and Chemical Engineering Quarterly*, vol. 21, no. 3, pp. 411–417, 2015.

[31] S. Sathyabama, M. Ranjith kumar, P. Bruntha Devi, R. Vijayabharathi, and V. Brindha Priyadharisini, "Co-encapsulation of probiotics with prebiotics on alginate matrix and its effect on viability in simulated gastric environment," *LWT—Food Science and Technology*, vol. 57, no. 1, pp. 419–425, 2014.

[32] S. Haas, J. Miura-Fraboni, F. Zavala, K. Murata, A. Leone-Bay, and N. Santiago, "Oral immunization with a model protein entrapped in microspheres prepared from derivatized α-amino acids," *Vaccine*, vol. 14, no. 8, pp. 785–791, 1996.

[33] A. J. Ribeiro, C. Silva, D. Ferreira, and F. Veiga, "Chitosan-reinforced alginate microspheres obtained through the emulsification/internal gelation technique," *European Journal of Pharmaceutical Sciences*, vol. 25, no. 1, pp. 31–40, 2005.

[34] T. Ž. Krunić, M. L. Bulatović, N. S. Obradović, M. S. Vukašinović-Sekulić, and M. B. Rakin, "Effect of immobilisation materials on viability and fermentation activity of dairy starter culture in whey-based substrate," *Journal of the Science of Food and Agriculture*, 2015.

[35] M. Chávarri, I. Marañón, and M. C. Villarán, "Encapsulation technology to protect probiotic bacteria," in *Probiotics*, E. R. Probiotics, Ed., chapter 23, InTech, Rijeka, Croatia, 2012.

[36] F. Saraei, N. M. Dounighi, H. Zolfagharian, S. M. Bidhendi, P. Khaki, and F. Inanlou, "Design and evaluate alginate nanoparticles as a protein delivery system," *Archives of Razi Institute*, vol. 68, no. 2, pp. 139–146, 2013.

[37] A. Poreda, T. Tuszyński, M. Zdaniewicz, P. Sroka, and M. Jakubowski, "Support materials for yeast immobilization affect the concentration of metal ions in the fermentation medium," *Journal of the Institute of Brewing*, vol. 119, no. 3, pp. 164–171, 2013.

[38] G. K. Gbassi, F. S. Yolou, S. O. Sarr, P. G. Atheba, C. N. Amin, and M. Ake, "Whey proteins analysis in aqueous medium and in artificial gastric and intestinal fluids," *International Journal of Biological and Chemical Sciences*, vol. 6, no. 4, pp. 1828–1837, 2012.

[39] M. Moresi and M. Bruno, "Characterisation of alginate gels using quasi-static and dynamic methods," *Journal of Food Engineering*, vol. 82, no. 3, pp. 298–309, 2007.

[40] C. X. Wang, C. Cowen, Z. Zhang, and C. R. Thomas, "High-speed compression of single alginate microspheres," *Chemical Engineering Science*, vol. 60, no. 23, pp. 6649–6657, 2005.

[41] S. V. Bhujbal, G. A. Paredes-Juarez, S. P. Niclou, and P. De Vos, "Factors influencing the mechanical stability of alginate beads applicable for immunoisolation of mammalian cells," *Journal of the Mechanical Behavior of Biomedical Materials*, vol. 37, pp. 196–208, 2014.

[42] E.-S. Chan, T.-K. Lim, W.-P. Voo, R. Pogaku, B. T. Tey, and Z. Zhang, "Effect of formulation of alginate beads on their mechanical behavior and stiffness," *Particuology*, vol. 9, no. 3, pp. 228–234, 2011.

[43] L. Y. Chen and M. Subirade, "Effect of preparation conditions on the nutrient release properties of alginate–whey protein granular microspheres," *European Journal of Pharmaceutics and Biopharmaceutics*, vol. 65, no. 3, pp. 354–362, 2007.

[44] S. L. Turgeon and M. Beaulieu, "Improvement and modification of whey protein gel texture using polysaccharides," *Food Hydrocolloids*, vol. 15, no. 4–6, pp. 583–591, 2001.

Hindawi Publishing Corporation
International Journal of Polymer Science
Volume 2015, Article ID 829795, 10 pages
http://dx.doi.org/10.1155/2015/829795

Research Article

Recycling of Cooking Oil Waste into Reactive Polyurethane for Blending with Thermoplastic Polyethylene

Anika Zafiah M. Rus,[1] N. Syamimi M. Salim,[1] and N. Haiza Sapiee[1,2]

[1]*Sustainable Polymer Engineering, Advanced Manufacturing and Material Center (AMMC), Universiti Tun Hussein Onn Malaysia, Batu Pahat, 86400 Parit Raja, Johor, Malaysia*
[2]*The University of Auckland (UoA), Auckland CBD 1010, New Zealand*

Correspondence should be addressed to Anika Zafiah M. Rus; zafiah@uthm.edu.my

Received 5 April 2015; Revised 25 June 2015; Accepted 2 August 2015

Academic Editor: Pratheep K. Annamalai

Driven by the need of growing to a more sustainable and environmentally friendly future, this research is started by mixing in-house produced biorenewable polymers (BP) from waste cooking oil with the standard low density polyethylene (LDPE) and high density polyethylene (HDPE) via melt-mixing at low ratios. These mixtures are then compounded via injection molding to produce tensile samples. By using the quality of individual compounds injected, the parameters obtained for all ratios of LDPE/BP were the same with neat LDPE whereas some adjustments were required for the HDPE/BP compounds. The corresponding mechanical behaviors of each ratio were also examined and the results showed that both tensile strength and strain of the LDPE/BP were better than neat LDPE. On the other hand, increasing the BP content in HDPE/BP will increase the toughness of the compound if compared to neat HDPE. Therefore, not only does the presence of BP provide renewable properties, but it also improves the mechanical properties. Moreover, the processing temperature and composition of BP will both influence the quality and mechanical behavior of the product made. Thus, this study may aid any intention on processing these in-house produced polymers by injection molding.

1. Introduction

Polymers in the form of plastics are the most abundant products that we use in our daily life. Nowadays, a majority of the consuming industries use polymers that are synthesized from petroleum sources, for example, polyethylene thermoplastics. Polyethylene is one of the most popular plastics globally and has the simplest structure of all commercial polymers. Two main types of polyethylene are low density polyethylene (LDPE) and high density polyethylene (HDPE) [1].

LDPE and HDPE are two of the most widely used plastics, especially in making plastic bottles, grocery bags, or containers [2]. These polyethylenes can be obtained from polymerization of ethylene. LDPE is produced via free radical polymerization at extremely high pressures, while HDPE is synthesised via Ziegler-Natta polymerization at atmospheric pressure [3]. LDPE is known for its relatively low density due to minor branching in the molecule. Meanwhile, HDPE is well known for its high strength to density ratio. Traditionally, different branch content polyethylenes are blended in order to improve the toughness or processability [4]. Ethylene comes from a nonrenewable source which is petroleum and does not undergo the process of sustainable degradation [5].

Due to the detrimental effects and dependency towards this limited source, there must be methods to replace or improve these plastics [6, 7]. Currently, there are extensive researches that are being done to accommodate the world's vision in growing to a more sustainable and environmentally friendly future [8]. This leads to a series of studies in producing biorenewable plastics which includes research being done using waste vegetable oil as an alternative feedstock for sustainable monomer [6, 7]. With the aim of gradually changing these plastics to renewable plastics, the renewable monomers are mixed with these standard thermoplastic polymers.

Braskem, one of the world's leading bioplastic producers, announced the expansion of its resin portfolio with plans to produce 30 kilotonnes of biobased low density polyethylene

(LDPE) annually. The product has been available on the market since January 2014. Braskem has been producing high density polyethylene (HDPE) and linear low density polyethylene (LLDPE) made from renewable feedstock on an industrial scale. Biobased polyethylene in all its variations has properties identical to those of traditional polyethylene; however, since it is derived from renewable materials, it has decisive advantages, such as reducing greenhouse gas emissions by sequestering carbon dioxide from the atmosphere [9].

Mixing these environmentally friendly hydroxylated biorenewable monomers and crosslinking agents allows biorenewable polymers (BP) to be produced [6, 7]. Combining the BP with the standard LDPE and HDPE is suggested to improve the photodegradation, which is polymer degradation due to light exposure. Even so, having biorenewable polymers without any means of processing them is a waste. The degradation being either photo or thermal may change in aspect of bond scission, chemical transformation, and formation of new functional groups [10]. Degradation rate of PE, exposed to heat or UV light involving thermo- or photooxidation, depends to a great extent on the nature of material and environment it is exposed to [11].

Injection molding is the most common, easy, and commercial method for processing or manufacturing of plastic parts into various products or even for material testing [12–14]. Since injection molding is one of the most widely used methods for processing thermoplastics, this paper aims to determine and understand the processing conditions of the LDPE/SP and HDPE/SP compound by injection molding [13]. An important advantage of injection molding is that complex geometries can be made easily in one production step in an automated process. The injection molding machine operates by first pouring the materials in the hopper which leads to the heated barrel equipped with a reciprocating screw [14]. After the material is heated to a molten state, the screw pushes the content into a mold via the nozzle with sufficient cooling time and the product will be ejected.

Being the most important process in manufacturing plastic product, injection molding produced mass-producing products since raw material can be converted into a solid shape by single procedure. It is undeniable that, for any process, the processing temperatures are one of the key factors which gives most impact on the properties or the processability of the product. Therefore, this research focuses on the parameters, mainly temperature, needed to produce several mixed ratios of these green polymers and LDPE or HDPE by injection molding. The presence of biorenewable polymers in the compound may lower the processing conditions required, which will save energy consumption. Besides that, the resulting mechanical properties of each of the injected samples will also be analysed.

2. Experimental

2.1. Raw Materials. The raw materials in this work included low density polyethylene (LDPE) (melt index = 5 g/10 min, density = 0.922 g/cm^3, and Vicat softening point = 93°C), high density polyethylene (HDPE) (melt index = 4 g/10 min, density = 0.957 g/cm^3, and Vicat softening point = 124°C), flexible and rigid polymethane polyphenyl isocyanate (modified polymeric MDI) (viscosity at 25°C = 120–160 cps, specific gravity at 25°C = 1.18–1.20 g/mL, NCO content, and % wt = 26.3–27.3), and biorenewable monomers (sustainable polyol).

2.2. Synthesis of Biorenewable Polyol. The biorenewable monomer conversions from waste vegetable oils were chemically manipulated at the laboratory scale using less than 1 L of vegetable oil [6, 7, 15].

The preparation of the hydroxylated biorenewable monomer was divided into two stages: the first stage is the preparation of catalyst to generate the epoxides from the unsaturated fatty compounds, while the second stage is the acid-catalysed ring-opening of the epoxides to form polyols.

The catalyst preparation was as follows: distilled water (0.6 mL) and hydrogen peroxide (1.26 mL, 30% w/w) were added and the solution was heated at 50°C and thoroughly stirred (for about 30 minutes) and cooled to room temperature and concentrated aqueous orthophosphoric acid (90 mg, 85% w/w) (1.2 mL) was poured in.

Waste vegetable oil (30 gm) was heated at 50°C and the catalyst prepared earlier was added, followed by water (50 mL). Orthophosphoric acid (15 gm, 85% w/w) and hydrogen peroxide (18 mL, 30% w/w) were added dropwise to the mixture. The mixture was heated at 90°C and stirred for 6 hours. This yielded the hydroxylated biorenewable monomer.

2.3. Preparation of Samples. In general, the hydroxylated biorenewable monomer is reacted with the crosslinking agent, namely, flexible or rigid modified polymeric 4,4-dimethylen-bis-(phenylisocyanate) (MDI), to produce biorenewable polymer (BP). BP were prepared by adding the hydroxylated biorenewable monomer (1 gm; 0.2 gm equivalent weight with polyol) with an appropriate amount of flexible or rigid MDI (0.5% equivalent weight of polyol). The mixture was mechanically stirred until a viscous compound resulted which was left to cure at room temperature for at least 6 hours until the disappearance of N=C=O groups as measured by IR spectroscopy.

Meanwhile, for the compounding process, liquidized BP (as prepared according to previous step but avoiding it to be left and cured at predetermined time) is mixed with LDPE and HDPE by manually stirring until the BP solidifies and adheres on the surface of LDPE or HDPE surfaces. The weights of compositions were determined based on ratio of BP and LDPE and HDPE, respectively. Samples were made with 1% of BP (wt/wt ratio) to 100% of LDPE or HDPE. The same method was used to mix 2%, 3%, 4%, and 5% of BP with LDPE and HDPE with either flexible or rigid crosslinkers.

The LDPE/BP and HDPE/BP specimens were then fed to the injection molding machine (Nissei Horizontal Screw Type Injection Molding NP7) equipped with a mold of tensile specimens according to ISO 527 (5A). Using the general processing conditions for pure LDPE and HDPE along with the TGA results as a guideline to determine the initial parameters, the quality of the resulting test bars was used as a benchmark to adjust the parameters for changing ratios.

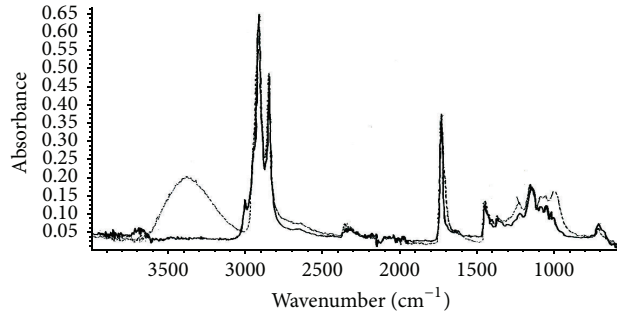

Figure 1: IR spectra of waste vegetable oil (bold line) and the corresponding biorenewable polyol (dotted line).

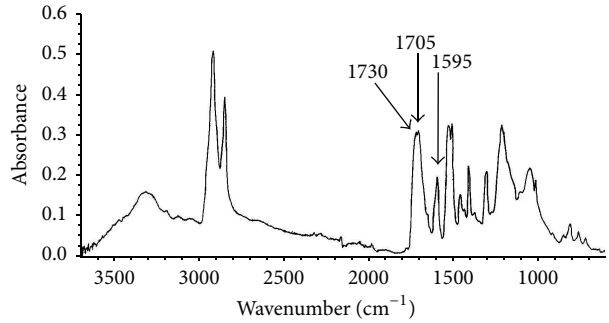

Figure 2: FTIR spectrum for biorenewable polymer of waste vegetable oil-based polyurethane.

2.4. Spectroscopic and Thermal Characterization. The starting vegetable oils and their hydroxylated monomers, namely, biorenewable monomer, are identified by means of Fourier transform infrared (FTIR) spectroscopy. The thermal gravimetric analysis (TGA) measurement of BP was performed using Linseis TGA to characterize the thermal properties of the BP according to ISO 11358. TGA is an analytical technique that measures the decomposition weight loss of a small polymer sample as a function of time or temperature. It provides a quantitative description of the thermal stability of a material and the amount of the corresponding residue. The weight loss and derivative weight loss were measured at 20°C to 900°C with heating rate of 10°C/min under oxygen atmosphere and flow rate of 0.3 μL using alumina crucible.

2.5. Mechanical Characterization. The Universal Tensile Machine AG-I, Shimadzu, 10 kN with a 5 mm/min crosshead speed, was used to analyse the respective mechanical properties of the specimens produced at each parameter [16]. Then tensile tests of five samples from each composition were tested and an average value was obtained. The tensile strength and strain of each specimen were obtained and tabulated to be examined.

2.6. Structural Characterization. In order to perform a fracture analysis on each specimen, the fractures were observed under a scanning electron microscope (SEM). The samples were initially coated with platinum and observed at different magnifications. However, the magnifications at 500x were carefully observed.

3. Results and Discussion

3.1. The Infrared Spectra of the Synthesized Biorenewable Polymer (Polyurethane) and Its Thermal Characterization. The IR spectra (Figure 1) of the biorenewable polyols show an intense, new broad peak at 3400 cm^{-1} that verifies the presence of hydrogen bonded hydroxyl (OH) groups in the synthesized product. (The OH group will then react with diisocyanate to form the polyurethane polymer, namely, biorenewable polymer (BP).) Otherwise, the principal IR bands are much in the same location for all four compounds.

The infrared spectra of the synthesized BP of waste vegetable oil-based polyurethane are shown in Figure 2. It is clearly seen that the polyurethane was fully cured. This is evidenced by the reduction and almost complete disappearance of the NCO peak at 2275 cm^{-1}. The following characteristic bands in the FTIR spectra were observed: 3300, 1720, 1525, 1220, and 1086 cm^{-1} (this band is attributed to the formation of urethane structures –NH [6, 7]), 2800–3000 cm^{-1} (CH stretching vibrations), 2919 cm^{-1} (asymmetric CH_2 stretching), and 2853 cm^{-1} (symmetric CH_2 stretching).

An absorption peak was observed at the 1595 cm^{-1} band corresponding to the C=C stretching vibration in the aromatic rings of MDI. A strong band, assigned to hydrogen bonded –(NH–C=O–O)– stretching vibrations, is present at 1705 cm^{-1}. A free (non-hydrogen bonded) C=O stretch appears as a shoulder on the high-wavenumber side of this band (at 1730 cm^{-1}, Figure 2).

Referring to Figure 3, the weight loss curves (TG), and derivative thermogravimetric (DTG) evaluation of SP samples, the initial temperatures for injection molding were ensured not to exceed the degradation temperature. The first peak appeared at the temperature range less than 100°C due to the beginning of weight loss of volatile material [17], moisture drying stage [18], moisture evolution of water [19], and water evaporation [20, 21] in the DTG evaluation profile of the samples.

Qualitative characterization of the degradation process is elaborated by the onset and maximum peak temperature of the first step T_{1on} and T_{1max} along with the same for second step T_{2on} and T_{2max}. The detail of TGA onset decomposition temperature (T_{onset}) and the maximum decomposition temperature (T_{max}) for BP is shown in Table 1. The onset degradation temperature T_{onset} and the maximum degradation rate temperature T_{1max} of the first BP degradation stage are 238°C and 419°C, respectively. The first peak of polymer decomposition temperature represents the hard segment, while the second peak represents the degradation of the soft segment. Figure 2 shows the derivative weight loss of BP is more than 93.7%. The weight loss of BP which started at less than 100°C indicated that the volatile matter in samples is equivalent to 4.3%.

Meanwhile, the decomposition temperature is attributed to the crosslinker of flexible isocyanate content. It has been suggested that the amount of weight loss at each degradation stage may be used as a quantitative measurement of the hard

Table 1: Thermal property of BP sample.

Samples	BP
First decomposition [°C]	238
T_{on} [°C]	94
T_{max} [°C]	283
Weight loss [%]	19.5%
Second decomposition [°C]	419
T_{on} [°C]	283
T_{max} [°C]	494
Weight loss [%]	57.4%
Third decomposition [°C]	567
T_{on} [°C]	494
T_{max} [°C]	678
Weight loss [%]	16.8%

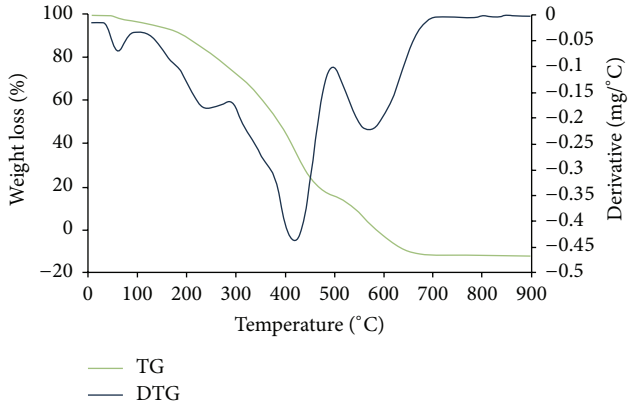

Figure 3: Thermogram (TG) and derivative weight loss (DTG) of BP samples.

and soft content in BP. This is indicated by the first weight loss of BP which is approximately similar to the first decomposition temperature at 238°C and second decomposition temperature is at 419°C, respectively.

3.2. Injection Molding Parameters. Based on the results obtained from the TGA, the injection molding temperatures of each zone were ensured not to exceed 238°C. This is to make sure that the BP does not decompose before injection. Then, by referring to the melting temperatures and typical injection molding temperatures of both pure LDPE and HDPE, the initial parameters were set. The next several temperature values with increasing BP composition were adjusted to ensure that the best samples were produced.

For all compositions of the LDPE/BP compound, regardless of the type of crosslinker used, there was no need to adjust the temperature values of feed, rear 1, rear 2, middle, front, and nozzle zones. These values are listed in Table 2.

Based on the values tabulated in Table 2, the LDPE/BP compounds were able to be processed at the same parameters as neat LDPE, regardless of the addition of BP. This is beneficial as the processing of these proposed biorenewable plastics will not require any additional cycle time. However,

Table 2: The main injection moulding parameters used for LDPE/SP compounds.

(a)

Injection pressure [MPa]	Injection rate [cm^3/s]	Holding pressure [MPa]	Holding time [s]	Cooling time [s]	Injection time [s]	Cycle time [s]
43.4	15.0	43.4	2.0	10.0	2.0	22.0

(b)

Temperature [°C]					
Feed	Rear 1	Rear 2	Middle	Front	Nozzle
50.0	165.0	170.0	175.0	180.0	185.0

if further development of the compound to be processed at lower temperature, lower injection pressure with reduction of cycle time should be considered. Due to lower temperature and injection pressure required for processing, less energy is consumed and thermal degradation of BP is reduced.

Meanwhile, for the HDPE/BP compounds, the parameters, mainly temperature, had to be adjusted to ensure the melt filled the mold entirely. All of the specimens injected were individually examined from any defect. The respective values are tabulated in Table 3.

According to these results, the parameters used for neat HDPE were the same at low percentages of BP with the flexible crosslinkers. However, when the composition of BP was increased, the temperatures had to be increased as silver streaks started to appear. Not only that, pressure also needed to be increased for the melt to completely fill the mold. This definitely opposed the initial idea of lowering processing conditions to save energy consumption.

The increase in values of the parameters may be due to the presence of HDPE. Its high density may have influenced the mixing conditions to increase. Nevertheless, in further research, the processing temperatures will be tried to be reduced and the resulting effects on the mechanical properties will be studied. This may significantly reduce the energy consumption for processing of these compounds. However, the visual observations cannot stand alone; henceforth, the corresponding mechanical properties for each compound were analyzed.

3.3. Mechanical Characterization. The mechanical properties of the compounds were analyzed based on their tensile strength and strain or elongation at break. These data were obtained through the tensile test performed. Table 4 shows the tensile test experimental data for all LDPE/BP compounds developed in this work.

The tensile strength measurement shows a peculiar trend as it significantly increases at low percentages of BP and gradually declines with addition of the BP. The same trend is observed for the elongation at break of the samples. This could be due to the soft properties of the BP blended with the strong properties of the LDPE producing a tough and strong compound. Not only does the presence of BP allow it to be more renewable, but it also improves the mechanical properties.

Table 3: The main injection molding parameters used for HDPE/BP compounds.

Parameters	HDPE					
	Neat	Flexible crosslinker				
		1% BP	2% BP	3% BP	4% BP	5% BP
Injection pressure [MPa]	96.6	96.6	96.6	104.7	104.7	104.7
Injection rate [cm^3/s]	25.0	25.0	25.0	15.0	15.0	15.0
Holding pressure [MPa]	96.6	96.6	96.6	104.7	104.7	104.7
Holding time [s]	2.0	2.0	2.0	2.0	2.0	2.0
Cooling time [s]	10.0	10.0	10.0	10.0	10.0	10.0
Injection time [s]	2.0	2.0	2.0	2.0	2.0	2.0
Cycle time [s]	22.0	22.0	22.0	22.0	22.0	22.0
Temperature [°C]						
Feed	50.0	50.0	50.0	60.0	60.0	55.0
Rear 1	175.0	175.0	175.0	185.0	185.0	175.0
Rear 2	165.0	165.0	165.0	175.0	175.0	165.0
Middle	180.0	180.0	180.0	190.0	190.0	180.0
Front	195.0	195.0	195.0	205.0	205.0	195.0
Nozzle	205.0	205.0	205.0	215.0	215.0	205.0
Parameters	HDPE					
	Neat	Rigid crosslinker				
		1% BP	2% BP	3% BP	4% BP	5% BP
Injection pressure [MPa]	96.6	104.7	104.7	104.7	104.7	104.7
Injection rate [cm^3/s]	25.0	15.0	15.0	15.0	15.0	15.0
Holding pressure [MPa]	96.6	104.7	104.7	104.7	104.7	104.7
Holding time [s]	2.0	2.0	2.0	2.0	2.0	2.0
Cooling time [s]	10.0	10.0	10.0	10.0	10.0	10.0
Injection time [s]	2.0	2.0	2.0	2.0	2.0	2.0
Cycle time [s]	22.0	22.0	22.0	22.0	22.0	22.0
Temperature [°C]						
Feed	50.0	55.0	55.0	55.0	55.0	55.0
Rear 1	175.0	175.0	175.0	175.0	175.0	175.0
Rear 2	165.0	165.0	165.0	165.0	165.0	165.0
Middle	180.0	180.0	180.0	180.0	180.0	180.0
Front	195.0	195.0	195.0	195.0	195.0	195.0
Nozzle	205.0	205.0	205.0	205.0	205.0	205.0

Table 4: The mechanical properties for the LDPE/BP injected sample.

Parameters	LDPE										
	Neat	Flexible crosslinker					Rigid crosslinker				
		1% BP	2% BP	3% BP	4% BP	5% BP	1% BP	2% BP	3% BP	4% BP	5% BP
Tensile strength [MPa]	8.9	11.3	10.9	10.6	10.1	9.9	11.8	11.3	10.8	10.2	9.9
Tensile strain [%]	67.6	71.4	70.2	69.2	68.3	67.8	79.6	74.8	72.1	71.4	66.0

Plasticization effect explains a change in the thermal and mechanical properties of a given polymer by the lowering of rigidity at room temperature. This can clarify the general increment of tensile strain. Polymer chains which possess a regular structure are able to crystallize under suitable conditions, either from the melt or from solution. This indicates that the chain molecules change from a coiled and disordered state to a tightly folded aligned and ordered state. Besides that, there was no significant difference seen between different types of crosslinkers. Further explanation can be provided by the fracture analysis which is done in the next section. On the other hand, Table 5 revealed the mechanical properties of the HDPE/SP compounds.

The HDPE provides ductility that exhibits brittle behaviour with a subsequent loss of toughness to the compounding materials [22, 23]. The addition of BP generally increases the toughness and decreases the strength of the compound. This could be due to the soft properties of the SP. Tensile strength measurements indicated that the mechanical property values decrease with increasing BP

Table 5: The mechanical properties for the HDPE/BP injected sample.

Parameters	Neat	HDPE									
		Flexible crosslinker					Rigid crosslinker				
		1% BP	2% BP	3% BP	4% BP	5% BP	1% BP	2% BP	3% BP	4% BP	5% BP
Tensile strength [MPa]	35.5	33.1	32.0	28.6	28.6	26.0	33.9	34.1	33.7	33.8	33.3
Tensile strain [%]	37.8	37.8	44.0	47.6	47.1	53.5	44.7	43.0	39.0	36.7	36.8

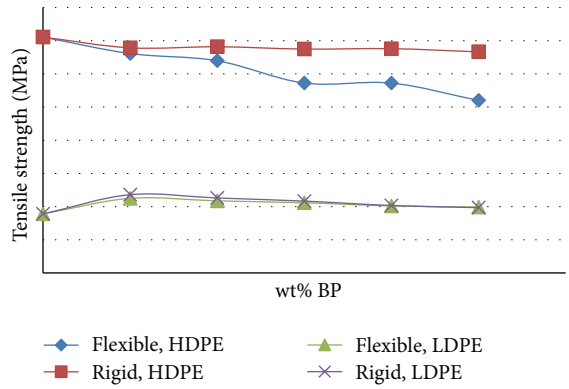

Figure 4: Tensile strengths for all specimens injected at respective compositions.

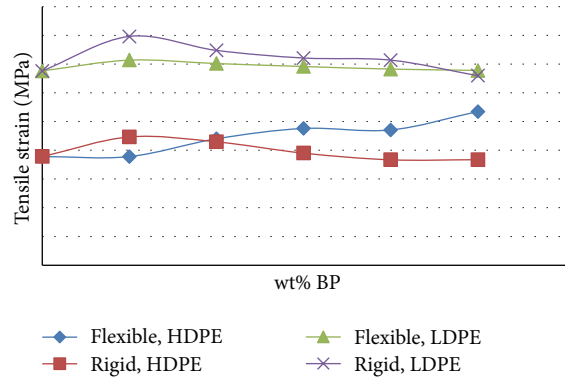

Figure 5: Tensile strains for all specimens injected at respective compositions.

content in the sample which used the flexible crosslinker. However, for the samples with rigid crosslinker, regardless of the BP content, the tensile strength remained approximately stagnant at 33 to 34 MPa. This is probably due to traits of the flexible and rigid crosslinkers. Flexible polyurethane is usually used for cushioning and packaging, while rigid polyurethane is used for insulation and packaging. The general declining trend may be due to the soft properties of the BP.

Meanwhile, the elongation at break increased for the sample with flexible crosslinker and vice versa for rigid crosslinker. The higher tensile strain of HDPE/BP compound compared to neat HDPE may also be due to plasticization effect. Based on these results, when the BP is added with flexible isocyanate, it may act as a filler as it improves the tensile strain values.

If both the samples of LDPE/BP and HDPE/BP compounds were to be compared, it can be said that the strength of HDPE/BP is significantly better than that of LDPE/BP. This can be seen in Figure 4.

The significant difference in tensile strength can be explained by the individual properties of HDPE and LDPE. HDPE is well known for its strong properties. Therefore, the same characteristics were observed even after addition of the BP with crosslinkers.

Besides that, the tensile strain of the LDPE/BP compound is observed to be higher than the HDPE/BP compound. This is shown in Figure 5.

The high value of elongation at break for the LDPE/BP compound is due to the more flexible properties. This allows it to significantly yield before breaking, leading to a high value of tensile strain. Therefore, LDPE/BP is comparatively more flexible than HDPE/BP.

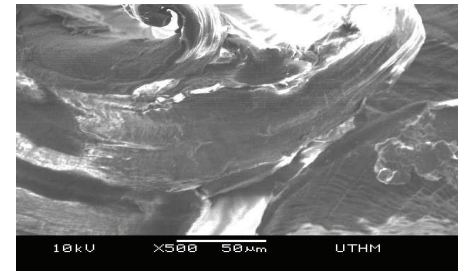

Figure 6: SEM image of fractured neat LDPE at 500x magnification.

Both these results are favorable as they do not alter the properties of the HDPE or LDPE too drastically and hence can allow the compound to gradually replace the usage of both HDPE and LDPE in industries.

3.4. Fracture Analysis. The fracture analysis was performed in order to understand and examine the fracture at a specific magnification. Besides that, it can also demonstrate the homogeneity of the compound injected. This can be done by placing the sample under a scanning electron microscope (SEM). Various magnifications were observed, but for the purpose of this study the images were taken at 500x magnification.

Figure 6 shows the SEM image obtained for neat LDPE, while Figure 7 shows the SEM images obtained for LDPE/SP compounds after fracture. The images show the general structure of the injected sample.

From Figure 6, it can be seen that the fracture is ductile. This is due to the significant elongation or necking before break. Also the plastic deformation which can be seen by

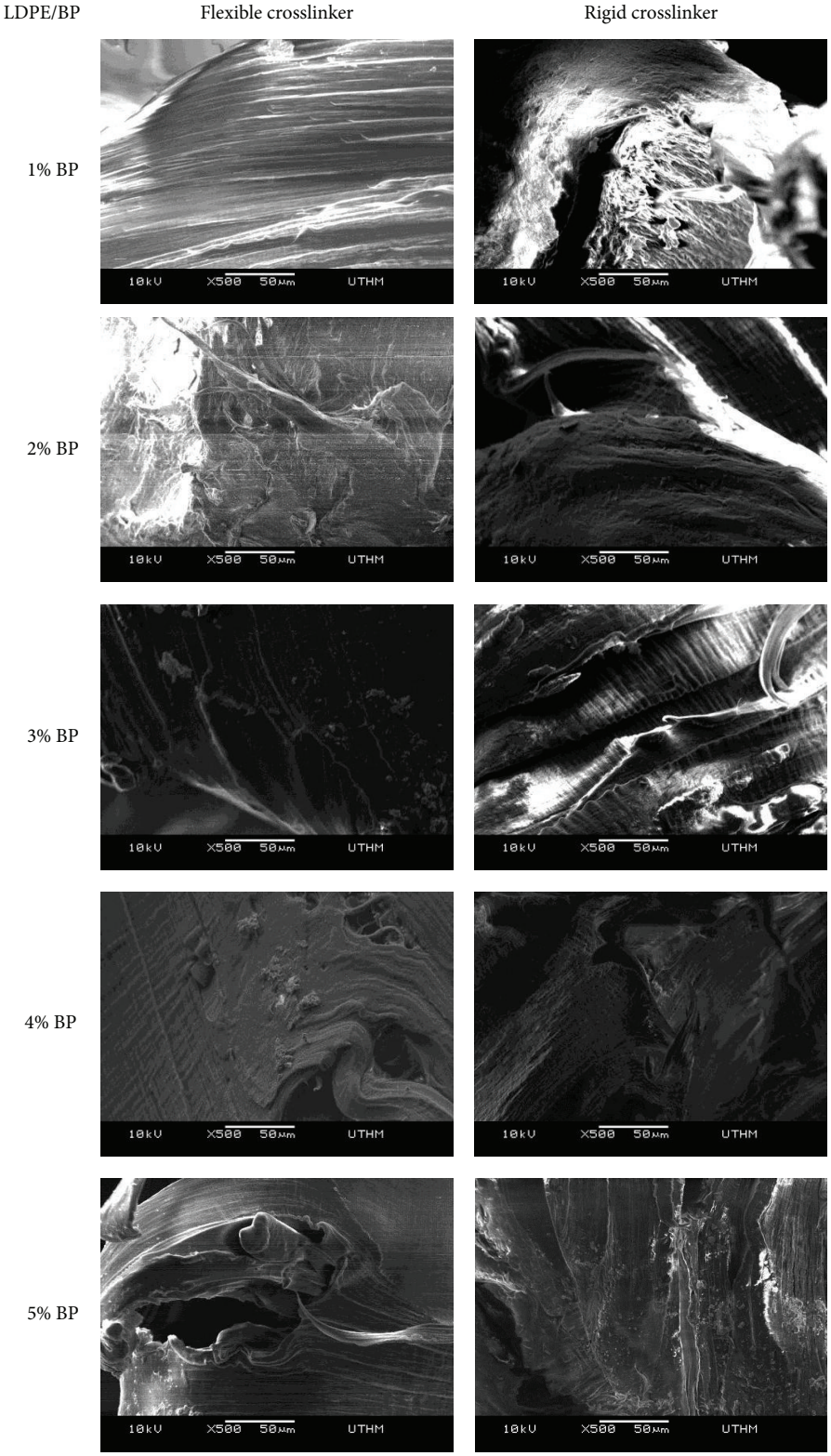

Figure 7: SEM images for all LDPE/BP specimens at 500x magnifications.

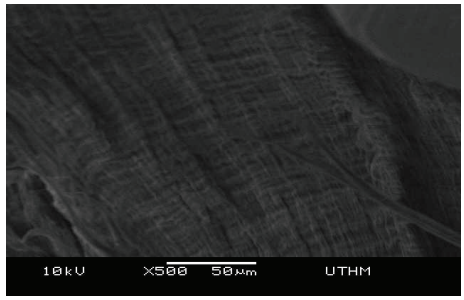

Figure 8: SEM image for fractured neat HDPE at 500x magnification.

the tear lines occurring on the fractured surface supported the deduction [24]. However, there might have been some stress points that could be observed due to the partially melted LDPE structure. The oval shaped structure appearing in the SEM of neat LDPE proves that these structures are not due to the BP as examined in Figure 7. Instead, they may be impurities or unmelted LDPE.

Various structures were observed through these images but it can be concluded that the BP content in the compound enables it to significantly elongate before breaking, in addition to the ductile properties of pure LDPE. Due to lower temperature and injection pressure required for processing, less energy is consumed and thermal degradation of BP is reduced. This can be proved via the long strands formed at each fracture. Having this property can allow these compounds to be used in diverse applications which require tough or highly ductile materials.

Besides that, blobs of material which are inhomogeneous to the entire sample are seen in the LDPE/BP compounds linked with flexible crosslinkers. The foamy structure may identify these blobs as the crosslinkers which may have not completely been mixed with the compound. It could also be due to the processing conditions during injection molding.

Since the blobs are not obviously seen in the LDPE/BP compound with the rigid crosslinker, it contributed to better mechanical properties than with the flexible crosslinker. Meanwhile Figure 6 shows the SEM image for neat HDPE and Figure 8 shows the SEM for all HDPE/BP samples.

The tear lines as seen in Figure 8 may represent plastic deformation and again can be proven by the tear lines, as in Figure 9. The image portrays that a homogeneous melt of HDPE was injected. The SEM images for the fractured HDPE/BP compounds are shown in Figure 9.

Based on the images, it can be seen that the structures may not be completely homogeneous as some rough surfaces can be seen. Some strands which demonstrate plastic deformation and a ductile failure can also be observed. If compared to the LDPE/BP images, no foamy structures were seen which may prove that the temperature used in injection molding is approximately accurate.

These findings can help support the fact that not only the composition of BP but also the parameters used in injection molding, mainly temperature, do give an impact on the mechanical properties of the HDPE/BP compound produced.

4. Conclusion

By using melt-mixing during the injection molding process, new compounding polymers based on different ratio of BP to LDPE or HDPE were successfully produced. The processing conditions of LDPE/BP and HDPE/BP, renewable plastics, by injection molding were determined and analyzed. The initial processing conditions of the standard LDPE and HDPE thermoplastic were used as a base point. It was concluded that the processing conditions of the LDPE/BP compound, a renewable plastic, by injection molding were exactly the same as that of neat LDPE while for the HDPE/BP compound an increase in the parameters used in injection molding was required. The corresponding mechanical properties of the compound were also examined. Tensile strength and elongation at break increased with increasing BP content at low compositions and started to decrease at high BP content for the LDPE/BP compound. However, the tensile strength and strain of the LDPE/BP compound were generally better than the neat LDPE. Therefore, not only does the presence of BP in the compound provide sustainable characteristics, but it also improves the mechanical properties. On the other hand, the tensile strength generally decreased for both HDPE/BP with flexible and rigid crosslinkers while the elongation at break increased. These results comply with the properties of pure LDPE and HDPE. Apart from the changing ratios of BP to LDPE or HDPE, the processing temperature was also considered to have an influence on the mechanical properties of the compound. By acting as a guideline, this study aids any intention on processing these in-house produced polymers via injection molding. Further research should be done in this area by decreasing the processing conditions to reduce the energy consumption.

Conflict of Interests

The authors declare that there is no conflict of interests regarding the publication of this paper.

Acknowledgments

The authors would like to thank the Malaysian Government, University Tun Hussein Onn Malaysia (UTHM), Johor, and Malaysian Technical University Centre of Excellence (MTUN CoE) for supporting this research study under research Grant

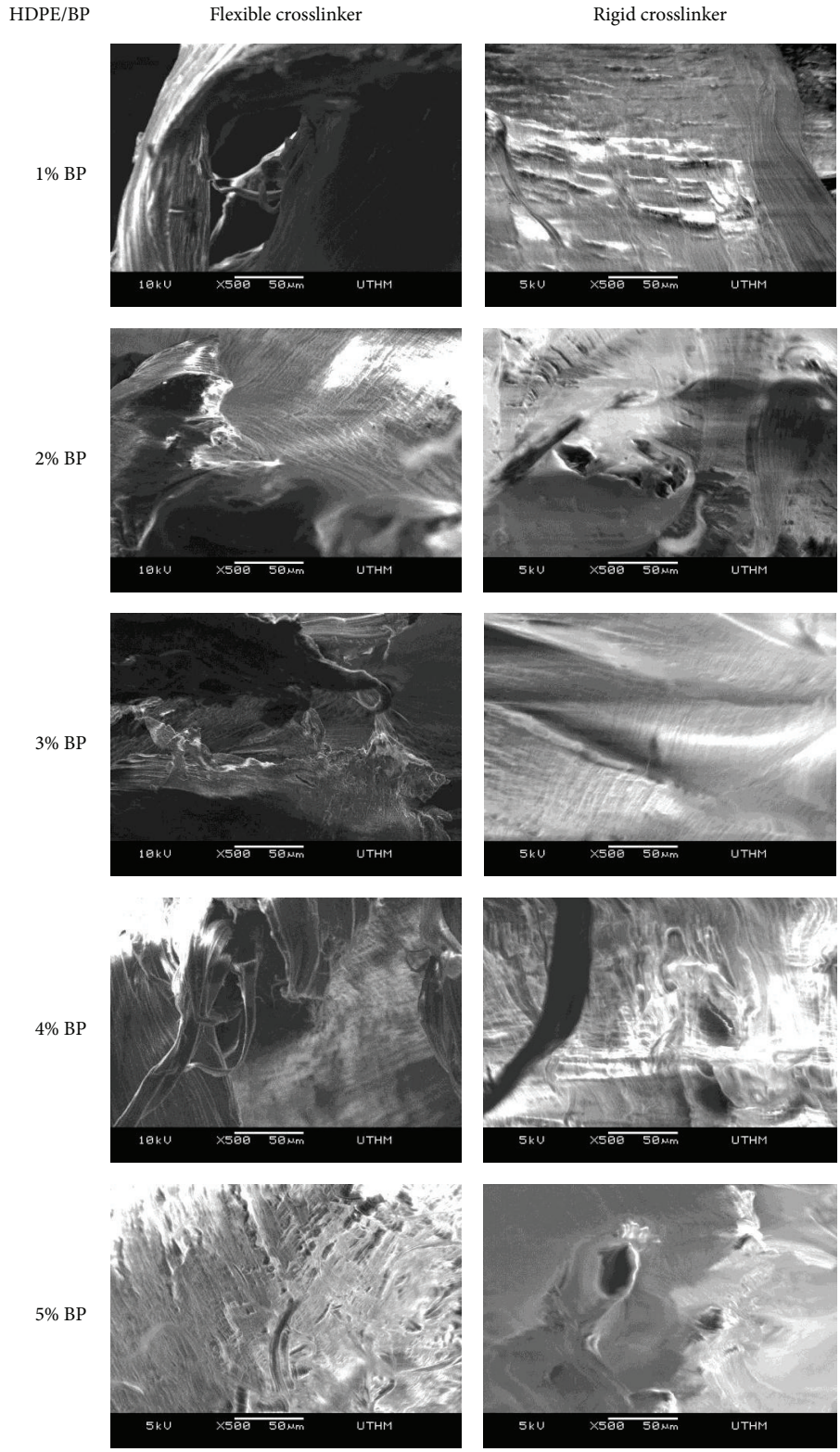

Figure 9: SEM images for all HDPE/BP specimens at 500x magnifications.

Vot C014 and Exploratory Research Grant Scheme (ERGS), E018. Not to forget, the authors express deep gratitude to the University of Auckland, New Zealand, for the research internship opportunity.

References

[1] B. John, K. T. Varughese, Z. Oommen, P. Pötschke, and S. Thomas, "Dynamic mechanical behavior of high-density polyethylene/ethylene vinyl acetate copolymer blends: the effects of the blend ratio, reactive compatibilization, and dynamic vulcanization," *Journal of Applied Polymer Science*, vol. 87, no. 13, pp. 2083–2099, 2003.

[2] M. Munaro and L. Akcelrud, "Polyethylene blends: a correlation study between morphology and environmental resistance," *Polymer Degradation and Stability*, vol. 93, no. 1, pp. 43–49, 2008.

[3] S. V. Canevarolo Jr., *Ciência dos Polímeros*, Editora Artliber Ltda, São Paulo, Brazil, 2006.

[4] J. Minick, A. Moet, and E. Baer, "Morphology of HDPE/LDPE blends with different thermal histories," *Polymer*, vol. 36, no. 10, pp. 1923–1932, 1995.

[5] J. H. Khan and N. Ahmed, "Photo-oxydative degradation of recycled, reprocessed HDPE: changes in chemical, thermal and mechanical properties," *Bulgarian Journal of Physics*, vol. 30, pp. 158–169, 2003.

[6] A. Z. M. Rus, "Polymer from renewable materials," *Science Polymer*, vol. 93, pp. 1–16, 2010.

[7] A. Z. Mohd-Rus, T. J. Kemp, and A. J. Clark, "Degradation studies of polyurethanes based on vegetable oils. Part 2. Thermal degradation and materials properties," *Progress in Reaction Kinetics and Mechanism*, vol. 34, no. 1, pp. 1–41, 2009.

[8] A. Min Min, T. G. Chuah, and T. R. Chantara, "Thermal and dynamic mechanical analysis of polyethylene modified with crude palm oil," *Materials & Design*, vol. 29, no. 5, pp. 992–999, 2008.

[9] European-Bioplastic, *Material Innovations-Biobased Low-Density Polyethylene*, 2014, http://en.european-bioplastics.org/.

[10] Y. Yildiz, N. Kizilcan, and N. Uyanik, "Effects of acetophenone-formaldehyde resin on the degradation of high-density polyethylene by UV-irradiation," *Pigment and Resin Technology*, vol. 35, no. 5, pp. 247–251, 2006.

[11] S. Ramarad, *Preparation and properties of kenaf fibre filled (plasticized polylactic asid) composites [M.S. thesis]*, Universiti Sains Malaysia, Penang, Malaysia, 2008.

[12] M. Ito and K. Nagai, "Degradation issues of polymer materials used in railway field," *Polymer Degradation and Stability*, vol. 93, no. 10, pp. 1723–1735, 2008.

[13] A. T. Bozdana and Ö. Eyercioğlu, "Development of an expert system for the determination of injection moulding parameters of thermoplastic materials: EX-PIMM," *Journal of Materials Processing Technology*, vol. 128, no. 1–3, pp. 113–122, 2002.

[14] S.-Y. Han, J.-K. Kwag, C.-J. Kim, T.-W. Park, and Y.-D. Jeong, "A new process of gas-assisted injection molding for faster cooling," *Journal of Materials Processing Technology*, vol. 155-156, no. 1-3, pp. 1201–1206, 2004.

[15] S. R. Mohid, A. Z. M. Rus, and N. H. Harun, "Influence of bio polymer composites as heat absorption coating," *Applied Mechanics and Materials*, vol. 315, pp. 404–407, 2013.

[16] D. R. Mulinari, H. J. C. Voorwald, M. O. H. Cioffi, M. L. C. P. da Silva, T. G. da Cruz, and C. Saron, "Sugarcane bagasse cellulose/HDPE composites obtained by extrusion," *Composites Science and Technology*, vol. 69, no. 2, pp. 214–219, 2009.

[17] J. M. Cervantes-Uc, J. V. Cauich-Rodríguez, H. Vázquez-Torres, and A. Licea-Claveríe, "TGA/FTIR study on thermal degradation of polymethacrylates containing carboxylic groups," *Polymer Degradation and Stability*, vol. 91, no. 12, pp. 3312–3321, 2006.

[18] S. S. Idris, N. A. Rahman, K. Ismail, A. B. Alias, Z. A. Rashid, and M. J. Aris, "Investigation on thermochemical behaviour of low rank Malaysian coal, oil palm sustainable mass and their blends during pyrolysis via thermogravimetric analysis (TGA)," *Sustainableresource Technology*, vol. 101, pp. 4584–4592, 2010.

[19] M. Ardanuy, M. Antunes, and J. I. Velasco, "Vegetable fibres from agricultural residues as thermo-mechanical reinforcement in recycled polypropylene-based green foams," *Waste Management*, vol. 32, no. 2, pp. 256–263, 2012.

[20] S. Ibrahim and M. R. Johan, "Thermolysis and conductivity studies of poly(ethylene oxide) (PEO) based polymer electrolytes doped with carbon nanotube," *International Journal of Electrochemical Science*, vol. 7, no. 3, pp. 2596–2615, 2012.

[21] S. Gopalakrishnan, N. T. Nevaditha, and C. V. Mythili, "Synthesis and characterization of bifunctional monomers for high performance polymers from renewable resource," *International Journal of ChemTech Research*, vol. 4, no. 1, pp. 48–54, 2012.

[22] P. S. Souza, E. F. Rodrigues, J. M. C. Prêta, S. A. S. Goulart, and D. R. Mulinari, "Mechanical properties of HDPE/textile fibers composites," *Procedia Engineering*, vol. 10, pp. 2040–2045, 2011.

[23] X. Zhao, R. K. Y. Li, and S.-L. Bai, "Mechanical properties of sisal fiber reinforced high density polyethylene composites: effect of fiber content, interfacial compatibilization, and manufacturing process," *Composites Part A: Applied Science and Manufacturing*, vol. 65, pp. 169–174, 2014.

[24] A. G. Supri, H. Salmah, and K. Hazwan, "Low density polyethylene-nanoclay composites: the effect of poly (acrylic acid) on mechanical properties, XRD, morphology properties and water absorption," *Malaysian Polymer Journal*, vol. 3, no. 2, pp. 39–53, 2008.